INVESTIGATION OF EXCITED ELECTRONIC SPECIES USING MOLECULAR BEAM TECHNIQUES

by

THOMAS ANDREW DAVIDSON

Thesis presented for the degree of

Doctor of Philosophy

University of Edinburgh

October, 1973.

To my parents

Abstract

This is an account of studies made on metastable mercury atoms using molecular beam techniques.

The metastable mercury atoms are produced by electron bombardment of a ground state mercury beam. Experiments involving an atomic beam decay technique and magnetic state selector have been used to determine the composition of the metastable mercury beam and the lifetimes of the states involved. The results suggest that there are two states in the beam, the 6^3P_2 and 6^3P_0, at energies below 10eV. A lifetime of $1.3 \pm 0.2 \times 10^{-3}$S was found for the 6^3P_2 which was tentatively attributed to a magnetic dipole transition to the 6^3P_1. Assuming that the excited mercury beam is not polarised, an estimate of the lifetime of the 6^3P_0 was found to be $1.3 \pm 0.4 \times 10^{-3}$S but no similar mechanism could be proposed for this decay.

Thermal energy collisions between metastable mercury and the alkali metals, sodium, potassium and rubidium have been studied in crossed molecular beam experiments. Interference structure was resolved in all cases suggesting that the atoms interact by a single effective potential in the attractive region probed at these energies. Potentials have been produced in all cases by inversion of the experimental cross sections and a critical evaluation of the method of inversion has been carried out.

Theoretical considerations of the excited mercury/alkali systems suggest that the single effective potential arises because the potential energy curves involved are not significantly different from each other and because the Hg*/alkali systems correspond to weak coupling cases.

No attenuation of the interference structure is observed so that quenching of the metastable state is not an important process along trajectories sampling only the attractive part of the potential.

ACKNOWLEDGEMENTS

I wish to express my sincere thanks to Dr K.P. Lawley and Dr M.A.D. Fluendy for many helpful suggestions and discussions. Their interest and encouragement helped tremendously in overcoming a host of problems which arose during three very interesting and enjoyable years.

My thanks also to the other members of the Molecular Beams Group at Edinburgh for their part in making the period of this research so unforgettable. I am especially indebted to J. Costello who, for the final twelve months, was a willing and able research colleague.

I wish to express thanks also to Mrs L. Campbell for her courage in undertaking the typing of the manuscript, her patience in deciphering it and her dexterity in typing it. My sincerest thanks also to Sheila for her encouragement and understanding over the past three years and her help in the unenviable task of proof reading.

I am indebted to the University of Edinburgh for provision of laboratory, library and computing facilities and also the Carnegie Trust for the Universities of Scotland for financial support during the period of this work.

Contents

Chapter 1

Introduction

1 Introduction

The major aim of this work is an investigation of metastable mercury atoms and a determination of the intermolecular potentials involved in collisions of these atoms with alkali atoms using molecular beam techniques.

Electronically excited atoms and molecules play an important role in flames, shocks, explosions, electrical discharges and photolysis and any knowledge of the intermolecular forces involved would aid the fundamental understanding of the physics and chemistry of these processes. Although, the investigation of these phenomena has given some information regarding cross sections for collisions of excited species, the identity of the particles involved must often be inferred and in most cases more than one species is involved. Therefore, it is virtually impossible to obtain potential functions for the interactions between excited and ground state particles from such experiments. However, provided the lifetime of the excited species is sufficiently long molecular beam scattering techniques can be used to determine cross sections for both elastic and inelastic scattering of these excited species together with the interaction potentials involved.

During the past decade, in particular, there has been increased activity in the fields of elastic, inelastic and reactive scattering using molecular beam techniques [FLU 1973(a)], [ROS 1966]. The majority of this effort has been directed towards ground state atoms and ions and very little work has been done on the investigation of differential scattering of metastable atoms [GRO 1968], [KAL 1973], [HAB 1973].

Elastic scattering experiments are primarily aimed at extracting intermolecular potentials and less directly any concurrent inelastic and reactive events. This arises because the elastic scattering behaviour of atoms and molecules is completely determined by their interaction potential, not only from classical considerations but also according to quantum theory. Unfortunately, the inversion of the scattering pattern to yield a potential is a difficult problem since experimental observations are limited in angular and energy range, are less than perfect in resolution and include some noise. For these reasons, previously existing data was fitted to simple model potentials. Unfortunately this led to ambiguities in results since the assumed form was by no means unique. Recently, however, the problem of direct inversion has been tackled with considerable success [BUC 1971(a)].

On the basis of experimental techniques elastic scattering can be divided into two parts; (1) the evaluation of the short range part of the potential by means of high energy beam scattering experiments and (2) the determination of the attractive well and long range part of the potential from scattering observations at thermal energies.

Unfortunately very little experimental information is as yet available on the superthermal scattering of mercury from alkali metals [DUC 1971] whereas the thermal energy scattering of these species has been extensively studied [MOR 1962(a)] [MOR 1962(b)] [HOS 1960] [HUN 1964] [HUN 1965] [BAR 1966]. These collisions between ground state Hg atoms ($^1S_0$) and alkali metal atoms ($^2S_{\frac{1}{2}}$) at thermal energies are necessarily elastic and occur under the influence of a single potential. Accurate scattering measurements on these systems have recently been

made by Buck and Pauly [BUC 1971(b)] [BUC 1972] and intermolecular potentials have been obtained by direct inversion of this data. The shape of the reduced potentials for these alkali/mercury systems determined by this inversion procedure are the same for all systems but they deviate significantly from that of model potentials commonly used.

The corresponding interactions between alkali atoms and the excited states of mercury are not so clearly understood [DAR 1971]. The lowest of such states are the 6^3P_0, 6^3P_1 and 6^3P_2 at, respectively, 4.64eV, 4.89 eV and 5.43 eV above ground. The 6^3P_0 and 6^3P_2 are metastable while the 6^3P_1 decays radiatively to the ground state and has a lifetime of 10^{-7} seconds. The thermal energy collisions of these excited atoms with other species is complicated not only by the possibility of energy transfer but also by the fact that a manifold of potentials arises from the separated atoms due to the possible spin pairings (if the partner is not a singlet atom) and m_J states of the Hg atom.

The photochemistry of the excited states of mercury and in particular of the $^3P_1$ atom is of great importance and has been extensively studied but the processes involved are by no means completely determined. The understanding of these fundamental processes of electronic energy transfer and their relation to curve crossing must begin with simple systems where a knowledge of the adiabatic potential curves can be obtained. The alkali metal/excited mercury system is a useful case for this purpose since both theoretical studies and the unravelling of potential energy curves through magnetic state selection offer the hope of a complete picture.

Inelastic events occuring in collisions of excited atoms, mercury in particular, are reviewed in chapter 2. Both experimental data and theoretical calculations are considered in order to supply some insight into the possible magnitude of such inelastic events.

The collision free environment in a molecular beam experiment offers the possibility of obtaining information on the polarisability, the electric and magnetic moments, the fine and hyperfine structure and the lifetimes of metastable atoms and molecules and although beam experiments involving metastable mercury have been in existence for some time [LIC 1958] considerable uncertainty still surrounds some of the major properties of the metastable beam species. In chapter 3 experiments are described in which the composition of the beam is determined and estimates made of the lifetimes of the species involved. The conclusions of this work are presented before embarking on any discussion of the scattering experiments since a knowledge of the beam composition and the lifetimes of the species involved is essential to any understanding of the scattering data.

In chapter 4 a theoretical description of the interaction between an excited mercury atom and a ground state potassium atom is given and results are presented for the calculated potential energy curves. Chapter 5 consists of a brief resumé of scattering theory and the analysis involved in interpreting the results of scattering experiments.

The experimental procedure and the results obtained are presented in chapter 6 together with the treatment and analysis of this raw scattering data. A method of inversion is described and critically

discussed and potentials are produced for the systems Hg*/Na, Hg*/K and Hg*/Rb by inverting the differential cross sections.

The evaluated potentials are discussed in chapter 7 and examined in the light of other experimental and theoretical knowledge before the conclusions are presented.

Chapter 2

Collisions of Excited Atoms

2 Collisions of Excited Atoms

Several types of collision between an excited atom or molecule and another particle may be distinguished.

$$A^* + B \rightarrow A^* + B \qquad (a)$$

$$A^* + B \rightarrow A + B \qquad (b)$$

$$A^* + B \rightarrow A + B^* \qquad (c)$$

$$A^* + B \rightarrow AB^+ + e \qquad (d)$$

$$A^* + B \rightarrow A + B^+ + e \qquad (e)$$

$$A^* + B \rightarrow A^+ + B + e \qquad (f)$$

Reaction (a) is straightforward elastic scattering, the other processes are all inelastic. Process (b) represents the conversion of excitation energy to the kinetic energy of separation of the products. An example of electronic energy transfer is given in process (c) whereas processes (d) and (e) are associative and Penning ionization respectively. Collisional ionization is represented by process (f).

Elastic scattering will not be treated here since it is discussed in Chapter 5. Processes (b) and (c) will be discussed initially and then a treatment of the ionization processes will be given. Finally, a short discussion of molecular beam experiments in this area of research will be presented.

A wide variety of experimental techniques have been employed to study the reactions of excited species. In general, the procedure is different according to whether the excited states concerned are metastable or not. Molecular beam experiments are useful for the study of metastable states due to their relatively long lifetimes. However, in cases

where the excited species involved is not metastable the progress of the reaction may be followed by observing the radiation emitted either in quenching or sensitized fluorescence experiments.

In the early development of the study of quenching a great deal of attention was paid to mercury vapour as a working substance, mainly because of its experimental convenience but also because of its effectiveness in the photosensitization of chemical reactions.

The quenching of $Hg(^3P_1)$ by Ar is an example of reaction (b). The $^3P_1$ state is deactivated directly to the ground state $^1S_0$ by collision and all the excitation energy appears as kinetic energy of the recoiling mercury and argon atoms because the energy of the $^3P_1$ state is insufficient to excite Ar to any of its excited states. Since the direct conversion of large amounts of electronic energy is very inefficient the cross section is small. This process can be explained in terms of figure [2-1].

If the collision partner is a diatomic or triatomic molecule the situation is very different. Accurate total quenching cross sections have been measured by Deech et al [DEE 1971] for a variety of collision partners with $Hg(^3P_1)$. Typical cross section values found were for H_2, D_2 and CO $\simeq 22\text{Å}^2$, for $CO_2 \simeq 10\text{Å}^2$, for $O_2 \simeq 60\text{Å}^2$ for $N_2{}^{14}$ and $N_2{}^{15} \simeq 0.75\text{Å}^2$ whereas for Xe $\leq 2 \times 10^{-3}\text{Å}^2$. The situation in the case of Xe is similar to that of Ar whereas the large H_2 and D_2 cross sections have been described to efficient collision complex formation which results in chemical quenching; HgH being the dominant channel. Pitre et al [PIT 1972] and Horiguchi et al [HOR 1971] have shown that the N_2 cross sections

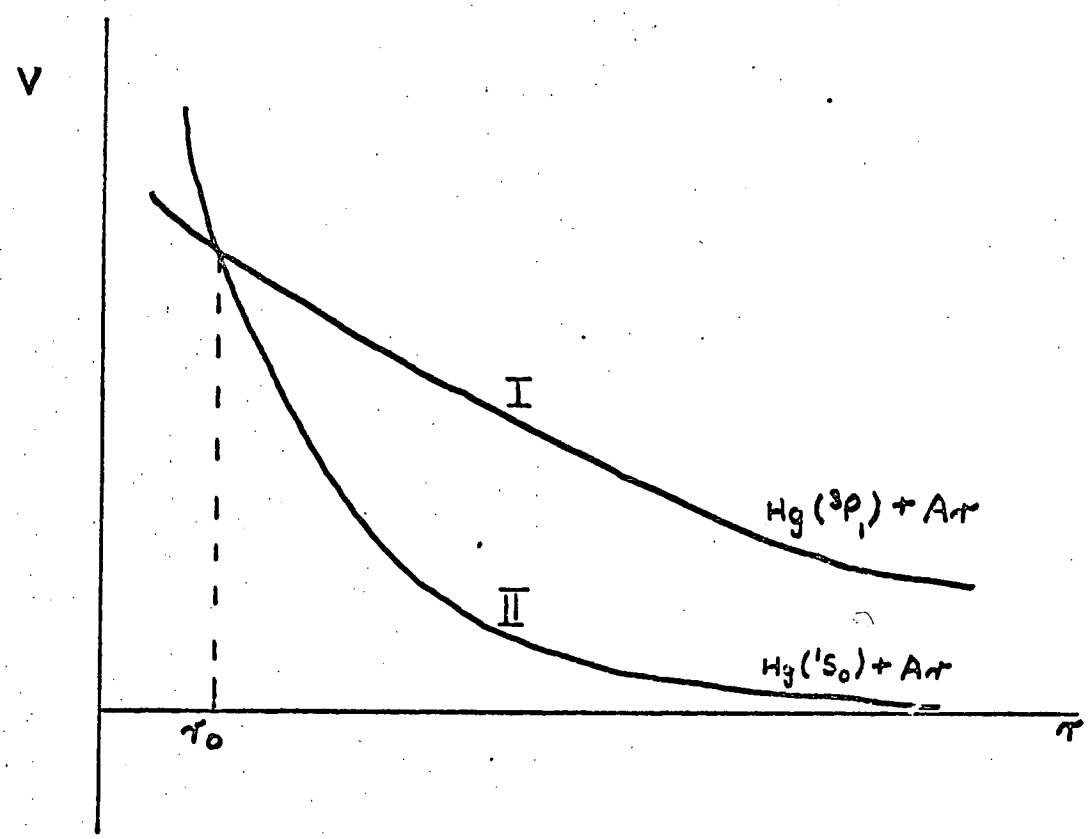

Quenching of an excited mercury atom by collisions of the second kind with an argon atom in its ground state.

Figure 2-1

for $^3P_1 \rightarrow {}^1S_0$ and $^3P_0 \rightarrow {}^1S_0$ are very small. This suggests that the results of Deech have to be interpreted as multiplet mixing cross sections; $^3P_1 \rightarrow {}^3P_0$. Because of the different vibrational energy levels of the two N_2 isotopic molecules; Deech's results provide evidence against a resonance effect in vibrational electronic energy transfer for $^3P_1 \rightarrow {}^3P_0$ transitions. Such a resonance effect was thought to be important previously. Vikis et al [VIK 1972] found that most molecules which they investigated predominantly induced $^3P_1 \rightarrow {}^3P_0$ transitions instead of quenching to $^1S_0$. CO_2 proved to be a notable exception for more than 99% was directly quenched to the ground state whereas CO caused mainly transitions to the $^3P_0$ state (~85%).

The fact that CO caused transitions to the $^3P_0$ means that the distribution of vibrational states in CO, described to quenching of $Hg(^3P_1)$, as observed by Polanyi et al [POL 1967] must be a result of CO quenching of the metastable 6^3P_0. Polanyi et al measured the infrared emission from specific vibrational states in order to determine how the energy is partitioned between vibration and kinetic energy of relative motion and to try to infer the mechanism of the energy transfer process. It appeared that for CO less than half of the amount of electronic energy involved is converted into vibrational energy.

A qualitative explanation of Polanyi's results was given by arguing that the excited Hg-CO potential energy curve must have a minimum which favours the formation of a relatively long lived collision complex. Moreover, the excited state potential energy curve should cross the ground state curve in a region which is

accessible at thermal energies. The electronic transition is assumed to occur as a sudden process at the crossing point so that nearly all the energy released is present as repulsion between Hg and the nearest atom in CO. The CO molecule then separates from the Hg atom due to this repulsion. The rotational and vibrational excitation of CO occurs during the separation. Within this model the experimental distribution of vibrational states after quenching could be explained theoretically [LEV 1972].

These are just some of the experiments on quenching which have been performed and include some of the more recent experiments. Earlier work is thoroughly reviewed by Massey et al [MAS 1971].

The other type of experiment, sensitized fluorescence is demonstrated with a classic example, the fluorescence of a mixture of mercury and thallium vapour irradiated with light from a mercury lamp. This process was first reported in 1922 [CAR 1922] and the direct proportionality of the thallium line intensity to thallium pressure and to the illumination intensity, and of decrease in mercury fluorescence with thallium pressure indicate clearly that the thallium atoms gain their excitation by collision with optically excited mercury.

One of the first detailed studies of the relative effectiveness of energy transfer from a given atom to different states of a second atom was carried out by Beutler and Josephy [BEU 1929] who studied the mercury sensitized fluorescence of the diffuse series of sodium. Their results seemed to show that the probability of transfer is greatest when the energy defect ΔE is least since the most favourable

process is:

$$Hg\ (6^3P_1) + Na\ (3^2S_{\frac{1}{2}}) \rightarrow Hg\ (6^1S_0) + Na\ (9^2S_{\frac{1}{2}})$$

where $\Delta E = +\ 0.19eV$. This "resonance" effect was the subject of great argument for sometime and Kraulinya [KRA 1970] found that this resonant behaviour was not present in the collisions HgTℓ, HgIn, HgCd and Hg Na and explained her results not in terms of collisions of the second kind but by long lived intermediate states. In view of Kraulinya's results Czajkowski et al [CZA 1973] have recently re-investigated the HgNa system at low Hg pressures. They found cross sections ranging over three orders of magnitude ($10^{-1} \rightarrow 10^2$ Å^2), showing a clear resonance dependence on the electronic energy difference ΔE and appear to have provided conclusive evidence in favour of such a resonance effect.

It should be noted that, until quite recently, there was essentially no theory of electronic energy transfer. At best a little could be said about general rules that sometimes apply and a modest amount about what kind of theories one could postulate, the implications of each and how one might go about setting up the problem. Most of the recent theories are still restricted to moderately specific and very limited classes of systems, eg. the transitions between the fine structure components of the ^2P terms of excited alkali atoms in alkali-inert gas collisions [NIK 1965] . In cases where larger amounts of energy are transferred the theories remain relatively primitive. Therefore the discussion which follows does not contain a formal treatment of inelastic scattering for energy transfer processes. It presents a very brief outline of the formalism and then proceeds to a discussion of a number of approximations and

theories used by a variety of authors in tackling their specific problem. A working knowledge for the theorist can be obtained [LEV 1969], [MOT 1965] and an outline of inelastic scattering is covered by Fluendy et al [FLU 1973].

There follows a simple example to illustrate the problems of theoretical investigation of electronic energy transfer. When two atoms A and B collide then the wave equation is as follows:

$$\left[\frac{\hbar^2}{2\mu}\nabla^2 - Ha(ra) - Hb(rb) - V(r,ra,rb) + E\right]\psi = 0 \qquad 2\text{-}1$$

where μ is the reduced mass of the system, ra and rb are the co-ordinates of the atomic electrons and V(r,ra,rb) is the interaction energy of the two atomic systems.

In order to calculate the probabilities of excitation, ionization or charge transfer on impact, a solution of equation [2-1] must be obtained which has the asymptotic form for large r

$$\psi = e^{ikr\cos\Theta}\,\psi_o(ra,rb) + \sum_{n=0}^{\infty} f_n(\Theta,\phi)\,\frac{e^{iknr}}{r}\,\psi_n(ra,rb) \qquad 2\text{-}2$$

where $k^2 = \frac{2\mu}{\hbar^2}\left[E - E_o\right]$

and $k_n^2 = \frac{2\mu}{\hbar^2}\left[E - E_n\right]$

Thus $\frac{kn}{2\pi}$ is the wave number of the relative motion after excitation of the nth state. The cross section for excitation of the nth state of the system by the impact is given by

$$Q_n = \int_o^{\pi}\int_o^{2\pi} \frac{kn}{k}\,|f_n(\Theta,\phi)|^2 \sin\Theta\, d\Theta d\phi \qquad 2\text{-}3$$

The usual method of calculating f_n approximately is to expand ψ in a series of the form

$$\psi = \sum_n F_n(r)\ \psi_n\ (ra,rb) \qquad 2\text{-}4$$

which on substitution in equation [2-1] gives

$$\sum_n \left[\frac{\hbar}{2\mu}\nabla^2 - V(r,ra,rb) + E - E_n\right] F_n(r)\ \psi_n(ra,rb) = 0 \qquad 2\text{-}5$$

Multiplying by $\psi_n^*(ra,rb)$ and integrating over the co-ordinate space of the electrons we obtain by virtue of the orthogonal properties of the atomic wave functions

$$\left[\frac{\hbar^2}{2\mu}\nabla^2 + k_n^2\right] F_n = \sum_m U_{mn}F_m \qquad 2\text{-}6$$

where $U_{mn} = \frac{2\mu}{\hbar^2}\iint V(r,ra,rb)\ \psi_n^*(ra,rb)\ \psi_m(ra,rb)\ d\tau_a d\tau_b$

The relations arrived at in 2-6 are hardly directly useful as they stand since not only is there an infinite number of them but most computational schemes would be carried out in terms of a partial wave expansion, multiplying, especially in the case of heavy particles, the number of equations still further. Almost inevitably it is necessary to close the set of coupled equations by selecting only a few channels for calculation. As an example, only two states o and n need to be considered when they are in close resonance but all other states are in poor resonance. The problem is then reduced to that of solving the coupled equations

$$\begin{aligned}\left[\nabla^2 + k^2 - U_{oo}\right] F_o &= U_{no}F_n \\ \left[\nabla^2 + k_n^2 - U_{nn}\right] F_n &= U_{on}F_o\end{aligned} \qquad 2\text{-}7$$

Having illustrated the problem in this analysis it is useful to discuss some of the theories and approximations used in a theoretical

description of the excitation transfer problem.

There are two general rules that have often been applied to interpret the process of electronic energy transfer. The rules are the Wigner spin selection rule which states that the total spin of the system is conserved throughout the inelastic collision and the energy resonance rule which is that excitation transfer is most efficient when the relative kinetic energy of the colliding species is most nearly conserved. However, it seems that neither of these rules can be treated as a general law. For example, the transfer of excitation from Ar* to N_2 was shown to conform nicely with the Wigner rule [FIS 1967] but the simple He* + He processes clearly violate this rule. In the other case, the transfer of excitation from Hg* has been shown in some systems to conform with the energy resonance rule whereas in other cases it does not.

The possible sorts of microscopic theories of electronic energy transfer can be put into three classes depending on how the interaction responsible for the transfer is described. These are:

1) Theories based on interactions describable in terms of radiation-like interactions, including true radiative transfer processes and interactions that can be written as multipole-multipole interactions.

2) Theories requiring explicit description of the states of the donor A* or of the acceptor B during the course of the collision but in which A and B essentially retain their identity.

3) Theories in which A and B become so strongly coupled that a description of the transfer process requires explicit consideration of the compound system.

At this stage in a general discussion it is useful to present the formal expressions of inelastic scattering since they provide a convenient store for all the information from which certain points can be selected.

The problem can be formulated so that the cross section into any final state is proprotional to the absolute square of the transition matrix element, ie $\langle\beta|T|\alpha)^2$ where β represents the final state of interest for the isolated system and $|\alpha\rangle$ represents the system as it is initially prepared, then $\langle\beta|T|\alpha\rangle$ is the projection of $\langle\beta|\psi\alpha^+)$ of the final state on the fully time developed system $|\psi_a + \rangle$ which began as α and experienced the collision [THO 1961]. The formal relationship between the T operator and the Hamiltonian of the full system, H, and the interaction potential U, the part of H that keeps states $|\alpha\rangle$ and $|\beta\rangle$ from being stationary throughout the collision can be written as

$$T = U + \lim_{\Sigma \to o} U\left[E - H + i\Sigma\right]^{-1} U \qquad 2\text{-}8$$

where E is the energy of the system and Σ serves as a convergence parameter.

The first decision in the solution of $\langle\beta|T|\alpha\rangle$ is a determination of how much of the system can be described classically and how much of it has to be stated in quantum mechanical terms. An impact parameter formulation is used in the classical case and a partial wave expansion in the quantum case. The impact parameter method

requires evaluation of the T matrices of many collision, each with its specified impact parameter and an average taken over all these impact parameters. The impact parameter method has been described by Callaway and Bauer [CAL 1965] in which changes in speed or in direction of particles during the collision are ignored. The partial wave method requires a knowledge of all the wave functions of the system and the total transition probability is given from the sum over all final angular momentum and the average over all initial states. For light particles, eg electrons and hydrogen and helium atoms, the partial wave method is suitable since a full partial wave calculation can be carried out. This method was used by Buckingham and Dalgarno [BUC 1952] to describe resonant energy transfer for He* + He.

The second decision is on what representation to use for the internal parts of the states $|\alpha\rangle$ and $|\beta\rangle$. The compound system may be described in terms of a simple product of functions for free A* and B in the incoming channel and for free A and B* in the outgoing channel, this is the simplest approximation and would be the most reasonable first approach for a weak interaction type of theory. This is the type of theory used by Callaway and Bauer [CAL 1965] for treating alkali $^2P_{\frac{1}{2}} \rightarrow {}^2P_{\frac{1}{2}}$ transitions due to collisions of excited alkali atoms with inert gas atoms. However, this method is unlikely to be successful for collisions involving large energy or momentum transfer and is certainly inapplicable to rearrangement collisions. A more sophisticated approximation would take account of one colliding partner acting on the other at the lowest level of perturbation theory, eg allowing for splitting of states that are

degenerate or allowing the wave function of B to be perturbed by the incoming A*. Nikitin has treated the theory of spin orbit relaxation at this level [NIK 1965]. Finally there is the perturbed stationary state or adiabatic strong coupling approximation. This is appropriate for collisions in which the AB complex behaves almost adiabatically so that few molecular states are excited or required in the calculation. This calculation is made using the stationary state wave functions for the full (AB)* complex system but with the nuclear kinetic energy omitted. The most commonly used criterion for the application of this method is that $\frac{\Delta E}{\hbar v} .a >> 1$, where ΔE and 'a' are respectively the energy difference between the two states and the range over which the transition occurs. Collisions with small impact parameters which are usually the most important in producing inelastic effects unfortunately involve large values of the radial velocity so that the approximation becomes least satisfactory in the important region.

The third type of judgement in constructing a theory of electronic energy transfer is a decision about what force is responsible for the interaction. For long range interactions U is presumably a multipole interaction operator, eg dipole-dipole or quadrupole induced dipole. This is the longest range and most weakly coupled form in which the pertubations of A and B on each other can be expressed. It requires that the charge distributions of A and B are essentially non-penetrating. In a theory of type 2 or type 3 the details of the interaction between A and B will need to be more specific.

Two types of operators may play the dominant role in the coupling mechanisms, the electrostatic potential terms or the nuclear kinetic energy. The former is sometimes sufficient especially if A and B are identical. In this case, the adiabatic Hamiltonian, and particularly the electron-electron terms $\frac{e^2}{r_{ij}}$ may be large enough that

$$H \text{ adiabatic} = U$$

One then only needs the matrix elements

$A_1^* A_2 \,|H \text{ adiabatic}|\, A_1 A_2^*$ to get a first approximation to the exchange probability [BUC 1952].

In Nikitin's description of the rare gas excited alkali collisions [NIK 1965] the adiabatic electrostatic terms are collected into two parts. The first expresses the long range behaviour of the interaction, and is the principal operator of Callaway and Bauer [CAL 1965]. The other part is the exchange interaction which has an exponential dependence on the distance between the atoms and can be represented as $A \exp[-\alpha R]$.

If one assumes that the unsymmetrical collision problem can be solved to arbitrary accuracy in the adiabatic or Born Oppenheimer approximation then one must use the nuclear kinetic energy operator to develop the coupling.

The kinetic energy of relative motion of A and B $(\frac{-\hbar^2}{2\mu})\nabla_R^2$ can be separated into angular and radial parts. The perturbations due to the radial part are apparently the most important ones for processes like pre-dissociation and autoionization. The angular momentum parts play a role in two ways. Firstly, there are direct couplings between electronic and nuclear angular momentum in which

rotational energy is transferred and the total angular momentum of the nuclei changes. In the second type of coupling the nuclear angular momentum is constant but its direction changes in a way that produces a re-orientation of the electronic angular momentum and thereby a change of electronic state and sometimes of transfer of electronic energy from one molecule to another [BAT 1962].

Despite all this complexity simpler qualitative microscopic models have been in existence for a long time, eg [KAL 1929]. These models all posed the question of how a system crossed from one potential curve to another with emphasis on the relation between the cross section and the distance at which the crossing or avoided crossing occurred. The essential explanation of fluorescence quenching by molecules, in these models, has been this. The molecule B and the excited metal atom A* approach on a curve lying between the ionic $A^{\pm}B^{-}$ curve and the ground state curve A-B. The ionic curve cuts the A*-B system, the system makes a transition to the attractive curve and accelerates towards collapse. Then the coulomb curve crosses the ground state A-B curve and either the entire system flies apart as in $Hg^* + H_2 \rightarrow Hg + 2H$ or a reaction occurs to dissociate the original molecule as in $Na^* + H_2 \rightarrow NaH + H$. In either case the system cannot find its way back to the curve giving A* + B and a quenching reaction occurs.

So far only excitation transfer processes have been considered but as mentioned previously there are a number of ionization processes which can occur in the collisional interaction of excited species with ground state atoms or molecules. These are

(c) $A^* + B \rightarrow AB^+ + e$ Associative ionization

(d) $A^* + B \rightarrow A + B^+ + e$ Penning ionization

(e) $A^* + B \rightarrow A^+ + B + e$ Collisional ionization

For associative ionization to occur in a thermal energy collision the energy required to ionize A* must be less than the dissociation energy of AB^+ into $A^+ + B$. Hornbeck et al [HOR 1951] studied the appearance potentials of He_2^+, Ne_2^+ and Ar_2^+ relative to those for He^+, Ne^+ and Ar^+ and demonstrated clearly that the diatomic molecular ion is generated by collision of an atom in its ground state with an atom in an excited state and not with an ion.

Penning ionization has also been recognised for many years since it was first reported by Kruithoff and Penning [KRU 1937] and along with associative ionization is one of the most important mechanisms for ion production in flames and other chemical systems.

In associative and Penning ionization processes there are three kinds of excited state of the initial excited reactant which may be involved. One type is the normal optically allowed short lived state like the 2^1P state of helium. Another is the relatively low lying metastable state like the 2^3S or 2^1S state of helium and finally there are relatively long lived highly excited states which are probably high Rydberg states which owe their long lifetimes to the small oscillator strength of the highly spread out states.

Information on specific state dependences was supplied by Muschlitz et al [HER 1968]. Their He* source was designed specifically to eliminate all low lying optically allowed states and also highly excited long lived states. The differences

between 2^1S and 2^3S He* were not found to be grossly different which suggests that the spin of the excited electron does not affect the ease with which it can gain enough energy to ionize.

In contrast to the various low lying states whose behaviour is relatively similar, the high lying states seem to differ considerably from the low lying metastables. Firstly highly excited states are capable of collisional ionization although

$$A^{**} + B \rightarrow A^+ + B + e$$

was only observed when B was at least triatomic suggesting that the energy for thermal collisional ionization comes from vibrational energy in B [HOT 1967]. Hotop et al [HOT 1967] also found that the reaction

$$Ar^{**} + H_2 \rightarrow ArH^+ + H$$

is the most favourable process with a cross section an order of magnitude greater than for Penning ionization and associative ionization is unobservable for this system. By contrast, Penning ionization of H_2 by He* is the most probable process almost a factor of 10 more probable than rearrangement ionization. Again associative ionization is less important than the other mechanisms but with He* or Ne* on H_2 it is an observable process.

Energy analysis of the electrons from Penning ionization can be used as a spectroscopic probe to locate states of the B^+ ion in the process $A^* + B \rightarrow A + B^+ + e$ if metastables of known energy are used or to locate metastable states of A* if known detector molecules B are used. Cermak has used this approach to study the states of molecule-ions and to determine various ionization potentials for the formation of these ions [CER 1966]. In many

cases the ionization potentials gave good agreement with values from photoelectron spectroscopy. The intensities and peak shapes indicate that Penning ionization is a Franck-Condon process in the sense that the distribution of vibrational states of the B^+ ion corresponds to the vertical excitation from the initial vibrational distribution of B.

The theory of such processes can be tackled by potential curve arguments.

It may generally be assumed that in a collision of A* with B the ground state of the ion AB^+ is attractive and exhibits a minimum. The next problem is to construct a potential curve or curves of the excited A* - B or (AB)* interaction.

1) (AB)* could correspond to an electron outside AB^+ in its ground state. In this case AB* lies below AB^+ and is attractive.

2) (AB)* could correspond to an electron bound to an excited AB^+ and also has an attractive well.

3) (AB)* could correspond to an electron bound to AB^+ in a repulsive state.

Heteronuclear diatomics have been studied by various workers, eg [CER 1966] [HOT 1968]. The rare gas-metal atom systems studied by Cermak have potentials corresponding to an electron bound to an excited AB^+ because the lowest excited states of the rare gases are well above the ionization potentials for the alkalis or mercury. Therefore the electrons released in Penning or associative ionization could carry away a large amount of energy or, in principle, could

leave the ionized system highly excited. The former is observed and in the reaction Hg + He (2^3S) → Hg^+ + He + e the electron carries away all the exoergicity which suggests that the potential curves for the initial and final states are essentially parallel. Electron energy deficiencies were observed for Hg + He (2^1S) and this was interpreted as implying that at the range of internuclear separations, where a transition occurs, points on the potential diagram [Fig 2-2] representing the initial state lie lower, relative to the asymptote of the initial state, than do the corresponding points of the final ionized state, relative to their own asymptote. Thus a downward vertical transition from (Hg He*) to $(Hg\ He)^+$ + e gives the electron less than the total exoergicity of the reaction leaving some as kinetic energy of relative nuclear motion.

As a final analysis in terms of potential curves an analysis of the relationship between Penning and associative ionization is considered.

In the case of He* - Ar the electron must carry away a large amount of energy and one must determine the relationship between the initial kinetic energy and the fraction of the energy carried away by the electron. Herman et al [HER 1966] considered a similar situation in terms of whether or not the A* - B system made its downward transition to a point to the left of the point Ro, the classical turning point for a pair of free particles A + B^+ with zero kinetic energy. Figure [2-3] shows a situation for which associative and Penning ionization differ only in so far as the Franck-Condon

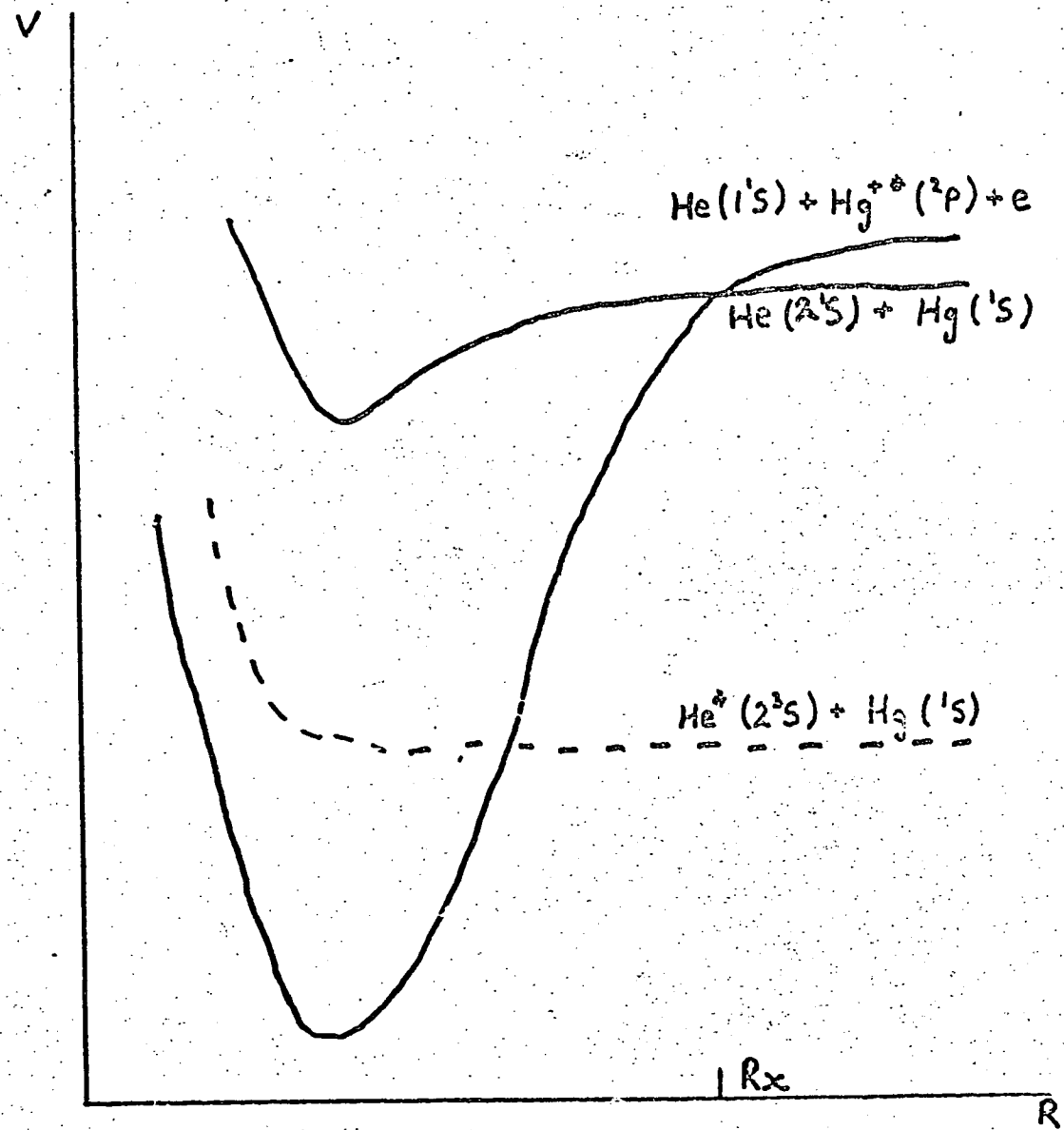

Potential curves for He* + Hg

Figure 2-2

transition from the upper curves turning point reaches above or below the dissociation limit of AB^+. The requirement for such a situation is that Ro for AB^+ falls to the left of Ro for A* - B so that both free and bound states of AB^+ are accessible via vertical transitions from the turning points of the potential for free A* + B. The ratio of AB^+ to B^+ is thus determined by the fraction of colliding pairs with relative kinetic energy above E_T. In non central collisions the principal effect of rotation is to raise more of the AB^+ curve above the dissociation limit and this moves Ro (AB^+) to the right. This in turn lowers E_T and therefore produces more Penning ionization and less associative ionization than one would infer from head on collisions only. It should also be noted that if Ro (A*B) is less than Ro (AB^+) then associative ionization is very improbable.

Miller [MIL 1970 (a)] has presented a thorough analysis of the theory of Penning and associative ionization in a classical, semi-classical and quantum mechanical framework and formulae for the total cross sections for the ionization processes, the angular distributions for ions and the distributions of ionized electrons are developed.

A brief resumé of the main points of Miller's work [MIL 1970(a) MIL 1970(b), MIL 1972] is presented here.

Figure [2.4] depicts the Born Oppenheimer potential Vo(R) for the AB system which dissociates to the states A* and B. V+(R) is the potential of the (AB^+) system which dissociates to the ground electronic species A and B^+. If the excitation energy of

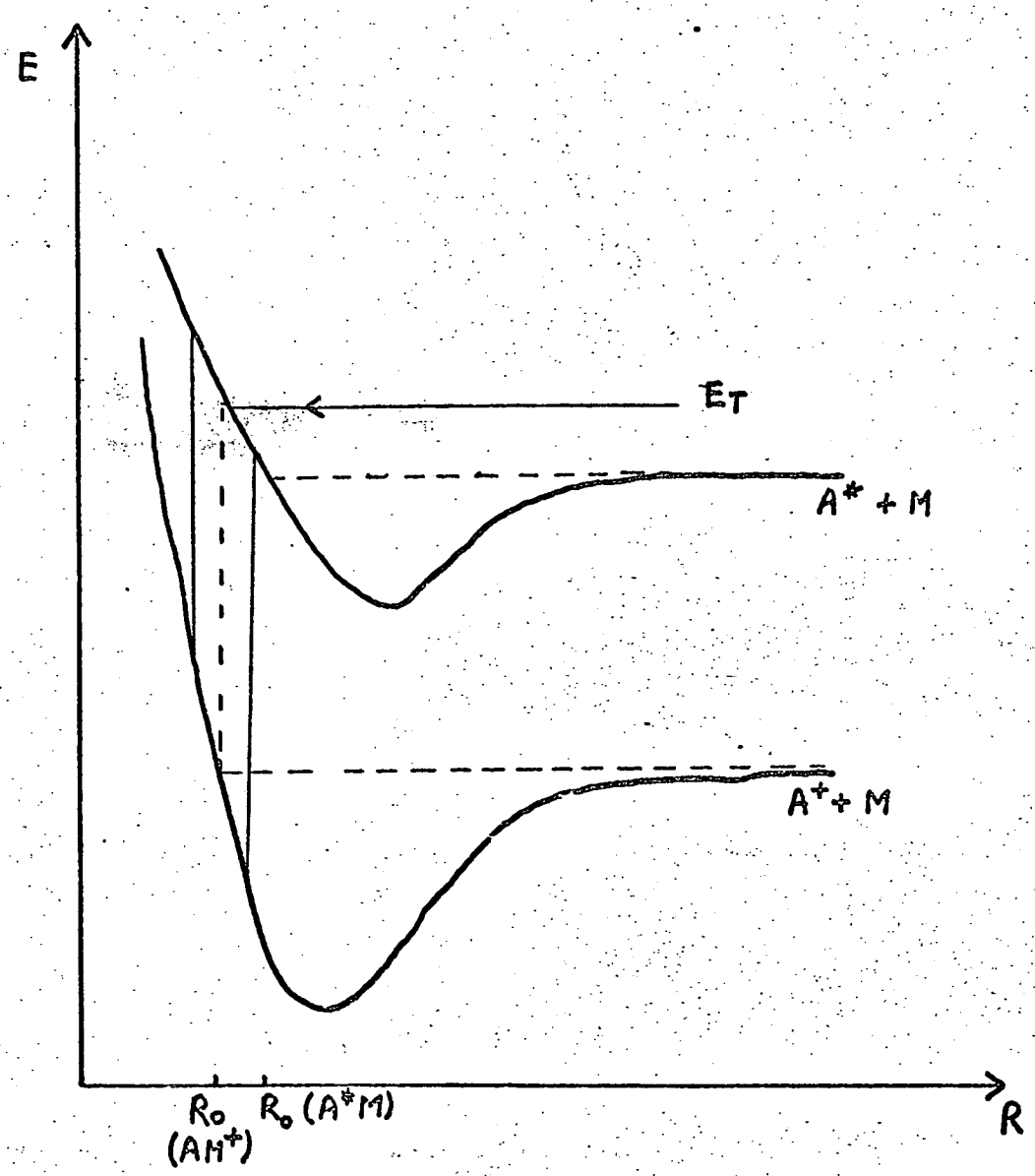

Model for associative ionization and Penning ionization when $E(A^* + M) > E(A + M^+ + e)$

Figure 2-3

A to A* is greater than the ionization potential of B, as indicated, then the $(AB)^+$ curve is the lower boundary for a continuum of potential curves of the system $(AB)^+ + e^-$, to a good approximation this continuum of potentials is $V_+(R) + \Sigma$ where Σ is the continuously variable energy of the ionized electron. For any fixed internuclear distance therefore the electronic state corresponding to the A* - B curve is embedded in a continuum of states of the $(AB)^+ + e$ type. Consequently for each internuclear distance R there is a width $\Gamma(R)$ (units of energy) associated with $V_o(R)$ for decay of the discrete electronic state into the continuum electronic state degenerate with it. At infinite separation the width vanishes, i.e. $\Gamma(R) \to 0$ as $R \to \infty$ since the coupling between discrete and continuum electronic states vanishes. The potentials $V_o(R)$, $V_+(R)$ and the width $\Gamma(R)$ are obtainable by fairly standard but not trivial electronic structure calculations.

In the complete quantum mechanical analysis of the Penning situation the appropriate matrix elements are

$$S_{\Sigma o}^{\ell} = -2i \left(\frac{2\mu}{\hbar^2}\right) \exp\left(i\eta_{\ell,o} + i\eta_{\ell\Sigma}\right) \langle \mu_{\ell o}(R) \, | V_{o,\Sigma} | \mu_{\ell\Sigma}(R) \qquad 2\text{-}9$$

where $\mu_{\ell\Sigma}(R)$ is the radial wave function of the potential $V_+(R)$ and $\mu_{\ell o}(R)$ is the radial wave function of the potential $V_o(R) - \frac{1}{2}i\Gamma(R)$. The function $V_{o,\Sigma}$ is the coupling between the two electronic states at internuclear distance R

$$V_{o,\Sigma}(R) = \int dr \chi_o(r;R) \left[H-E\right] \chi_\Sigma(r;R) \qquad 2\text{-}10$$

where r denotes all electronic co-ordinates, $\chi_o(r;R)$ is the discrete electronic state which dissociates to A* + B and $\chi_\Sigma(r;R)$ is the continuum electronic state which dissociates to $A + B^+ + e^-(\Sigma)$. The width is given by

$$\Gamma(R) = 2\pi \, |V_{o\Sigma}(R)|^2 \qquad 2\text{-}11$$

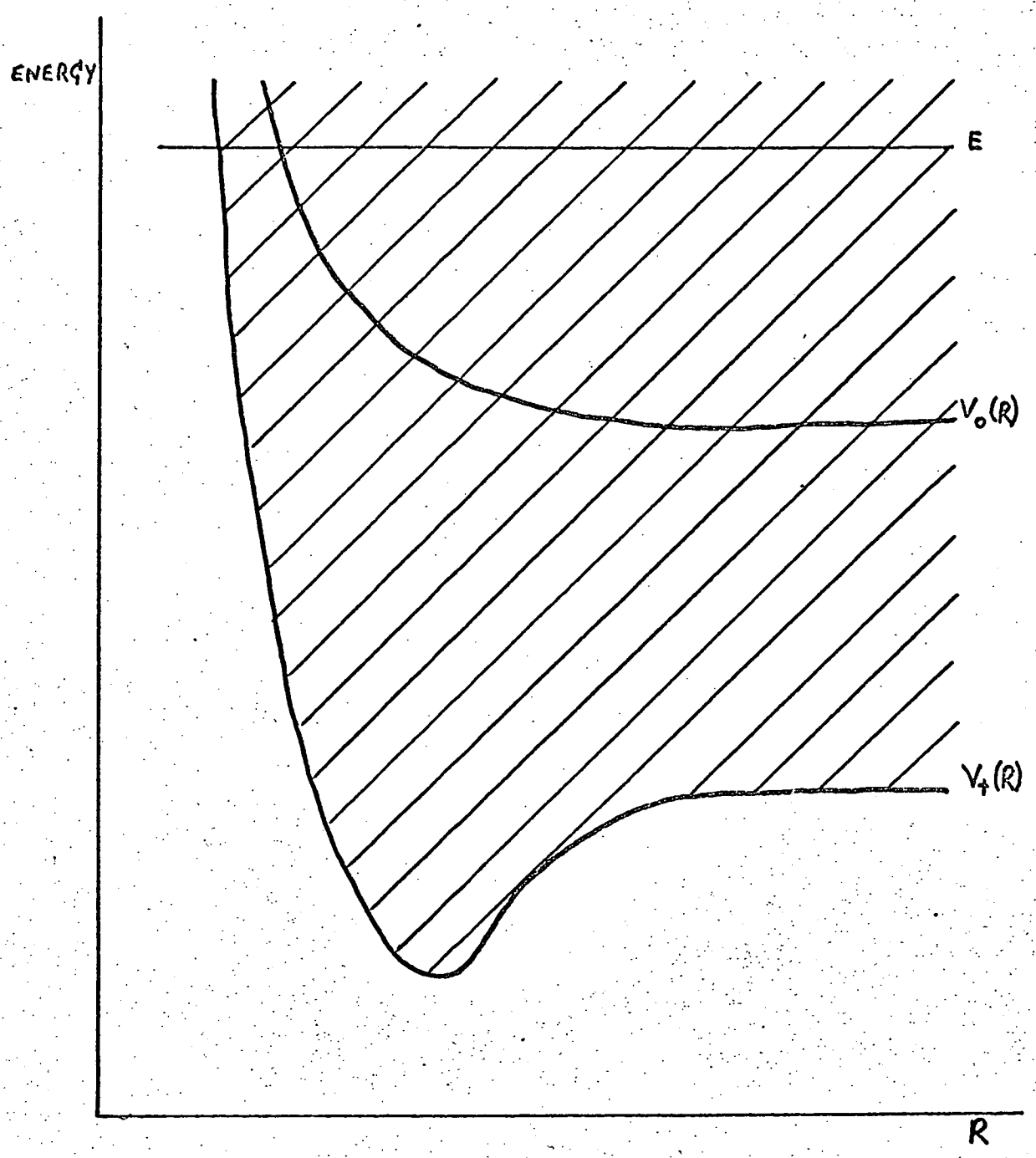

$V_o(R)$ represents the A* - B potential
$V_+(R)$ represents the A - B^+ potential.
The shaded area indicates a continuum of potential curves which dissociate to the states A, B^+ + e.

Figure 2-4

Similar expressions can be derived for the associative ionization. Miller points out that many of the salient features of Penning ionization and associative ionization are apparent by casual inspection of $V_o(R), V_+(R)$ and the width $\Gamma(R)$.

Miller et al [MIL 1970(b)] have carried out a simplified theoretical treatment of Penning ionization of the hydrogen atom by helium metastables. In this calculation they used a configuration interaction technique using the same basis set for the description of the N electron A* - B state and for the (N -1) electron ($A - B^+$) state. The basis set was chosen to provide an accurate description of the helium 1S and 2S atomic orbitals and the hydrogen 1S atomic orbital. Molecular calculations were then carried out and the ground state potential for He H^+ and excited states of HeH were produced.

Although the ratio of Penning ionization to associative ionization cross sections cannot be rigorously evaluated without a knowledge of the width $\Gamma(R)$ one can employ a simple model, which does not include this width, at low collision energies. The model is applicable only at energies sufficiently low for classical orbiting to occur in the A* - B potential. In Miller's calculation the resulting expression for the total ionization cross section is given by

$$\sigma TOT(E) = \pi R^2 \left[1 - V_o(R)/E\right] \qquad 2\text{-}12$$

where $R \equiv R(E)$ is the larger root of the equation

$$E = V_o(R) + \tfrac{1}{2} R V_o{}^1(R) \qquad 2\text{-}13$$

where $V_o(R)$ is the A* - B potential and E is the collision energy.

The associative ionization cross section

$$\sigma AI(E) = \pi R^2 \left[1 - V_o(R)/E\right] \qquad 2\text{-}14$$

but where $R \equiv R(E)$ is the root of

$$E = V_o(R) + \tfrac{1}{2} R V_+^1 (R) \qquad 2\text{-}15$$

where $V_+(R)$ is the $A - B^+$ potential .

A recent calculation [MIL 1972] presents the use of the auto-ionization width $\Gamma(R)$ as a function of internuclear distance which allows rigorous evaluation of the total ionization cross sections and relative amounts of He H^+ and He + H^+ obtained together with the energy and angular distribution of the heavy particles.

In this paper they use the relationship

$$\Gamma(R) = 2\pi\rho \; |< \chi \mid H - E \mid \psi >|^2 \qquad 2\text{-}16$$

where ψ is the initial discrete electronic state, χ is the final electronic continuum state which is energetically degenerate with ψ, H is the electronic Hamiltonian, E is the electronic energy of the discrete state and ρ is the density of final continuum states. Equation [2-16] can be solved to find $\Gamma(R)$. Using classical and semi-classical techniques the total ionization cross section is given by

$$\sigma = \int_o^\infty dR \; 4\pi R^2 \left(\frac{\Gamma(R)}{h v_o}\right) \left[1 - V_o(R)/E\right]^{\frac{1}{2}} \qquad 2\text{-}17$$

where v_o is the radial velocity.

Expressions were also derived for the associative ionization cross section together with the energy and angular distribution of the ionized electrons and the angular distributions of the heavy particles. Total ionization cross sections were found to be 30→40 $Å^2$ [Fig 2-5]. Associative ionization is found to be 22% of

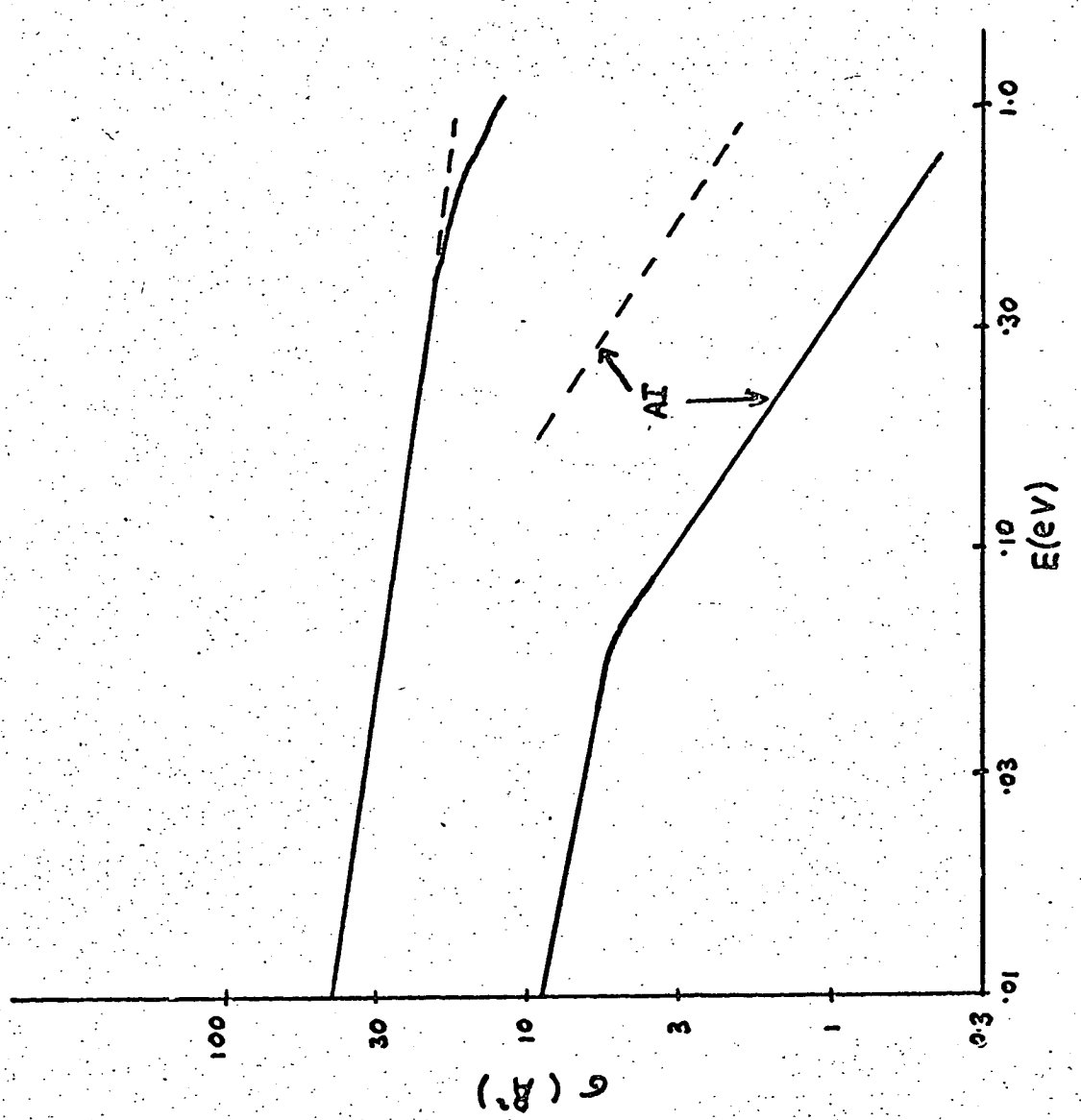

The total ionization cross section for $He^* + H \rightarrow He + H^+ + e$, $HeH^+ + e$ as a function of collision energy E; AI indicates the cross section for HeH^+. The dashed lines are the results of the orbiting model.

Figure 2-5

the total ionization cross section in the limit of zero collision energy. This fraction decreases with increasing energy being about 18% at the collision energy corresponding to 300°K. A comparison of these results with those obtained by the orbiting model shows that the model is adequate in predicting the total ionization cross sections but is less accurate for more detailed collision properties.

Miller's work seems to offer an accurate theoretical analysis of the physical situation and therefore the situation appears to be more clearly resolved than in excitation transfer processes.

Molecular Beam Scattering Experiments

The metastable states of helium have received most attention experimentally because (a) helium is an important constituent of the universe (b) the radiative lifetime of these states is long enough for them to be studied under a variety of experimental conditions (c) they are sufficiently energetic (19 → 20ev) to ionize any collision partner (d) helium is sufficiently simple electronically to allow theoretical treatments from first principles.

Studies of excited electronic species by molecular beam techniques prior to 1966 are well reviewed by Muschlitz [MUS 1966]. Rothe et al [ROT 1965] observed the velocity dependence of the total cross section of He (2^3S_1) colliding with Ar and Kr. They interpreted their results in terms of a L-J (12:6) potential. Grosser et al [GRO 1968] performed the first differential cross section measurement for a metastable atom in which they investigated the systems He* - He and He* - Ar and determined limits on the values

of Σ and Rm for a L-J (12:6) potential. Unfortunately they were unable to make an independent determination of Σ and Rm.

Since that time the rare gas metastables have been studied in detail from the point of view of inelastic processes by Muschlitz et al [PEN 1968], [KRA 1972], [TAN 1972] and by Hotop and Niehaus [HOT 1968], [HOT 1969(a)],[HOT 1969(b)], [HOT 1970]. In the first mentioned of the experiments by Muschlitz et al the relative cross section for ionization of H_2, HD and D_2, using thermal energy beams of 2^3S and 2^1S helium atoms, were measured. They found that the cross section for production of H_2^+, HD^+ and D_2^+ increased in that order. The isotope effect is explained in terms of the initial formation of a pre-ionization state that may either dissociate or ionize. In the second experiment a thermal energy beam of metastable He 2^1S, 2^3S or Ne ($^3P_2$,o) produced by electron impact enters a collision chamber into which a known pressure of gas B has been introduced. Penning and associative ions are formed and extracted by a small electric field, mass analysed and counted. Ratios of the cross section for associative to total ionization cross sections have been measured. By determining the ratio as a function of the collision chamber pressure and by measuring the relative intensity of the secondary product ion B_2^+ the cross sections for

$$AB^+ + B \rightarrow A + B^+ + B \qquad (1)$$

$$AB^+ + B \rightarrow A + B_2^+ \qquad (2)$$

have been determined. The effect of a change in the ratio of 2^1S to 2^3S helium in the metastable beam has also been investigated by changing the exciting beam energy. In collisions of He* with both argon and krypton the ratio of associative to total cross section is greater for 2^3S than for 2^1S. The large size of the

cross sections for process (1) which range from 210 $Å^2$ for $NeAr^+$ - Ar to 470 $Å^2$ for $HeKr^+$ - Kr suggests that the associative ions are formed very close to their dissociation limit. The final experiment in this group mentioned, concerns an investigation of the velocity dependence in the thermal energy range of total ionization cross sections of Ar, Kr and Xe in their ground states on impact of a velocity selected beam of metastable neon atoms in the $^3P_2$ (16.6eV) and $^3P_0$ (16.7eV) states. The composition of the beam was measured using an inhomogeneous field deflecting magnet. The ionization measurements were of sufficient precision to allow simultaneous determination of both secondary electron ejection efficiency and the cross section. Analysis of the results indicates that the interaction leading to ionization is short ranged.

No survey of recent excited metastable atom collisions would be complete without a mention of the work performed by Hotop and Niehaus. In their first study [HOT 1968] they report on ionizing collisions of long lived excited species with atoms and molecules using a crossed molecular beam technique. Relative cross sections for the production of ions are presented. This work was followed [HOT 1969(a)] by an analysis of the Penning electrons produced in thermal collisons of He (2^1S) and He (2^3S) with Ar, Kr, Xe and Hg. Their third contribution [HOT 1969(b)] is a measurement of the relative cross sections for Penning and associative ionization by the helium metastables and in the fourth report intermolecular potentials are determined for the Penning electron distributions. These distributions, arising from the ionization of Na and K by helium metastables, as well as the absolute cross section for

P e n n ing ionization of Na by He (2^3S) and relative cross sections for ionization of Na and K by He (2^1S) and He (2^3S) were measured. The cross section was found to be of the order of 15 $Å^2$ for Penning ionization of Na and the ratio of cross sections for He (2^1S) to He (2^3S) were found to be 1.20 ± 0.10 in the case of Na and 1.14 ± .10 for K.

The results from the work of these two groups, which overlap, are similar.

TABLE 2.1

Ratios R, of AI to the sum of AI and PI

SYSTEM	R	T (^oK)*	REFERENCE
He* - Ar	0.252	90	HOTOP et al
	0.161	320	HOTOP et al
	0.145 ± 0.005	330	MUSCHLITZ et al
He* - Kr	0.273	90	HOTOP et al
	0.125	320	HOTOP et al
	0.114 ± 0.004	330	MUSCHLITZ et al
Ne* - Ar	0.343 ± 0.005	330	MUSCHLITZ et al
Ne* - Kr	0.319 ± 0.005	330	MUSCHLITZ et al

*Temperatures listed are those of the metastable beam.

The results of Table 2.1 show, as predicted, that the ratio of associative to total ionization decreases with increasing temperature. Other metastable species which have received considerable attention in molecular beam experiments are the metastable levels of mercury (6^3P_2,0). Van Itallie et al [VAN 1972] have reported the relative intramultiplet quenching cross sections for the transitions $Hg(6^3P_2) \rightarrow Hg(6^3P_1)$ for a variety of collision partners. In this experiment crossed molecular beams were used and the phosphorescence

of $Hg(6^3P_1)$ from the interaction region was monitored. They also showed that the energy resonance with vibrational states in the other collision partner does not appear to be a major factor in determining the magnitude of the intramultiplet cross sections for the process. Their results for collisions with the rare gases He and Xe exhibit very small cross sections compared to N_2, CO and NO etc which indicates that internal degrees of freedom are required for significant cross sections when the quencher lacks excited states below $Hg(6^3P_2)$.

The mercury metastables have also been studied by Krause et al [KRA 1973] . In this experiment the de-excitation of metastable mercury atoms have been studied by a modulated cross beam method using H_2, D_2, N_2, NO and CH_4. The molecular beam was velocity selected and the photon emission at 2537 Å was studied versus the molecular speed. In this work quenching experiments were performed and signals at wavelengths other than 2537 Å were sought in an effort to indirectly detect the presence of mercury photon emission from higher states. Light emission corresponding to four strongly allowed transitions that terminate on 6^3P was not detected at excitation voltages between 5eV and 16eV. ($^3D_3{}^o$ metastables might be readily quenched to any number of well known short lived Hg states such as 6^3D_2 (8.85eV) or 7^3S_1 (7.73eV). These short lived Hg states radiate to 6^3P_2 at 3656 Å and 5461 Å respectively. They also cascade to 6^3P_1 at 3127 Å and 4358 Å). The relative cross sections obtained are similar to those of VAN ITALLIE et al [VAN 1972] since there is only weak energy dependence of the quenching cross section and therefore velocity selected and velocity averaged cross sections for the two experiments

should be in good agreement. The results are in good agreement with a model [BYK 1964] which assumes that quenching occurs when the potential energy surfaces that describe the interaction of $Hg(6^3P_2)$ + M and the interaction $Hg(6^3P_1)$ + M* intersect. The quenching efficiency then depends on the energy separation of the initial and final states of the quasimolecule.

Relative Penning and associative ionization cross sections were determined for collisions of $Hg(6^3P_2,o)$ with the alkali metals [MAR 1972]. The relative cross sections were obtained by following the changing alkali cross beam flux with a hot wire detector and the ion production using a quadrupole mass filter. The associative/Penning ionization cross sections for sodium and potassium were 0.28 and 0.028 respectively. No associative ionization was observed for rubidium and cesium. A study of the reaction observed by Josephy and Beutler [BEU 1929] for $Hg(6^3P_1)$ was carried out for $Hg(6^3P_2,o) + M \rightarrow Hg(^1S_o) + M^*$ by Martin [MAR 1972]. No Na* fluorescence was observed.

There are other works in the field of excited atom collisions but these are too numerous to mention here. Those mentioned, cover some of the work which is more relevant to this study of collisions of metastable mercury atoms.

It is obvious that some of the experimental results, now available, contain a wealth of information about the processes which occur in excited atom collisions. This is especially true of the molecular beam technique where collisions of individual atoms and molecules can be studied and in which photon, ion or excited atom emission

from the collision region can be monitored. This information can be used to test formal theories or provide necessary information for use in approximate methods.

The situation in the case of energy transfer processes is still complex as can be seen from the number of approximate theories in use. Formal theory results in vast computational problems and is likely to be limited to simple systems involving light particles. A number of recent approximate theories have appeared which are still restricted to moderately specific and very limited classes of systems and are relatively untested. For one set of processes, however, the transitions between the fine structure components of the ^2P terms of excited alkalis in alkali/inert gas collisions, a theory has been developed [NIK 1965] which seems to promise a quantitatively accurate analysis of the physical situation. In other cases where larger amounts of energy are transferred the situation is not as bright. In these cases it seems that the results from experiments, such as those by Polanyi et al [POL 1967], will form the basis of some potential energy curve argument in an attempt to resolve the physics of the situation.

Perhaps because of the ease of detecting ions, a significant amount of data is now at hand on ionization processes especially with excited helium. This has proved especially useful since helium is sufficiently simple electronically to allow theoretical treatments from first principles and a full theory has been developed for the Penning and associative ionization processes [MIL 1972]. It should be possible to extend this theory to other excited atoms e.g. mercury, admittedly with an increase in the

computational effort if a complete formal solution is to be obtained. However, it may be possible to make realistic assumptions to reduce the computational effort.

Potential energy surface arguments are found in numerous places in this discussion and therefore any information obtained about these surfaces will help to unravel some of the problems. With increased theoretical expertise and sophisticated experiments the future determination of the physics of excited atom collisions is bright.

Chapter 3

Properties of the Metastable Beam

3 Properties of the Metastable Beam

Electron bombardment of a beam of mercury atoms results in the production of two or possibly three metastable states depending on the excitation energy. These states are the $^3P_0$, $^3P_2$ and possibly $^3D_3$ [LIC 1958]; located at 4.64, 5.43 and 9.05eV respectively above the ground state [Fig 3-1]. An experiment by Borst [BOR 1969], using the trapped electron technique has indicated that the excitation cross sections for $^3P_{0,2}$ excitation are much larger than those of the other metastable states e.g. the cross section for the $^3P_2$ is approximately 100 times greater than for the $^3D_3$ state and therefore the important metastables in the beam would seem to be the $^3P_2$ and $^3P_0$ at an excitation energy of 10eV.

The $^3P_2$ and $^3P_0$ states are metastable for the following reasons. The $^3P_0 \rightarrow {}^1S_0$ transition is forbidden for all types of radiation by the rule $J=0 \not\leftrightarrow J=0$ whereas the transition $^3P_2 \rightarrow {}^1S_0$ is rigorously forbidden for electric dipole and magnetic dipole radiation since $\Delta J=2$, and for electric quadrupole radiation by the parity rule. The 6^3P_2 state can decay, however, to the $^3P_1$ state via magnetic dipole radiation. Lifetimes in the absence of specific effects might thus be expected to be of the order 1s.

Previously reported experimental values for the lifetime of the $^3P_0$ state varied from 4.2×10^{-4} seconds [KIM 1960] to 7.5×10^{-3} seconds [MCA 1965] while the reported values for the lifetime of the $^3P_2$ state were 1.3×10^{-4} seconds [TIT 1965] and 1.2×10^{-3} seconds [BAL 1965]. Since these values are in considerable disagreement an attempt has been made to find the lifetimes of these

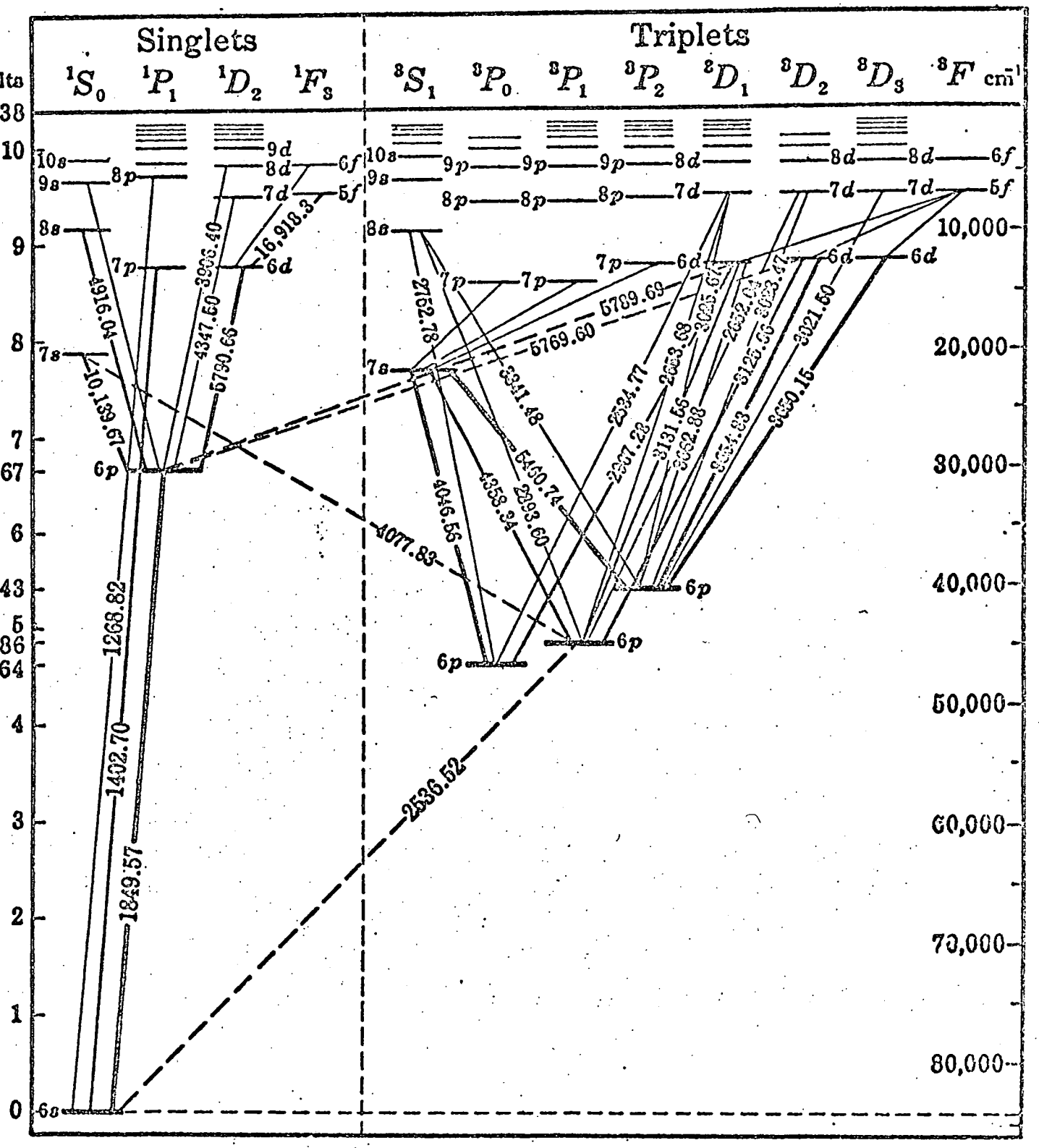

Term diagram for mercury

Figure 3-1

species together with the ratio of the cross sections for excitation, by electron bombardment, of the $^3P_2$ and $^3P_0$ which McConnel et al [MCC 1968] have predicted to be 5:1.

Lifetimes of excited species are affected not only by the presence of electric or magnetic fields but also by collisions with other atoms or molecules. The molecular beam technique provides an excellent means for the determination of field-free space lifetimes since it is only necessary to measure the decrease in intensity of the beam as it passes through a good vacuum. When a thermal source of molecules is used without velocity selection the velocity distribution of the atoms must be considered with the result that the intensity of excited molecules of velocity in the range v to v + dv remaining in the beam at a distance L from the point of excitation is

$$I_L(v)dv = I_o(v)dv \exp\left(-\frac{L}{\tau v}\right) \qquad 3\text{-}1$$

where τ is the mean lifetime and $I_o(v)dv$ the corresponding intensity at the point of excitation. The latter quantity is given by the usual Maxwell-Boltzmann distribution.

$$I_o(v)dv = 4\pi I_o \left(\frac{m}{2\pi KT}\right)^{\frac{3}{2}} v^2 \exp\left(-\frac{mv^2}{2KT}\right) dv \qquad 3\text{-}2$$

The reason for this is that although the effusion process contributes a factor of v to the normal distribution, the probability that a molecule will be excited by electron impact is proportional to v^{-1}. By varying the position of the detector with respect to the source an estimate of the lifetime can be obtained from the equation [3-1][LIC 1957].

Lifetime estimates can also be achieved by measuring the inverse of the velocity distribution, the time of arrival distribution, which is the time it takes an atom or molecule to drift from a pulsed electron bombarder to the detector [FRE 1967].

The velocity distribution in a beam of ground state molecules which has been formed by effusion through a thin slit is the Maxwell-Boltzmann v^3 distribution.

As has been pointed out the production of metastables by electron bombardment leads to a modified velocity distribution. However, when pulsed bombardment is used this correction applies only to the fastest molecules, those with velocities greater than vc = L/tp where L is the length of the bombarder, and tp is the duration of the bombarding pulse. Species with velocities less than vc are all bombarded for the same length of time so that the third power of v is correct. The time of arrival expression is then:

$$N_L(t) = -C \frac{L^{n+1}}{t^{n+2}} \exp\left(-\frac{L^2}{\alpha^2 t^2} - \frac{t}{\tau}\right) \qquad 3\text{-}3$$

where $N_L(t)$ is the number of atoms arriving after time t at a distance L from the source, $\alpha = (\frac{2KT}{M})^{\frac{1}{2}}$ and C is a constant.
($n = 3$ for $v < v_c$, $n = 2$ for $v > v_c$).

An estimate of the lifetime can be obtained by using a fitting procedure for the values c and τ. Equation [3-3] neglects the finite length of the bombarder and it also assumes a known velocity distribution.

A method incorporating both experimental techniques has been developed by Johnson [JOH 1972] in which a pulsed source is used and

the time of arrival distribution of a thermal beam of metastable molecules is sampled and detected at two positions. The theory, using Johnson's notation is as follows:

The total number Ni(v) of metastables with velocity v that are counted at detector i is therefore

$$Ni(v) = \Sigma_k \, Ci(k) \, n_o \, (v,k) e^{-\frac{ti}{\tau_k}} \qquad 3\text{-}4$$

where $C_i(k)$ is a constant efficiency factor of the i'th detector. The ratio of the number of metastable molecules in the same velocity interval at two spatially separated detectors yields the expression:

$$R = \frac{N_2(v)}{N_1(v)} = \frac{C\Sigma_k \, n_o(v,k) e^{-\frac{t_2}{\tau_k}}}{\Sigma_k \, n_o(v,k) e^{-\frac{t_1}{\tau_k}}} \qquad 3\text{-}5$$

which is independent of the two detector efficiencies except for the normalisation constant C. Also, the initial velocity distribution, determined not only by the effusion from the source slit but also by the excitation process in the electron gun is the same for all states k; therefore the ratio R is independent of the initial velocity distribution.

If all the metastable states in the beam decay at the same rate $\tau_k = \tau$ then:

$$R = Ce^{-t/\tau} \qquad 3\text{-}6$$

Therefore a plot of $\log_e R$ versus time of flight $t = (t_2 - t_1)$ is a straight line whose slope yields τ. However, if the metastable states have different decay rates, then $\log_e R$ versus t is no longer a straight line; any curvature in the plot indicates that metastable states with different decay rates are present in the beam.

Although the apparatus used in this work does not offer the possibility of having two different flight paths at the same time it was felt that Johnson's method could be adapted to experiments performed on different occasions with different flight paths provided the initial conditions could be reproduced. This method was preferred since it combines the major points of both previous methods and it does not require any prior knowledge of the velocity distribution since $\log_e R$ versus t is independent of velocity distribution whereas any fitting procedure requires that the exact velocity distribution is known.

Magnetic deflection analysis of the beam is a powerful tool in the determination of the constituents of the beam since all atoms with non zero effective moment are deflected in an inhomogeneous magnetic field. The technique was first used in the classic experiment of Stern and Gerlach [STE 1921] which demonstrated the spatial quantization of angular momentum in the case of silver atoms.

In a non homogeneous magnetic field a neutral atom or molecule experiences a force F_z given by

$$F_z = \mu\text{eff} \frac{dB}{dZ} \qquad 3\text{-}7$$

where μ eff = effective dipole moment of the particle in the field

$\frac{dB}{dZ}$ = magnetic field gradient, the Z axis being taken as the direction of the magnetic field

The effective dipole moment has a magnitude given by

$$\mu\text{eff} = m_J g \mu_o \qquad 3\text{-}8$$

where m_J is the magnetic quantum number in the case where the much smaller nuclear magnetic moment is neglected. In the above

expression g is the Landé factor and μ_o is the Bohr magneton.

$$\mu_o = \frac{e\hbar}{2mc} \qquad 3\text{-}9$$

m_J can take on 2J+1 values where J is the total angular momentum quantum number of the atom.

Thus if an atomic or molecular beam is sent transversely through an inhomogeneous magnetic field, the beam splits into components corresponding to various magnetic substates and each component undergoes a deflection determined by the length of the magnet, the field gradient, the mass and velocity of the atom or molecule since the deflection D is given by:

$$D = \frac{A}{v^2} \qquad 3\text{-}10$$

$A = \frac{F_Z}{2M}\ (l_m + 2l_d l_m)$ where M = mass of the atom, l_m is the length of the magnet, l_d is the length from the magnet exit to the detector.

In a sufficiently large inhomogeneous field the $^3P_2$ state of mercury should therefore be split into five components whereas the $^3P_0$ should be unaffected. (The field should be sufficiently large to decouple the electronic and nuclear motions for the mercury isotopes with non zero nuclear spin). Unfortunately in the present apparatus the detector is fixed and therefore there is no possibility of detecting the $m_J = \pm 2, \pm 1$ states separately. However, by making the exit aperture of the magnet very narrow it should be possible to detect only those atoms which remain undeflected in the magnetic field. A computer program, which calculates the expected deflection pattern produced by passing a beam of metastable Hg atoms (in a particular J state) through a non homogeneous magnetic field is discussed in Appendix I. From the results of this program it is possible to select the values of the slit

widths required for the magnet apertures so that only those atoms with zero effective moment are transmitted. The signal in this case is then made up from the $m_J=0$ state of the $^3P_2$ atoms and the total amount of $^3P_0$ atoms in the beam. Assuming that the m_J states are populated equally in the $^3P_2$ atom the total signal contains $^3P_0$ atoms + $\frac{1}{5}$ of the whole amount of $^3P_2$ atoms in the beam. By measuring the transmitted current with the magnet on and off information should be obtained about the constituents of the beam.

Experimental

The apparatus used in the present experiment is shown schematically in figure [3-2].

Vacuum System

The vacuum system consists of a stainless steel frame measuring 22 inches along all sides and 12 inches high. Side plates are bolted to this frame and sealed with rubber rings. One of the side plates has electrical and water feed throughs while another has a perspex viewing window. The metastable atom detector is bolted to one of the other sides. The bottom plate holds a water cooled chevron baffle for a 12 inch diffusion pump. The lid, which can be lifted by means of a hoist, contains a large copper liquid nitrogen cold trap. Copper curtains are bolted to the cold trap on all four sides so that when the cold trap is filled very high pumping speeds for easily condensible material are achieved.

Source

The ground state mercury beam is formed by effusion through

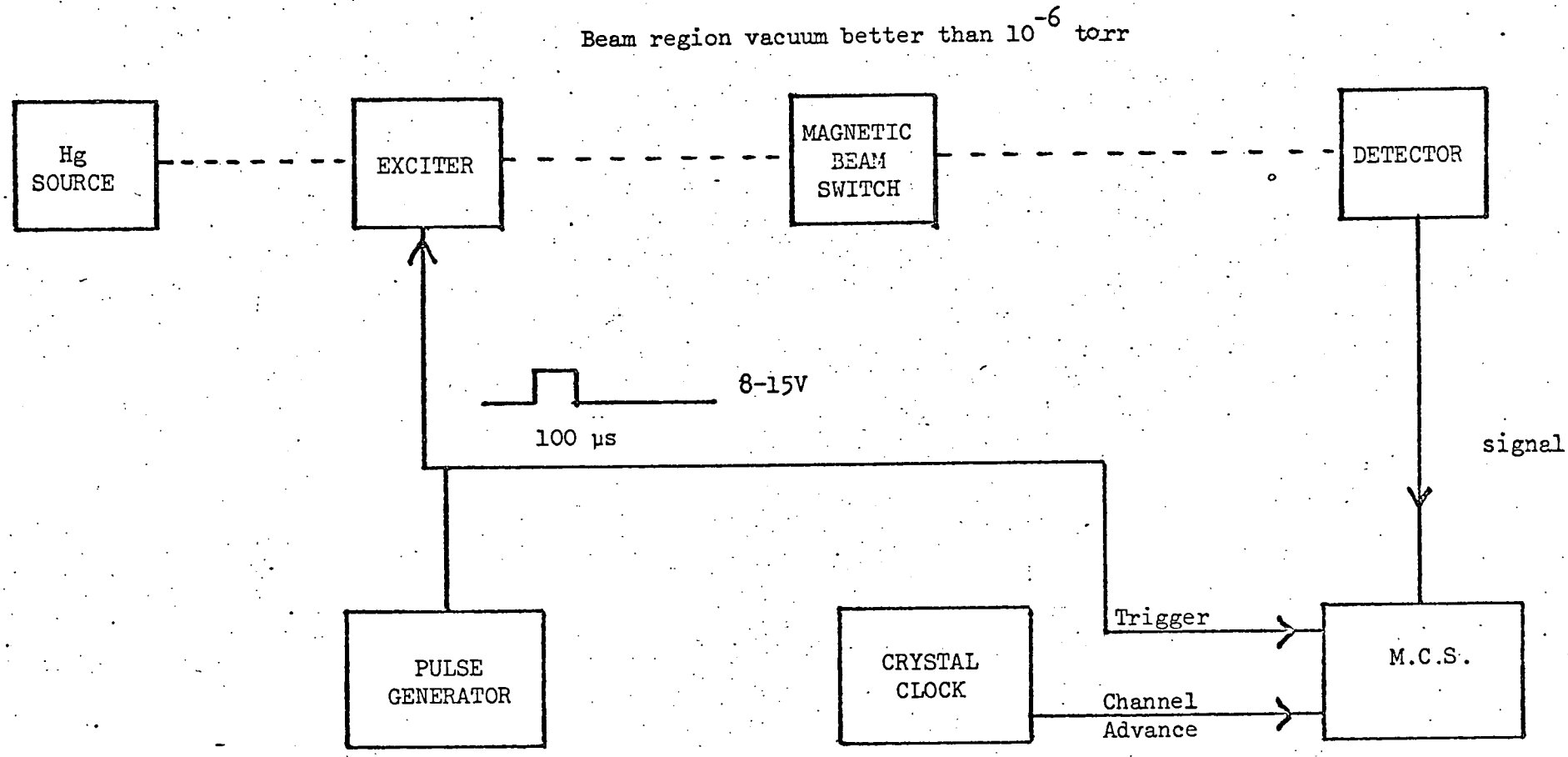

Figure 3-2

Apparatus schematic showing metastable atom source, magnetic selector to remove atoms having an effective magnetic moment and timing electronics.

a glass capillary array plate from a carefully thermostated oven. This oven, which is made throughout of stainless steel, was designed by Darwall [DAR 1972].

Exciter

The beam is excited by a magnetically collimated flux of electrons of controlled energy. The electron gun is mounted in front of the mercury oven but separate from it [Fig 3-3]. This gun consists of an anode with a groove down its entire length through which the Hg beam is passed. The cathode is mounted underneath the slit in the anode as close to the anode as possible but insulated from it by thin mica strips. Standard uncured oxide cathodes from PL36 pentode valves, supplied by Mullard, are used. These cathodes are heated indirectly, the heating filaments also being supplied by Mullard. At an anode-cathode voltage of 10V, the emission current is of the order of 8 ma. A magnetic field is provided by two "Eclipse" C magnets as shown in figure [3-3]. The magnetic field is 600 gauss, measured by a Hall probe, with the result that the electrons leaving the cathode travel in a helical path. The cathodes are replaced before each experiment.

The method of excitation is rather inefficient since perhaps only 1 in 10^5 of the atoms are excited, but it does have the advantage over discharge sources of being more selective in so far as only those states with energies less than the excitation energy can be excited. It might be expected that the effects of recoil would destroy the collimation thus making such a method unsuitable for cases where very close beam definition is necessary.

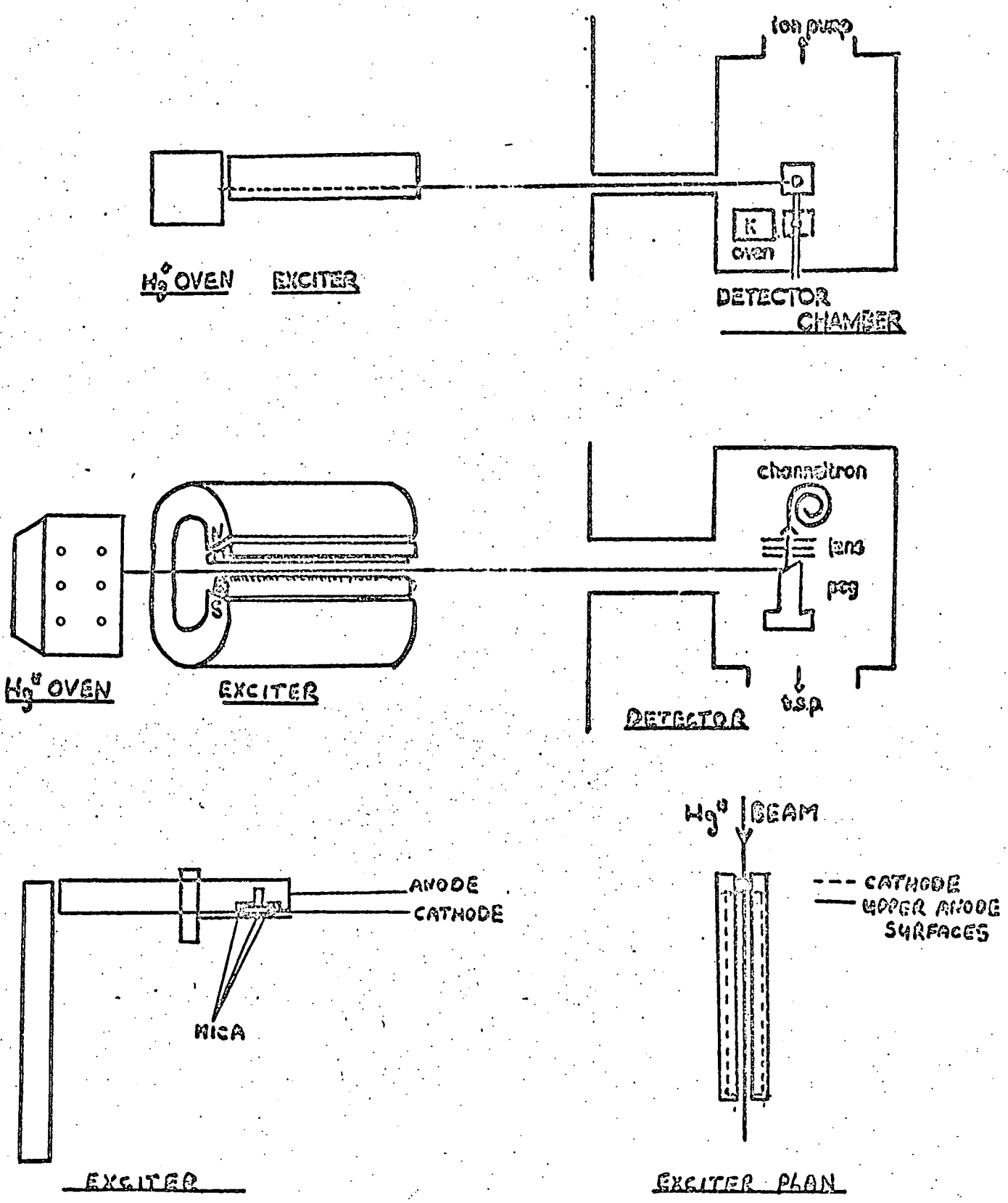

Schematic showing the main feature of the exciter and detector

Figure 3-3

However, if the electron gun is placed very close to the source slit the loss of intensity by scattering out of the beam is not great since it is at least in part compensated by scattering of particles into the beam. At an excitation energy of 10eV the $^3P_1$ state is produced together with the metastable $^3P_2$ and $^3P_0$. The production of $^3P_1$ results in the emission of photons at 2536.5 Å since this state is radiatively connected to the ground state. The photons emitted by the exciter which reach the detector have been measured and are discussed later. A mercury 2536.5 Å discharge has also been observed, viewed through the perspex window, with a high source pressure ($\sim$ 10 torr) and a high excitation voltage ($\sim$ 16V).

Magnetic State Selector

The magnetic state selector is an inhomogeneous magnetic field of the two wire type [RAM 1956]. The magnet is 10 cm in length, the other important dimensions are shown in figure [3-4]. The field strength can be varied over a limited range by varying the exciting current between 0 and 30 amps. A plot of magnetic field strength, measured with a Hall probe versus exciter current is shown in figure [3-5].

In Appendix I a program for the calculation of the predicted deflection patterns for a given velocity distribution is discussed. As a result of these calculations the magnetic field was provided with entrance and exit apertures $\sim$ 0.006 cm in width. Figure [3-6] shows, for a magnetic field of 7.5 kilogauss, an entrance aperture of 0.006 cm, an exit aperture of 0.006 cm, that the fraction of metastables with non zero effective moment which are transmitted

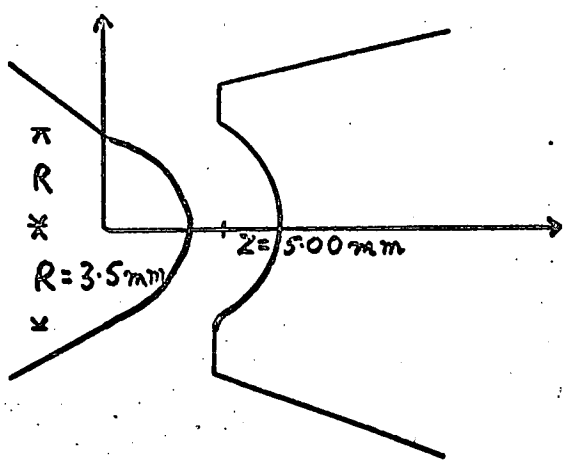

Schematic showing the dimensions of the magnet pole pieces.

Figure 3-4

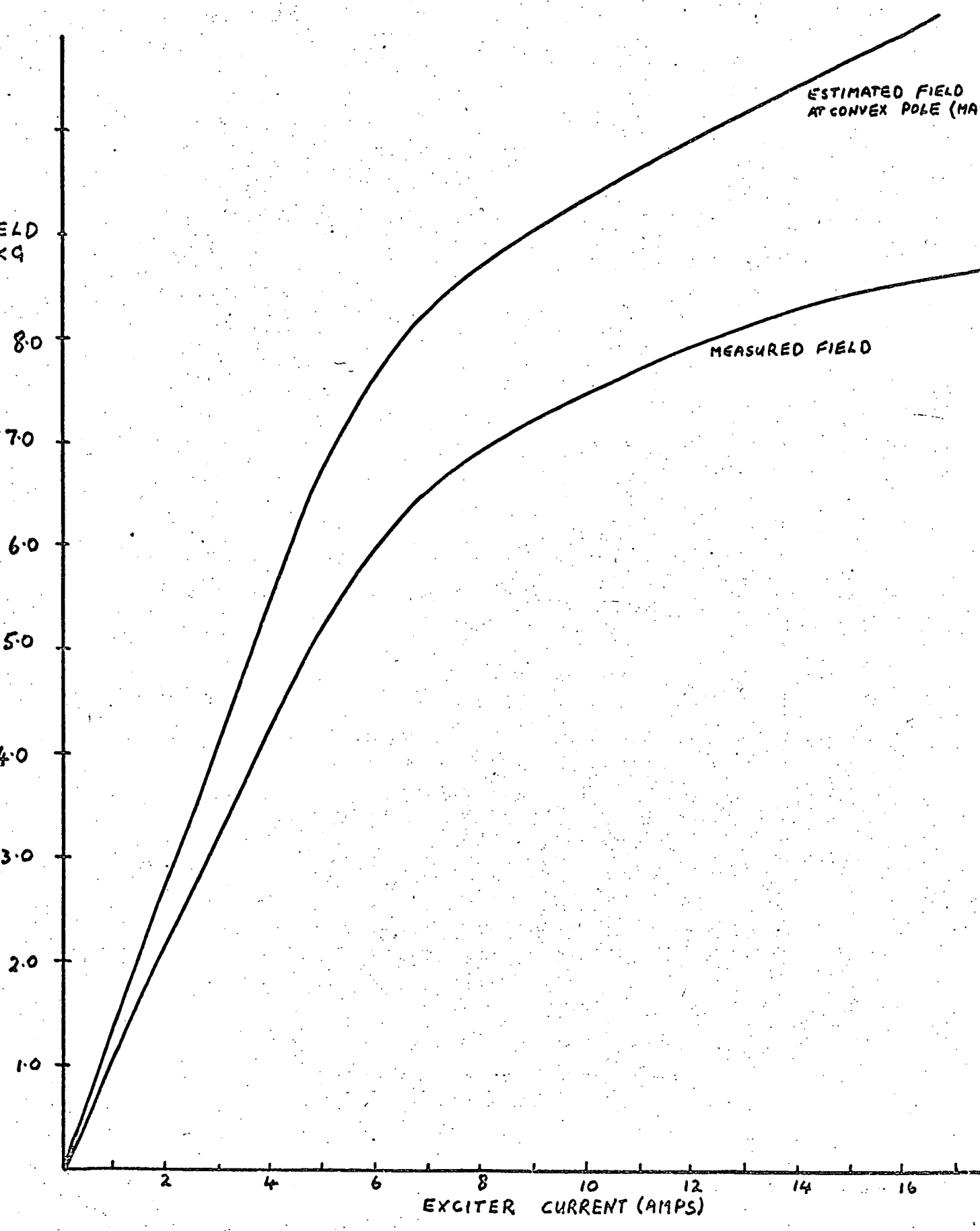

Magnetic field strength versus exciter current for the state selector

Figure 3-5

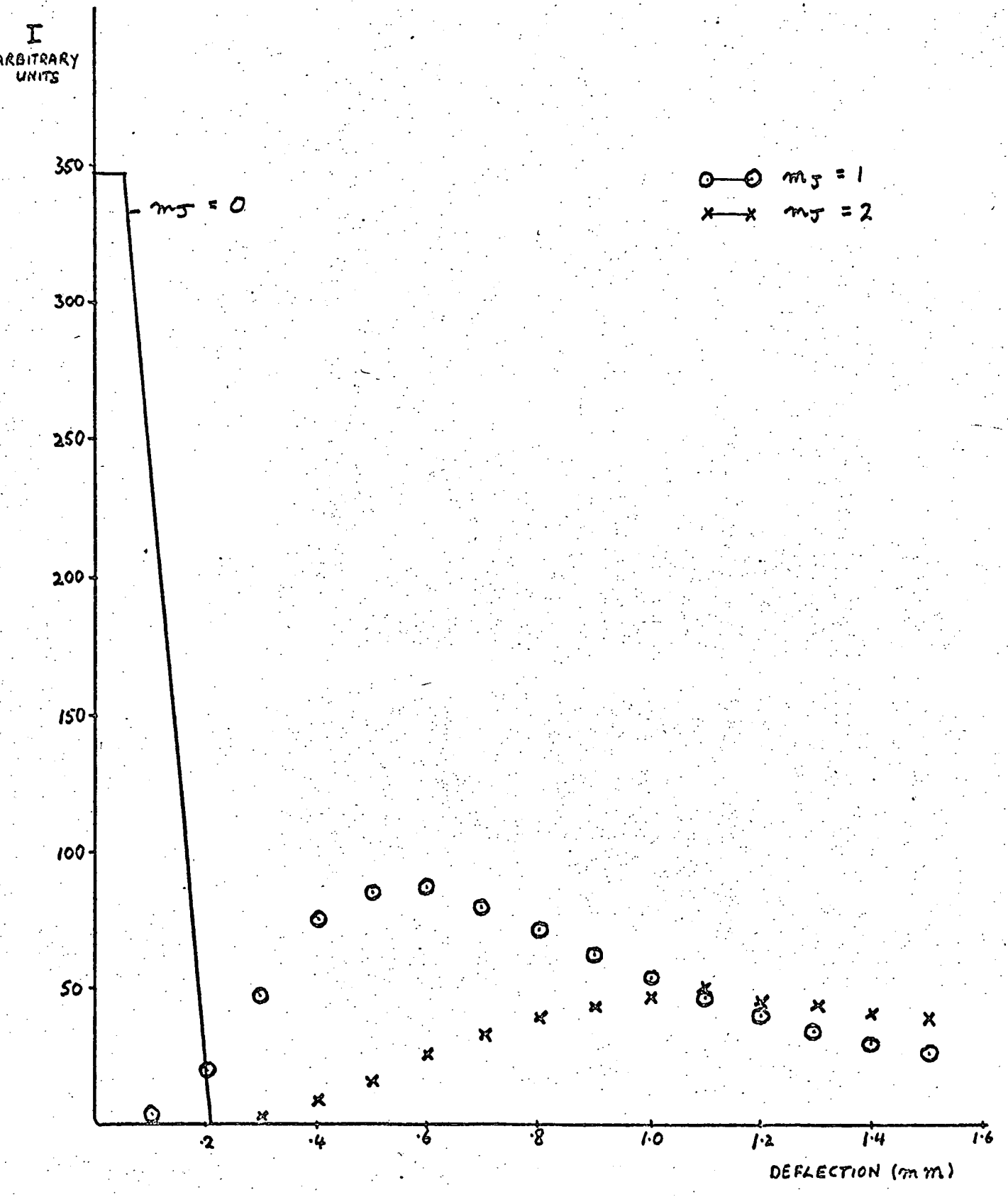

Plot showing the computed deflection for the m_J = +2 and +1 states of Hg* for a magnetic field of 7.5 KG and an entrance aperture of .01 cm mapped onto a detector .01 m from the exit of the magnet.

Figure 3-6

is predicted to be negligible. This design feature was checked by a saturation plot showing that with the magnet fully excited less than ∿ 3% of atoms with a non zero effective moment were transmitted [Fig 3-7].

At thermal velocities the magnetic field therefore acted as a switch; with the field off the beam was transmitted without loss while with the field on only atoms with zero effective moment were transmitted since at a field of 7.5 kilogauss nuclear coupling effects can be ignored.

Metastable Detector

This piece of equipment has been described in detail by Darwall [DAR 1972]. A short treatment of the main points will be presented here.

The detector is based on an Auger process by which the electronic energy of the metastable is transferred to an electron in the conduction band of a metal. In cases where the energy of the metastable is greater than the work function of a metal then Auger electrons may be ejected from the metal surface when the atom collides with the surface. The metal surface used is potassium deposited on a tungsten peg. The measured work function for potassium is

$$2.177 \pm 0.004 \quad \text{at} \sim 206^{\circ}K$$
$$2.217 \pm 0.004 \quad \text{at} \sim 300^{\circ}K \qquad [\text{GAR } 1961]$$

The metastable states of mercury $^3P_{0,2}$ have sufficient energy to eject electrons from the potassium surface since they have energies of 4.64eV and 5.43eV respectively. The conduction band

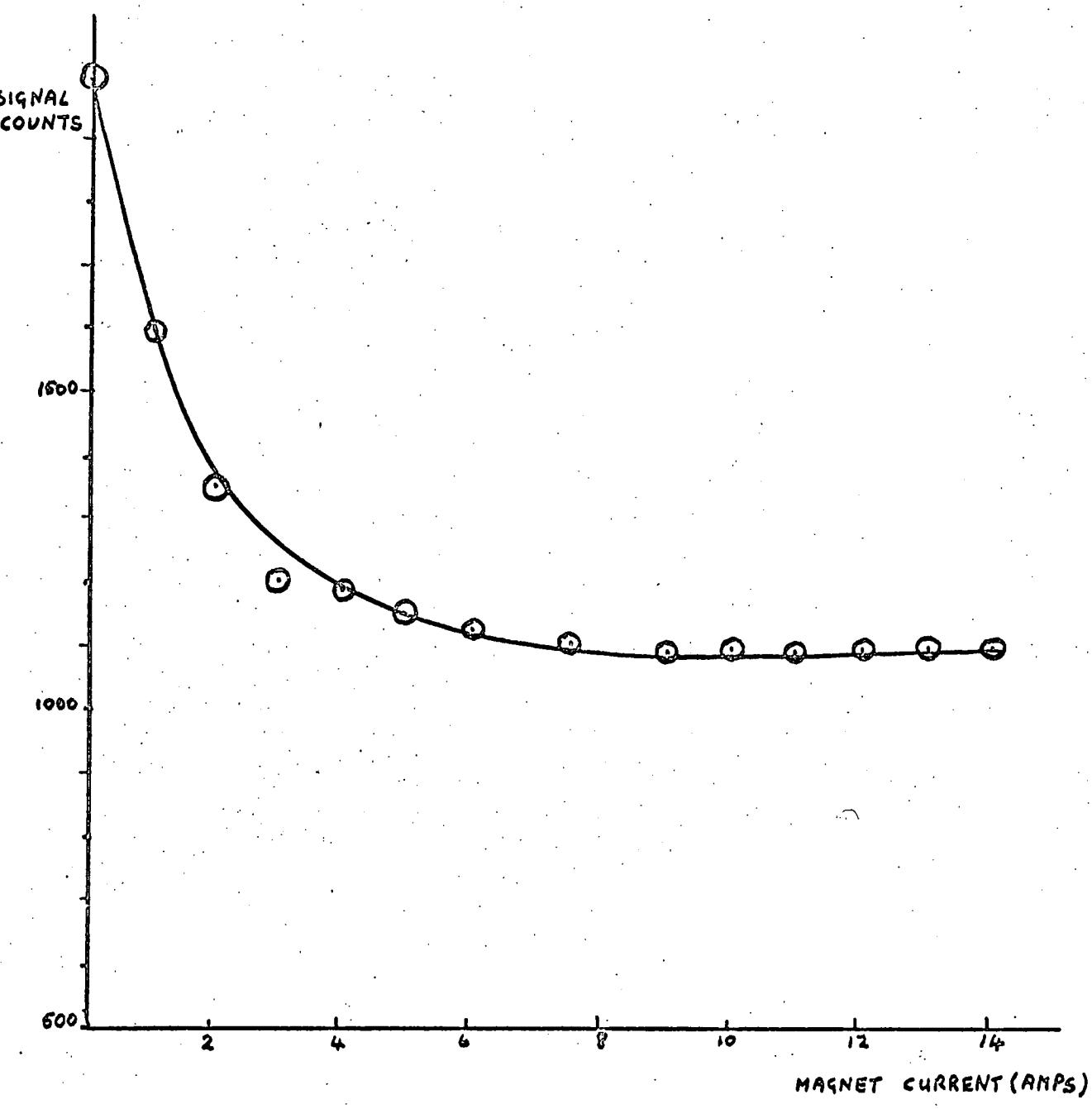

Plot of transmitted signal versus magnet current showing saturation (The transmitted signal includes photons).

Figure 3-7

of potassium extends from ∿ 2.2V to 4.6V below the vacuum level [KIT 1956] and since both metastables have energy in excess of 4.6V the surface should be a very useful detector for both species.

The detector is mounted in a separate U.H.V. chamber which is made of stainless steel throughout. It is connected to the main chamber via a bakeable valve and a slit and it is pumped by a Ferranti 80 ls^{-1} ion pump and a liquid nitrogen cooled Titanium sublimation pump.

The detector consists of a tungsten peg [Fig 3-8] mounted so that it can be transversely moved out of the path of the Hg* beam to a position in front of a small oven filled with potassium. The tungsten peg is insulated from ground by a P.T.F.E. sleeve so that it can be floated at a convenient voltage. A three element electrostatic lens is mounted above the position of the peg when it is situated inthe path of the Hg* beam. The whole assembly is mounted on a 6" diameter flange so that the entire unit can be withdrawn from the vacuum chamber for cleaning or re-filling of the alkali oven. Copper shielding is positioned so that the C.E.M. is protected from the oven heater wires and further shielding was added to reduce the amount of alkali sprayed around the chamber when the tungsten peg is being plated. An adequate film of potassium can be deposited on the peg after 30 minutes exposure to the potassium beam, with the oven at 230°C. Once deposited the potassium surface would last several months and many experiments provided the pressure was maintained below 1 x 10^{-9} torr.

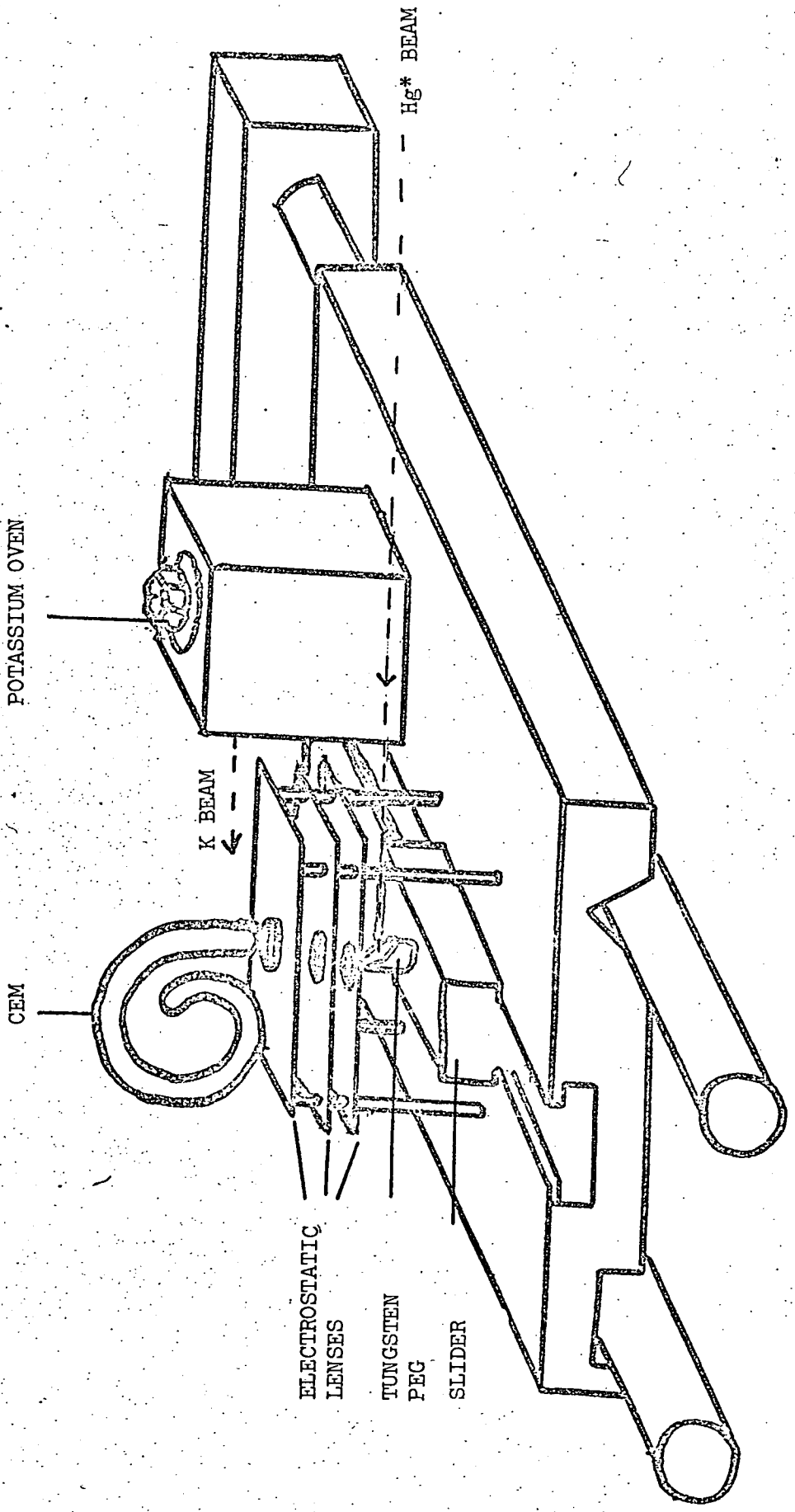

The Detector

Figure 3-8

Electrons ejected from this surface are focussed into a Mullard Channel Electron Multiplier by the electrostatic lens. In the C.E.M. each electron produces an avalanche of electrons which is treated as a single pulse. Typical voltages during the experiments are shown in Table [3-1] and typical background counts were about 100 second^{-1} while typical signal counts were 60,000 second^{-1}. The background count rate was largely due to photons produced from the hot cathode.

Table 3-1

Unit	Voltage
Peg	-80V
Lens 1	+70V
Lens 2	-71V
Lens 3	-80V
C.E.M. entrance	0
C.E.M. collector	2.8KV

Since the collector end of the C.E.M. is at 2.8KV, the output pulses are taken off by a 00.001 μF capacitor. This is followed by a protection circuit after which the signal is fed into a Keighley III amplifer which in turn is followed by a Hewlett Packard HP462A amplifer and a discriminator and pulse shaper circuit which have been described by Cowley [COW 1968]. The signals are then counted into two scalers, in the case of the scattering experiments, or into a multichannel scaler in the lifetime determination experiments.

By plotting the observed metastable signal at the detector against the exciter voltage the excitation function for Hg* may be obtained. The excitation function A is plotted in figure [3-9] together with excitation function B produced by Darwall [DAR 1972].

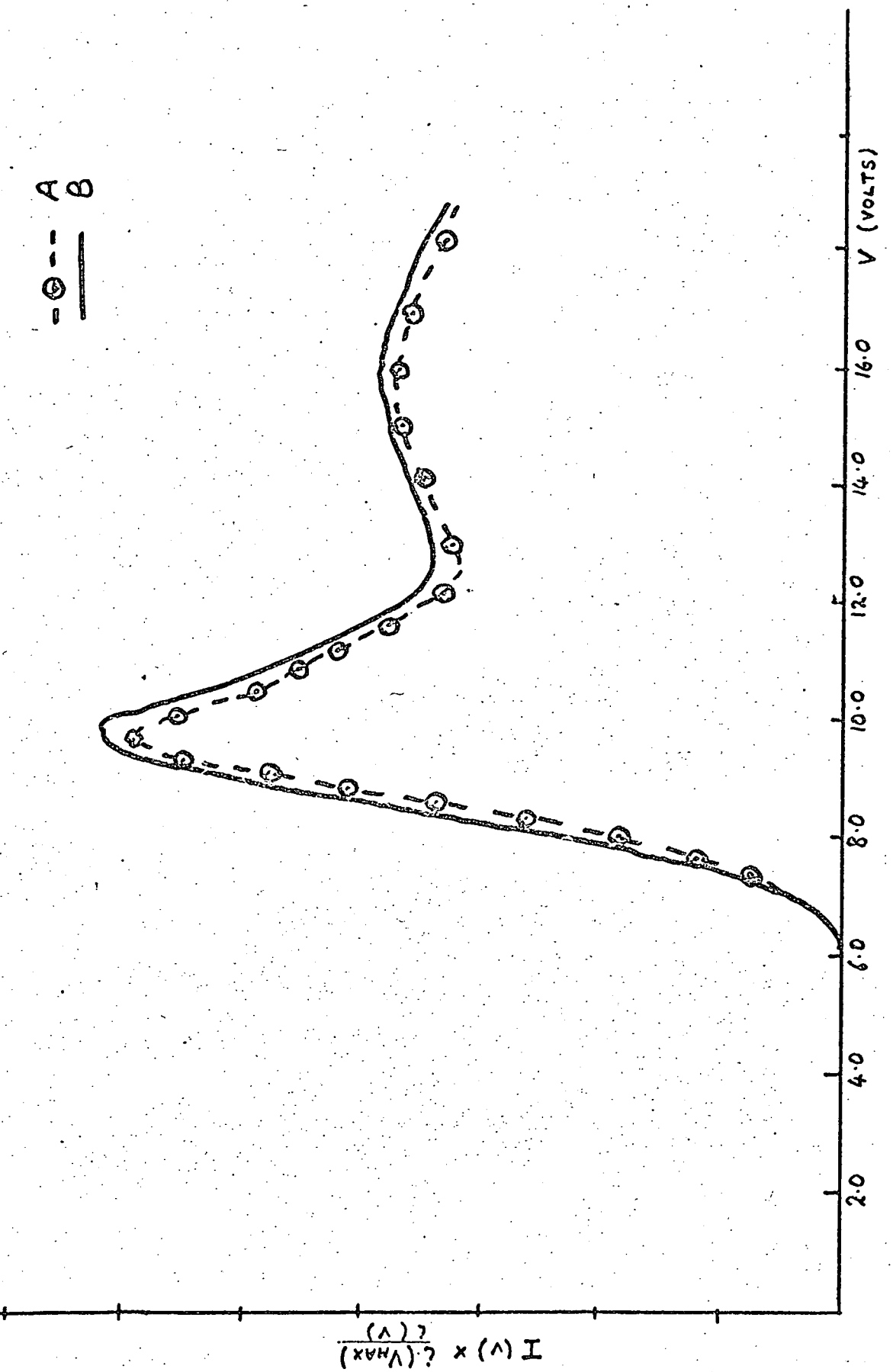

Excitation functions for Hg* detected on potassium

A This work
B Darwall

Figure 3-9

Both excitation functions were obtained using a potassium surface. At each voltage the observed signal i(V) has been multiplied by the factor $\frac{i(V\ max)}{i(V)}$ where i(V) is the exciter current at voltage V. This is to compensate for the larger currents flowing at higher voltages giving rise to greater signals. The results exhibit a threshold around 6V with two subsequent maxima at 9.5V and 15V. The curves are in good agreement with those obtained by Lichten [LIC 1958]. The first peak is attributed to the $^3P_{0,2}$ whereas the peak at 15V will contain contributions from $^3P_{0,2}$ and perhaps ^3D, although a significant part of this signal is probably due to photons.

Signal

After discrimination the signal pulses, in this experiment, were counted in a multichannel scaler. Timing information was obtained by pulsing the excitation voltage on for 10 μs at 20 ms intervals and triggering the sweep of the channel address for the multiscaler in synchronism. The metastable counts were thus collected as a function of their flight time in 10 μs wide channels spaced by 10 μs intervals of dead time during which the channel advanced. In the experiments with the magnet the store of the multiscaler was divided into two halves, the first half being used to collect signals while the magnet was on and the second for signals while the magnet was off. The two types of observation were made in alternate periods of 5 minutes until sufficient precision was obtained [Fig 3-10]. The data, counts versus arrival time were finally output on papertape for computer analysis. In the experiments to evaluate the lifetime of the $^3P_2$ state the distributions shown

in figure [3-11] were obtained for two different flight paths. In this case magnetic selection was not used and the signal was counted into all the channels of the multiscaler, otherwise the situation was identical.

By inserting a delay into the excitation pulse circuit it was possible to open the multichannel scaler before applying the excitation pulse. In this mode it was possible to observe the instantaneous arrival of photons, the majority of which are presumably 2536.5 Å photons, a plot of signal versus arrival time is shown in Figure [3-12]. As shown in Table [3-2], increasing the excitation voltage increases the ratio of photons to metastables and the number of metastables produced appears to be approximately constant. Since these photons arrive instantaneously they will have no effect on the lifetime or magnetic selection experiments in which the multiscaler channels are opened in synchronism with the excitation pulse. However, the effect of photons will need to be considered in the scattering experiments and it is obvious from Table [3-2] that in these experiments the exciter should be operated at the lowest possible voltage.

TABLE 3-2

Voltage	Metastables	Photons	Metastables/ Photons
10.0V	19,000	20,000	0.95
12.5V	18,500	30,000	0.62
15.0V	19,000	50,000	0.38

The number density of Hg atoms at the exit of the exciter was calculated as $\sim 10^{12}$ atoms cm^{-3} and the background pressure was 10^{-6} - 10^{-7} torr in the flight path so that removal of excited species by

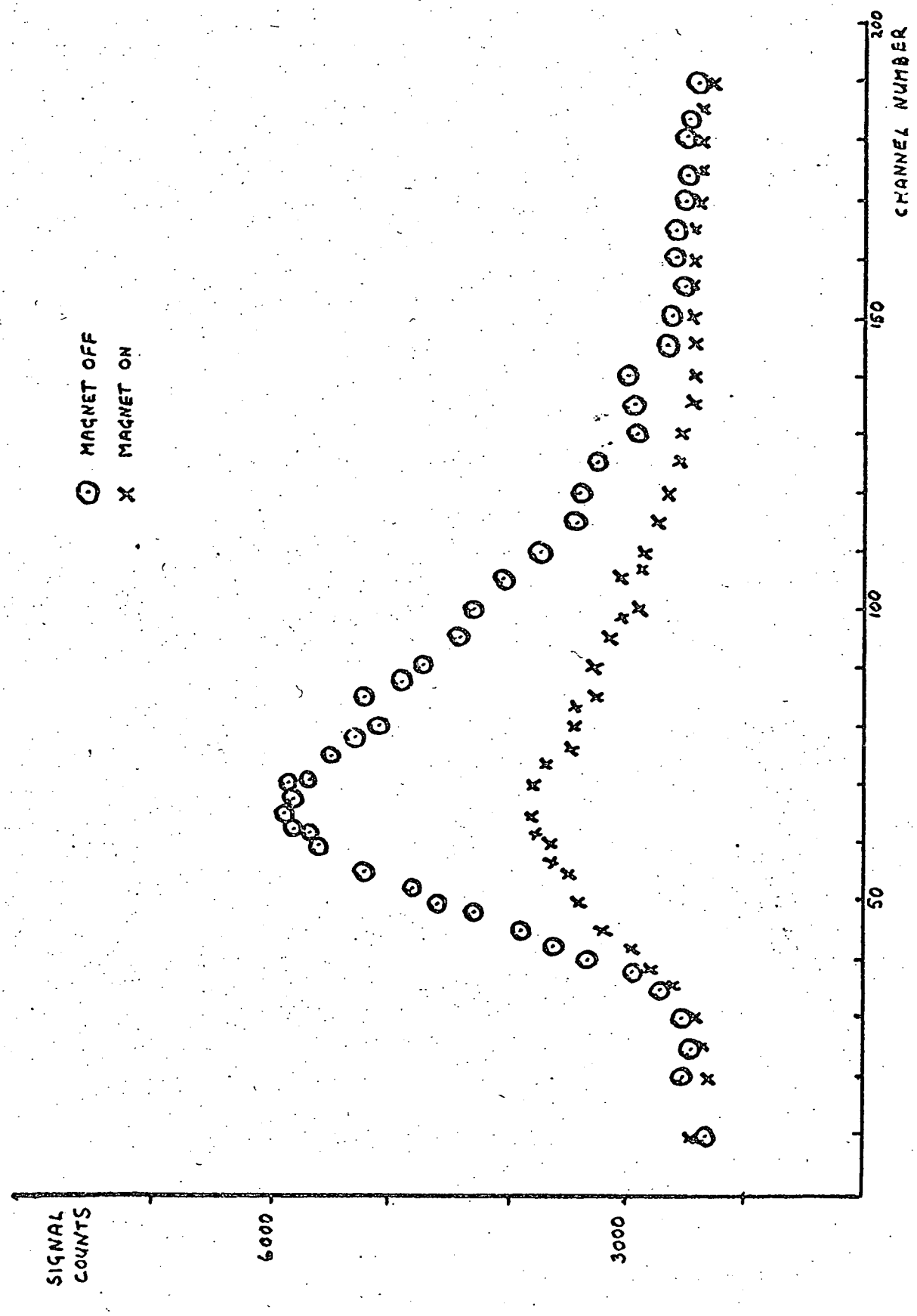

Time of flight distributions for magnet on and off

Figure 3-10

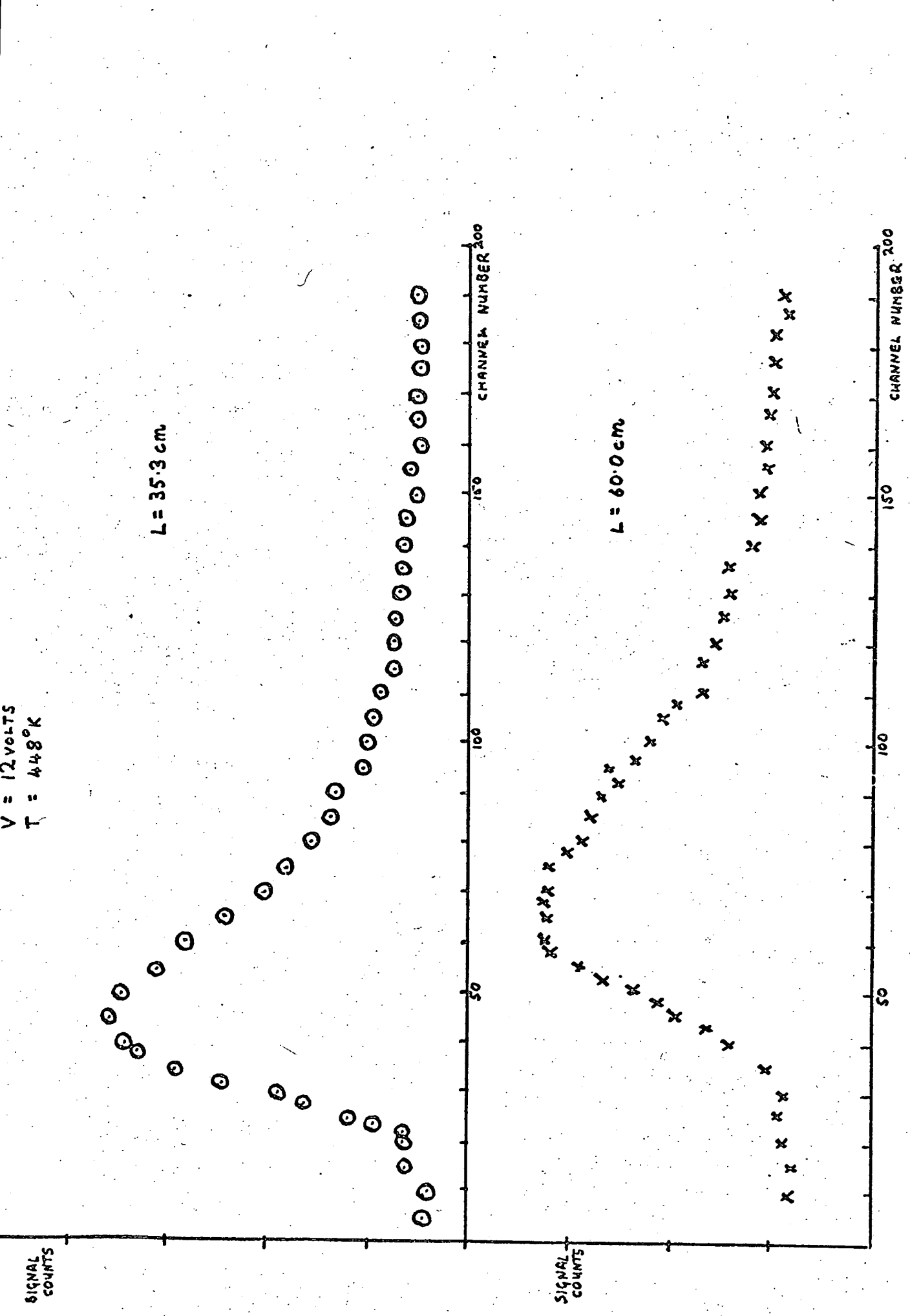

Time of flight distributions for two different flight paths

Figure 3-11

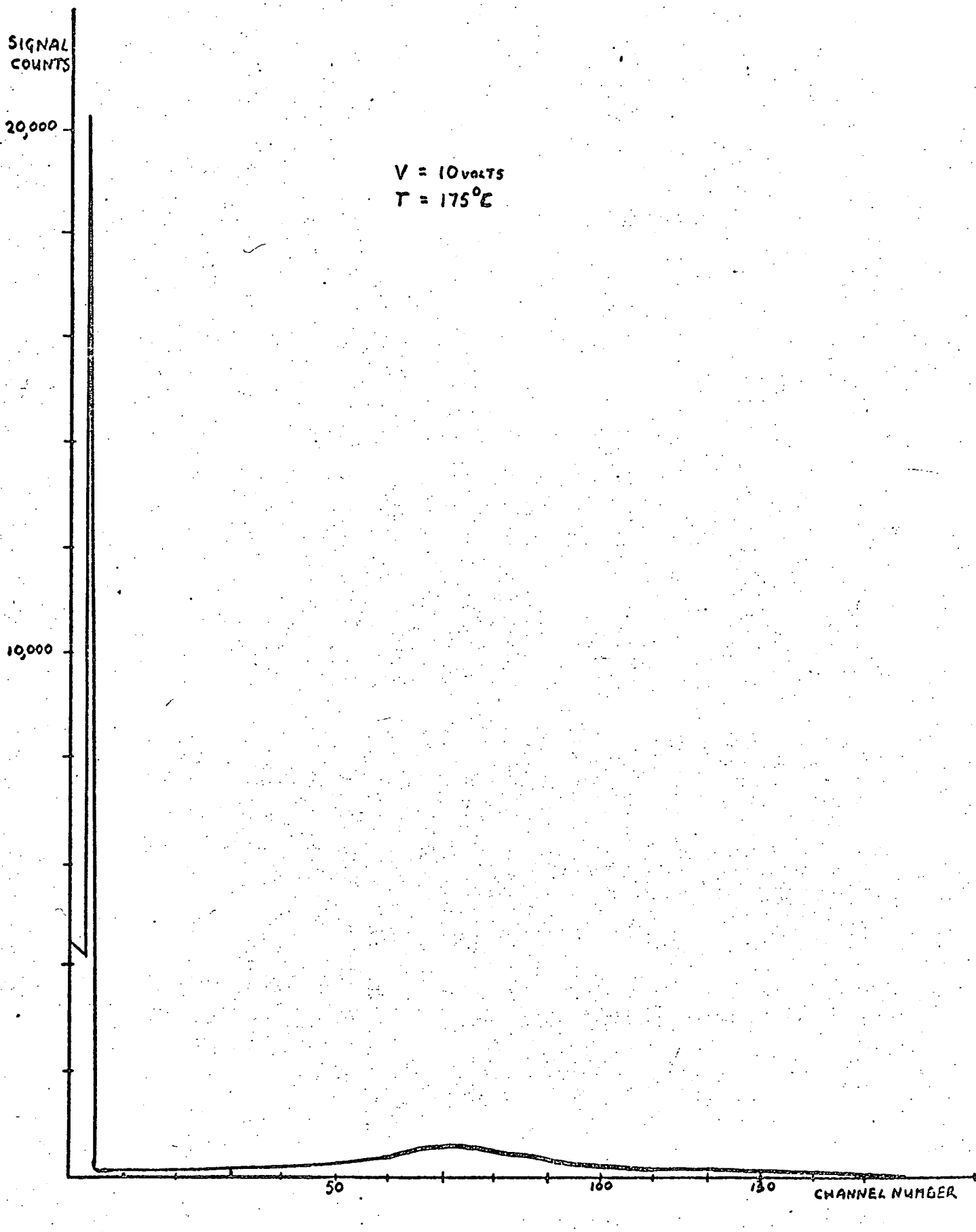

Time of flight distribution in which the instantaneous arrival of photons is recorded.

Figure 3-12

self scattering or by collision with background gas was negligible ($\lambda f \sim 10^3 - 10^4$cm). A calculation similar to that of Borst and Zipf [BOR 1971] showed that any photon contribution to the signal due to decay in flight was less than 0.1% of the total signal. Radiation trapping of the 2536.5 Å line is also negligible at the beam density used [ALP 1949]; finally the dimer fraction in the beam at the source pressures used (< 5 torr) is entirely unimportant.

Analysis and Results

State Selected Measurements

At excitation energies between 6 and 10eV the only long lived states of Hg accessible are the 6^3P_2 and 6^3P_0. Since the electrons producing the excitation are spiralling along the magnetic lines of force of the collimating field which is perpendicular to the velocity of the atom no polarisation effects can arise and all the magnetic substates of the $^3P_2$ must be equally populated. If $\underline{S}^H(t)$ and $\underline{S}^o(t)$ are the beam signals at flight time t with the magnet on and off respectively, then

$$\underline{S}^H(t) = \underline{x} + (1 - 5\underline{x}) \qquad 3\text{-}11$$

and

$$\underline{S}^o(t) = 5\underline{x} + (1 - 5\underline{x}) \qquad 3\text{-}12$$

where x is the apparent fraction of the beam in each magnetic substate of the $^3P_2$ and the qualification apparent is used since this fraction will include the effect of any differential sensitivity between the $^3P_0$ and $^3P_2$ states in the detector.

The apparent composition of the beam is now

$$I^{3P_2}(t) = \frac{5}{4}\,(\underline{S}^{o}(t) - \underline{S}^{H}(t)) \qquad 3\text{-}13$$

$$I^{3P_0}(t) = \underline{S}^{H}(t) - \tfrac{1}{4}\,(\underline{S}^{o}(t) - \underline{S}^{H}(t)) \qquad 3\text{-}14$$

The ratio of these compositions as a function of flight time in the beam can be related to the lifetimes of the states τ_2, τ_0 and their cross sections for excitation σ_2 and σ_0.

$$\frac{I^{3P_2}(t)}{I^{3P_0}} = \underline{C}\,\frac{\sigma_2\, e^{-\frac{t}{\tau_2}}}{\sigma_0\, e^{-\frac{t}{\tau_0}}} \qquad 3\text{-}15$$

$$\text{or} \quad \mathrm{Ln}\,\frac{I^{3P_2}(t)}{I^{3P_0}} = \ln\left(\underline{C}\,\frac{\sigma_2}{\sigma_0}\right) + t\left(\frac{1}{\tau_0} - \frac{1}{\tau_2}\right) \qquad 3\text{-}16$$

Thus the difference in the lifetimes of the two states can be obtained from the slope of a log plot of this relation, while an additional assumption about $\underline{C}$ the relative detector efficiencies will enable the ratio of the cross sections to be determined. Since the work function of the potassium surface used in the detector is considerably lower than the energy of both metastable states, $\underline{C}$ can plausibly be taken as unity. A typical plot of this type is shown in figure [3-13] and the results of a least mean square fit for data taken at several excitation voltages are given in Table [3-3]. The error bars are two standard deviations long and are computed from counting statistics assuming no correlation between the noise in the $\underline{S}^{o}$ and $\underline{S}^{H}$ observations. Making an initial estimate of the half life of the $^3P_2$ state of 1ms enables the difference in half-life of the two states to be estimated. These estimates are also shown in Table [3-3].

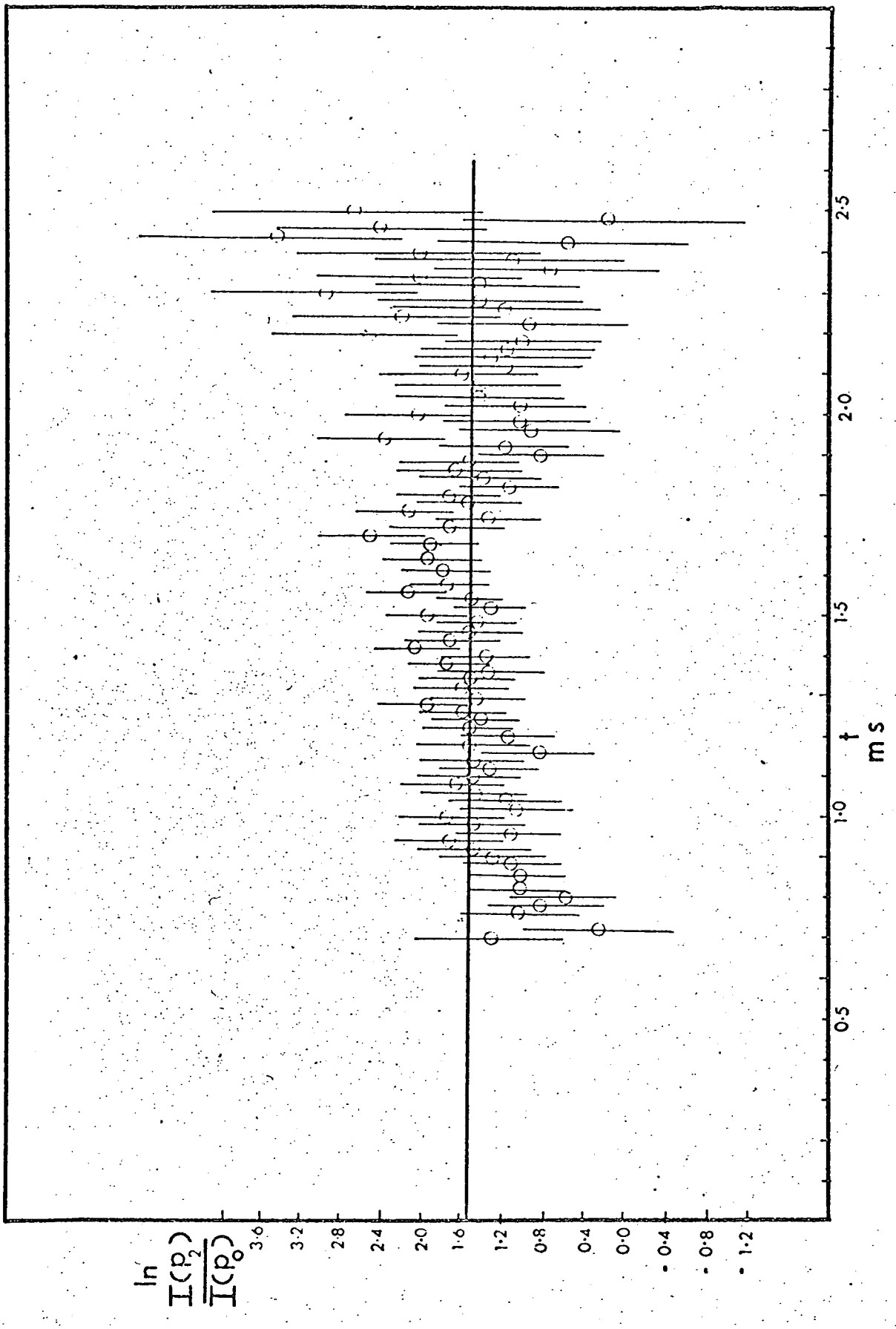

Composition of the metastable beam as a function of flight time

Excitation voltage = 10V

Figure 3-13

TABLE 3-3

Magnetic Deflection Experiments

Excitation Voltage E	$\frac{\sigma(^3P_2)}{\sigma(^3P_0)}$ (E)	Gradient of plot $(\frac{1}{\tau_0} - \frac{1}{\tau_2})$ms.	Estimated life-time differences ms.
10	4.62 ± 0.6	- 0.02 ± 0.06	0.02 ± 0.06
12	4.76 ± 0.8	- 0.02 ± 0.06	0.02 ± 0.06
15	4.14 ± 0.8	0.007± 0.07	- 0.07 ± 0.06

The lifetimes of the two states are identical within the experimental error. The ratio of cross sections is only rather approximately determined but it is close to the statistical ratio for the states.

Lifetime of $^3P_2$ state

To extract absolute values of the lifetimes of the two states it is necessary to make decay measurements at more than one detector source distance [JOH 1972]. However, since the lifetime of both states is the same, the magnetic selecting field is not required in these experiments.

The ratio of the fraction of metastables in a velocity interval v to v + dv after flight paths of length ℓ_1 and ℓ_2 is

$$R(v) = \frac{N(v, \ell_1)}{N(v, \ell_2)} = \frac{G \times I(v) e^{-\frac{t_1}{\tau}}}{G \times I(v) e^{-\frac{t_2}{\tau}}} \qquad 3\text{-}17$$

where I(v) is the initial velocity distribution and the convolution G accounts for the finite length of the exciter and pulse widths etc.

The ratio R(v) is independent of the actual velocity distribution

and yields a relation for the metastable lifetime.

$$\text{Ln } R(v) \alpha \left(\frac{t_2 - t_1}{\tau}\right) \quad ; \quad v = \frac{\ell_1}{t_1} = \frac{\ell_2}{t_2} \qquad 3\text{-}18$$

A typical plot of this type is shown in figure [3-14] and the complete results are given in Table [3-4].

TABLE 3-4

Lifetime for $^3P_2$ state

Exciter Voltage	Path Length ℓ_1 cm	Path Length ℓ_2 cm	Source Temperature T_1 ^oK	Source Temperature T_2 ^oK	Lifetime $^3P_2$ ms.
10V	35.3	60.0	448	448	1.25 ± 0.30
12V	35.3	60.0	448	448	1.26 ± 0.40
15V	35.3	60.0	448	448	1.30 ± 0.50
10V	36.2	60.0	448	448	1.40 ± 0.30
12V	36.2	60.0	448	448	1.35 ± 0.40
			Mean Estimate		1.30 ± 0.17
10V	35.3	60.0	433	448	1.05 ± 0.25
15V	35.3	60.0	433	448	1.00 ± 0.20

Once again the estimates are least mean square fits to the data. An error occurs because the electron bombardment region is finite. This leads to an uncertainty in the effective distance between the two detectors. Taking half of the bombardment length as the total distance error one obtains a maximum error bound for the lifetime of ± 0.2 ms, well within the statistical uncertainty of the present experiment.

The plots show no sign of curvature at any excitation energy and although the photon output rises very sharply at higher voltages the metastable signal remains fairly constant [Table [3-2]]. There is

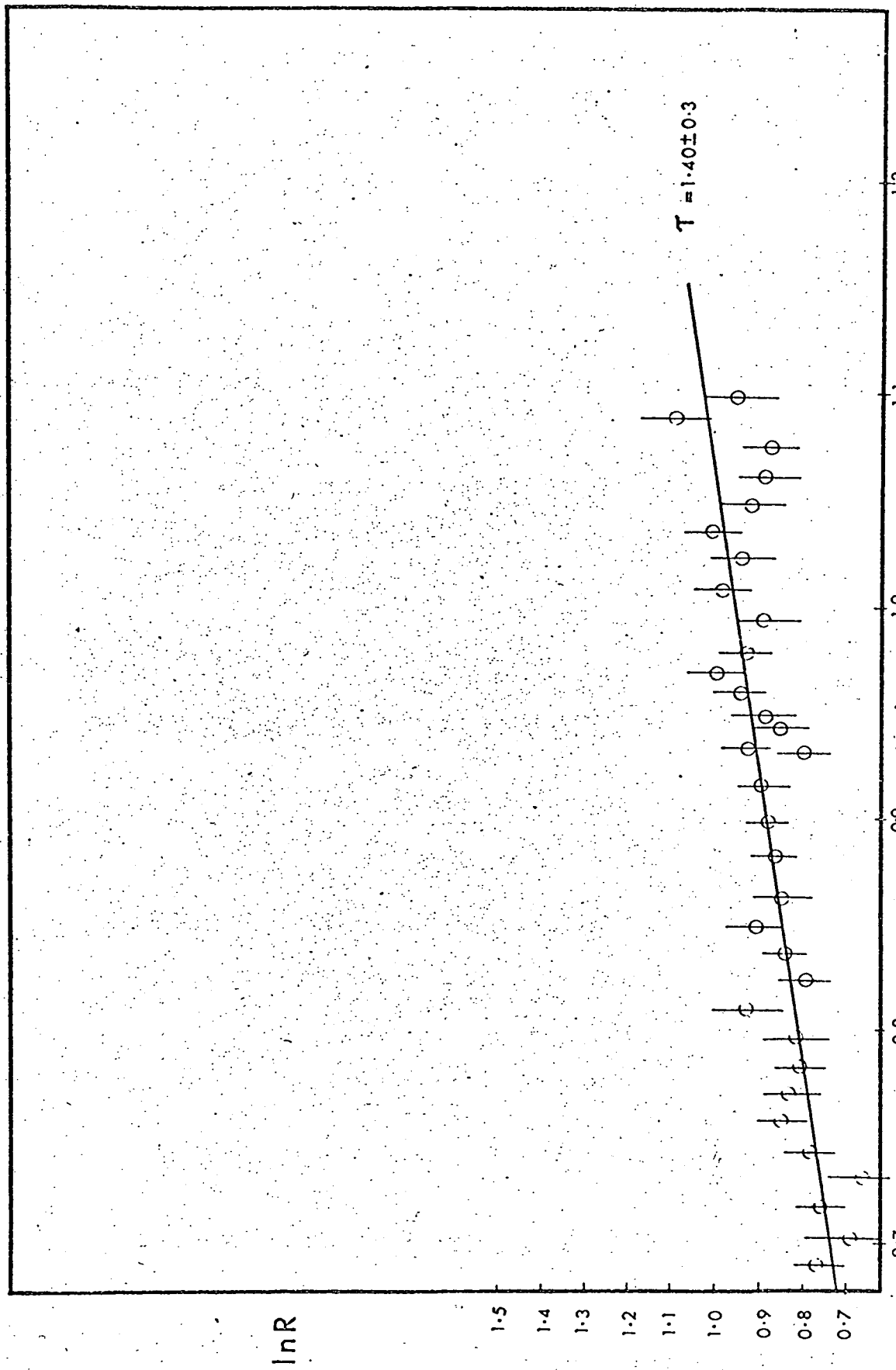

Plot of lnR versus $t_2 - t_1$ showing the lifetime of the $^3P_2$ state

Figure 3-14

no evidence for any contribution from the $^3D_3$ state. This predominance of the P states is in accordance with the cross section measurements by Borst [BOR 1969].

Because of the mechanical changes required to alter the beam path these experiments had to be performed on different occasions. As the precision depends upon the reproducibility of the velocity distribution it was necessary to determine the stability of these results to possible variations, in particular in the source temperature. The observations at the bottom of Table [3-4] illustrate this point. Since the possible temperature drift is only 1-2°K at most, any error from this source is small in comparison with the statistical uncertainty.

On first consideration of the results it appeared that the half life obtained was rather short. The value of 1.3×10^{-3} seconds means that a large percentage ($\sim$ 80%) of the metastable beam has decayed before reaching the detector in the case of the longer flight path. An attempt to verify this value was made by fitting a Maxwellian distribution to the data obtained for the longer flight path by using the expression obtained in equation [3-3]. An estimate for the half life of 2.1 ms was achieved. By convoluting the excitation pulse width and exciter dimensions an estimate of 1.5 ms was obtained. Therefore the value of 1.3 ms ± .17 seems additionally confirmed.

Conclusions

The measured ratio for the excitation cross sections to the $^3P_2$ and $^3P_0$ states was found to be almost independent of energy in

the range 10 - 15eV and within experimental error identical to that calculated by McConnel et al [MCC 1968].

The lifetime of the $^3P_2$ state, $1.3 \pm 0.2 \times 10^{-3}$s, found in this work is in excellent accord with that observed by Baltayan et al [BAL 1965] who monitored the $^3P_2$ concentration by using the absorption corresponding to the $6^3P_2 \rightarrow 7^3S_1$ transition. Both these results, however, differ substantially from the value 1.3×10^{-4}S reported by Tittel [TIT 1965] on the basis of line broadening measurements. This latter work was primarily directed to the measurement of line broadening cross sections for the rare gases and the natural life may be in error due to residual background impurities, possibly N_2 in the cell. Since the present results and those of Baltayan et al using a quite different technique are in agreement, the longer lifetime would seem secure.

The $^3P_0$ lifetime, $1.3 \pm 0.4 \times 10^{-3}$s, is rather different to that reported by McAlduff et al [MCA 1965] but as the error limits on their rate constant correspond to lifetimes between 4 and 20 ms the disagreement is not severe. In earlier work Kimbell et al [KIM 1960] found a half life of 4.2×10^{-4}s by absorption measurements on the forbidden line at 2656 Å ($6^3P_0 \rightarrow 6^1S_0$). It is possible that this value may be appropriate for Hg isotopes with nuclear spin.

For isotopes with zero nuclear spin (about 70% of the natural abundance are of this type) J is a good quantum number and transitions from the 6^3P_0 to the ground state are forbidden for electric dipole, quadrupole and magnetic dipole radiation. Transitions from the 6^3P_2 are similarly forbidden though this state can decay via

magnetic dipole radiation to the $^3P_1$.

In contrast, isotopes with nuclear spin have F as a good quantum number and can interact with the $^3P_1$ state so that their natural life will be considerably shorter. Radiation for the $^3P_2$ and $^3P_0 \rightarrow {}^1S_0$ transitions in respect of these isotopes has been observed [RAY 1927], [FUK 1926], [MRO 1945], [KES 1950]. The natural life of these states of mercury would therefore be expected to depend upon the isotope and the F quantum number. Recent values for the lifetime of the 6^3P_0 state for the odd isotopes of mercury were $\tau_{199} = 1.7S$, $\tau_{201} = 2.65S$ [BIG 1967] and these values are in considerable disagreement with the value for the lifetime of the $^3P_0$ obtained in this work ($\tau = 1.3 \pm 0.4 \times 10^{-3} S$).

It was pointed out that the apparently short lifetimes determined in this experiment might be due to attenuation of the metastable beam by background gas. The fact that the lifetime evaluated is due to decay and not to scattering by the background gas can be confirmed by considering the ratio of the metastable removed by background scattering to that lost by decay. In this work even with a pessimistic assumption of 10^3 $\mathring{A}^2$ for the total cross section the scattering loss is only $\sim$10% of that due to decay. In the experiments of Van Dyck et el [VAN 1972(b)] the corresponding ratio was about 25% and they were able to demonstrate by changing the background pressure that their measured lifetime was not perturbed at this level. The questions now remain about possible modes of decay for the two states since the beam decays by more than 30% between the two detector positions and there seems little doubt that the decay measured is due to the dominant species in the beam (i.e. zero spin isotopes).

The decay of the 6^3P_2 state is presumably by magnetic dipole to the $^3P_1$. However, no similar mechanism can be proposed for the $^3P_0$ state and in view of the lack of decay processes (even two photon electric dipole radiation is forbidden) it would appear that the lifetime values found for the odd isotopes of mercury (τ_{199}=1.7S, τ_{201}=2.6S) [BIG 1967] are more plausible than the values of the $^3P_0$ lifetime found in this work ($\tau \simeq 1.3 \pm 0.4 \times 10^{-3}$S). It is thus possible that the initial assumption that all m_J states of the $^3P_2$ are equally populated is incorrect and that some degree of polarisation exists in the beam i.e. $m_J = 0$ is preferentially populated. On the other hand the assumption may be correct and then some other decay process for the $^3P_0$ state must be sought.

Chapter 4

Theoretical Interatomic Potential Energy Curves

4 Theoretical Interatomic Potential Energy Curves.

Although collisions involving metastable atoms are an important process in gas phase experiments, there are relatively few theoretical papers on the subject eg [BUC 1952], [MAS 1967], [KOL 1969]. Most theoretical papers on collisions of excited species treat the cases of optically allowed excitation [WAT 1967].

The description and understanding of many of the most interesting processes in atomic and molecular physics involves a knowledge of the molecular wave functions and potential surfaces accessible to a set of interacting atoms. This can be looked upon as the calculation of the interatomic potential energy curve in a diatomic molecule [BRO 1971].

This chapter presents a crude calculation of the theoretical potential curves for the molecular states involved in a collision between Hg* ($^3P_2$) and an alkali metal M. Such potentials, together with the ground state potential curves for (Hg-M) and (Hg-M)+ are required in a consideration of possible inelastic processes which might occur in these collisions.

In the present work the systems of interest involve the collisional interactions of Hg*($^3P_2$) with Na, K and Rb. This discussion will be limited to the interaction of Hg*($^3P_2$) and K($^2S_{\frac{1}{2}}$) as a typical case. Firstly, a description of the metastable atom will be given followed by a description of the possible molecular states which arise in the collision. A method for the calculation of the interatomic potentials for diatomic systems using the Heitler-London [HEI 1927] method is then presented.

A computer program for the calculation of the terms involved is then discussed and the application of this method to the system $Hg^*(^3P_2) + K(^2S_{\frac{1}{2}})$ is then considered. Finally theoretical potential energy curves for this calculation are presented.

Metastable Mercury.

Considering only the two outermost 6S and 6p electrons of Hg and writing the determinental wave function for these electrons as

$$S\alpha P_o\beta = \frac{1}{\sqrt{2}} \left| 6S\,\alpha(1)\ 6po\ \beta(2) - 6po\,\alpha(1)\ 6S\ \beta(2) \right\rangle$$

where α, β refer to the spin wave functions and the subscripts to the n_l quantum numbers, then the Russel Saunders wave functions for the (J,m_J) states may be written in terms of the Clebsch-Gordan coefficients as:

$$
\begin{array}{lll}
^3P_2 & M_J = 2 & \psi = S\alpha p_1\alpha \\
 & M_J = 1 & \psi = \tfrac{1}{2}\left[S\alpha p_1\beta + S\beta p_1\alpha\right] + \frac{1}{\sqrt{2}}\ S\alpha p_0\alpha \\
 & M_J = 0 & \psi = \frac{1}{\sqrt{3}}\left[S\alpha p_0\beta + S\beta p_0\alpha\right] + \frac{1}{\sqrt{6}}\left[S\beta p_1\beta + S\alpha p_{-1}\alpha\right] \\
 & M_J = -1 & \psi = \tfrac{1}{2}\left[S\alpha p_{-1}\beta + S\beta p_{-1}\alpha\right] + \frac{1}{\sqrt{2}}\ S\beta p_0\beta \\
 & M_J = -2 & \psi = S\beta p_{-1}\beta \\
^3P_1 & M_J = 1 & \psi = \tfrac{1}{2}\left[S\alpha p_1\beta + S\beta p_1\alpha\right] - \frac{1}{\sqrt{2}}\ S\alpha p_0\alpha \\
 & M_J = 0 & \psi = \frac{1}{\sqrt{2}}\left[S\beta p_1\beta - S\alpha p_{-1}\alpha\right] \\
 & M_J = -1 & \psi = \tfrac{1}{2}\left[S\alpha p_{-1}\beta + S\beta p_{-1}\alpha\right] + \frac{1}{\sqrt{2}}\ S\beta p_0\beta \\
^3P_0 & M_J = 0 & \psi = \frac{1}{\sqrt{3}}\left[S\beta p_1\beta + S\alpha p_{-1}\alpha\right] - \frac{1}{\sqrt{6}}\left[S\alpha p_0\beta + S\beta p_0\alpha\right]
\end{array}
$$

4.1

Wave functions for the 6S and 6p electrons have been calculated by Darwall et al [DAR 1970] [DAR 1972]. Limited HARTREE-FOCK wave functions were computed for the ^3P states of mercury in which exchange between the 6S and 6p electrons was included explicitly

and the exchange of both outer electrons with the core was represented by an approximation due to Slater [SLA 1951] using Herman-Skillman core wave functions [HER 1963].

$$V_{\text{exch: core}} = -6\left[\frac{3}{32\pi^2}\sum_{\text{core}} 2(2\ell+1)\,\psi_{n\ell}(r)^2/r^2\right]^{\frac{1}{3}} \qquad 4\text{-}2$$

The computed wave functions were tested by calculating the polarisability of the atom but unfortunately the values obtained did not agree particularly well with the experimental values [DAR 1972] although they did provide better agreement than coulomb wave functions used by McConnell et al [MCC 1968]. It was decided to use Darwall's wave functions for the 6S and 6p electrons of mercury in this calculation. A one electron coulomb wave function was chosen for the potassium 4S electron. The coulomb and Hartree-Fock orbitals were fitted by a linear combination of three Slater orbitals [TABLE 4.1].

$$\psi = A_1 r^{n_1} \exp(-\alpha_1 r) + A_2 r^{n_2}(-\alpha_2 r) + A_3 r^{n_3} \exp(-\alpha 3 r) \qquad 4\text{-}3$$

TABLE 4.1

Orbital	A_1	A_2	A_3	n_1	n_2	n_3	α_1	$\alpha 2$	$\alpha 3$
Hg 6S	-6.132	31.44	-33.38	2	1	1	1.20	1.60	2.00
Hg 6p	13.52	-11.09	-11.24	1	1	2	1.00	1.20	1.80
K 4S	.2877	.4597	-1.263	2	1	1	.5663	.7762	1.0194

Molecular States.

In a collision between two atoms the system will start off in a state corresponding to Hund's case (c) but as the interatomic separation (R) decreases so it will tend more towards Hund's case (a). For Hund's case (c) the spin orbit coupling between L and S is strong compared with the axial interatomic field. In this case

L and S couple to give J and it is only the components of J along the internuclear axis that will couple together. In this instance only the component Ω of the sum of the two angular momenta J along the axis is well defined.

$$\Omega = | M_{J_1} + M_{J_2} | \qquad 4\text{-}4$$

At smaller separations the interatomic field may become sufficiently strong that both the L's are coupled to it. In this case it is only the projections M_L along the internuclear axis that are well defined and the total angular momentum quantum numbers of the molecule about the axis are given by

$$\Lambda = | M_{L_1} + M_{L_2} | \qquad 4\text{-}5$$

The electronic angular momentum Ω is given by adding Λ and S vectorially, where S, the spin angular momentum quantum numbers are given by adding the spins of the two atoms vectorially. This is known as Hunds case (a). However, it should be noted that even at the distance of closest approach the system may only be described by some intermediate form of coupling of the angular momenta. This is particularly true for systems involving heavy atoms.

Table [4.2] presents the molecular states in Λ S notation for Hunds case (a), in which the bonding interaction is much greater than the spin orbit coupling.

TABLE 4.2

Type	Number
$^4\pi$ $M_J = {}^5/_2, {}^3/_2, \frac{1}{2}, \frac{1}{2}$	8
$^4\Sigma$ $M_J = {}^3/_2, \frac{1}{2}$	4
$^2\pi$ $M_J = {}^3/_2, \frac{1}{2}$	(Two kinds)4 X2
$^2\Sigma$ $M_J = \frac{1}{2}$	(Two kinds)2 X 2

There is a total of 24 states and unfortunately no information is available on the energy ordering of these states. One could say fairly confidently that one of the $^2\Sigma$ will show a pronounced minimum in the potential corresponding to a normal bond [Fig 4.1(a)], whereas the $^4\Sigma$ state would probably be highly repulsive [Fig. 4.1(b)]. Table [4-3] shows the states involved for Hund's case (c). Here the Ω designation is appropriate where the J state of the heavy atom is left intact.

TABLE 4.3

Atomic States	(JJ) States
$^3P_2 + {}^2S_{\frac{1}{2}}$	$^5/_2$, $^3/_2$, $\frac{1}{2}$, $\frac{1}{2}$, $^3/_2$
$^3P_1 + {}^2S_{\frac{1}{2}}$	$^3/_2$, $\frac{1}{2}$, $\frac{1}{2}$
$^3P_0 + {}^2S_{\frac{1}{2}}$	$\frac{1}{2}$

A total of 18 states is produced in this case although there are also an additional 6 states from the $^1P_1$ state of atomic Hg, to be considered, making a total of 24 states in all. Unfortunately it is not possible to unambiguously correlate the states characterised by Ω and the molecular states. No spectroscopic data is available to shed light on any of these systems.

In attempting to produce a correlation diagram the following assumptions might be used:

1) The $^2\Sigma$ state with the outer pairing lies lowest and the $^2\Sigma$ state with the inner pairing lies highest.

2) The $^4\pi$ states lie lower than the $^4\Sigma$ states.

3) The $^2\pi$ state with inner pairing will lie close to the $^4\pi$.

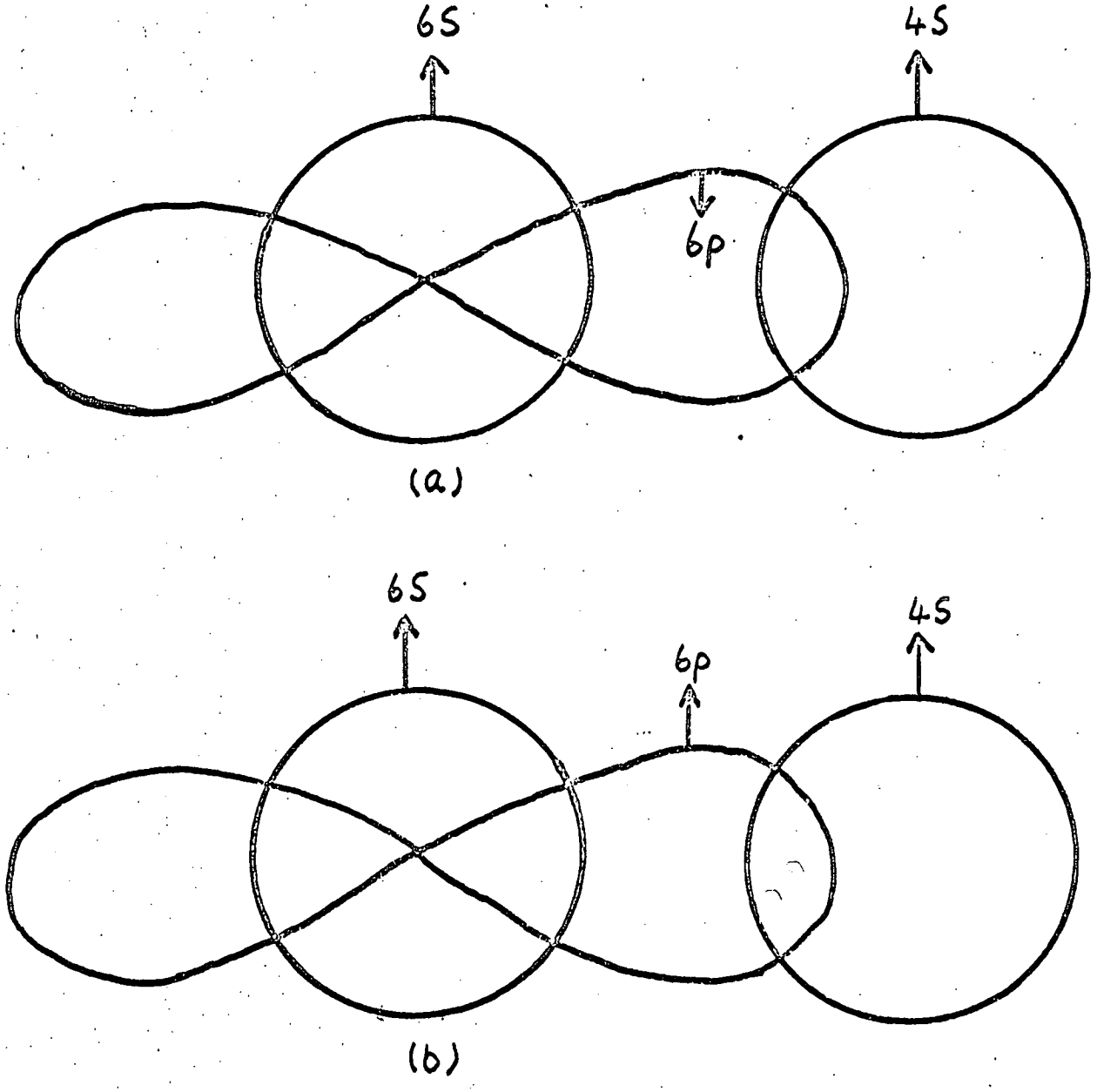

Schematic showing bonding schemes

a) $^2\Sigma$ outer

b) $^4\Sigma$

Figure 4-1

4) The $^4\Sigma$ is close in energy to the $^2\Sigma$ (inner) since the outer electron configuration is identical.

It is certain that the $^4\pi_{5/2}$ state must come from $^3P_2$ and that the $^1P_1$ state can only give rise to doublet states.

With reservations two possible correlation diagrams are shown in Fig [4.2]. There is a personal preference for Fig [4.2(a)] since the $^2\Sigma$ and $^4\Sigma$, which have the same outer configuration, are close together.

It should be noted that five molecular states evolve from the interaction of $Hg(^3P_2)$, the dominant species in the metastable beam experiment, with $K(^2S_{\frac{1}{2}})$. Depending on the order of the molecular states the following tentative correlations may be made [TABLE 4.4].

TABLE 4.4

M_J	M_S	Ω	Molecular State
2	$^1/_2$	$^5/_2$	$^4\pi\ ^5/_2$
2	$-\frac{1}{2}$	$^3/_2$	$^4\pi\ ^3/_2$
1	$\frac{1}{2}$	$^3/_2$	$^4\Sigma\ ^3/_2$
1	$-\frac{1}{2}$	$^1/_2$	$^4\pi\ ^1/_2$
0	$^1/_2$	$^1/_2$	$^4\Sigma\ ^1/_2$

Wave functions for these states are required in any potential calculation. The simplest wave function is that of the $|2\ 2\rangle$ state of Hg combining with the $|\frac{1}{2}\ \frac{1}{2}\rangle$ state of K which can be written as a single determinant.

$$||\ 6S\,\alpha\, 6p_1\,\alpha\, 4S\,\alpha\ ||$$ 4-6

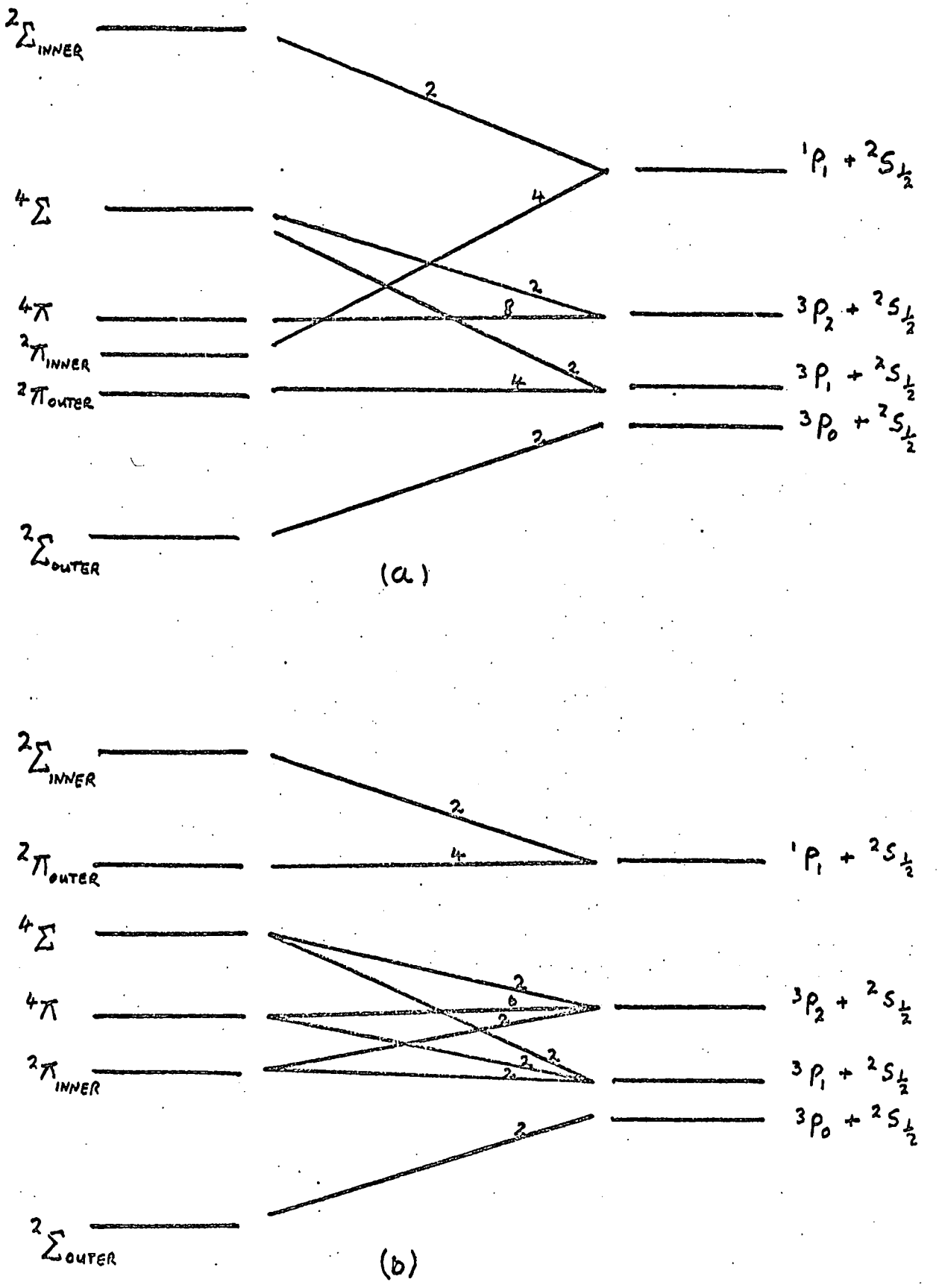

Two possible correlation diagrams for Hg* + K

Figure 4-2

Zeroth order molecular wave functions of this kind are used in the calculation.

Potential Energy Curve Calculations.

The method of calculation is that introduced by Heitler and London for the hydrogen molecule [HEI 1927]. The essential feature of this method is the assumption that the electronic structure of the atoms is largely preserved in a molecule and that the energy of the covalent bond is associated with exchange of electrons between atoms [PAU 1935] [SLA 1963].

Kodaira et al [KOD 1971] calculated potential energy curves for the system He* + He by the Heitler London method using Slater type orbitals and their results for the collisional transfer of triplet excitations between helium atoms agree reasonably well with calculations based on more rigorous potentials [KOL 1969]. A similar method is proposed here but firstly it is useful to examine the potential energy curves for two hydrogen atoms in order to understand the exact mechanism of the binding as described by the Heitler London method.

The hydrogen atom in its ground state has an electron in a 1 S orbital. If the nucleus is labelled a and the electron 1 then the wave function can be written as

$$\psi_a = a\,(1) \qquad 4\text{-}7$$

The second atom (nucleus b, electron 2) has a wave function

$$\psi_b = b\,(2) \qquad 4\text{-}8$$

The wave function for the total system can be represented as

$$\psi_{\pm} = \left[2 \pm 2S^2\right]^{-\frac{1}{2}} \left[a(1)\,b(2) \pm a(2)\,b(1)\right] \qquad 4\text{-}9$$

$$\text{where } S = \int a(1)\,b(1)\,dv_1 \qquad 4\text{-}10$$

Equation [4-9] satisfies the condition that the wave function for H_2 must give equal chance of each electron being around the two nuclei. When spin is included in the wave function then since ψ_+ is symmetric to electron exchange it must be combined with an anti-symmetric spin function in order to satisfy the Pauli exclusion principle. This results in a singlet state

$$^1\psi_+ = [2 + 2S]^{-\frac{1}{2}} [a(1)b(2) + a(2)b(1)] \frac{1}{\sqrt{2}} [\alpha(1)\beta(2) - \alpha(2)\beta(1)] \qquad 4\text{-}11$$

whereas ψ_- becomes a triplet state

$$^3\psi_- = [2 - 2S]^{-\frac{1}{2}} [a(1)b(2) - a(2)b(1)] \begin{cases} \alpha(1)\alpha(2) \\ \frac{1}{\sqrt{2}}[\alpha(1)\beta(2) + \alpha(2)\beta(1)] \\ \beta(1)\beta(2) \end{cases} \qquad 4\text{-}12$$

The Hamiltonian for the system is

$$H = H_a + H_b + H^1 \qquad 4\text{-}13$$

where H_a and H_b are the Hamiltonians for atoms a and b and H^1 is given by:

$$H^1 = -\frac{1}{ra_2} - \frac{1}{rb_1} + \frac{1}{r_{12}} + \frac{1}{R} \qquad 4\text{-}14$$

where ra_2 is the distance from electron 2 to nucleus a

rb_1 is the distance from electron 1 to nucleus b

r_{12} is the distance between electron 1 and 2

R is the internuclear separation.

The energy of the system is then given by

$$E = \int \psi H \psi \qquad 4\text{-}15$$

Making use of the fact that a(1) is an eigen function of H_a and b(2) is an eigen function of H_b then

$$E = 2E_H + \iint \psi H^1 \psi \, dv_1 dv_2 \qquad 4\text{-}16$$

where $\psi = \psi_+$ the energy is given by

$$E_+ = 2E_H + \frac{Q + A}{1 + S^2} \qquad 4\text{-}17$$

and where $\psi = \psi_-$ the energy is

$$E_- = 2E_H + \frac{Q - A}{1 - S^2} \qquad 4\text{-}18$$

in which

$$Q = \iint a^2(1)\, b^2(2) \left[-\frac{1}{rb_1} - \frac{1}{ra_2} + \frac{1}{r_{12}} + \frac{1}{R} \right] dv_1 dv_2 \qquad 4\text{-}19$$

and

$$A = \iint a(1)\, b(1) \left[-\frac{1}{rb_1} - \frac{1}{ra_2} + \frac{1}{r_{12}} + \frac{1}{R} \right] a(2) b(2) dv_1 dv_2 \qquad 4.20$$

Q is called the coulomb integral and A is termed the exchange integral. The majority of the integrals which have to be calculated

e.g. $$\iint a^2(1)\, b^2(2) \left[-\frac{1}{rb_1} \right] dv_1 dv_2$$

can be evaluated analytically [COU 1942].

However integrals of the type

$$\iint a^2(1)\, b^2(2) \frac{1}{r_{12}}\, dv_1 dv_2$$

and more especially

$$\iint a(1)\, b(1) \frac{1}{r_{12}}\, a(2)\, b(2)\, dv_1 dv_2$$

are extremely difficult to determine.

The evaluation of such integrals is normally carried out by using the Neumann expansion for $1/r_{12}$ in terms of elliptical co-ordinates. However, the mathematical structure of the expansion is unfortunately not all that simple. Huzinaga [HUZ 1967] recently reviewed the literature on the evaluation of such molecular integrals and he also gave a thorough coverage of the evaluation of integrals over Gaussian basis sets. The Gaussian basis sets render evaluation of such integrals easier. However, they have a drawback in that when viewed as representing atomic wave functions they behave very poorly

near the origin and at large distances from the nucleus. In this respect Slater type functions are the better of the two and it is essential to discover whether the marked simplicity in the evaluation of these integrals involving Gaussian orbitals offers enough compensation for the poor characteristics as atomic functions. For the case considered in this chapter the integrals at intermediate and large separations are of greatest interest and therefore Slater type orbitals are used.

A general integral program is an essential part of the calculation of potential energy curves and the next section presents a simple approximate method of evaluation of $\frac{1}{r_{12}}$ type integrals free from the mathematical complexities of the other formulations.

A method for Solution of Coulomb and Exchange $\frac{1}{r_{12}}$ Integrals

These calculations were carried out on the IBM 360/50 at the Edinburgh Regional Computing Centre. A flow diagram of the computer program is shown in Appendix II.

In this program an internuclear axis is defined and two nuclei are placed at positions A and B on this axis at a distance R apart [Fig 4-3]. A field of integration is then defined in the first quadrant and divided up into a number of boxes of equal volume. The centres of these boxes are then considered to be the possible positions of the electrons.

In the outer cycle of the routine the co-ordinates of all possible positions of electron 1 are set up. The wave functions for the electrons can be read in either in tabulated form or as Slater

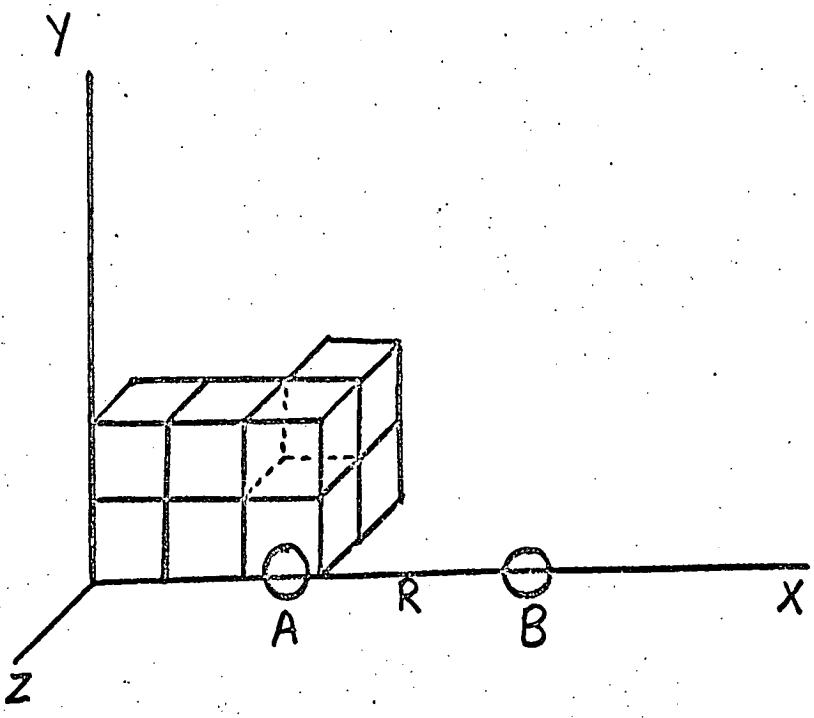

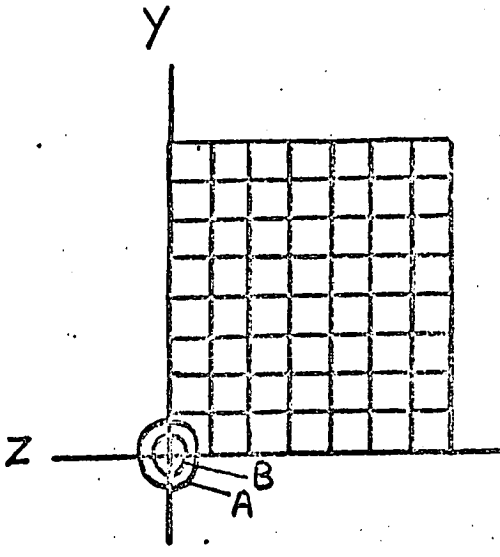

Schematic illustrating the division of the integration field into boxes

Figure 4-3

fitted combinations of atomic orbitals. The values of the wave functions for electron 1 with respect to nuclei A and B are then generated for a fixed position of electron 1 and the value of $a^2(1)$ or $a(1)b(1)$ is found where $a(1)$ is the value of wave function of electron 1 with respect to nucleus A. This essentially determines the amount of charge at the centre of each box. This amount of charge is taken to be uniform throughout the box. For each position of electron 1, electron 2 can move to every position in all four quadrants and the wave function for electron 2 with respect to A and B is evaluated each time and therefore $b^2(2)$ and $a(2)b(2)$ can be determined (Provision is make for the possibility of electrons 1 and 2 being located in the same box. This situation is treated as two overlapping cubes of uniformly distributed charge). The distance between the electrons is then computed and values for $a^2(1)\ b^2(2)\frac{1}{r_{12}}$ and $a(1)b(1)\frac{1}{r_{12}}\ a(2)b(2)$ are obtained. A summation is then carried out over all positions of electron 2 in the four quadrants while electron 1 remains in the same position. In the outer cycle electron 1 is then moved to a new position and the procedure is repeated keeping a running total in the outer loop. Electron 1 moves only throughout the first quadrant. The complete sum is then multiplied by four to take into account all four quadrants.

Since extensive calculations have been performed on H+ H e.g. [MCL 1960] it seemed sensible to test this method using two hydrogen 1S orbitals which were:

$$\psi = \pi^{-\frac{1}{2}}\ e^{-r} \qquad 4.21$$

Table [4-5] shows the values obtained for two internuclear separations by this method and also those obtained by Slater [SLA 1963] for the integrals

$$\int \psi^2(1)\ \psi^2(2)\frac{1}{r_{12}}\ dv_1 dv_2$$

TABLE 4-5

Internuclear Separation	Integral Value	
	Slater	This Work
3 a.u	.3198	.3170
4 a.u	.2476	.2454

These values were obtained with a box volume of 0.4219 $(a.u)^3$ and a field of integration of 18 a.u along the X axis and 6 a.u on both the Y and Z axes. Nuclei A and B were situated at 6 a.u and 9 a.u and 10 a.u respectively.

A variety of other values for the field and box dimensions was tried. It was found that greatly increasing the field of integration had little effect since the values of the wave functions at these distances are very small. Not surprisingly it was also found that the smaller the value of the internuclear separation (R) then the smaller the box size required to give the same accuracy.

Unfortunately as the accuracy was increased so was the amount of computing time required. It was therefore decided to normalise these integrals using the knowledge that

$$N = \int \psi^2(1)\ \psi^2(2)\ dv_1 dv_2$$

should equal unity. By dividing the computed value of the integral by the value of N obtained in the calculation the following results were obtained [Table 4.6].

TABLE 4-6

Ra.u	Coulomb $1/r_{12}$ Slater	Coulomb $1/r_{12}$ This Work	Exchange $1/r_{12}$ Slater	Exchange $1/r_{12}$ This Work	Normalisation
1.5	.4904	.4905	.2969	.2965	.980
2.0	.4259	.4263	.1842	.1840	.975
2.5	.3684	.3685	.1066	.1062	.975
3.0	.3198	.3202	.0585	.0584	.990
4.0	.2476	.2478	.0156	.0156	.990

These results were very encouraging although evaluation of these integrals at each separation required about 10 minutes of computer time. These values were obtained with the same dimensions mentioned previously. It seemed reasonable to attempt to use this method, with normalisation, for the Hg* - K case although the computer time might be considerable if an accuracy of $0.96 < N \leqslant 1.0000$ is required.

Before embarking on the computations for Hg* - K the method was further tested by a consideration of hydrogen fluoride. This seemed a useful test for the program since S and P electrons are involved in the binding, a situation which is similar to that in Hg* - K. The data for comparison in this case was that obtained by Ransil [RAN 1960].

Cartesian axes were chosen with the hydrogen nucleus at $(x_1, 0, 0)$ and the fluorine nucleus at $(x_2, 0, 0)$. The value of the bond length used was 1.733 a.u and the Slater type functions were as follows

$$\psi_1 = \psi\ (F,1S) = \left(\frac{\Sigma_1^3}{\pi}\right)^{\frac{1}{2}} \exp(-\Sigma_1 r)$$

$$\psi_2 = \psi\ (F,2S) = \left(\frac{\Sigma_2^5}{3\pi}\right)^{\frac{1}{2}} r \exp(-\Sigma_2 r)$$

$$\psi_3 = \psi\ (F,2p_x) = \left(\frac{\Sigma_2^5}{\pi}\right)^{\frac{1}{2}} x \exp(-\Sigma_2 r)$$

$$\psi_4 = \psi\ (F,2p_z) = \left(\frac{\Sigma_2^5}{\pi}\right)^{\frac{1}{2}} Z \exp(-\Sigma_2 r)$$

$$\psi_5 = \psi\ (F,2py) = \left(\frac{\Sigma_2^5}{\pi}\right)^{\frac{1}{2}} y \exp(-\Sigma_2 r)$$

$$\psi_6 = \psi\ (H,1S) = \left(\frac{\Sigma_3^3}{\pi}\right)^{\frac{1}{2}} \exp(-\Sigma_3 r)$$

where $\Sigma_1 = 8.7$, $\Sigma_2 = 2.6$, $\Sigma_3 = 1.0$

The results which were obtained are shown in Table [4-7] in which $I = \mu\gamma \frac{1}{r_{12}} \lambda\sigma$ where μ, γ, λ and σ are atomic wave functions. I_1 are the results of Ransil, I_2 are the results of this work and N is the normalisation used in this work.

TABLE 4-7

μ	γ	λ	σ	I_1	I_2	N
6	6	2	2	.5016	.4998	.9897
6	2	6	2	.1642	.1638	.9897
6	3	6	3	.1121	.1112	.9707
6	6	3	3	.5277	.5259	.9707
6	6	4	4	.4886	.4864	.9900
6	4	6	4	.0277	.0274	.9900

These results were obtained with a field of integration measuring 16 a.u on the X axis and 6 a.u on the Y and Z axes. The hydrogen nucleus was situated at 6.0 a.u along the x axis and the fluorine nucleus at 7.733 a.u. The box volume used was 0.4219 $(a.u)^3$ and the above calculations took 13 minutes of computer time. The amount of computer time was again large for the required accuracy. However it was decided to continue and use this method in a crude calculation of the potential surfaces for $Hg^*(^3P_2) + K(^2S_{\frac{1}{2}})$ since the accuracy was good.(i.e. greater than 98% in all cases [Table 4-7].)

Calculation of the interatomic potential energy curves for $Hg^*(^3P_2) + K(^2S_{\frac{1}{2}})$

Calculations of the interatomic potential in the m_J, m_S coupling scheme were made using the limited Hartree Fock Slater two electron orbitals already calculated for the $^3P_2$ state of Hg [DAR 1972]. These were combined with the wave function for potassium to form linear combinations of Slater determinants that preserved J and m_J as good quantum numbers. The wave functions which were used are listed in Table [4-1].

The simplest interaction arises from the collision of $^3P_{22} + ^2S_{\frac{1}{2},\frac{1}{2}}$ and can be represented by the following zeroth order Heitler London three electron Slater determinant [4-22].

$$\psi = \frac{1}{\sqrt{6}} \begin{vmatrix} 6S\,\alpha(1) & 6p_1\,\alpha(1) & K\,\alpha(1) \\ 6S\,\alpha(2) & 6p_1\,\alpha(2) & K\,\alpha(2) \\ 6S\,\alpha(3) & 6p_1\,\alpha(3) & K\,\alpha(3) \end{vmatrix} \qquad 4\text{-}22$$

An approximate Hamiltonian using the core potentials (with exchange) of the unperturbed atoms together with the specific electron/electron repulsion terms among the three valence electrons was then chosen.

$$H = -\tfrac{1}{2}\nabla_1^2 - \tfrac{1}{2}\nabla_2^2 - \tfrac{1}{2}\nabla_3^2 - VHg(1) - VHg(2) - VHg(3) - VK(1) - VK(2) - VK(3) + \frac{1}{r_{12}} + \frac{1}{r_{23}} + \frac{1}{r_{13}} + \frac{Z_A Z_B}{R} \qquad 4\text{-}23$$

where $(-\tfrac{1}{2}\nabla_1^2)$ = kinetic energy of electron 1

$VHg(1)$ = potential energy between the mercury core and electron 1

$\frac{1}{r_{12}}$ = electron/electron repulsion term

$\frac{Z_A Z_B}{R}$ = nuclear/nuclear repulsion term with the cores taken to be point charges.

When the wave function [4-22] is combined with the Hamiltonian [4-23] and substituted in the expression for the energy of the state [4-15] then a vast number of terms require to be computed. A more detailed analysis is performed in Appendix III for this specific example although it is obvious by inspection that terms such as

$$\int K\,\alpha\,(2)\,\left[-VHg(1)\right]\,K\,\alpha\,(2) \qquad 4\text{-}24$$

$$\int 6p\,\alpha\,(3)\,\left[-VK(3)\right]\,6p\,\alpha\,(3) \qquad 4\text{-}25$$

$$\int 6p\,\alpha\,(1)\,K\,\alpha\,(2)\,\frac{1}{r_{12}}\,6p\,\alpha\,(1)\,K\,\alpha\,(2) \qquad 4\text{-}26$$

$$\int 6S\,\alpha\,(1)\,K\,\alpha\,(2)\,\frac{1}{r_{12}}\,6S\,\alpha\,(1)\,K\,\alpha\,(2) \qquad 4\text{-}27$$

$$\int 6S\,\alpha\,(1)\,K\,\alpha\,(1) \qquad 4\text{-}28$$

are required in the computation.

A list of all the possible integrals required was then drawn up and computed for the various internuclear separations required. However due to the orthogonality of the wave functions and the fact that the overlap integral $\int 6p_1\,\alpha\,(1)\,K\,\alpha\,(1)$ is zero then the total number of terms required was reduced.

Wherever possible the integrals were evaluated analytically by the methods of Coulson [COU 1942] eg [4-24], [4-25] and [4-28] whereas $\frac{1}{r_{12}}$ type integrals eg [4-26] and [4-27] were evaluated using the summation method presented previously.

All the required integrals were computed at the one time for a specific internuclear separation since this only required one evaluation of the interelectron distances. Initially, for a normalisation factor greater than .96, the complete computation at one internuclear separation required 89 minutes. This is excessive and therefore calculations were attempted with a larger box size and hence with less accuracy. A comparison of the values obtained for

certain integrals with the two normalisation values is shown in Table [4-8].

TABLE 4-8

Inter-nuclear Separation	Integral	Normal-isation	Normalised Value	Time Required
13 a.u	$6p(1)6p(1)\frac{1}{r_{12}}4S(2)4S(2)$	0.9705	0.0799	89
13 a.u	$6p(1)6p(1)\frac{1}{r_{12}}4S(2)4S(2)$	0.8867	0.0804	11
13 a.u	$6p(1)4S(1)\frac{1}{r_{12}}6p(2)4S(2)$	0.9705	0.0005	89
13 a.u	$6p(1)4S(1)\frac{1}{r_{12}}6p(2)4S(2)$	0.8867	0.0005	11
7 a.u	$6p(1)6p(1)\frac{1}{r_{12}}4S(2)4S(2)$	0.9865	0.1455	69
7 a.u	$6p(1)6p(1)\frac{1}{r_{12}}4S(2)4S(2)$	0.8957	0.1470	10
7 a.u	$6p(1)4S(1)\frac{1}{r_{12}}6p(2)4S(2)$	0.9865	0.0278	69
7 a.u	$6p(1)4S(1)\frac{1}{r_{12}}6p(2)4S(2)$	0.8957	0.0282	10

The results are in good agreement and therefore the method using the larger box size was adopted. Once the integrals had been computed the relevant algebra was performed for all possible states (Appendix III) for each internuclear distance and a value for the potential energy was obtained. These values were calculated for internuclear separations between 5 a.u and 14 a.u. The results are displayed graphically. [Figs [4.4] [4.5] [4.6] [4.7] [4.8].]

Although the values obtained for each term are accurate to within 2% the total error bars are large due to the addition of errors in the summation of all the terms involved for each point.

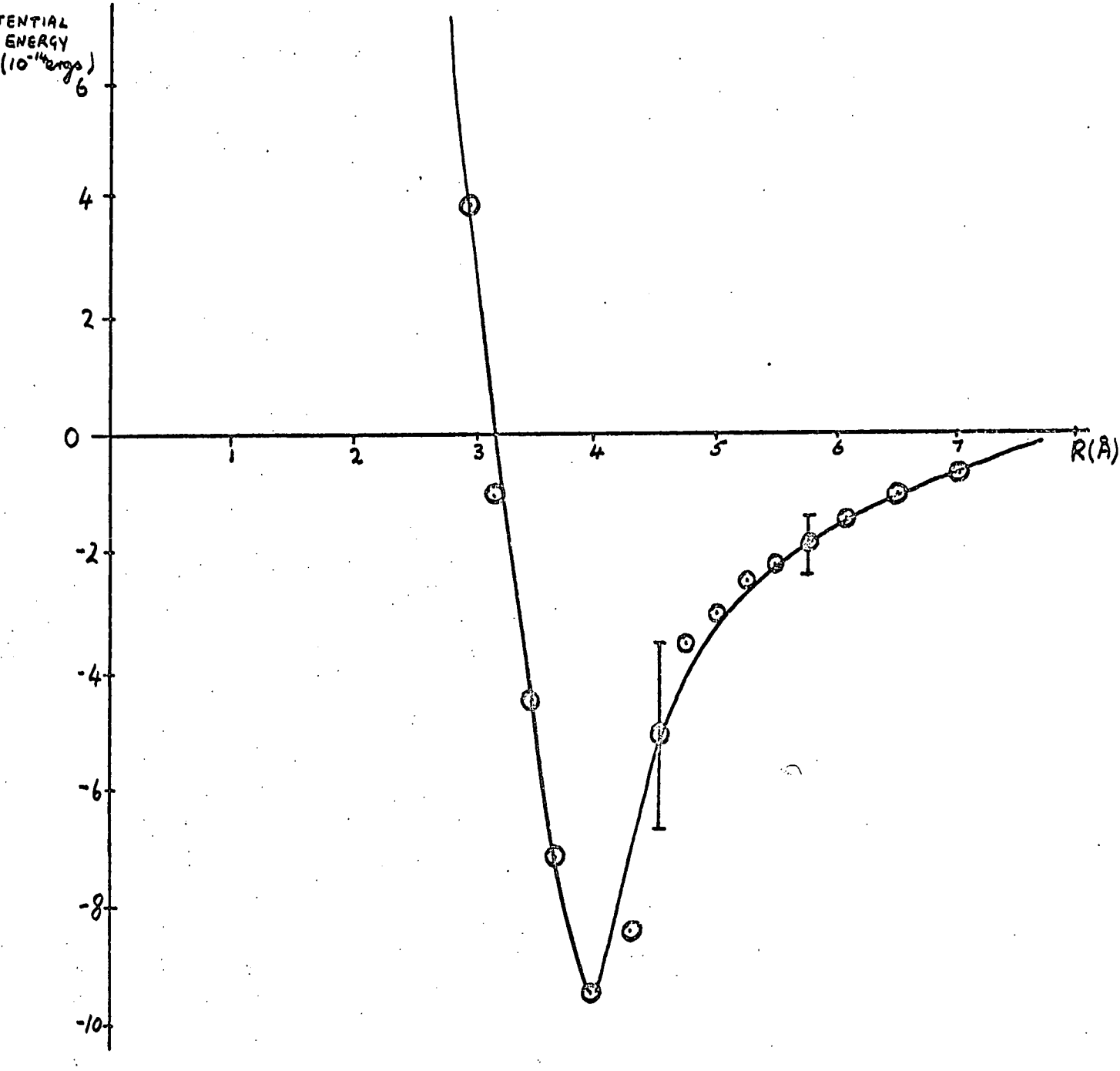

Potential Calculation of $Hg(^3P_2) + K(^2S_{\frac{1}{2}})$ $(m_J = \frac{5}{2})$

Potential Energy v Internuclear Separation

Figure 4-4

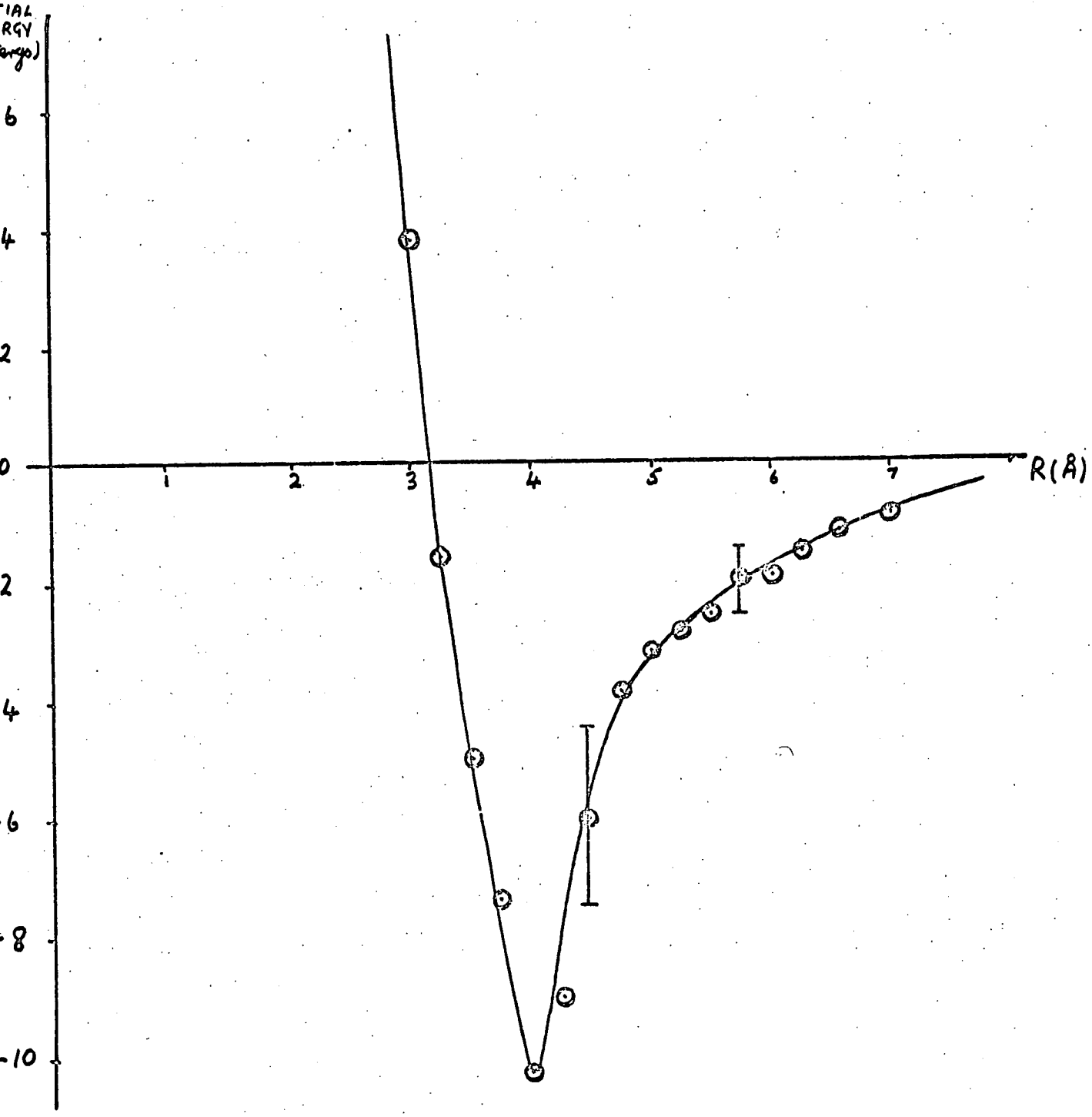

Potential calculation of $Hg(^3P_2) + K(^2S_{\frac{1}{2}})$ $(m_J = \frac{3}{2})$

Potential Energy v Internuclear Separation

Figure 4-5

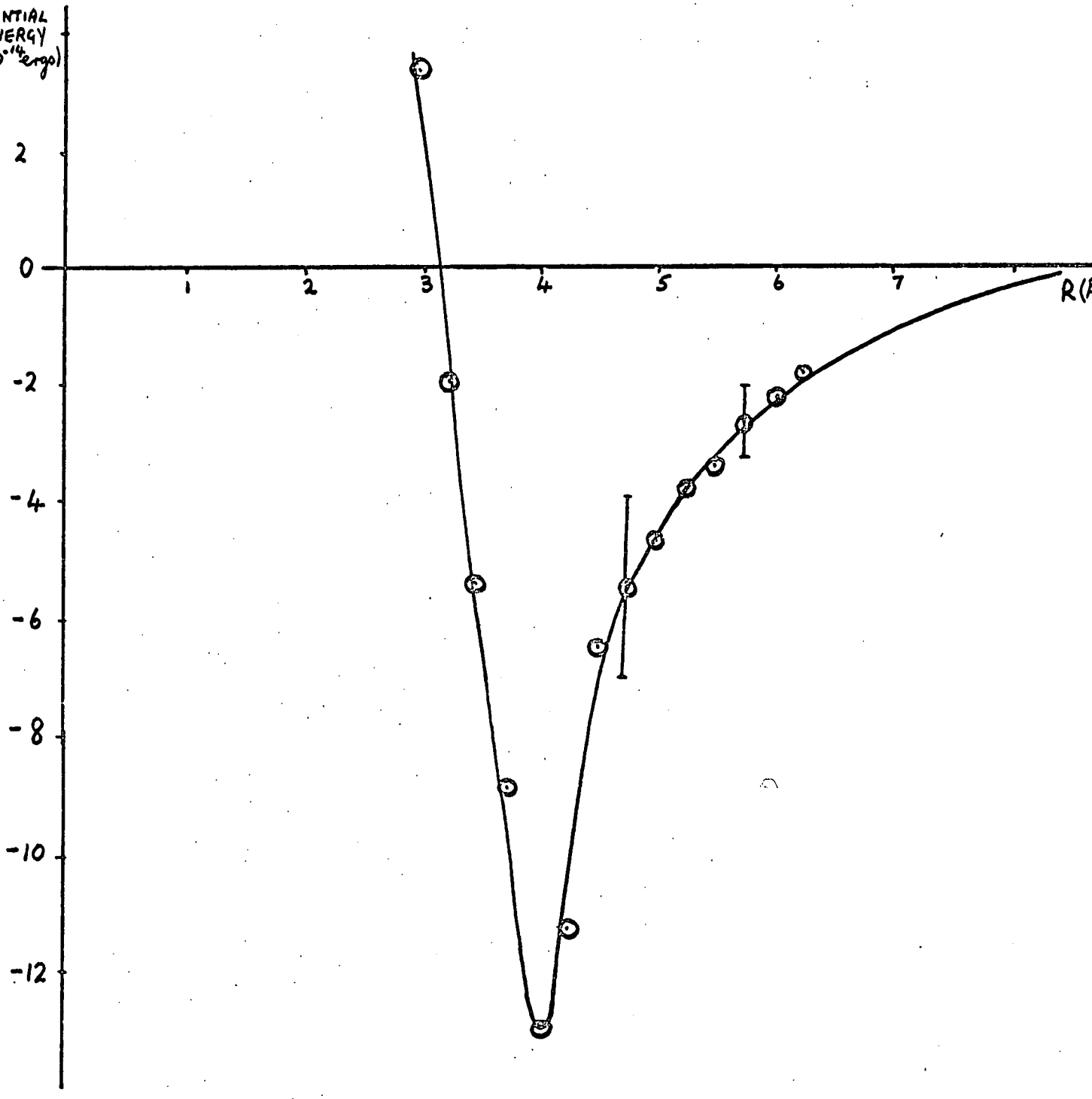

Potential calculation of $Hg(^3P_2) + K(^2S_{\frac{1}{2}})$ $(m_J = \frac{1}{2})$

Potential Energy v Internuclear Separation

Figure 4-6

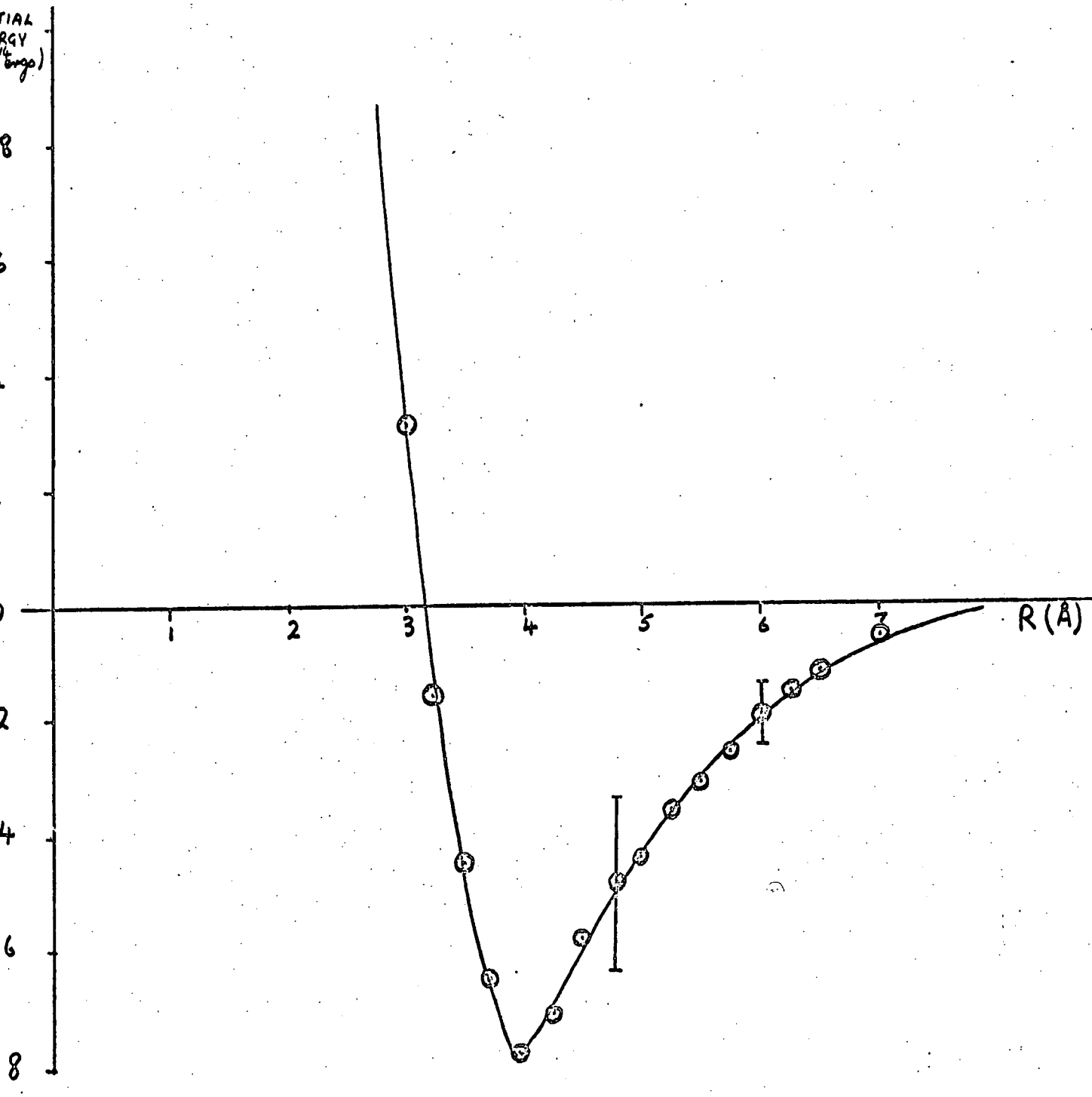

Potential calculation of $Hg(^3P_2) + K(^2S_{\frac{1}{2}})$ $(m_J = \frac{1}{2})$

Potential Energy v Internuclear Separation

Figure 4-7

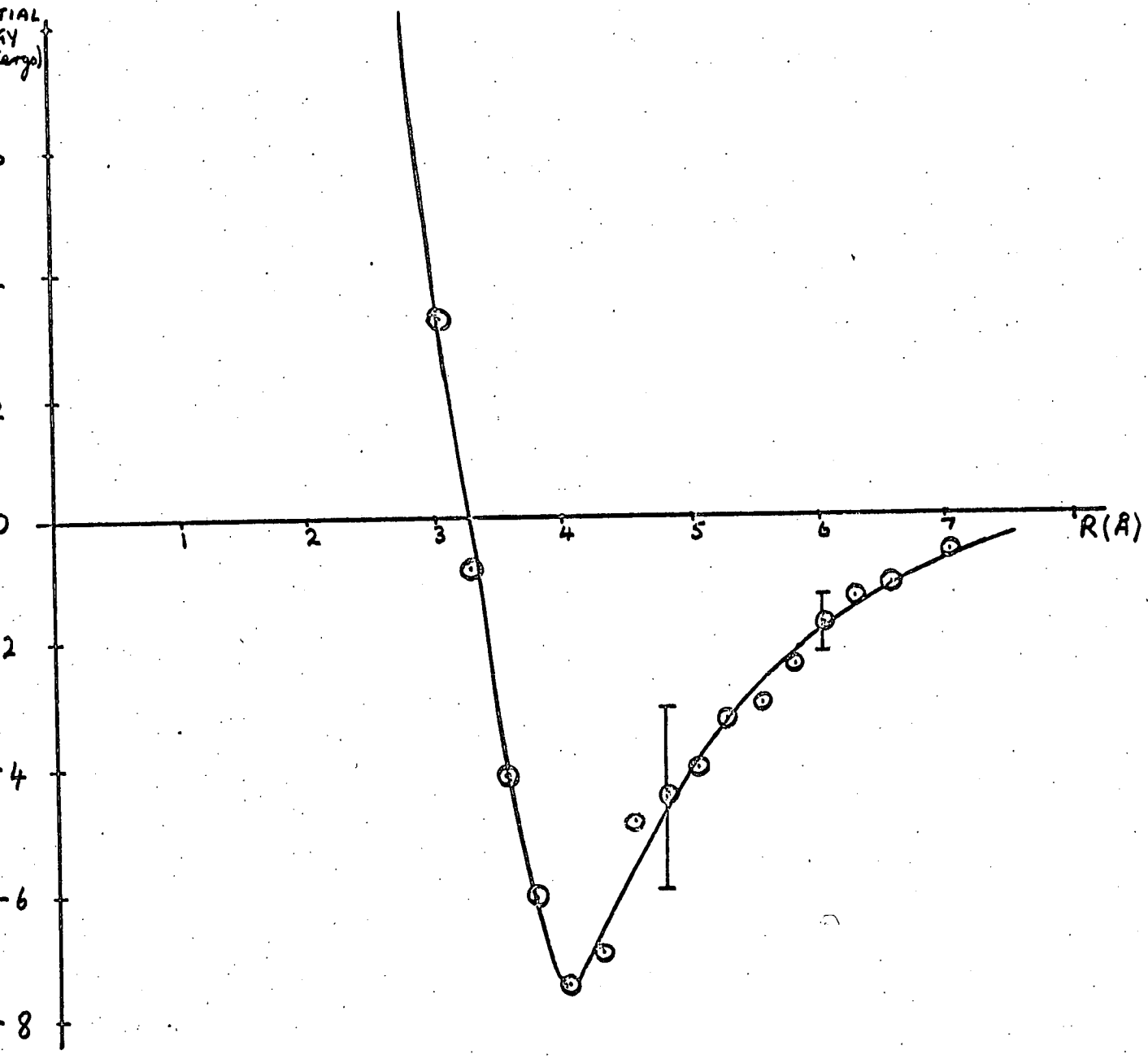

Potential calculation of $Hg(^3P_2) + K(^2S_{\frac{1}{2}})$ $(m_J = \frac{3}{2})$

Potential Energy v Internuclear Separation

Figure 4-8

Relatively shallow wells are obtained with depths ranging from 8×10^{-14} ergs to 13×10^{-14} ergs, all much less than the spin orbit splitting in mercury. The positions of the potential minima are roughly constant at 4Å.

These calculated potentials are similar to the ground state potential where the well depth is $8.40 \pm 0.29 \times 10^{-14}$ ergs and $r_m = 4.91 \pm 0.03$ Å [BUC 1972]. However a smaller value of r_m is obtained. This may be due to the fact that the core-core repulsion in the Hamiltonian was expressed as that for point charges. This means that the value of the potential at internuclear separations which are less than the sum of the two core radii will be incorrect. Therefore for values of R less than 2.5Å this is certainly true since the ionic radii of Hg^{2+} and K^+ are 1.1 and 1.33Å respectively and it may be true for larger values of R.

These calculated potentials will be compared with those derived from experimental scattering patterns in a later chapter. However, it should be remembered that this calculation is rather crude. An approximate Hamiltonian has been used [Appendix III] as well as zeroth order molecular wave functions. It is probable, however, that the neglect of terms in the Hamiltonian will have little effect since the major terms have been included. Configuration interaction has also been omitted and it should be noted that it is primarily the interaction of states with the same Ω value arising from different separated atomic states that leads to the lowering of the $^2\Sigma$ from $^3P_0$ [Fig. 4.2]. However provided the states computed here are not involved this omission will have little effect. In conclusion one

should be wary of leaning too heavily on this calculation because of the assumptions used and the fact that the experimental polarisability was not reproduced too well with these wave functions.

Chapter 5

Elastic Scattering Theory and Interpretation of Thermal Energy Scattering Results

5 Elastic Scattering Theory and Interpretation of Thermal Energy Scattering Results.

Scattering Theory

As the subject has been thoroughly reviewed elsewhere (e.g. Bernstein [ROS 1966] and Pauly et al [BAT 1965])only a brief outline will be presented here. The theory can be treated classically or quantum mechanically. Classical mechanics can be used successfully for the treatment of transport and other bulk properties of gases whereas quantum mechanics is generally required only to describe the properties of individual molecules.

Classical Mechanics

Although the detailed predictions of classical mechanics are generally not applicable to collisions between atoms in which quantum mechanics plays an essential part, the concepts which arise in classical mechanics are useful in the description of any scattering system [GOL 1964].

By separating out the motion of the centre of mass of the system the two body collision problem can be formally reduced to the problem of one particle interacting with a central force field, V(R). This single particle has a mass

$$\mu = \frac{M_1 M_2}{M_1 + M_2} \qquad 5\text{-}1$$

where M_1 and M_2 are the masses of the colliding particles. The particle moves in the field with a velocity $Vr = V_1 - V_2$ where V_1 and V_2 are the velocities of the colliding particles.

Using the conservation of energy and of angular momentum, the angle of deflection χ is obtained as a function of impact parameter.

$$\chi(b) = \pi - 2b\int_{ro}^{\infty} \frac{1}{R^2} \left[1 - \frac{b^2}{R^2} - \frac{V(R)}{E}\right]^{-\frac{1}{2}} dR \qquad 5\text{-}2$$

where E is the relative kinetic energy of the system and R_o is the distance of closest approach given by;

$$R_o^2 \left[1 - \frac{V(R)}{E}\right] = b^2 \qquad 5\text{-}3$$

The deflection function for a typical interatomic potential [Fig 5-1(a)] is shown in Fig [5-1(b)]. For small values of b the potential is repulsive and $\chi(b)$ is positive. As b increases so the potential becomes attractive and $\chi(b)$ falls to a minimum and then goes to zero as b is further increased. From Fig. [5-1(b)] it is obvious that the scattering at angles χ which are less than χr, the rainbow angle, results from three impact parameters. Classically, the differential scattering cross section is expressible directly in terms of the deflection function by the relationship

$$\sigma(\chi) = \sum_i \frac{bi}{\sin \chi \left|\frac{d\chi}{dbi}\right|} \qquad 5\text{-}4$$

where the summation is over all possible branches of the deflection function contributing to the scattering at an angle χ.

Equation [5-4] highlights some of the failures of classical theory in that it predicts singularities at the glory impact parameter where $\chi = 0$ and at the rainbow angle where $\frac{d\chi}{db} = 0$. Such singularities are never observed in reality and classical mechanics also fails to explain the oscillatory structure and the angular dependence of small angle scattering.

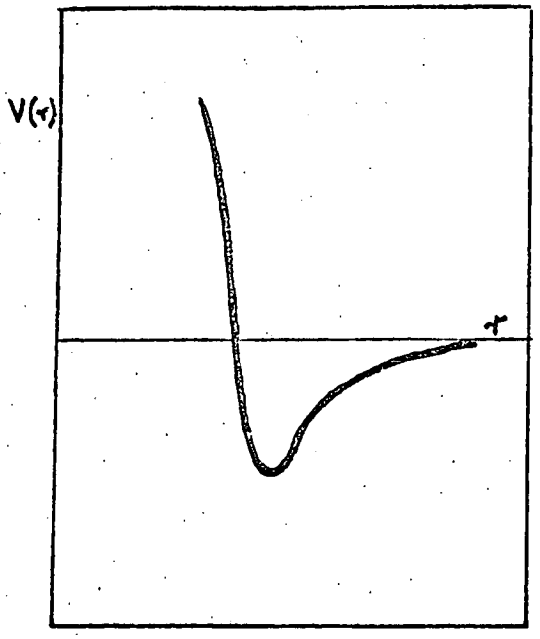

(a)

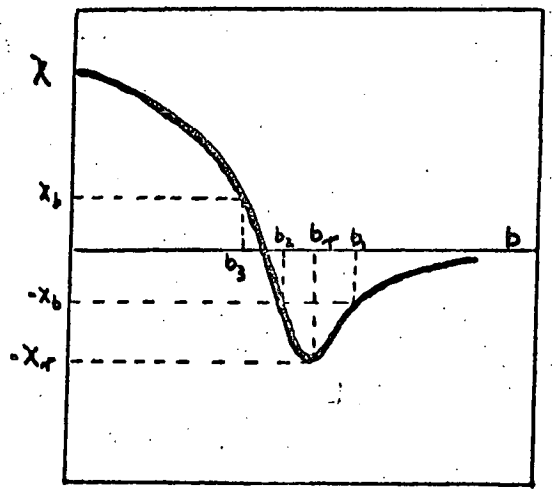

(b)

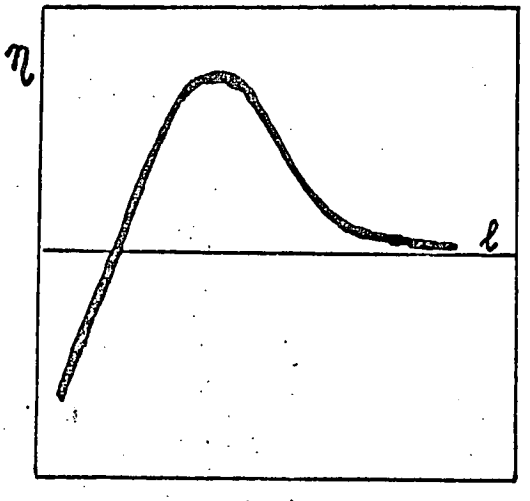

(c)

a) Potential energy curve
b) Deflection function
c) Phase shift curve

Figure 5-1

Quantum Scattering

In the quantum mechanical description of scattering the singularities mentioned previously become finite in accord with experiment and the various scattered contributions at an angle χ do not simply add together but there is a phase relationship between the contributions and interference effects occur.

The quantum mechanical treatment of scattering may be found in detail in the books by Mott and Massey [MOT 1965] , Wu and Ohmura [WU 1962], Fluendy and Lawley [FLU 1973] and a review by Bernstein [ROS 1966] deals with the salient features.

As in the classical case the problem reduces to a consideration of the scattering of a particle of reduced mass μ and energy E from a central force. Associated with the particle is a wave function ψ which must contain information about the particle before and after scattering. The situation can be described by a plane wave incident on the potential and a spherical wave scattered outwards from it. The wave function may be written as

$$\psi = e^{ikz} + \frac{f(\chi)}{R} e^{ikR} \qquad 5\text{-}5$$

where $k = \frac{\mu V}{\hbar}$ and Z is the axial direction.

The differential cross section is given by

$$\sigma(\chi) = | f(\chi) |^2 \qquad 5\text{-}6$$

and the total cross section by

$$Q = 2\pi \int_0^{\pi} \sin \chi \; | f(\chi)|^2 \, d\chi \qquad 5\text{-}7$$

The incident wave may be expressed as an infinite sum of partial waves each with a specific orbital angular momentum. This method

finally gives

$$f(\chi) = \frac{1}{2ik} \sum_{o}^{\infty} (2\ell + 1)(e^{2i\eta\ell} - 1) P_{\ell}(\cos \chi) \qquad 5\text{-}8$$

where η_{ℓ} is the phase shift between the ℓ^{th} partial wave scattered by the potential V(R) and the same partial wave for the case where V(R)=0. $P_{\ell}(\cos \chi)$ are the Legendre functions.

It may also be shown that the total cross section Q is given by

$$Q = \frac{4\pi}{k^2} \Sigma_{\ell}(2\ell + 1) \sin^2\eta_{\ell} \qquad 5\text{-}9$$

The problem is now reduced to finding η_{ℓ}. This can be done by solving the so called radial equation (see Bernstein [ROS 1966]). Although this gives exact phase shifts it is very laborious for atomic collisions where the maximum value of ℓ is typically more than 1000. Provided the collision is not between slow moving light atoms the JWKB method [MOT 1965] can be used where

$$\eta_b = k\left[\int_{Ro}^{\infty} \left(1 - \frac{b^2}{R^2} - \frac{V(R)}{E}\right)^{\frac{1}{2}} dR - \int_{b}^{\infty} \left(1 - \frac{b^2}{R^2}\right) dR\right] \qquad 5\text{-}10$$

The impact parameter is related to ℓ by

$$b = \frac{1}{k}\left[\ell + \tfrac{1}{2}\right] \qquad 5\text{-}11$$

and R_o is the distance of closest approach.

In the differential cross sections reported later the computer program, Monoenergy Forward [COW 1968], was used to calculate differential cross sections in centre of mass and laboratory co-ordinates. This program calculates phase shifts by the above method until η is less than 0.1 radians, higher order phase shifts being derived using the Born Approximation [MOT 1965].

Semi-Classical Scattering

Most phase shift functions are smooth functions of ℓ [Fig 5.1(c)] and for thermal scattering are greater than $\frac{\pi}{2}$ over most of their range so that $e^{2i\eta_\ell}$ in [5-8] is oscillatory. To handle this situation the technique of stationary phase is used for approximating the partial wave summation [FOR 1959].

The partial wave summation for $f(\chi)$ is first replaced by an integration and the integral is split into two parts

$$f(\chi) = \frac{-1}{2ik}\left\{\int_o^\infty (2\ell + 1)e^{2i\eta_\ell} P_\ell(\cos \chi)d\ell - \int_o^\infty (2\ell +1) P_\ell(\cos \chi)d\ell \right. \qquad 5\text{-}12$$

The second integral in [5-12] is a delta function and so vanishes for $\chi \neq 0$. Next an approximation for the Legendre polynomials in the first integral of [5-12] is introduced for large values of ℓ

$$P\ell(\cos \chi) \approx \left[\tfrac{1}{2}(\ell + \tfrac{1}{2})\, \pi \sin \chi\right]^{-\frac{1}{2}} \sin\left[(\ell + \tfrac{1}{2})\, \chi + \frac{\pi}{4}\right] \qquad 5\text{-}13$$

which when substituted gives

$$f(\chi) = \frac{-1}{k(2\pi \sin \chi)^{\frac{1}{2}}} \int_o^\infty (\ell + \tfrac{1}{2})^{\frac{1}{2}} \left\{ e^{i\phi_+(\ell)} - e^{-i\phi_-(\ell)} \right\} d\ell \qquad 5\text{-}14$$

where

$$\phi_\pm(\ell) = 2\eta(\ell) \pm (\ell + \tfrac{1}{2})\, \chi \pm \frac{\pi}{4} \qquad 5\text{-}15$$

The contribution of a range of ℓ values of width $\Delta\ell$ around some value ℓ_1 to $f(\chi)$ can be examined by expanding $\eta(\ell)$ in a Taylor series about ℓ_i so that the phase ϕ becomes:

$$\phi_\pm(\ell) = 2\eta(\ell_i) + 2\left(\frac{d\eta}{d\ell}\right)_{\ell=\ell i} (\ell - \ell_i) + \left(\frac{d^2\eta}{d\ell^2}\right) (\ell - \ell_i)^2$$

$$+ - - - \pm (\ell + \tfrac{1}{2})\, \chi \pm \frac{\pi}{4} \qquad 5\text{-}16$$

Now $$2\frac{d\eta_\ell}{d\ell} = \chi \qquad 5\text{-}17$$

so that neglecting higher terms than the quadratic in [5-16] a region of stationary phase in $\phi(\ell)$ centred about ℓ_χ is found where ℓ_χ satisfies

$$2\left(\frac{d\eta_\ell}{d\ell}\right)_{\ell=\ell_\chi} = \pm\, \chi_{obs} \qquad 5\text{-}18$$

The width $\Delta\ell$ of the stationary phase region in which $\phi_\pm$ changes by less than π is seen from

$$\phi_+(\ell) \simeq 2\eta(\ell_\chi) - 2(\ell_\chi + \tfrac{1}{2})\eta'(\ell_\chi) + \eta''(\ell_\chi)(\ell - \ell_\chi)^2 + \frac{\pi}{4} \qquad 5\text{-}19$$

to be proportional to $\eta''(\ell_\chi)^{-\frac{1}{2}}$ but need not be specified if we use the following standard integral to evaluate [5-14] when [5-19] is substituted.

$$\int_{-\infty}^{+\infty} e^{\pm iax^2} dx^2 = \left(\frac{\pi}{a}\right)^{\frac{1}{2}} e^{\pm i\frac{\pi}{4}} \qquad 5\text{-}20$$

so that

$$f(\chi) = -k^{-1}\left\{\frac{\ell_\chi}{2\,|\eta''|\,\sin\chi}\right\}^{\frac{1}{2}} e^{i\alpha_\pm\chi} \qquad 5\text{-}21$$

where

$$\alpha_+(\chi) = 2\eta(\ell_\chi) - 2(\ell_\chi + \tfrac{1}{2})\eta'(\ell_\chi) + \frac{\eta''}{|\eta''|}\,\frac{\pi}{4} \qquad 5\text{-}22$$

The main semi-classical approximation to $\sigma(\chi)$ is then

$$\sigma(\chi) = |f(\chi)|^2 = \frac{\ell_\chi}{\left[2k^2\left|\frac{d^2\eta_\ell}{d\ell^2}\right|\sin\chi\right]} \qquad 5\text{-}23$$

Interfering Branches of the Deflection Function

There is one respect in which [5-23] may be in error and this arises from the possible presence of more than one region of stationary phase in $\phi_\pm$. The condition for stationary phase is that ℓ satisfies [5-18] and this may well be fulfilled by more than one

value of ℓ. In particular, for values of χ less than the rainbow angle there will always be three solutions of [5-18].

If the energy of the collision is such that the rainbow angle is greater than 2π, the situation is even more complicated because trajectories that suffer a deflection of $\chi + 2\eta\pi$ are experimentally indistinguishable from those deflected through χ and each contributes a region of stationary phase and is a separate branch of the deflection function. In order to obtain the correct phase to $|2\pi|$ between all these branches, a new phase β is defined that replaces α in [5-22].

$$\beta = 2\eta(\ell_\chi) - 2(\ell_\chi + \tfrac{1}{2})\eta'(\ell_\chi) - \left(2 - \frac{\eta'}{|\eta'|} - \frac{\eta''}{|\eta''|}\right)\frac{\pi}{4} \qquad 5\text{-}24$$

where the term $\frac{\eta'}{|\eta'|}\ \frac{\pi}{4}$ provides the relative phase change of $\frac{\pi}{2}$ in passing from the positive to the negative branch of the deflection function. Each of the 3 regions ℓ_1, ℓ_2 ℓ_3 [Fig 5(1b)] gives a contribution to $f(\chi)$ of the form [5-21] and their sum is the resultant amplitude. The semi-classical differential cross section then becomes

$$\sigma(\chi) \simeq \left| \sum_n f_n(\chi) \right|^2 \qquad 5\text{-}25$$

$$\simeq \sum_n |f_n(\chi)|^2 + \sum_{\substack{n \\ n \neq m}} \sum_m |f_n(\chi)||f_m(\chi)| \cos(\beta_n - \beta_m) \qquad 5\text{-}26$$

where the second term represents an oscillatory contribution in the presence of the dominant first term which is in fact the classical value of $\sigma\chi$

Therefore $\underset{\text{semi classical}}{\sigma(\chi)} = \sum_{\substack{n \\ \text{all branches}}} \underset{\text{classical}}{\sigma(\chi)} +$ interference terms between all branches

For heavy particle scattering the second term in equation [5-24] is dominant and so remembering that $\eta'(\ell_\chi)$ changes sign in passing

from ϕ_+ to ϕ_- then:

$$\beta_n - \beta_m \simeq (\ell_n \mp \ell_m)\,\chi \qquad 5\text{-}27$$

the upper sign referring to the case in which both branches come from ϕ_+ and the lower sign to one branch from ϕ_+ and the other from ϕ_-. Defining the periodicity Δ of the modulations as

$$\cos(\beta_n - \beta_m) = \cos 2\pi\, \chi/\Delta \qquad 5\text{-}28$$

$$\Delta = \frac{2\pi}{|\ell_n \mp \ell_m|}$$

Therefore the periodicity of the oscillations in the differential cross section yields information about the range of the deflection function.

Transformation from Centre of Mass to Laboratory Co-ordinates

In order to compare theoretical and experimental results it is necessary to transform centre of mass angles χ to the laboratory angles Θ. The relationship between the centre of mass and laboratory scattering angles are well known, eg [MOR 1962].

For elastic scattering between beams intersecting at some angle ψ, the transformations can be made by means of the Newton diagram. The Newton diagram for the case of ^{4}He-K is shown in Fig [5-2].

If the masses and velocities of the two beams are M_1, V_1 and M_2, V_2 respectively then the initial resultant velocity V^1 is

$$V^1 = \left[V_1^2 + V_2^2 - 2V_1 \times V_2 \cos\psi\right]^{\frac{1}{2}} \qquad 5\text{-}29$$

The velocity of the incident primary beam particle 1 relative to the centre of mass is $V_1{}^1$; its magnitude is

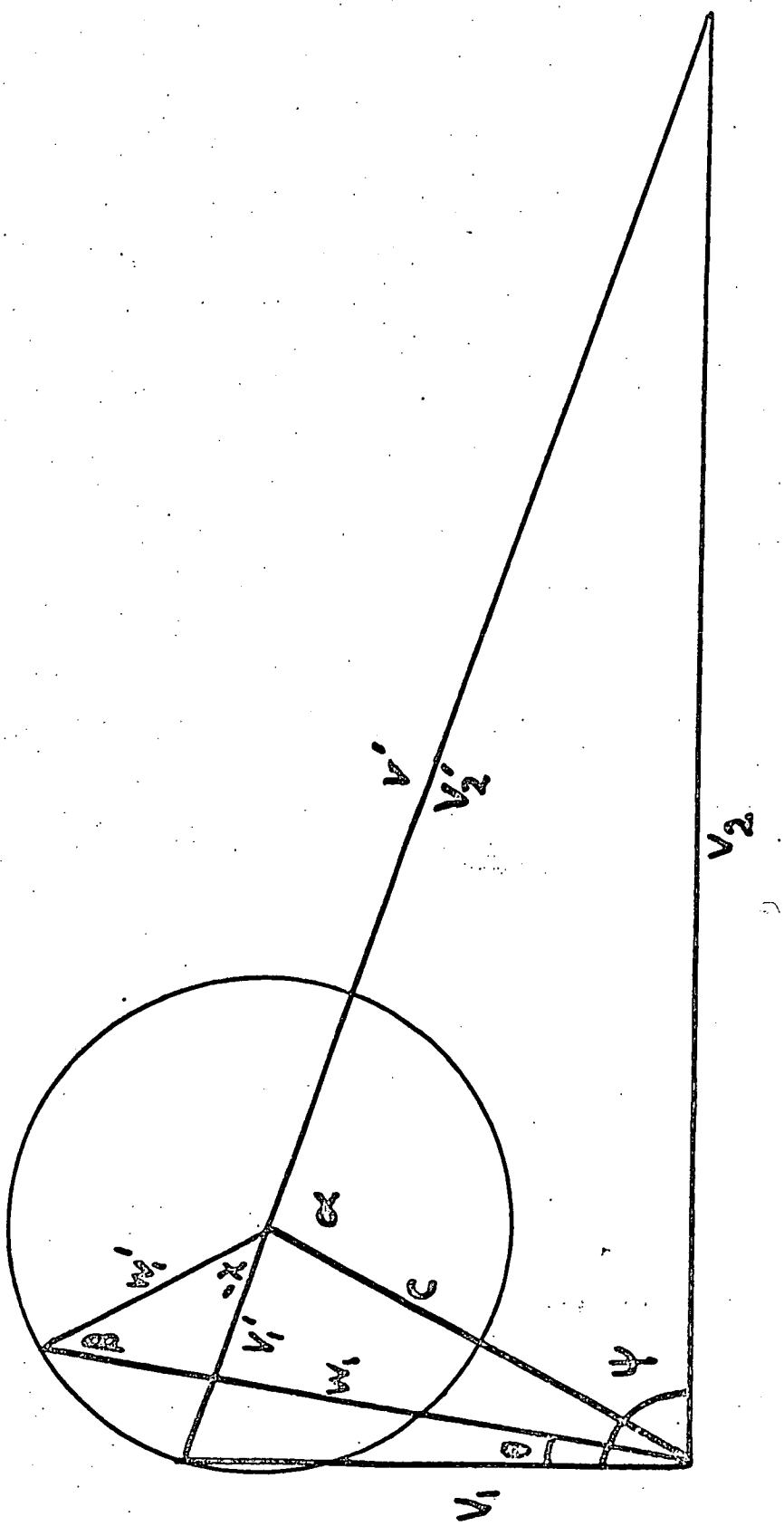

Newton Diagram for Hg*/K

Figure 5-2

$$V^1{}_1 = \frac{M_2}{M_1+M_2} V^1 \qquad 5\text{-}30$$

The velocity of the cross beam particle 2 relative to the centre of mass is

$$V_2{}^1 = \frac{M_1}{M_1+M_2} V^1 \qquad 5\text{-}31$$

The speed of the centre of mass is given by

$$C = \frac{1}{M_1+M_2} \left[M_1{}^2V_1{}^2 + M_2{}^2V_2{}^2 - 2M_2M_1V_2V_1\cos\psi \right]^{\frac{1}{2}} \qquad 5\text{-}32$$

For the case of elastic scattering the final relative velocities $W_1{}^1$ and $W_2{}^1$ of particles 1 and 2 are respectively:

$$|W_1{}^1| = |V_1{}^1| \quad \text{and} \quad |W_2{}^1| = |V_2{}^1| \qquad 5\text{-}33$$

The final relative velocity W^1 being rotated through an angle χ relative to the initial relative velocity V^1. The problem is to find the laboratory angle θ at which particle 1 scattered through the centre of mass angle χ will appear. Now:

$$\theta = \cos^{-1} \left[(V_1{}^2 + W_1{}^2 - 4\, W_1{}^{1^2}\sin^2(\tfrac{\chi}{2})) \,/2V_1{\times}W_1 \right] \qquad 5\text{-}34$$

where

$$W_1 = \left[W_1{}^{1^2} + C^2 + 2CW_1{}^1\cos(\alpha+\chi) \right]^{\frac{1}{2}}$$

$$\alpha = \cos^{-1} \left[(C^2 + V_2{}^{1^2} - V_2{}^2)/2CV_2{}^1 \right]$$

$$W_1{}^1 = \frac{M2}{M_1+M_2} W^1 \text{ and } W_2{}^1 = \frac{M_1}{M_1+M_2} W^1$$

In the transformation of differential cross sections from the centre of mass to the laboratory co-ordinates,

$$I(\theta,V_1,V_2) = I(\chi,V^1) \frac{d\omega}{d\Omega} \qquad 5\text{-}35$$

where $d\omega$ is the solid angle subtended in the centre of mass system, and $d\Omega$ is the solid angle in the laboratory system, it is necessary to know $\frac{d\omega}{d\Omega}$.

Consider an area dA normal to $W_1{}^1$

$$dW = \frac{dA}{W_1{}^{1^2}} \qquad 5\text{-}36$$

and in the laboratory system

$$d\Omega = \frac{dA \cos \beta}{W_1{}^2} \qquad 5\text{-}37$$

Now $$\cos \beta = \frac{W_1{}^2 + W_1{}^{1^2} - C^2}{2W_1W_1{}^1} \qquad 5\text{-}38$$

So $$d\Omega = \frac{dA\ (W_1{}^2 + W_1{}^{1^2} - C^2)}{2W_1{}^3W_1{}^1} \qquad 5\text{-}39$$

and therefore

$$\frac{d\omega}{d\Omega} = \frac{2W_1{}^3}{W_1{}^1(W_1{}^2 + W_1{}^{1^2} - C^2)} \qquad 5\text{-}40$$

The situation is simplified by the fact that in this case the angle between the beams in 90^o.

Interpretation of Results

Scattering experiments with molecular beams have in recent years contributed significantly to the determination of intermolecular potentials.

The potential well depth Σ and the equilibrium distance R_m have been determined for a large number of systems [BER 1967] although only under the assumption of simple model potentials. The main reason for this is that the formal inversion of a differential cross section to yield a potential is a difficult problem. For cases in which a very few partial waves are involved, eg nuclear scattering, rather sophisticated procedures have been evolved [W U1962]. These have not, however, been extended to thermal molecular scattering where the effective range of the potentials is much greater and thousands of partial waves are involved. Experimental observations in thermal

elastic scattering are limited in angular and energy range, are less than perfect in resolution, include some noise and under these conditions any formal inversion is unreliable. Alternative ways of treating the data include

a) Applying all available information from other sources to estimate the potential and choosing an analytical form for it.

b) Identifying and using any key features in the scattering observations, eg rainbows or glories to refine the original estimates of the potential parameters.

c) Carrying out a fitting operation between a forward calculation of the expected scattering pattern and the observed scattering pattern if the data is of high enough resolution.

The method that has been almost universally used to date and must still be used if the data is not sufficiently well resolved is to represent the interaction potential V(R) by some parametric form and to vary the parameters until certain distinctive features of the calculated scattering pattern agree with the same features as observed experimentally. A typical parametric form is the Lennard-Jones (n:6) potential

$$V(R) = \frac{6\Sigma}{n-6}\left[\left(\frac{R_M}{R}\right)^n - \frac{n}{6}\left(\frac{R_M}{R}\right)^6\right] \qquad 5\text{-}41$$

where Σ = well depth, R_M = equilibrium distance. In situations where quantum interference structure has been resolved to wide angles [BAR 1966] the usual forms of Lennard-Jones potential (n, Σ and R_M being adjustable) have proved inadequate. Buck and Pauly [BUC 1968] fitted a parameter dependent potential which contained four

adjustable parameters in addition to the well depth and equilibrium separation. Duren et al [D UR 1968] fitted a modified form of the Lennard-Jones potential which contained five adjustable parameters in addition to the well depth and equilibrium separation. The computational effort in the usual fitting procedure is increased greatly in these more flexible multi-parameter forms. The difficulties involved in all such methods can be avoided if it is possible to apply an inversion procedure, i.e. the determination of the potential directly from measured cross sections.

Recently the inversion of data based on classical mechanics and due to Firsov [FIR 1953] has been used. This method relates the deflection function $\chi(b)$ and the potential. For scattering at an energy E the potential is defined by the equations

$$r_m = b \exp \left\{\frac{1}{\pi} \int_b^\infty \frac{\chi(b^1)}{\sqrt{b^{1^2} - b^2}} db^1 \right. \qquad 5\text{-}42$$

where b^1 is a dummy impact parameter

$$V(r_m) = E \left(1 - \frac{b^2}{r_m^2}\right) \qquad 5\text{-}43$$

The significance of the Firsov formula lies in the fact that it provides a direct means of calculating numerical potentials from scattering data. It is then possible to progress from fitting parameter dependent potentials to experimental data, to the determination of more accurate numerical potentials. This method has been extended by Buck [BUC 1971(a)] who allowed the deflection function to have both positive and negative branches, as it should. The deflection function is obtained by a fitting process based on a semi-classical approximation to $\chi(b)$ in terms of b. The advantage of this process is that the potential is obtained pointwise rather

than as a constrained function. The procedure uses as essential starting information, in the nonmonotonic part only, the angular positions of the measured extrema of the rainbow oscillations. Neither the absolute value of the differential cross section nor its relative shape is required. This has the great advantage that these extrema positions are almost independent of various angular and energy averaging processes in the primary and secondary beams. Buck et al [BUC 1971(b)], [BUC 1972] have successfully used this method for their mercury / alkali thermal energy scattering experiments.

Certain features of the differential cross section are useful in the determination of a potential or a deflection function. The rainbow location is largely dependent on the reduced energy and only weakly on the length parameter whereas the extrema in the scattering pattern give information about the range of the potential. For smoothly varying potentials, eg Lennard-Jones potentials, the high frequency structure, in the scattering pattern, arises from interference between the two inner branches of $\chi(b)$ [Fig 5-1(b)]. The spacing of the interference pattern is given by semi-classical arguments.

$$\Delta\chi = \frac{2\pi}{\ell_2 + \ell_3} \qquad 5\text{-}44$$

Lower period structure, arising out of interference of two branches on the attractive side is given by

$$\Delta\chi = \frac{2\pi}{\ell_1 - \ell_2} \qquad 5\text{-}45$$

Such information could be useful in the construction of a deflection function.

Therefore, the interpretation of the results obtained in this work, CHAPTER 6, is as follows:

d) Construction of the deflection function using all available data.

e) Inversion of the deflection function by Firsov's procedure to yield V(R) pointwise without making any assumptions about its mathematical form.

f) Use of the evaluated V(R) to obtain a scattering pattern by a forward calculation.

g) Comparison of the experimental and calculated scattering patterns.

However, it should be noted that apart from the case where V(R) is a monotonic function of R it is not possible to find a unique potential to account for the observed scattering. This has been illustrated by Luoma [LUO 1970] and Boyle [BOY 1971] has shown that even in cases of well resolved structure the ambiguity is by no means resolved.

Chapter 6

Experimental Procedure and Analysis of Results

6 Experimental Procedure and Analysis of Results

The apparatus used in the scattering experiments has been in existence for some time. The vacuum system was designed for high angular resolution differential cross section measurements at small angles [COW 1968] [HOR 1969]. The apparatus was then modified for the present experiments involving metastable mercury [DAR 1972].

A complete description of the apparatus has already been presented [COW 1968] as well as a description of the modulation scheme [HOR 1969]. A brief resumé of the experimental procedure will be given in which the main points of the experiment will be highlighted.

The experimental set up is shown schematically [Fig 6-1]. The two beam sources rotate on a turntable in front of a fixed detector which is located in a differentially pumped chamber. The metastable mercury source and the detector have been described previously. After leaving the exciter the metastable atom beam is collimated and then crossed by a modulated target beam of alkali atoms. The cross beam oven is similar to that described by Cowley [COW 1968] but it has a much larger capacity so that a large number of long duration sweeps can be studied.

Exact alignment of the components involved in a molecular beam experiment is of critical importance. In these experiments the alignment was checked optically, care being taken to ensure that the Hg* beam is aligned along the axis of the oven support rails. The alignment of the oven was checked by use of a small electric bulb in the oven and sighting pins on the oven support rails. When viewed through a telescope the oven slit, the exciter slit, the collimating

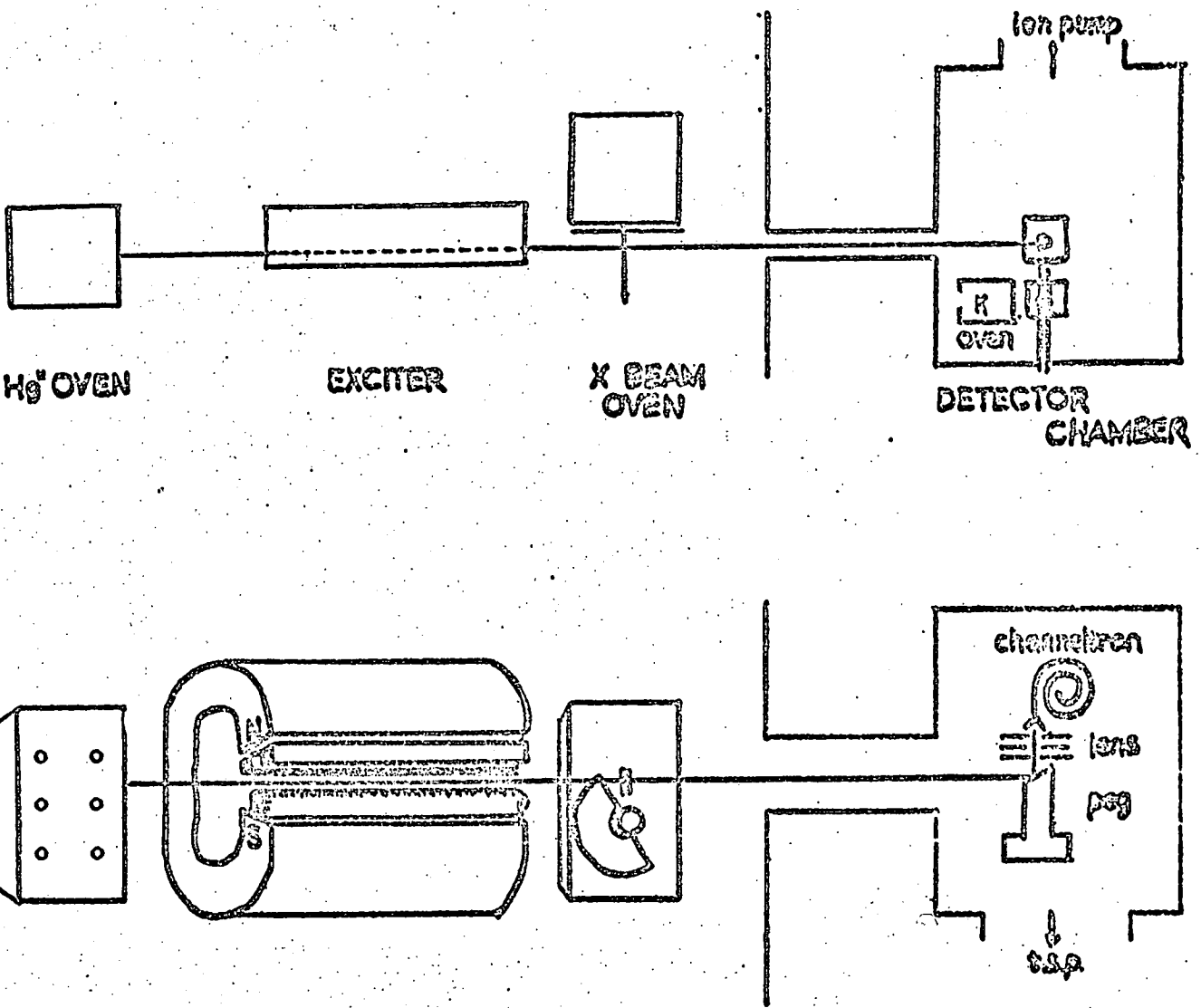

Apparatus schematic showing electron gun for metastable excitation and auger detector.

Figure 6-1

slit and the sighting pins should define a straight line. If this is the case the mercury oven is in the correct position. The alignment of the cross beam oven was then checked by rotating the turntable through 90^{o} and performing the same operation ensuring that there is no discrepancy in the height of the two ovens. This alignment was checked reasonably frequently.

The alignment of the detector was checked in a different manner. The apparatus subframe, carrying the rotatable turntable, was placed in its position, governed by two stops on rails inside the main vacuum chamber. The rear flange of the detector chamber was removed and the tungsten peg moved out of its position under the electrostatic lenses so that a clear view of the scattering chamber was achieved. A laser beam (Spectra Physics Model 155 He/Ne gas laser) was then used to locate the Hg oven slits. The beam passed through the entrance channel of the detector, the collimating slits and the exciter and it produced a well defined image of the slits inside the mercury oven. The detector peg was then returned to its position under the electrostatic lens so that it interrupted the laser beam. The position at which this occured was noted. The detector was then aligned, this alignment was checked only infrequently since the entire apparatus subframe could be reproducibly replaced inside the chamber.

Before each experiment the exciter cathode was replaced, the ovens were filled and all components in the vacuum were checked to ensure working order [LAB 1972]. The lid was then bolted down and the pumps switched on. When a pressure of 1×10^{-5} torr had been achieved, the liquid nitrogen cold trap was filled and the pressure reduced to $\sim 10^{-6} \rightarrow 10^{-7}$ torr. At this stage the mercury oven was heated up to

$\sim 130^{\circ}C$ and the oxide cathode was activated [LAB 1972]. If the exciter was performing adequately (i.e. giving about 8 milliamps at 10V) the valve between the main chamber and the detector chamber was opened and a search made for the beam centre by rotating the turntable.

When found the main beam signal was tuned up for maximum counts by altering the lens voltages while keeping the exciter voltage as low as possible, $\sim$ 10V, because of the excessive number of photons produced at higher voltages. When a reasonable beam intensity had been achieved (60,000 counts per second) the cross beam oven was heated. An attenuation of 10 $\sim$ 15% should be achieved when the cross beam is at the correct operating temperature. If this is not the case then either the oven is below operating temperature or a significant proportion of the main beam signal is attributable to photons which are hardly attenuated. Table [6-1] shows the % attenuation for three exciter voltages during the same experiment and indicates that increasing the excitation voltage reduces the percentage attenuation as predicted.

TABLE 6-1

Voltage	Attenuation
10V	12%
12V	10%
15V	5%

The results are consistent with those mentioned previously [Chapter 3] which showed that although the number of metastables remained almost constant the number of photons increased rapidly with increasing voltage.

When a steady main beam, cross beam and attenuation had been achieved angular sweeps were started. The temperature of the ovens in the experiments reported here are shown in table [6-2].

TABLE 6-2

System	Main Oven	Cross Oven
Hg*/Na	135°C	424°C
Hg*/K	132°C	332°C
Hg*/Rb	134°C	265°C

Sweeps were always started on the anti-clockwise side of the main beam and swept through in a clockwise direction. Sweeps were carried on as far as the apparatus dimensions allowed ($\sim 20^{\circ}$). At the end of each sweep the position of the main beam centre was checked to ensure that the shaft rotation indicator, which monitored the angular position, was performing properly and another sweep was started on the anti-clockwise side of the main beam.

The modulation scheme in the present apparatus [HÖR 1969] used a chopper disk, rotating at 70 cycles per second, mounted in front of the cross beam oven. At the instant that this chopper interrupted the cross beam it also intercepted a light beam between a bulb and a photocell, the output of which was used to drive an "in phase" detector system. This "in phase" counting system consisted of two delay width lines, the yellow and the blue line, and two counters [Fig 6-2]. The counters were Hewlett Packard 5245L and 3734A units. These counters shall be referred to as the blue counter and the yellow counter respectively.

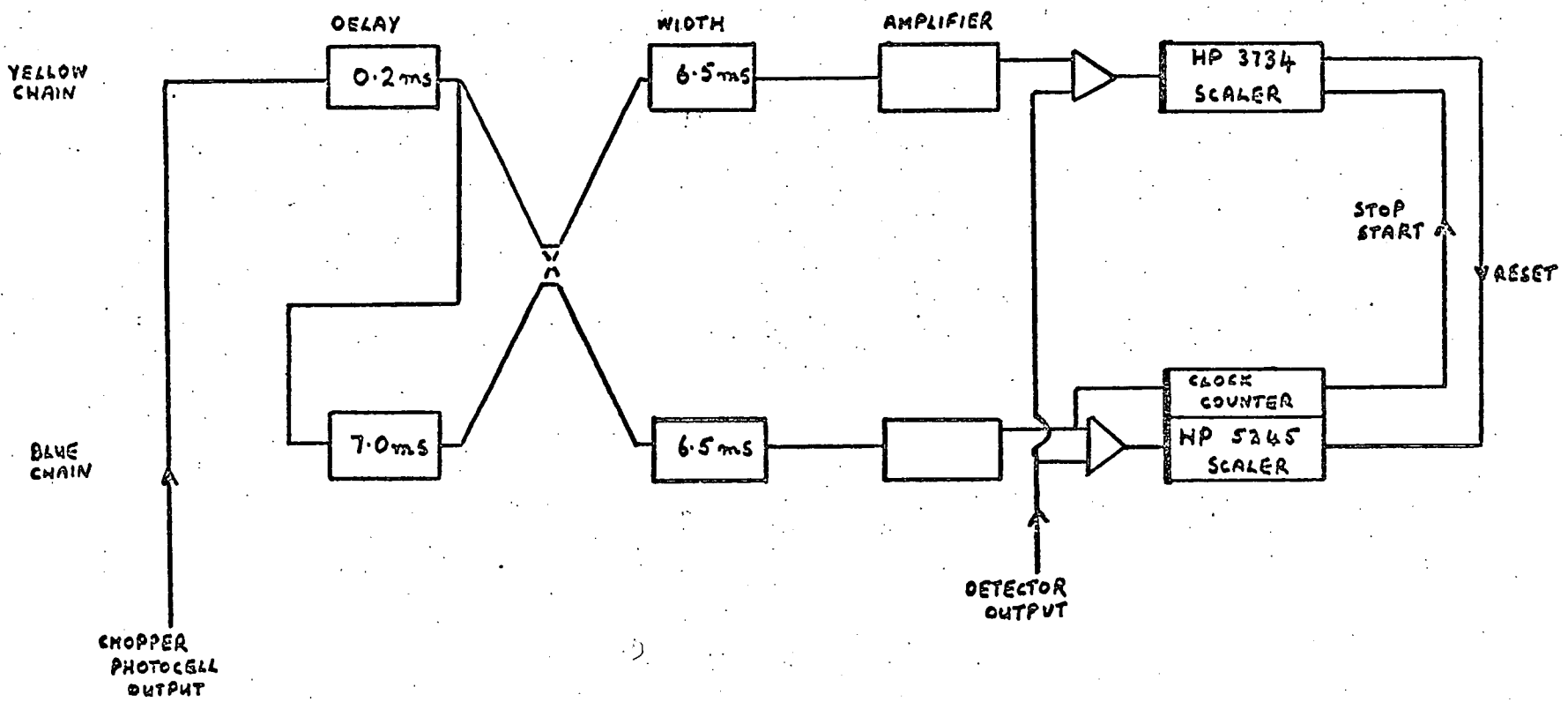

Figure 6-2 The Counting System

A signal from the photocell when the cross beam was on triggered the delay of the "signal + noise" line which was set at 0.2 ms. The output from the delay was fed to a 7 ms delay at the start of the "noise" line and a 6.5 ms width unit in the "signal + noise" line. For the duration of that width "signal + noise" was being counted in one of the counters. The delay at the start of the "noise" line triggered the "noise" width unit after the chopper had shut off and therefore that counter received only noise pulses during that period. To compensate for slight differences in the open time of the two counters, the roles of the two width counter lines were reversed after each batch of 100 modulation periods. Thus if for the first batch one scaler counted "signal + noise" then for the second batch of 100 it counted "noise". A clock counter registered these 100 pulses before triggering this interchange and also triggering the punch unit which punched out the accumulated counts from the two counters after which the scalers were reset to zero.

Sentences of sixteen lines of information were produced onto paper tape and the information was distributed as follows

5 lines for the "yellow" counter output, or Angle or Manual Codes
6 lines for the "blue" counter output
2 lines for condition codes
3 lines for separator codes.

The separator codes always appear in the same unique order so that any corruption in the data can be noticed. The relative position of the turn table was measured by an S.G Brown "Minitac" shaft rotation indicator coupled by a rubber tyred friction wheel to a quadrant attached to the turntable. (The motion of the "minitac" against the

quadrant produces a set of Moiré finges which are counted enabling the relative motion of the turntable to be determined). The output from the encoder displayed the turntable position on an electronic counter to an accuracy of 0.05^{o}. The manual codes are set by the operator and can be used to signal different types of information being collected but are more commonly used to signify the beginning and end of a sweep. The condition codes signify the type of information collected, i.e. whether it is signal on data, signal off data, angle etc.

At any position of the turntable the following collection sequence was carried out automatically: first the angular position of the turntable was punched along with the relevant condition code. (The number of times that the angle was recorded being fixed by the operator). The next information to be supplied was the background noise. At this stage the main beam exciter voltage was switched off and the detector output was accumulated in the two counters for the two cases where the cross beam was on and off. The outputs from both counters should be the same in this case and therefore this supplies a check that there is no "in phase' spurious signal. Finally the main beam was switched on and measurements made for the "signal + noise" when the cross beam was on and "noise" when the cross beam was off. (Again the number of measurements was controlled by the operator). After the final measurement was taken the turntable was automatically moved to a new position and the procedure repeated. (The angle step size was initially set by the operator).

In some of the experiments the punched output unit was not used due to breakdown. In these circumstances the data was recorded, by hand, in exactly the same manner so that all the data could be processed in the same way.

Data Analysis

A full description of the data analysis procedure has been given by Cowley et al [COW 1968] and although there have been a few changes the basic format is still the same and therefore only a brief summary will be given here. The new version is well documented [LAB 1972].

In the first phase the binary tape is translated into decimal and the complete sentence is checked for consistency; if any discrepancy is discovered the entire sentence is deleted. At each angle the mean and standard deviation are calculated for all observations. The original data is compared with the mean ± 2 standard deviations and any readings outside these limits are discarded. After these rejections the mean and standard deviation are recalculated and passed onto the second phase.

In the second phase smoothing and deconvolution of the raw data is performed. The main beam centre is found and all observations are related to it. A check is made to ensure that there is no noise in phase with the signal (noise in this case means the difference between counts when the cross beam is on and off, the exciter voltage being zero in each case). At small angles the scattered signal appears to be negative since the detector observes the main beam attenuated by the cross beam. A correction is made for this attenuation from one of the scans and added to the signal at each angle. Using the values calculated from this scan a best approximation to the signal and standard deviation are achieved. The signals from all the scans are then merged ensuring that in each scan the beam centre which

has been calculated is reproduced. A suitable filter function is then calculated from the main beam profile which is used in the smoothing.

The convolution equation

$$h(x) = \int_{-\infty}^{+\infty} f(y)\, g(x-y)\, dy = f*g \qquad 6\text{-}1$$

has been used to describe experimental broadening due to the main beam width only. (The true apparatus function is multidimensional). Here h(x) is the measured spectrum; f(y) is the corresponding ideal spectrum and g(z) is the apparatus resolution function. The observed spectrum would be ideal if g(z) were a delta function i.e. if the main beam shape had no broadening effect. In this experiment g(z) may be taken to be the observed distribution in the primary beam and h(x) the observed scattered signal. The method of solution of equation [6-1] has been described by Morrison [MOR 1963] and uses the Van Cittart iterative procedure. Finally the smooth and deconvoluted signal and standard deviations are calculated and line printer and graphical output is produced.

Results and their treatment

This output is the laboratory distribution for Hg* scattered from an alkali cross beam. The distribution for Hg* scattered from sodium is shown in figure [6-3]. Figure [6-4] shows the result of deconvoluting the data using the observed main beam profile as a filter function. The deconvoluted results are rather noisy but structure partially resolved before deconvolution can now be clearly seen. Figures [6-5] and [6-6] present the deconvoluted results for Hg* scattered from K and Rb respectively. The corresponding scattering

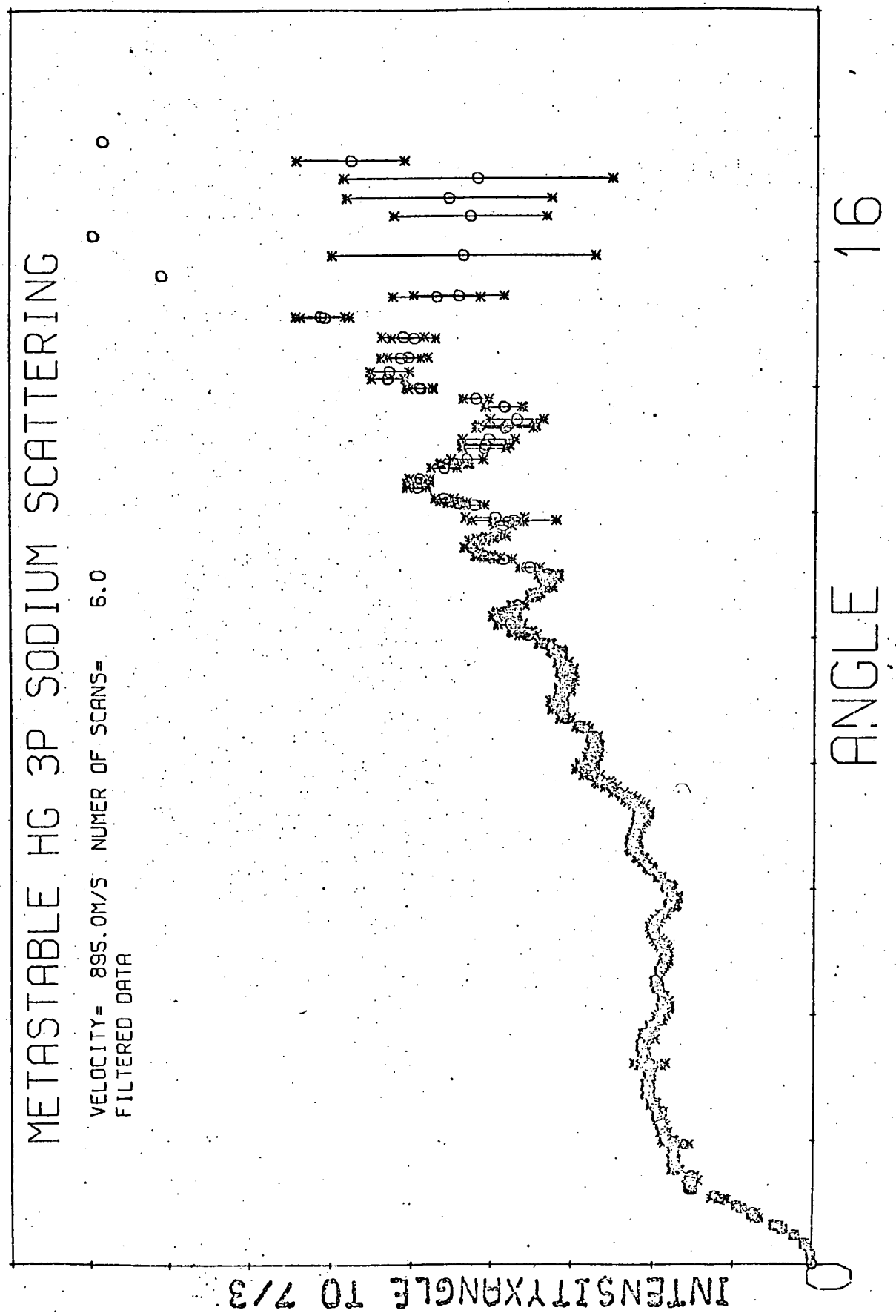

Laboratory differential cross section for Hg*/Na

Figure 6-3

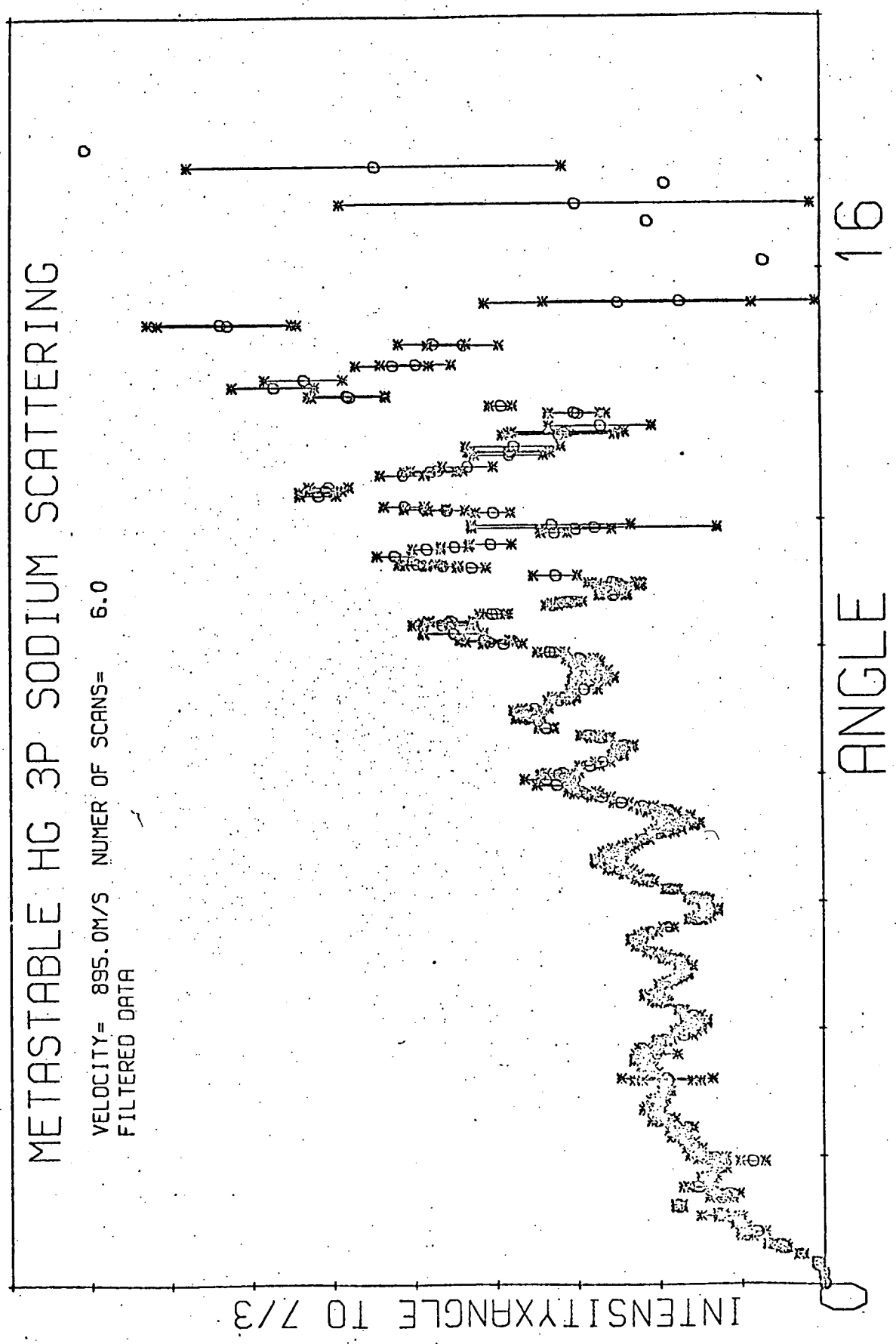

Laboratory differential cross section for Hg*/Na deconvoluted using the main beam profile

Figure 6-4

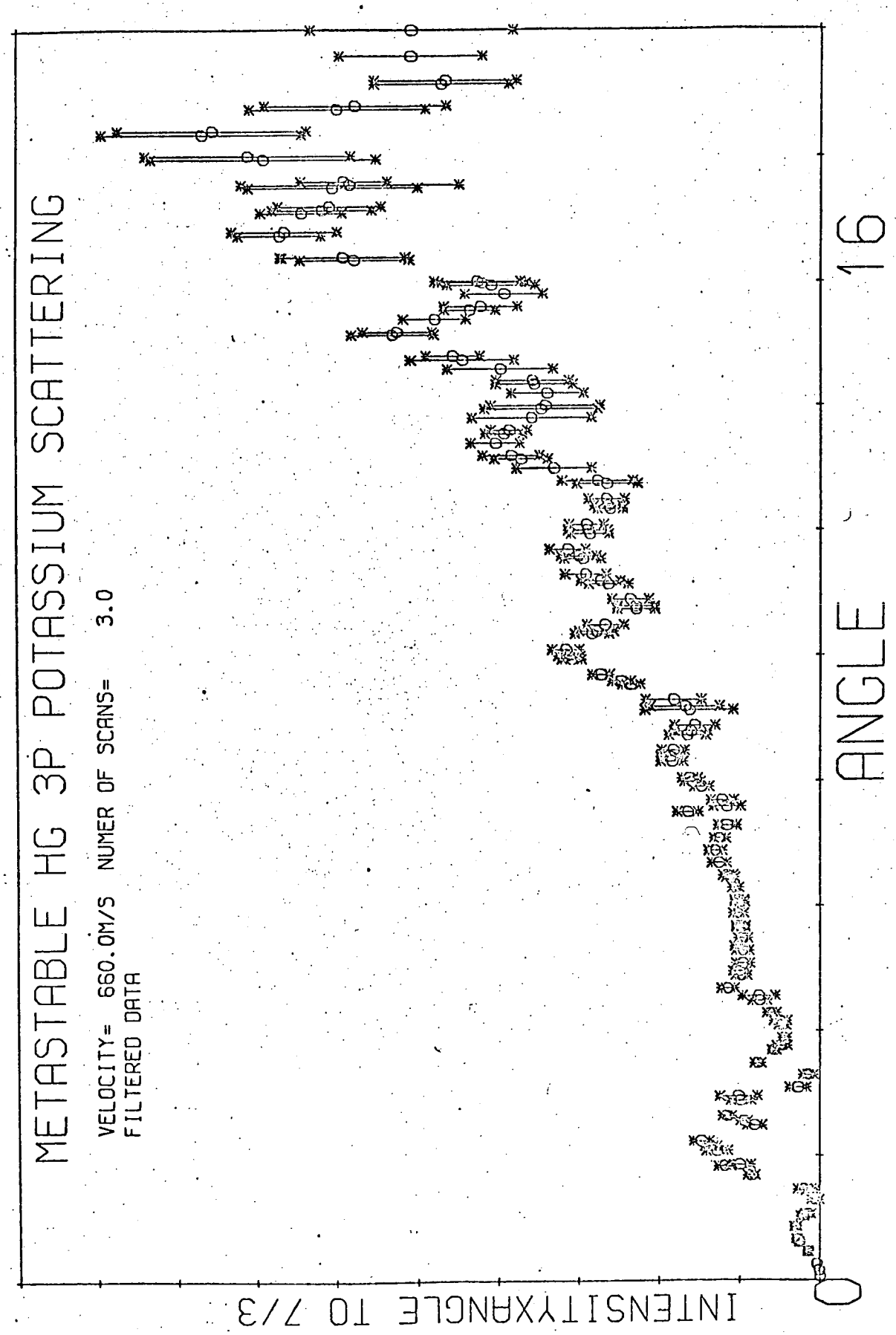

Laboratory differential cross section for Hg*/K deconvoluted using the main beam profile

Figure 6-5

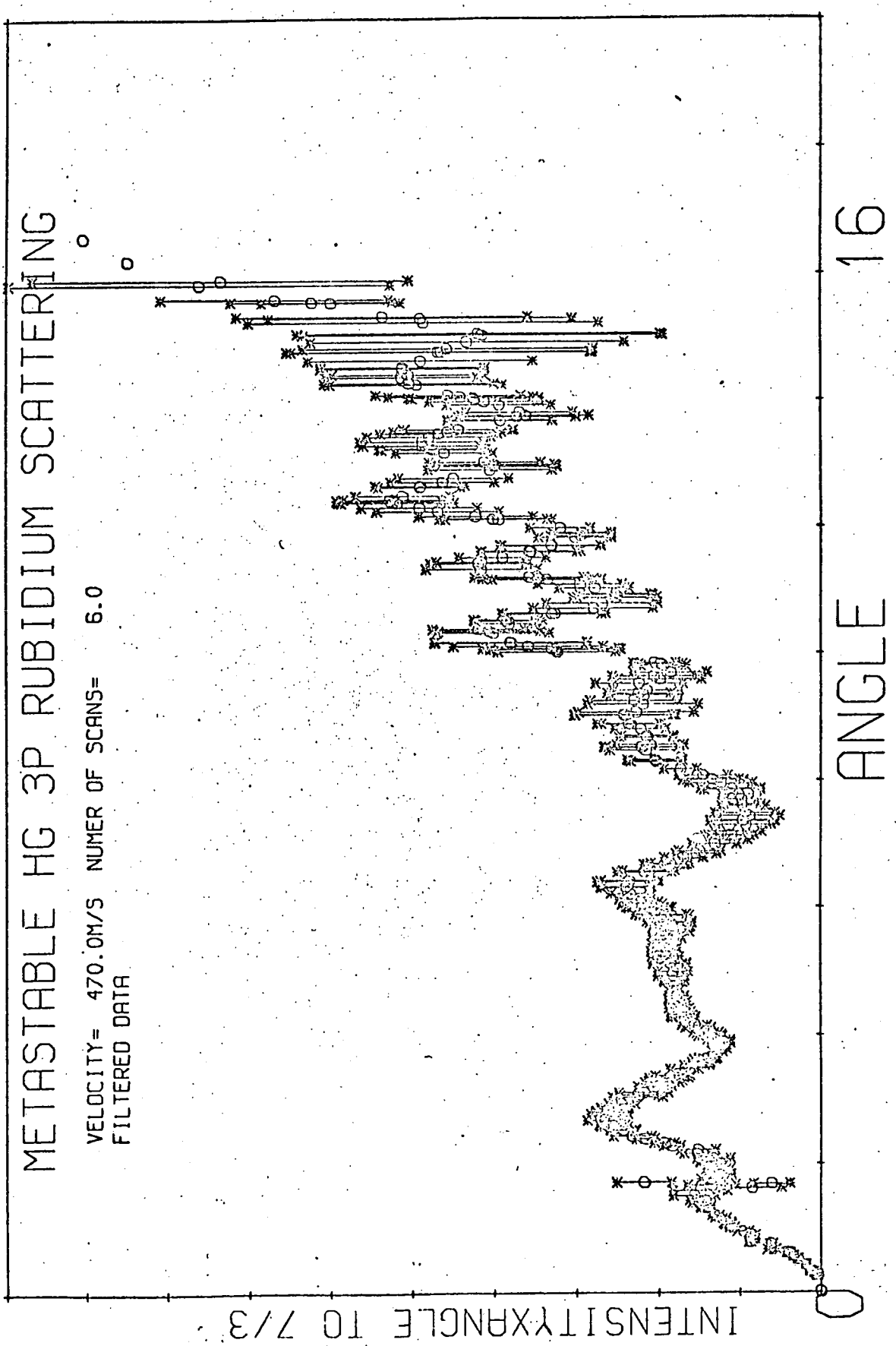

Laboratory differential cross section for Hg*/Rb deconvoluted using the main beam profile

Figure 6-6

patterns for Hg*/Na, Hg*/K and Hg*/Rb in the centre of mass system are shown in figures [6-7], [6-8] and [6-9]. Because the $^3P_2$ Hg atom decays appreciably during transit from scattering centre to detector, the Hg* velocity distribution is considerably distorted from the initial v^2 Maxwellian one out of the exciter. The appropriate velocity distribution at a distance L from the source is

$$I(v) = I(v_o^*) \left(\frac{v}{v_o^*}\right)^2 \exp\left\{\left[1 - \left(\frac{v}{v_o}\right)^2\right] - \frac{L}{\tau v}\right\} \qquad 6\text{-}2$$

where v_o^* is the most probable velocity at source and τ is the lifetime. At a distance L downstream the most probable velocity of the Hg* is $\sim$ 38% greater than that for a stable species at the same temperature. The relative velocity distribution is not affected so much, the full width at half height being reduced by <10%. The most probable velocity also changes slightly with the angle of scattering (< 10%). The relative masses and velocities are such that at a given laboratory angle of observation there are two centre of mass angles contributing, leading to fast and slow scattered components. However, partly because of the ratio of Jacobians but also because of the substantially greater decay, the slow component is <10% of the fast component. Also it is fortunate that in the cases considered the forward and backward contributions to the laboratory scattering patterns arise from the same range of centre of mass scattering angles (Figs [6-10], [6-11] [6-12]). Therefore it has been possible to achieve an estimate for the backward contribution and to subtract it from the forward distribution. The centre of mass scattering patterns presented here have been obtained by the following iterative procedure. Each laboratory angle corresponds to two centre of mass angles CMA(1) and CMB(1). CMA(1) represents the angle which corresponds to

Centre of mass differential cross section for Hg*/Na

Figure 6-7

Centre of mass differential cross section for Hg*/K

Figure 6-8

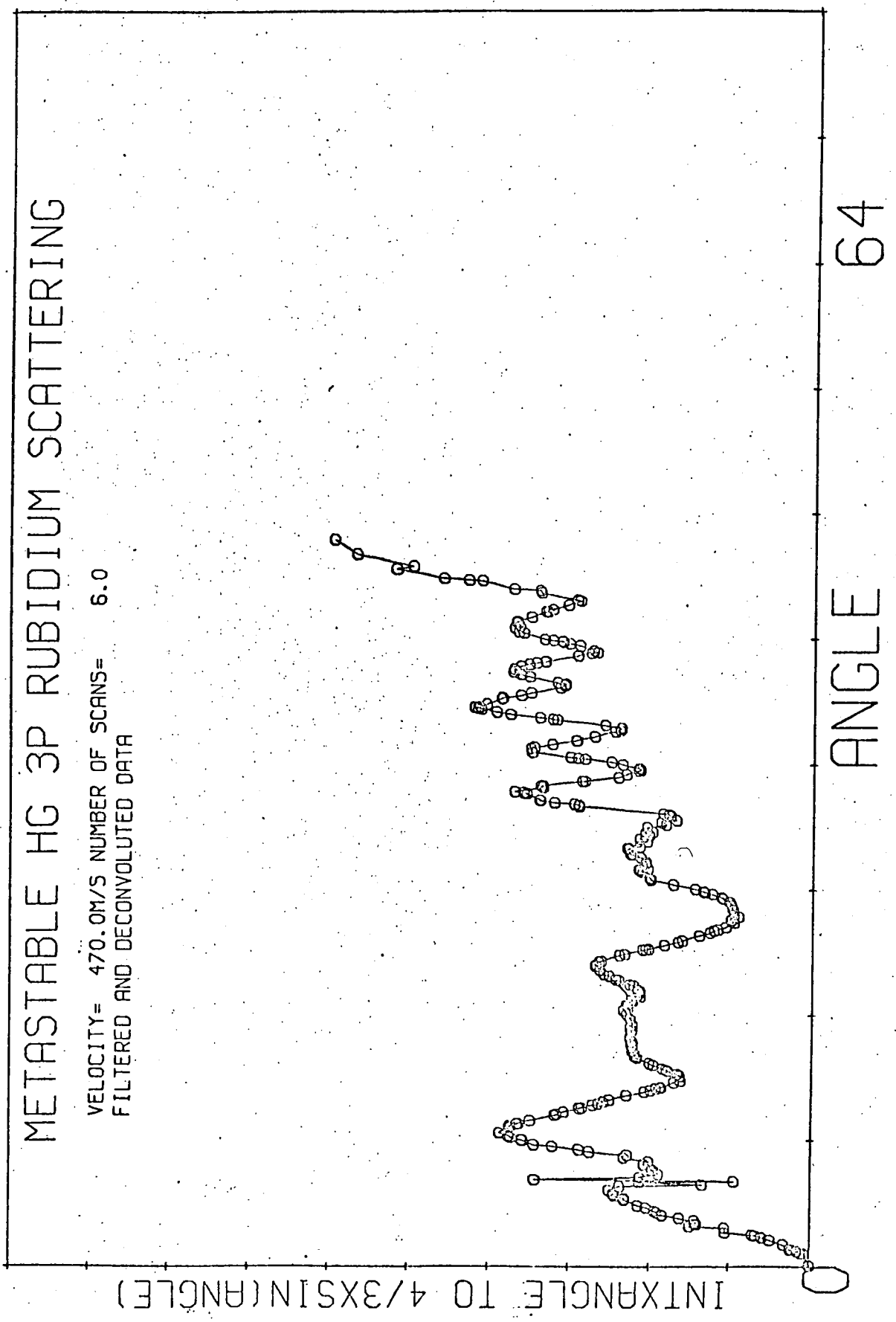

Centre of mass differential cross section for Hg*/Rb

Figure 6-9

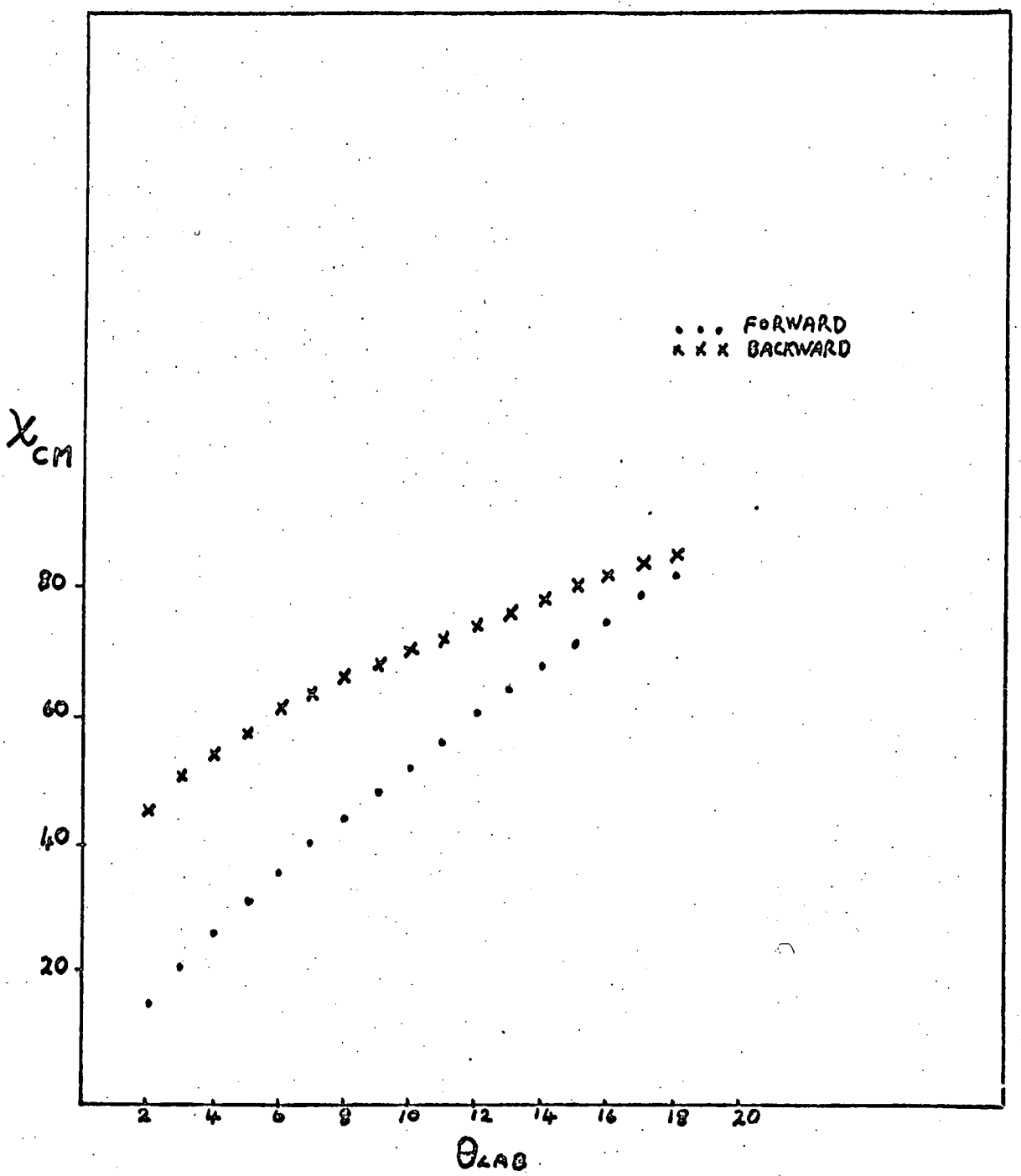

Centre of mass scattering angles v laboratory angles for Hg*/Na

Figure 6-10

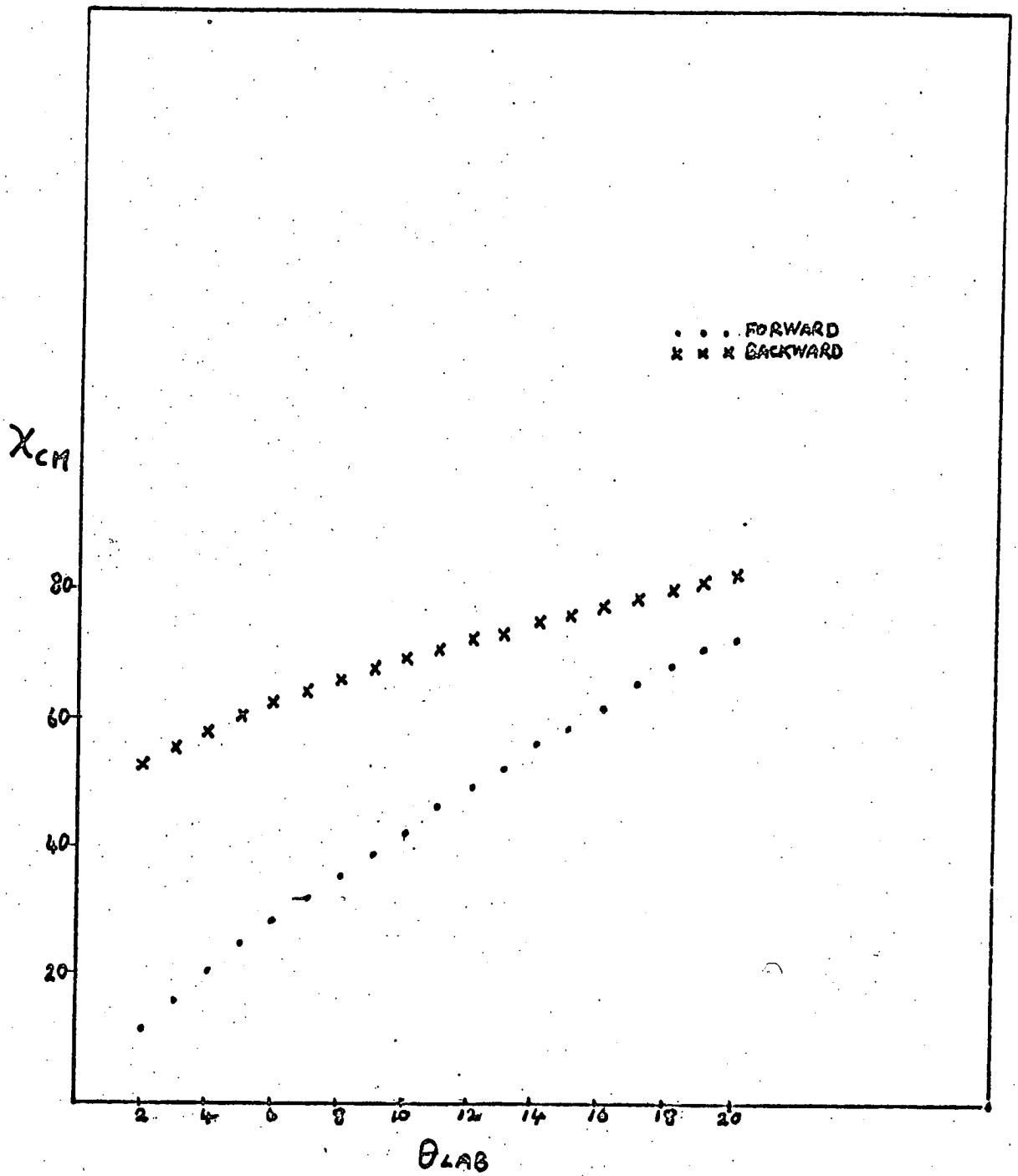

Centre of mass scattering angles versus laboratory angles for Hg*/K

Figure 6-11

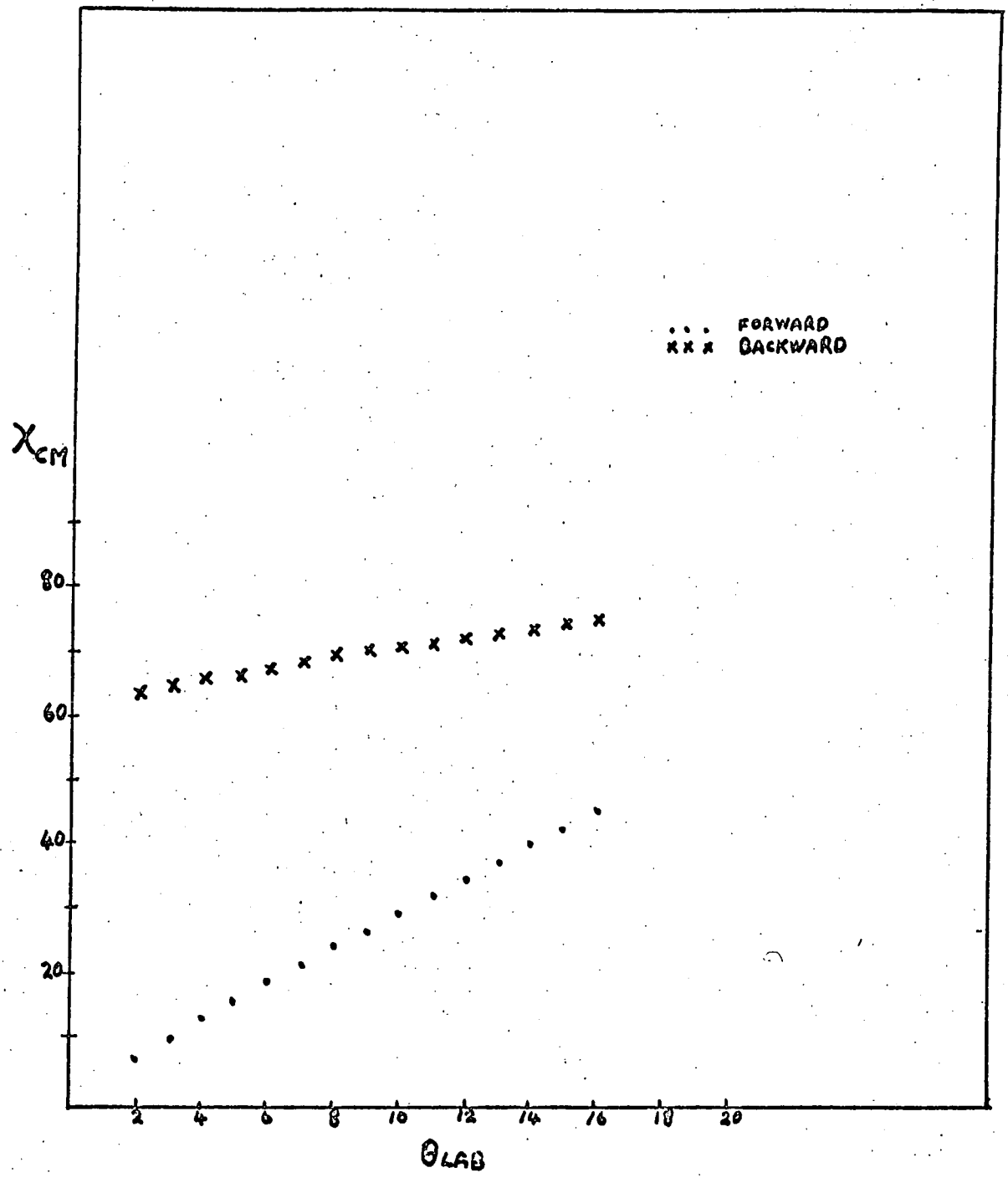

Centre of mass scattering angles versus laboratory angles for Hg*/Rb

Figure 6-12

forward scattering whereas CMB(1) represents the backward scattering angle. Now CMB(1) is equal to another angle CMA(2) which is an angle corresponding to forward scattering. The signal at CMA(2) multiplied by the ratio of the Jacobians is taken to be the backward scattered signal for CMB(1) in the first approximation and is subtracted from the signal at CMA(1). Thus a new set of values for the signal at all angles is produced and the procedure repeated until the signal values converge. In all cases convergence was reached after 3 iterations.

Preliminary Analysis

The most striking qualitative feature of these results is the presence of strong undulations in the differential cross section which cover the whole angular range of observation with undiminished amplitude. This rather simple oscillatory structure is similar to that expected from a single potential at collision energies leading to orbiting or a rainbow well beyond the angular range since if several different potentials, as would be expected from the different m_J states, with similar weights were operating the net interference structure would be much weakened by the superposition of the separate patterns.

With reference to Figure [6-7] analysis of the angular periods in the interference structure can be made using the semi-classical relation

$$\Delta\chi = \frac{2\pi}{\ell_1 - \ell_2}$$

where ℓ_1 and ℓ_2 are the orbital angular momenta values for two interfering branches on the attractive side of the deflection function

(Fig [6-13]). By measuring the separation of the maxima and minima a deflection function can be calculated from their positions (Table [6-3]).

TABLE 6-3

θ LAB	χ CM	Δχ	Δℓ
.75	6.5		
		3.0	120 ± 10
1.25	9.5		
		3.5	104 ± 10
1.75	13.0		
		3.5	104 ± 10
2.35	16.5		
		4.0	80 ± 10
3.10	20.5		
		4.0	80 ± 10
3.75	24.5		
		4.0	80 ± 10
4.50	28.5		
		4.0	80 ± 10
5.25	32.5		
		5.0	72 ± 10
6.45	37.5		
		5.5	67 ± 10
7.80	43.0		
		5.0	72 ± 10
8.90	48.0		
		5.0	72 ± 10
10.30	53.0		
		5.0	72 ± 10
11.80	58.0		
		5.0	72 ± 10
13.00	63.0		
		5.5	67 ± 10
14.35	68.5		

Highfrequency structure which is evident has been used to locate the range of the potential. The interference spacing of this high frequency structure is given by

$$\Delta\chi_{HF} = \frac{2\pi}{\ell_2+\ell_3}$$

ℓ_2 and ℓ_3 converge at $\chi=0$ and therefore for small angles

$$\Delta\chi \simeq \frac{\pi}{\ell_o} \simeq \frac{\pi}{kb_o} .$$

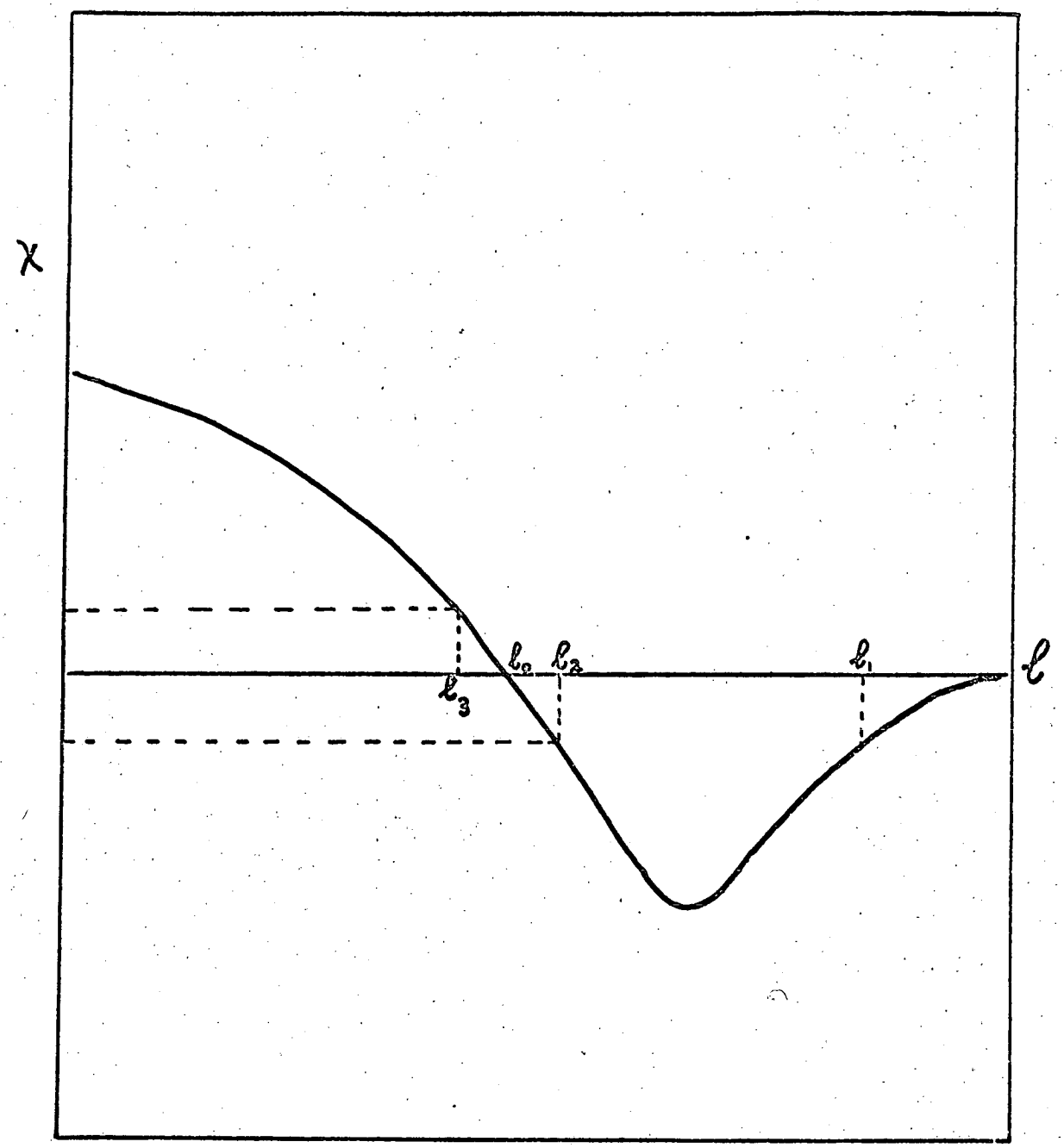

Typical deflection function

Figure 6-13

The value obtained in the case of sodium was ℓ_0=180 since at narrow angles the spacing of the high frequency structure was $\sim 1.0^{\circ}$. This value of ℓ_0 is useful in locating the range of the potential. A deflection function calculated in this manner from the Hg*/Na data is shown in figure [6-14]. Unfortunately the rainbow angle was not observed in this experiment and so the value of the rainbow angle is uncertain. Three possible deflection functions (Fig [6-14]), with a reasonable guess made for the rainbow angle were then inverted using the Firsov procedure and three potentials were obtained (Fig [6-14]). A forward calculation using the computer program, Monoenergy forward, was then obtained and it was found that the deeper of the three potentials gave best agreement with the experimental scattering pattern (Fig [6-15]).

The agreement between the two sets is not outstanding but is reasonable enough to suggest that the initial assumption that the scattering pattern is due to interfering branches of the deflection function is secure.

Detailed Inversion

Since the simple analysis described produces acceptable agreement with experimental results and suggests a single effective potential it should be possible to utilise the more sophisticated method of Buck [BUC 1971(a)] in a treatment of the results. This method involves a construction of the deflection function from the measured differential cross section and uses as essential starting information only the angular positions of the measured extrema i.e. neither the absolute value of the differential cross section nor its relative

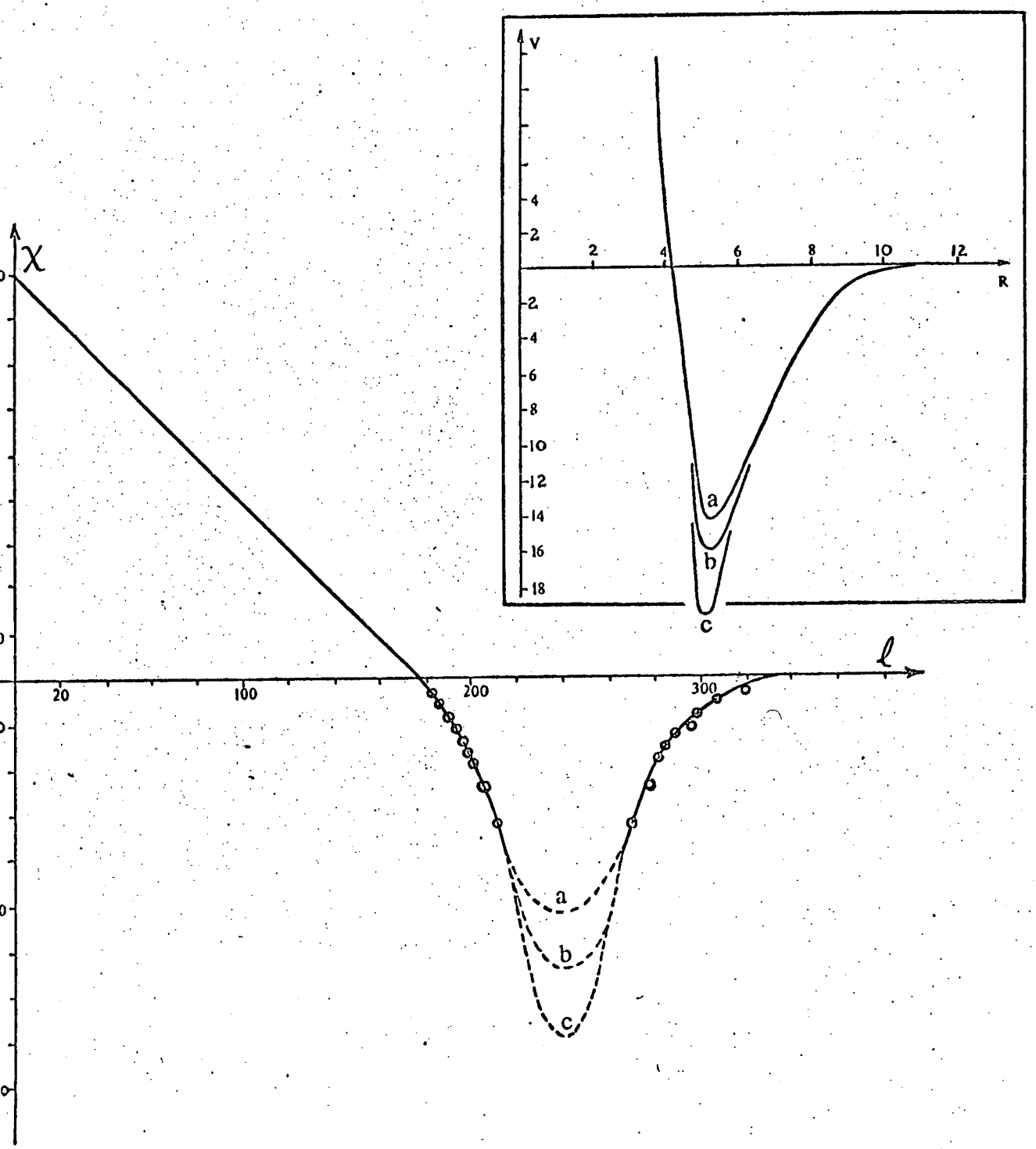

Set of three possible deflection functions for Hg*/Na from preliminary analysis. The corresponding potentials are also shown.

Figure 6-14

Comparison of the observed and calculated cross section for Hg*/Na. A monoenergy forward calculation has been carried out on the preliminary analysis data of figure 6-14.

Figure 6-15

shape is required. According to Buck, this has the great advantage that these extrema positions are almost independent of various angular and energy averaging processes in the beams.

The measured cross section M can be used to determine the deflection function in the general case in the following way. The cross section M is in every situation only a function of the impact parameter b and the angle χ. If an inverse function $b=f^{-1}(\chi)$ of the function $\chi=f(b)$ exists, then the experimental quantity M can be written as $M=M\left[f^{-1}(\chi),\chi\right]$ and this depends only upon χ, although implicitly. M in this form can then be compared directly with the experimental values and $f^{-1}(\chi)$ can be determined from this comparison. Therefore the deflection function is constructed from arbitrary monotonic functions f with $\chi = \Sigma_i f_i$; the cross section is calculated using f_i and f_i is determined by minimising the expression

$$\sum_j (Mj, \text{expt} - Mj)^2 \qquad 6\text{-}3$$

where j is the number of data points.

From the Berry approximation [BER 1966] the calculated differential cross section is given by

$$\sigma(\chi) = \pi(\sigma_2^{\frac{1}{2}} + \sigma_1^{\frac{1}{2}})\ |Z|^{\frac{1}{2}}\ \mathrm{Ai}\ (-|Z|) + \pi\ (\sigma_1^{\frac{1}{2}} - \sigma_2^{\frac{1}{2}})\ |Z|^{-\frac{1}{2}}\ A_1^{\prime 2}\ (-|Z|\ ) \qquad 6\text{-}4$$

where $\sigma_i(\chi) = \dfrac{bi}{\sin\chi\left|\frac{d\chi}{db}\right|}$ is the classical differential cross section, A_i and A_i' are the Airy function and its first derivative respectively, and $\frac{4}{3}Z^{\frac{3}{2}} = |\Delta\gamma|$.

$$\Delta\gamma = \gamma_2 - \gamma_1 = 2\eta(b_2) - 2\eta(b_1) + k\theta(b_2 - b_1)$$

($\Delta\gamma$ are the phase differences of the interfering partial waves).

The positions of the extrema in the cross section are noted and the maxima are counted as integers and the minima as half integers, starting with the classical rainbow. The equation used to calculate Z is

$$(N - \tfrac{3}{4})\, 2\pi = \tfrac{4}{3} Z_N^{\frac{3}{2}} \qquad 6\text{-}5$$

where N is the index of the peak. The values of Z calculated from this equation are given in table [6-4].

Table 6-4

Values of Z_N calculated for various indices

N	Z_N	N	Z_N	N	Z_N
1.0	1.115	5.5	7.941	10.0	12.38
1.5	2.320	6.0	8.489	10.5	12.82
2.0	3.261	6.5	9.019	11.0	13.26
2.5	4.081	7.0	9.535	11.5	13.69
3.0	4.826	7.5	10.04	12.0	14.11
3.5	5.516	8.0	10.53	12.5	14.52
4.0	6.166	8.5	11.01	13.0	14.93
4.5	6.783	9.0	11.47	13.5	15.34
5.0	7.373	9.5	11.93	14.0	15.73

Z_N is then considered as an experimental quantity and can be written

$$Z_N = (0.75 \{ 2n(b_2(\chi)) - 2n(b_1(\chi)) + k\chi_N b_2(\chi_N) - k\chi_N b_1(\chi_N) \})^{\frac{2}{3}} \qquad 6\text{-}6$$

Simple mathematically invertible functions are chosen for f_i. The region of the zero crossing is represented by a straight line, the minimum by a parabola, the asymptotical behaviour by a C^6/b^6 representation and the region in between by an inverse power [Fig 6-16].

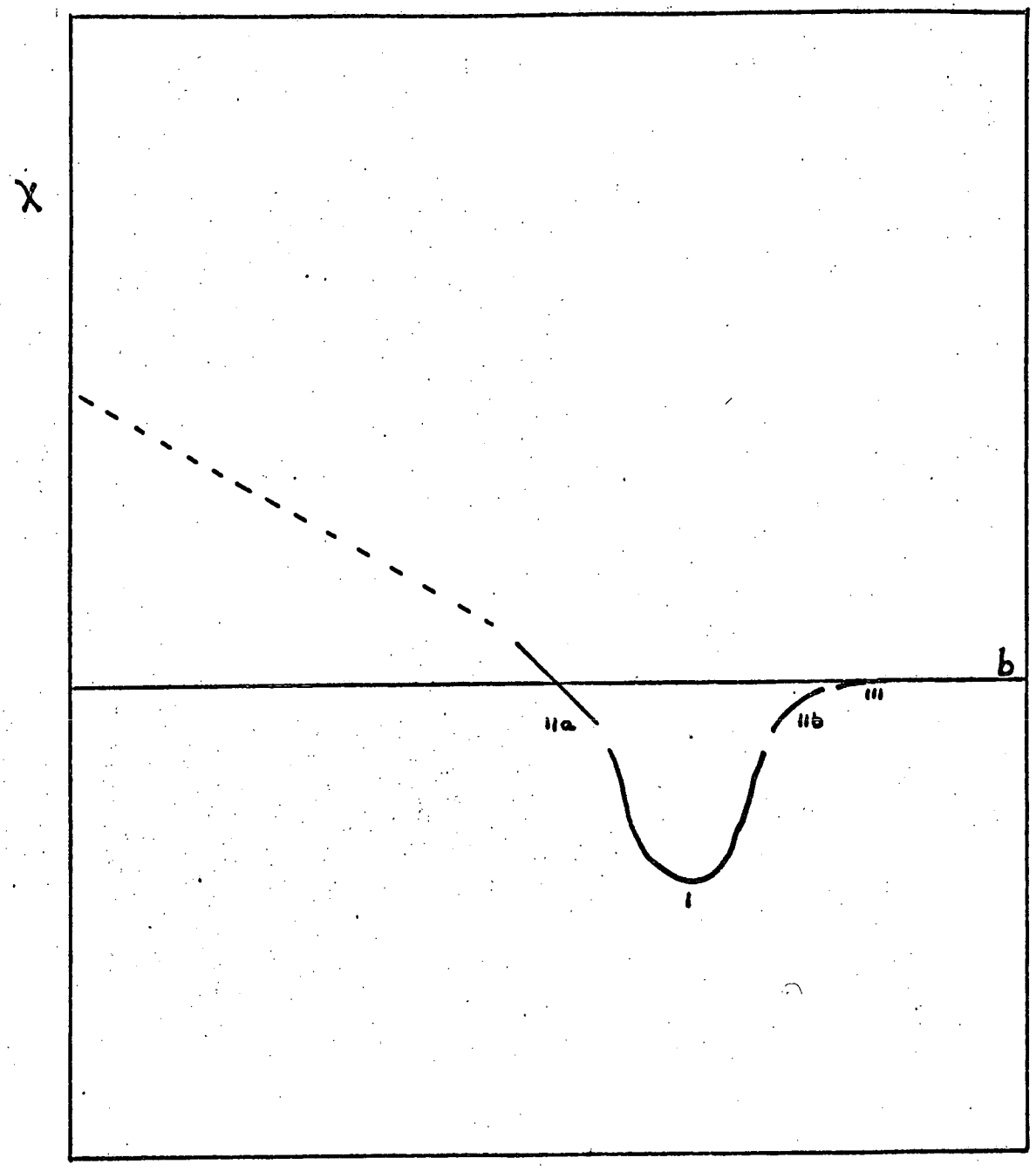

Parameterised deflection function

(i) Parabolic region
(iia) Straight line region
(iib) Exponential region
(iii) $\frac{C^6}{R^6}$ region.

Figure 6-16

The quantities Z_N as a function of χ_N can then be calculated.

1) In the region of the minimum

$$\chi(b) = -\chi r + q\,(b_{2,1} - b_R)^2 \qquad 6\text{-}7$$

$$Z_N = k^{\frac{2}{3}} q^{-\frac{1}{3}} (\chi_R - \chi_N) \qquad 6\text{-}8$$

where χ_R is the rainbow angle, b_R is the impact parameter corresponding to the rainbow and q is the curvature of the parabola.

2) In the region next to the minimum

$$\chi(b) = -a_1 (b_2 - b_0) \qquad a_1 > 0 \qquad 6\text{-}9a$$

$$\chi(b) = -c_1 b_1^{-C_2} \qquad 6\text{-}9b$$

$$Z_N = 0.75^{\frac{2}{3}}\left[2\eta_0 + kb_0\,\chi_N + \tfrac{1}{2}\,ka_1^{-1}\,\chi_N^2 - kC_1^{\alpha}\,(1-\alpha)^{-1}\,\chi_N^{(1-\alpha)}\right]^{\frac{2}{3}} \qquad 6\text{-}10$$

where η_0 is the maximum phase and $\alpha = C_2^{-1}$.

3) In the asymptotic region the formulae [6-9] and [6-10] are valid but the substitution

$C_1 = (\frac{15}{16})\,\pi\,(\frac{C}{E})$; $C_2 = 6$ is used where C is Van der Waals constant.

A minimisation procedure is then used in determining the unknowns while taking account of the continuity equations at the intersections of the regions. Altogether the following coefficients must be determined.

Region (1) χ_R, q, b_R

(11) η_o, b_o, a_1, c_1, c_2

(111) C

Buck's data was used in a preliminary test of the method and the same potential was obtained. In this calculation the parameter C was fixed and the value calculated by Darwall was used [DAR 1972], the other parameters were variable. Initial guesses for these

parameters were determined from the shape of the deflection functions obtained from the relationships:

$$\Delta\chi = \frac{2\pi}{\ell_1 - \ell_2} \quad , \quad \Delta\chi_{HF} = \frac{2\pi}{\ell_2 + \ell_3}$$

Unfortunately in these experiments the rainbow angle was not observed and therefore a number of different indexing schemes were tested in order to achieve the best fit to the data. The errors between the calculated and experimental values of Z_N are shown for different indexing schemes in table [6-5] and are displayed graphically in figure [6-17].

Table 6-5
Calculated Errors for various indexing schemes

SYSTEM	1st PEAK	INDEX	ERROR
Hg*/Na	69.5°	6	.20777
Hg*/Na	69.5°	8	.17015
Hg*/Na	69.5°	10	.15034
Hg*/Na	69.5°	12	.16987
Hg*/Na	69.5°	14	.17932
Hg*/Na	69.5°	16	.19006
Hg*/K	70.4°	6	.67654
Hg*/K	70.4°	8	.54562
Hg*/K	70.4°	10	.46925
Hg*/K	70.4°	12	.41810
Hg*/K	70.4°	14	.44604
Hg*/K	70.4°	16	.46513
Hg*/Rb	40.6°	12	.074234
Hg*/Rb	40.6°	18	.068607
Hg*/Rb	40.6°	20	.063348
Hg*/Rb	40.6°	22	.061020
Hg/*Rb	40.6°	24	.059438
Hg*/Rb	40.6°	26	.060273
Hg*/Rb	40.6°	28	.062540

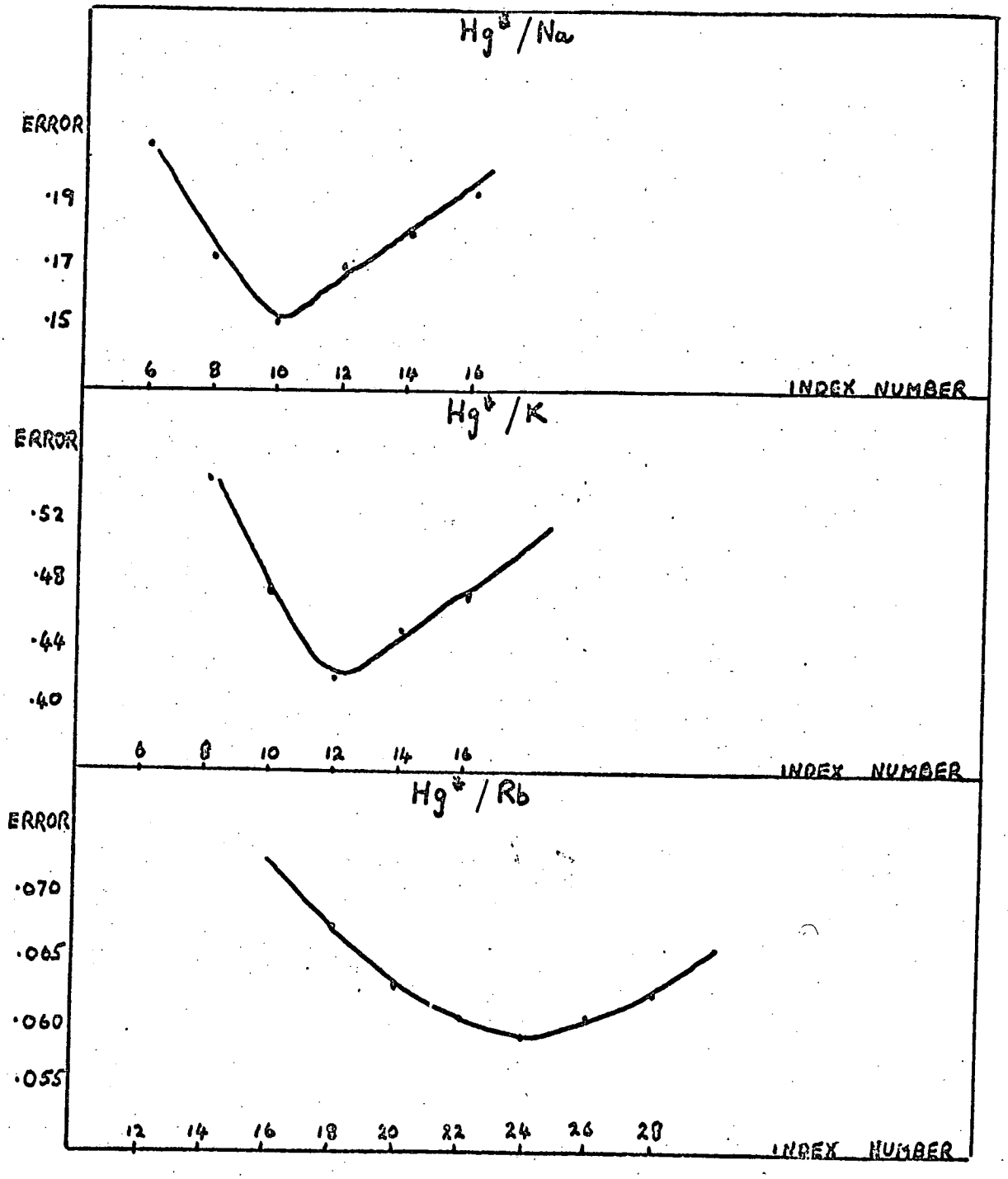

Calculated error versus index number for all three systems in the fitting routine.

Figure 6-17

The data is fitted for 21 extrema in the case of sodium, for 37 extrema in the case of potassium and for only 10 extrema in the case of rubidium. The Rb data was not so well resolved and because the centre of mass transformation is less favourable in this case a smaller angular range was available than for the other systems.

At a glance the agreement between experimental and calculated extrema positions appears to be best in the case of Hg*/Rb and worst in the Hg*/K situation. However, it should be pointed out that the error is the sum of the squares of the differences between experimental and calculated values of Z_N and is greatest for Hg*/K since a much larger number of extrema points have to be fitted using the same limited number of variable parameters. This highlights the great weakness of this method of analysis since it is obvious that a greater number of variable parameters is required to produce an accurate fit in cases where a large number of extrema are resolved. On this point I should like to criticize the work of Buck et al since they appear to use only five extrema to produce a best fit to their data when they have five variable parameters despite the fact that as many as 27 extrema are resolved. This is a great waste of data. A more accurate fit to the data should be possible by increasing the number of variable parameters to match the number of data points but unfortunately this has not yet been achieved since it has proved difficult to evaluate Z_N when the deflection function is not made up from simple mathematically invertible forms such as the straight line, the parabola and the exponential, already incorporated. Work is in progress in the laboratory at Edinburgh in an attempt to resolve this.

Bearing in mind the inadequacies of the above technique, deflection functions were obtained for the Hg*/alkali systems. The results for the best fits for Z_N and the angular position are shown in tables [6-6], [6-7] and [6-8]. Using the Firsov formulae,

$$r_m = b \exp \left\{ \frac{1}{\pi} \int_b^\infty \frac{\chi (b^1)}{\sqrt{b^{12}-b^2}} \, db^1 \right\},$$

$$V(r_m) = E \left(1 - \frac{b^2}{r_m^2}\right)$$

the deflection functions were then inverted and potentials were produced for the interactions Hg*/Na, Hg*/K and Hg*/Rb and are listed in tables [6-9], [6-10], and [6-11] (The Firsov inversion program was tested for a Lennard Jones (12:6) potential and was found to be correct). The calculated potentials are displayed graphically in figures [6-18], [6-19] and [6-20].

Table 6-6

Best fit achieved for Hg*/Na.

N	Z EXPT	Z calc	χ EXP	χ calc
10.0	12.386	12.285	69.50	68.87
10.5	12.828	12.832	66.10	66.12
11.0	13.263	13.476	62.10	63.22
11.5	13.691	13.814	60.00	60.76
12.0	14.112	14.087	58.30	58.14
12.5	14.528	14.457	56.00	55.86
13.0	14.937	14.811	53.80	53.02
13.5	15.341	15.262	51.00	50.52
14.0	15.739	15.745	48.00	48.03
14.5	16.133	16.131	45.60	45.59
15.0	16.521	16.485	43.40	43.17
15.5	16.905	17.000	40.20	40.78
16.0	17.285	17.276	38.40	38.37
16.5	17.661	17.730	35.00	35.54
17.0	18.033	18.093	32.40	32.86
17.5	18.401	18.381	30.40	30.31
18.0	18.765	18.739	28.00	27.86
18.5	19.126	19.016	26.40	25.72
19.0	19.484	19.441	23.50	23.30
19.5	19.838	19.850	21.00	21.11
20.0	20.189	20.291	18.40	18.70

Table 6-7

Best fit achieved for Hg*/K

N	Z EXP	Z calc	χ EXPT	χ calc
12.00	14.112	14.293	70.40	71.10
12.50	14.528	14.614	69.00	69.36
13.00	14.937	14.980	67.40	67.58
13.50	15.341	15.300	66.00	65.82
14.00	15.739	15.650	64.60	64.08
14.50	16.133	16.089	62.70	62.36
15.00	16.521	16.513	60.70	60.66
15.50	16.905	16.857	59.20	58.98
16.00	17.285	17.223	57.60	57.32
16.50	17.661	17.635	55.80	55.68
17.00	18.033	18.047	54.00	54.06
17.50	18.401	18.413	52.40	52.45
18.00	18.765	18.779	50.80	50.86
18.50	19.126	19.100	49.40	49.30
19.00	19.484	19.394	48.20	47.78
19.50	19.838	19.786	46.40	46.17
20.00	20.189	20.153	44.80	44.64
20.50	20.537	20.610	42.80	43.00
21.00	20.883	21.008	40.80	41.20
21.50	21.225	21.109	39.00	38.38
22.00	21.565	21.420	37.20	36.42
22.50	21.901	21.808	35.00	34.53
23.00	22.236	22.208	32.80	32.69
23.50	22.568	22.656	30.40	30.80
24.00	22.897	22.923	29.00	29.15
24.50	23.224	23.313	27.00	27.35
25.00	23.549	23.762	24.60	24.87
25.50	23.872	24.007	23.20	23.80
26.00	24.192	24.286	22.00	22.59
26.50	24.511	24.606	20.40	20.17
27.00	24.827	24.837	19.60	19.69
27.50	25.141	25.141	18.22	18.22
28.00	25.453	25.373	17.60	18.05

Table 6-8

Best fit achieved for Hg*/Rb

N	Z EXPT	Z calc	χ EXPT	χ calc
24.00	22.897	23.007	40.60	41.10
24.50	23.224	23.310	39.00	39.40
25.00	23.549	23.512	38.00	37.80
25.50	23.877	23.705	37.00	36.20
26.00	24.192	24.214	35.40	35.54
26.50	24.511	24.523	34.00	34.09
27.00	24.827	24.837	32.60	32.68
27.50	25.141	25.103	31.60	31.31
28.00	25.453	25.435	30.00	29.97
28.50	25.764	25.796	28.40	28.60

Table 6-9

The potential for Hg*/Na

The potential parameters are calculated to be

$r_m = 4 \cdot 829$ Å $\Sigma = 23 \cdot 06 \times 10^{-14}$ ergs

r(Å)	V($\times 10^{-14}$ ergs)	$\frac{r}{r_m}$	$\frac{V}{\Sigma}$
4.2495	+1.406	.8800	.0610
4.2939	+0.7148	.8892	.0310
4.3330	-0.8416	.8973	-.0365
4.3930	-2.5366	.9098	-.1100
4.4410	-4.5059	.9197	-.1954
4.4930	-6.9133	.9306	-.2998
4.5498	-8.5529	.9422	-.3709
4.6097	-10.065	.9546	-.4365
4.6392	-19.232	.9607	-.8340
4.7670	-20.795	.9873	-.9018
4.8291	-23.060	1.000	-1.0000
5.0994	-22.179	1.056	-.9618
5.5678	-18.939	1.153	-.8213
5.8237	-16.879	1.206	-.7320
6.2294	-14.449	1.290	-.6266
6.6398	-12.341	1.375	-.5352
7.0841	-9.743	1.467	-.4225
7.6394	-7.653	1.582	-.3319
8.0934	-5.562	1.676	-.2412
8.5618	-4.391	1.773	-.1904
9.1654	-2.370	1.898	-.1028
9.9670	-0.828	2.064	-.0359
10.449	-0.403	2.164	-.0175

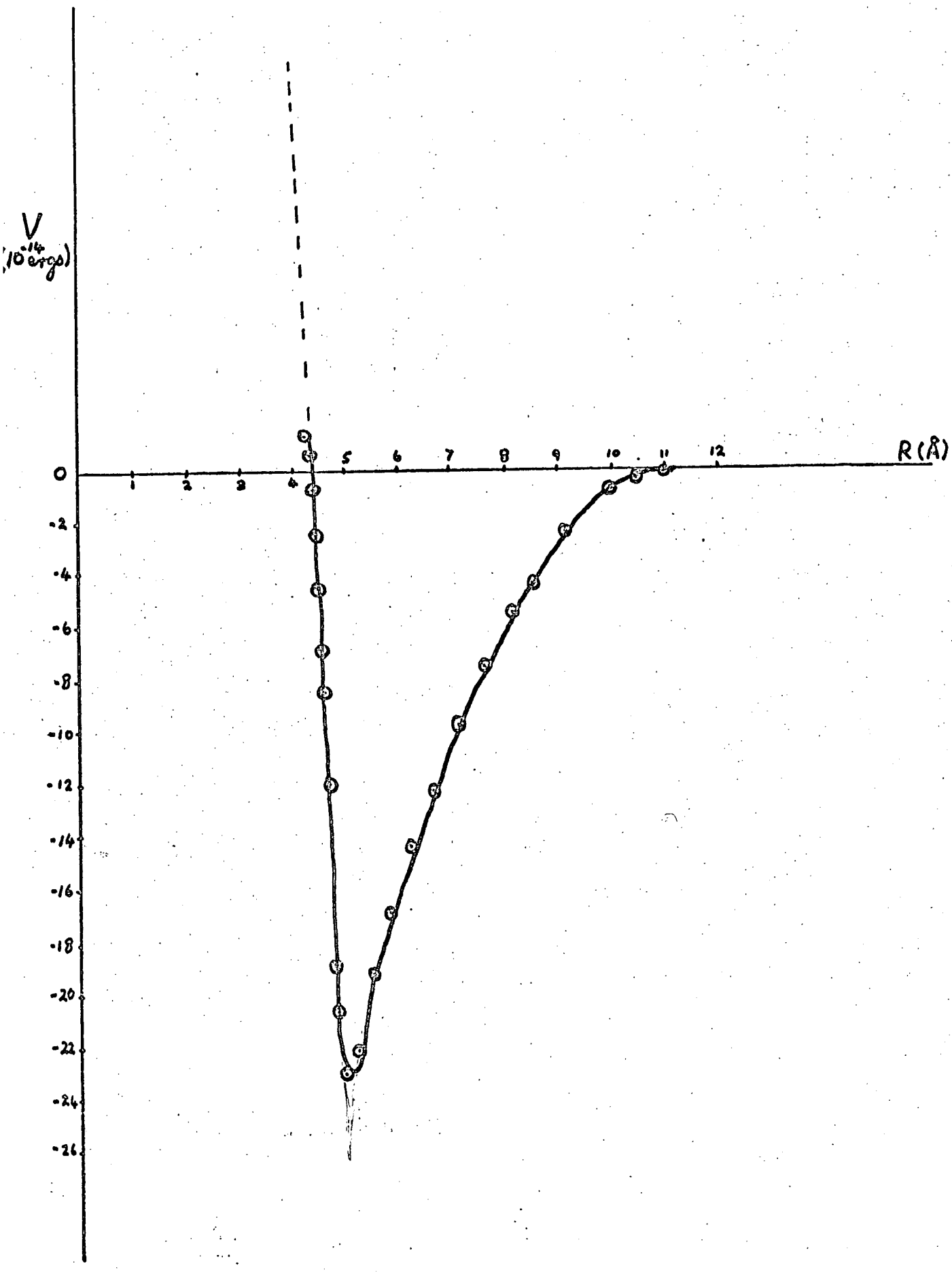

The potential for Hg*/Na

Figure 6-18

Table 6-10

The potential for Hg*/K

The potential parameters are calculated to be

r_m = 5.05 Å $\Sigma = 22.73 \times 10^{-14}$ ergs

r(Å)	$V \times 10^{-14}$ ergs	$\frac{r}{r_m}$	$\frac{V}{\Sigma}$
4.443	+1.751	.8798	+.0769
4.481	-0.364	.8873	-.0160
4.521	-1.058	.8952	-.0465
4.564	-2.509	.9037	-.1103
4.609	-3.985	.9126	-.1753
4.656	-5.481	.9219	-.2411
4.704	-6.995	.9314	-.3079
4.753	-8.532	.9411	-.3739
4.800	-10.11	.9504	-.4400
4.841	-18.46	.9586	-.8121
4.893	-22.57	.9689	-.9938
5.050	-22.73	1.000	-1.000
5.289	-21.77	1.047	-.9577
5.609	-19.91	1.110	-.8759
6.011	-17.44	1.190	-.7672
6.495	-14.63	1.286	-.6436
7.060	-11.73	1.398	-.5160
7.705	-8.908	1.525	-.3919
8.418	-6.326	1.666	-.2783
9.182	-4.078	1.818	-.1794
9.959	-2.239	1.971	-.0985
10.680	-0.908	2.114	-.0399
11.130	-0.421	2.200	-.0255
11.47	-0.251	2.271	-.0110
11.79	-0.152	2.334	-.0066
12.09	-0.094	2.394	-.0039
12.38	-0.058	2.451	-.0021
12.66	-0.036	2.507	-.0012

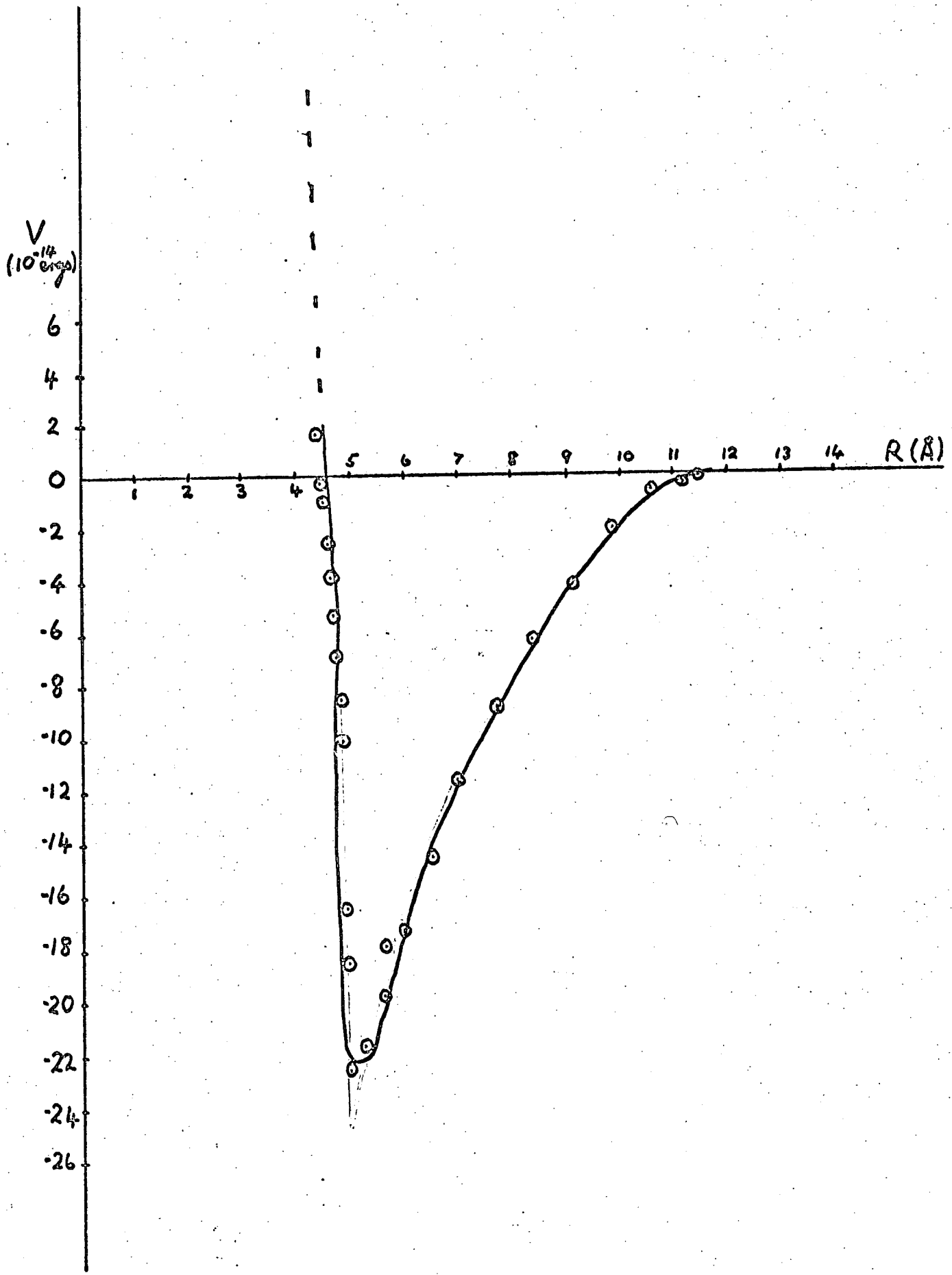

The potential for Hg*/K

Figure 6-19

Table 6-11

The potential for Hg*/Rb

The potential parameters are calculated to be

r_m = 5.20 Å $\Sigma = 22.03 \times 10^{-14}$ ergs

r(Å)	V($\times 10^{-14}$ ergs)	$\frac{r}{r_m}$	$\frac{V}{\Sigma}$
4.579	+1.4319	.8807	+.0650
4.633	+0.6829	.8910	+.0310
4.669	-1.1940	.8979	-.0542
4.715	-2.6568	.9068	-.1206
4.769	-4.4016	.9173	-.1998
4.835	-6.6112	.9298	-.3001
4.890	-8.3758	.9404	-.3802
4.945	-10.4246	.9511	-.4732
5.038	-18.8202	.9689	-.8543
5.200	-22.030	1.000	-1.0000
5.574	-20.9285	1.072	-.9500
5.902	-18.4832	1.135	-.8390
6.333	-15.5003	1.218	-.7036
6.853	-12.7025	1.318	-.5766
7.472	-9.9333	1.437	-.4506
8.153	-7.7523	1.568	-.3519
8.866	-4.1835	1.705	-.1899
9.505	-2.9167	1.828	-.1324
9.906	-2.1964	1.905	-.0997
10.244	-1.6037	1.970	-.0728
10.535	-0.6432	2.026	-.0293
10.795	-0.4692	2.076	-.0213

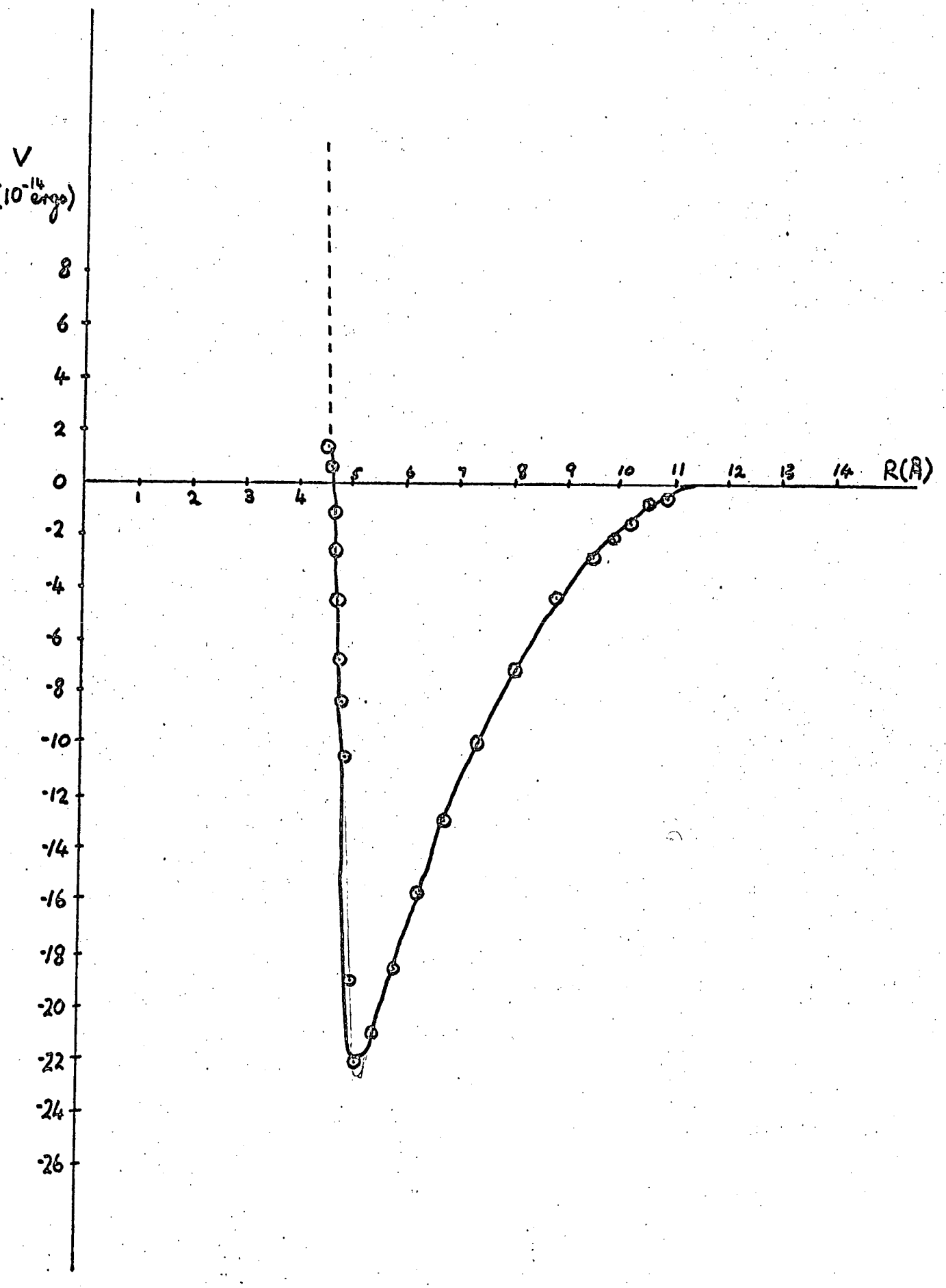

The potential for Hg*/Rb

Figure 6-20

At this stage it is worthwhile to consider the accuracy and uniqueness of these potentials. An attempt has been made to estimate the sensitivity of the potentials to changes in the deflection function. In figure [6-21(a)] a deflection function is shown for Hg*/K together with the potential calculated from it. This deflection function has been altered to make the bowl steeper and deeper, the potential obtained by its inversion is shown beside it. The major effect of this change is that the calculated potential energy well has become deeper and the value of r_M has also been decreased slightly while the asymptotic behaviour for large values of r remains unaltered. These are important points since the rainbow is not observed in these experiments and therefore the angular position of the rainbow and the well depth of the potential are uncertain.

As a consequence it is difficult to rule out the possibility that a deflection function such as that shown in figure [6-21(b)] might be the one appropriate to the scattering pattern produced. In figure [6-22] the same deflection function has been altered so that it is more attractive for large values of the impact parameter, i.e. the asymptotic approach to zero for large values of b is more gradual. The only effect that this has on the potential function is to make it more attractive at large separations [Fig 6-22(b)]. Unfortunately, the asymptotic behaviour, which contributes largely to narrow angle scattering, can not be determined very accurately from the scattering patterns obtained (these patterns supply their best information from between 20° and 60° in the centre of mass). It is therefore difficult to ascertain whether the potentials produced here have

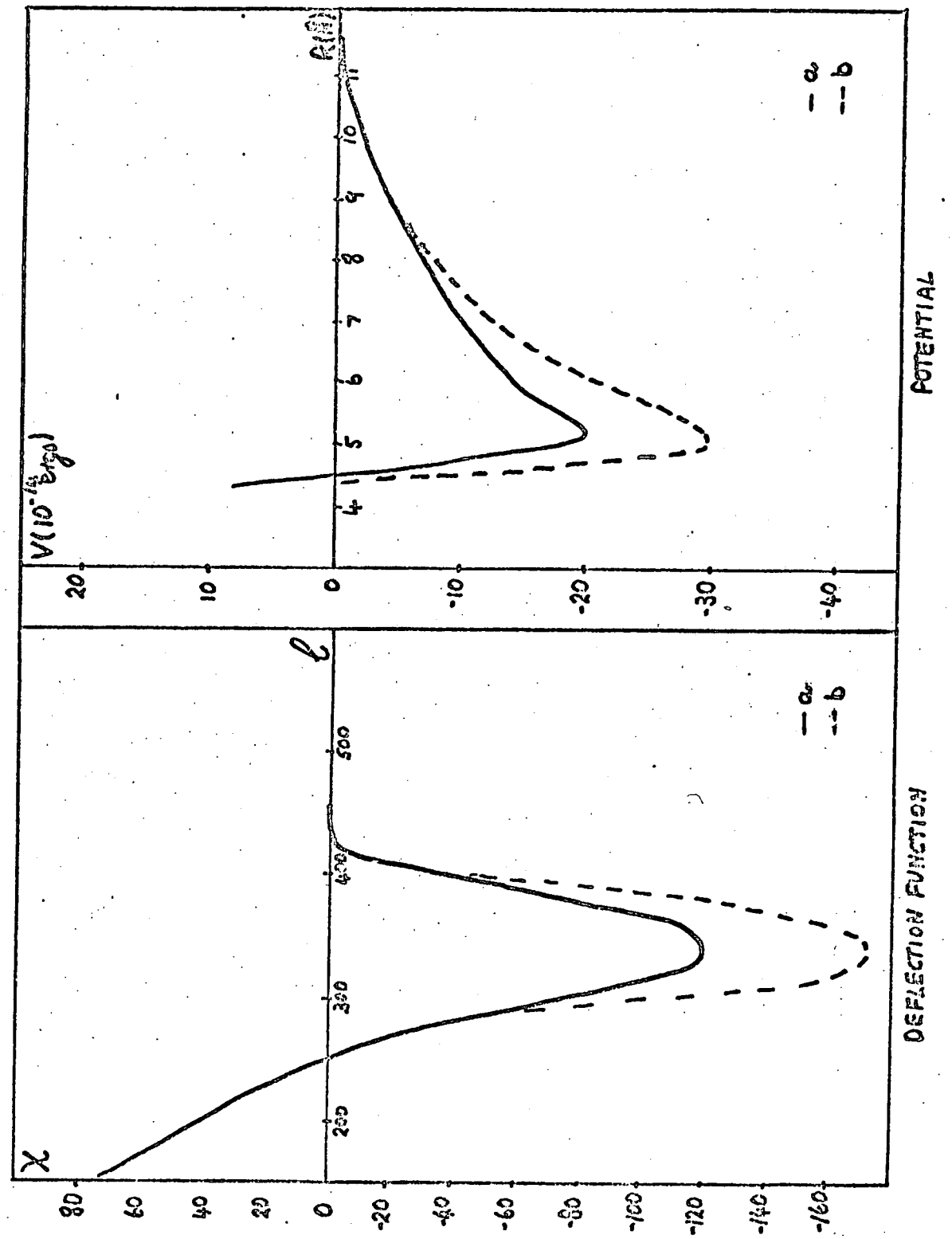

Potential changes produced by altering the deflection function

Figure 6-21

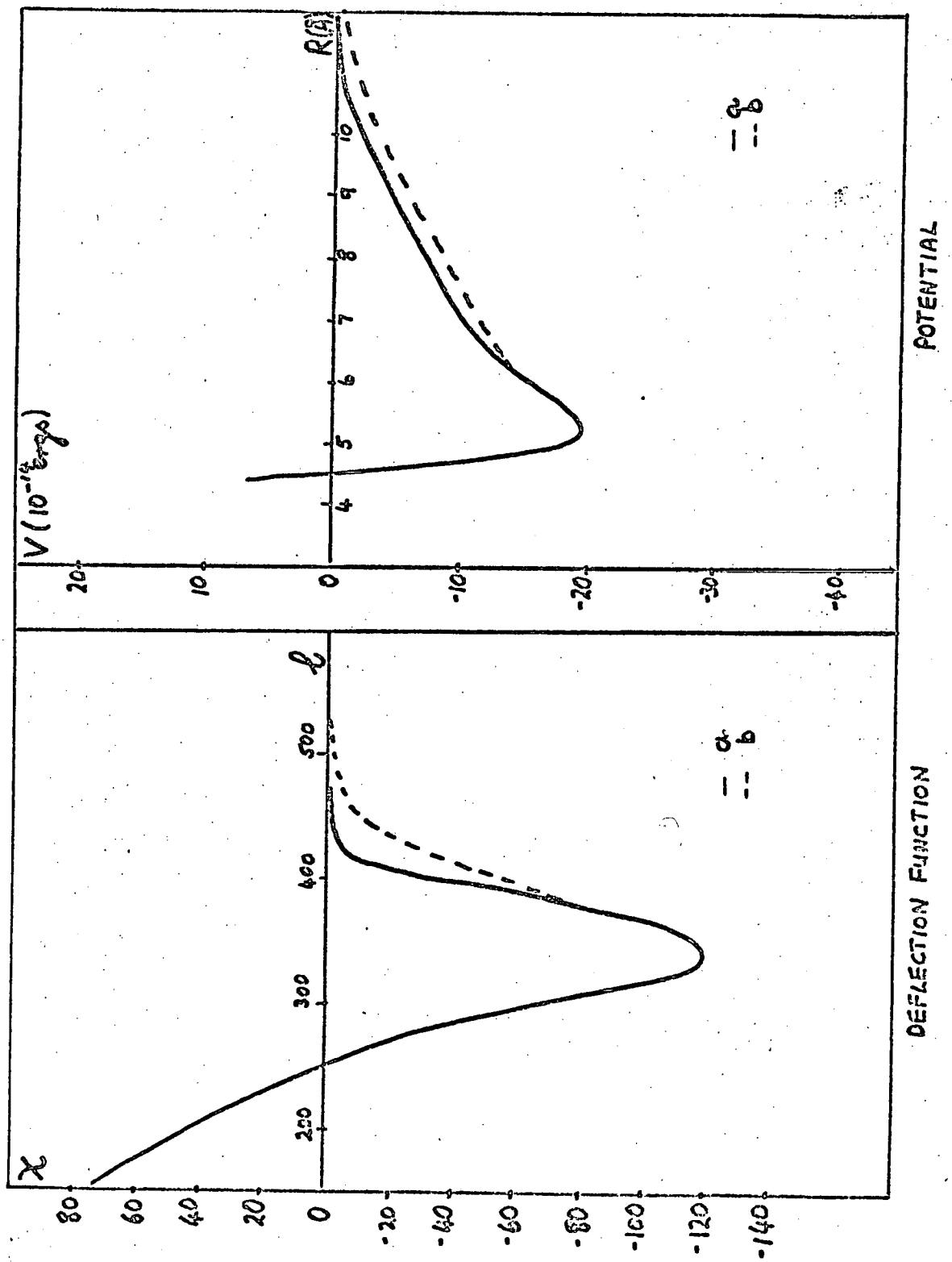

Potential changes produced by altering the deflection function

Figure 6-22

the correct asymptotic form for large values of the internuclear separation.

The potentials which have been obtained have an unusual shape [Figures 6-18, 6-19, 6-20] but I think this is largely due to the parameterised form of the deflection function which requires that the form of this function at the crossing point on the inner branch is given by a straight line of slope a_1. Varying the slope of the deflection function, in the fitting procedure, while keeping b_o, the impact parameter for the crossing, fixed results in a change in the outer branch of the fitted deflection function and also in the potential. It is possible therefore that the shape of the potential function is not correct although a reasonable fit to the extrema has been achieved.

Boyle [BOY 1971] has shown that one cannot rely very heavily on potentials fitted solely to the angular positions of the main rainbow oscillations taken at a single energy since he points out that only the area bounded by the deflection function determines the positions of the main oscillations in the cross section, i.e. the position of rainbow oscillations will remain unaltered provided the area bounded by the deflection remains the same. Therefore construction of the deflection function by the above method is by no means unique. The major uncertainty is that the derivatives of the branches of the deflection function are not known. A guess has been made for the slope of the inner branch in the fits shown so that a smooth transition is achieved between the parabolic region and the straight line portion of the deflection function.

Unfortunately since neither the rainbow angle nor the exact transition between the two regions, straight line and parabola, are known this method is suspect but at this stage in development it is the only route available for analysis of the data. This problem is well illustrated in figure [6-23] where the two possible deflection functions have widely different values of b_2 but the area enclosed by both functions is the same. Work is now in progress at Edinburgh to use the shape of the scattering envelope to determine $\frac{d\chi}{db}$ from the classical relationship $\sigma(\chi) = \frac{b}{\sin \chi \left|\frac{d\chi}{db}\right|}$ and this work should provide constraints on the slope of the deflection function.

At this stage of development it seemed reasonable to attempt a characterisation of the deflection functions in terms of the areas enclosed by them. The best fits to the deflection functions for Hg*/Na, Hg*/K and Hg*/Rb are shown in figures [6-24, 6-25 and 6-26]. The area between $\chi = -40^{\circ}$ and $\chi = -\chi_R$ has been evaluated in the three cases and is shown in table [6-12]. This area acts as a check on the consistency of the method since the spacing between two maxima is equivalent to a change of 2π in the area bounded by the deflection function between the two angles considered. The number of maxima is given by:

$$(N-1) \times \frac{2\pi}{k} = \int_{b_1}^{b_2} \chi db \qquad 6\text{-}11$$

Therefore the calculated value of N should be equal to the number of maxima between 40° and χr in the cross section. This is found to be the case for all three systems [table 6-12].

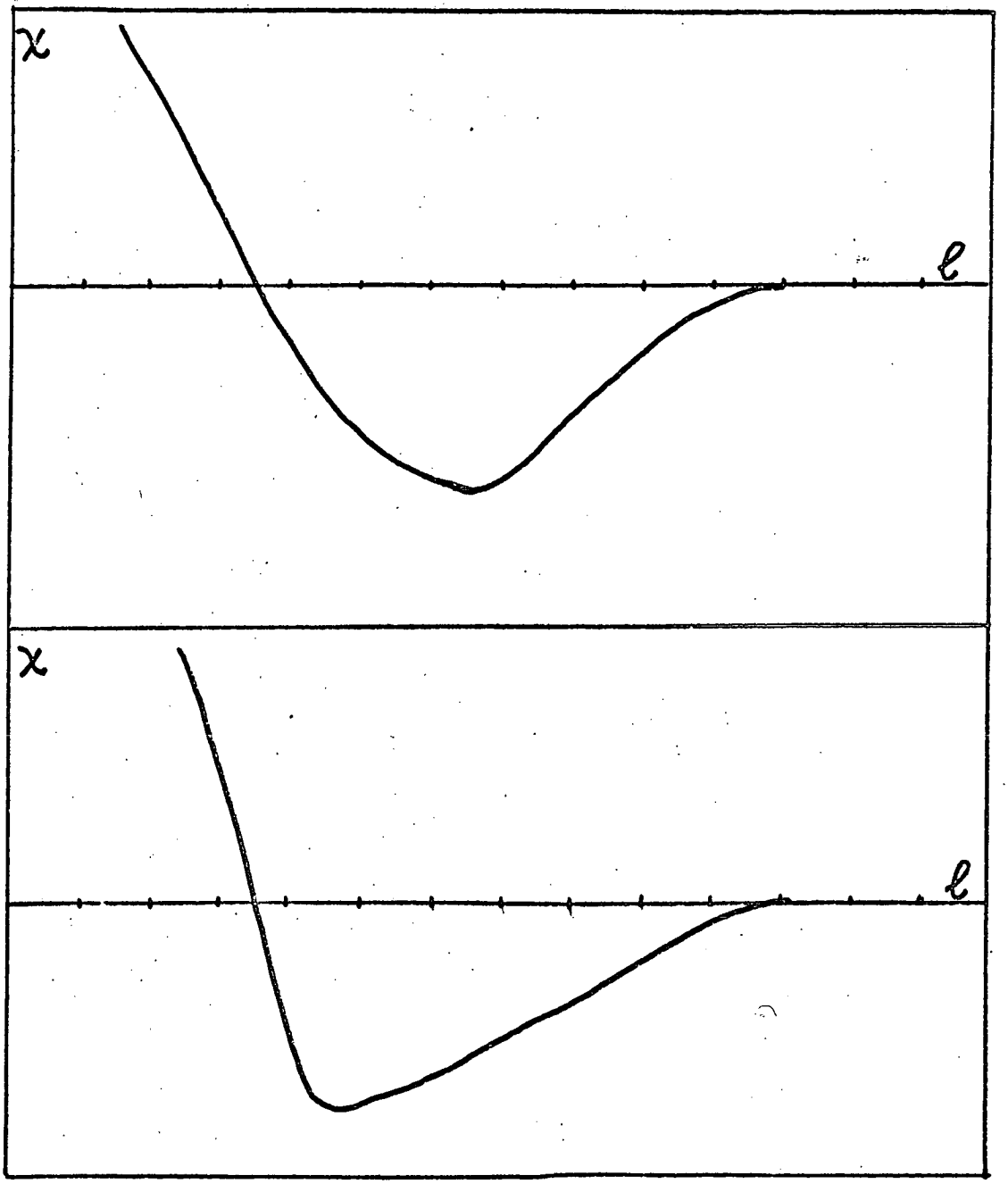

Two different deflection functions which when inverted predict the same extrema positions

Figure 6-23

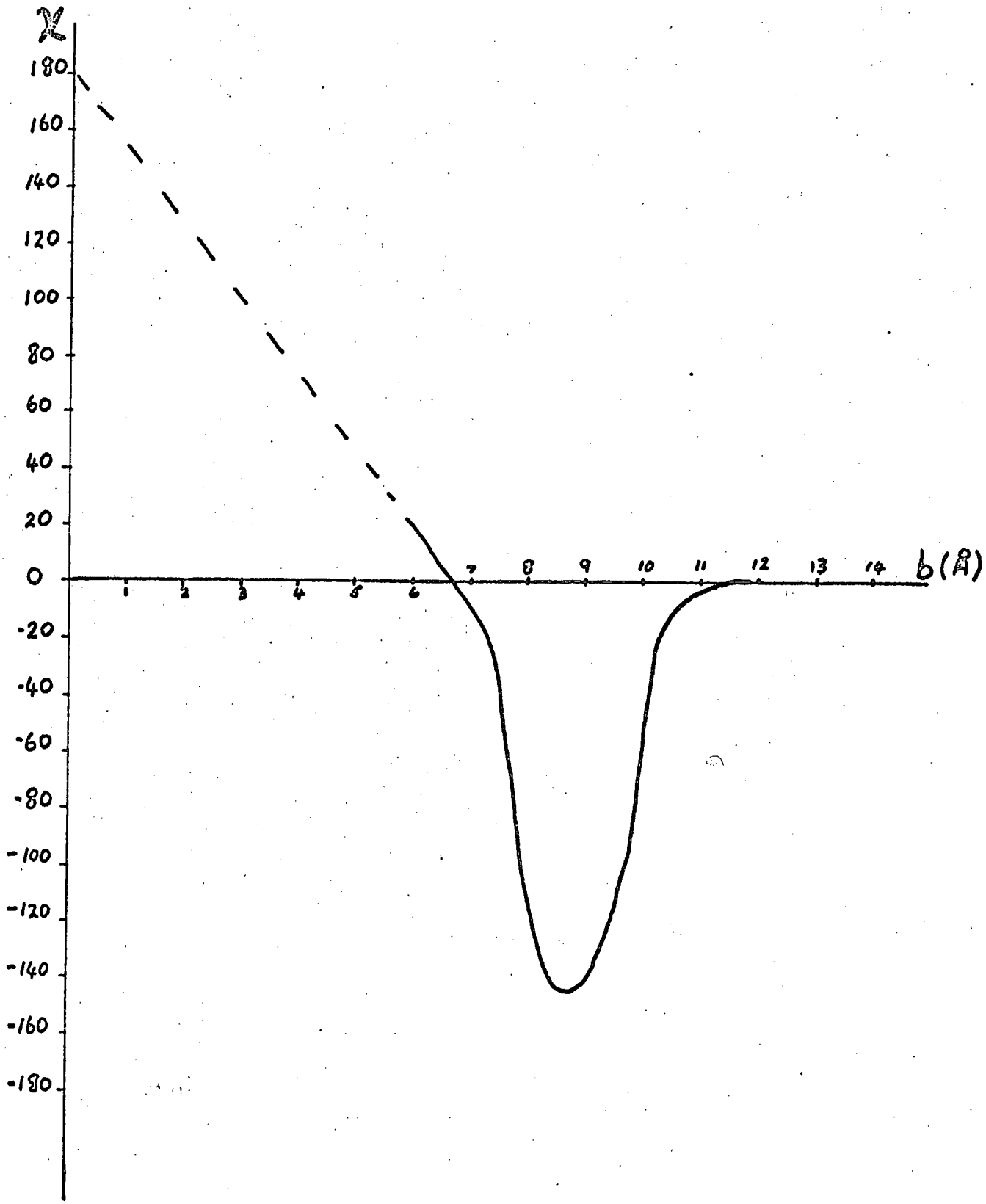

The deflection function for Hg*/Na

Figure 6-24

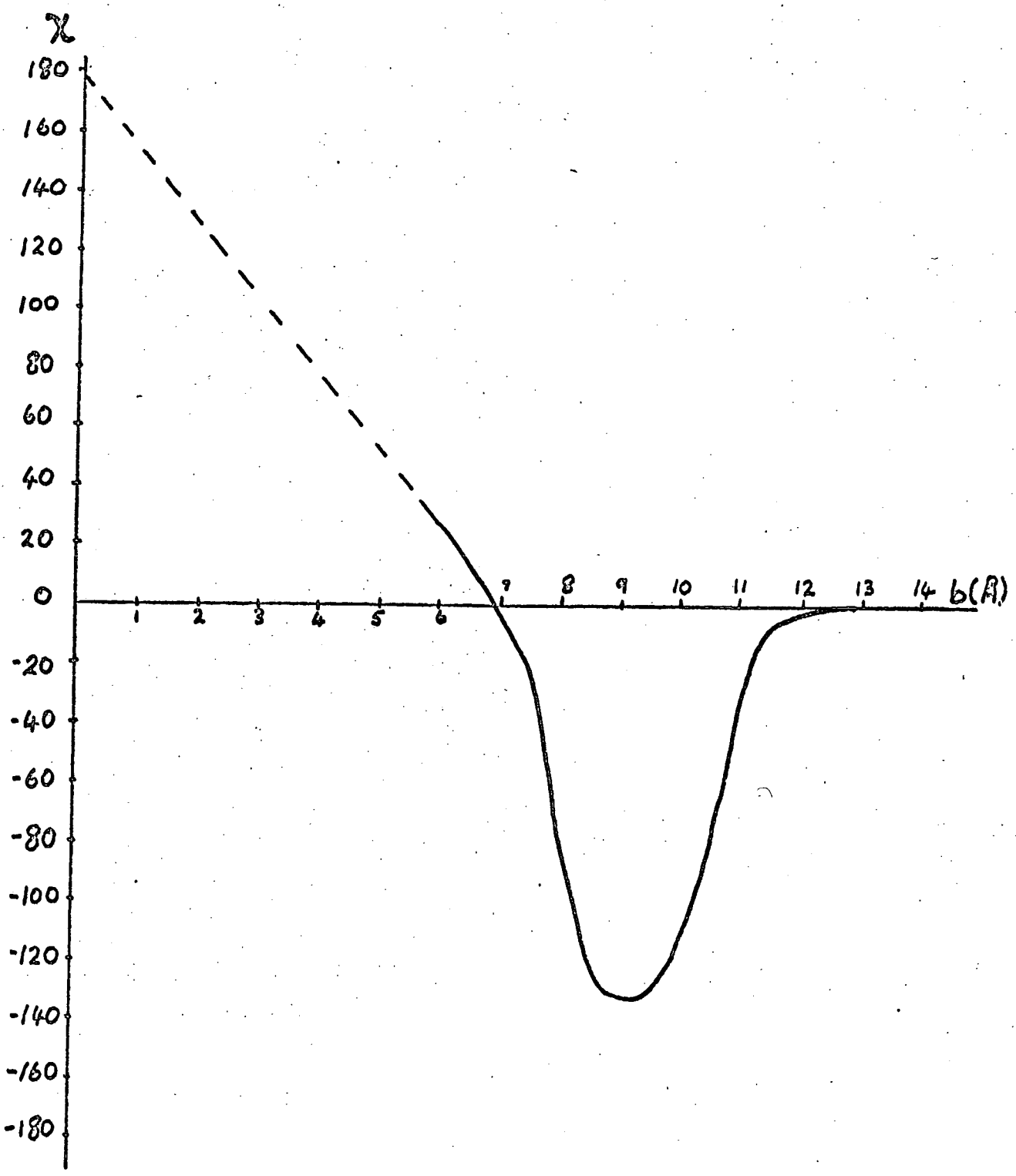

The deflection function for Hg*/K

Figure 6-25

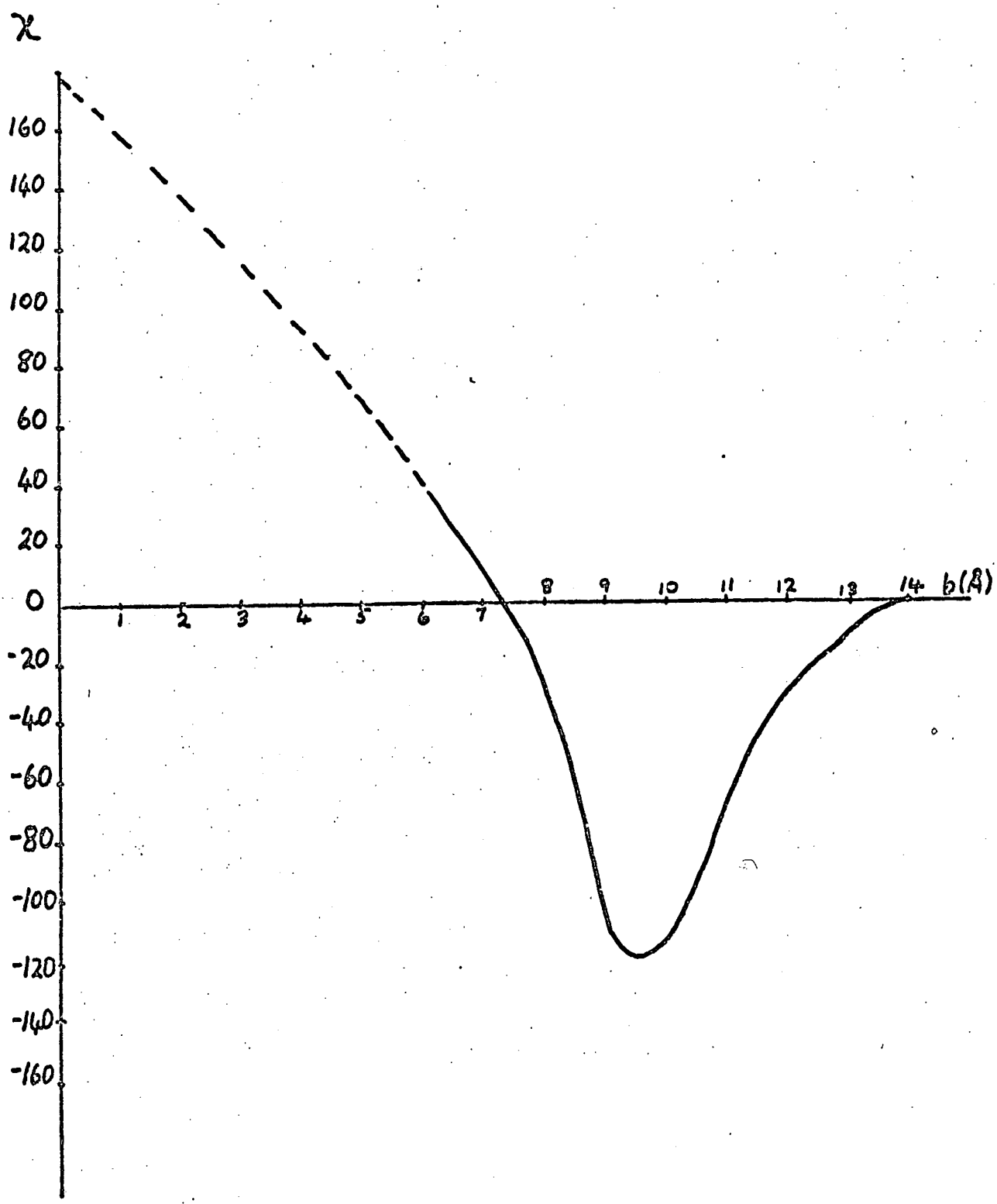

The deflection function for Hg*/Rb

Figure 6-26

Table 6-12

The areas bounded by the deflection function and a comparison of the index numbers.

SYSTEM	XR (Degrees)	k ($\AA^{-1}$)	Areas arbitrary units	N INDEX	N CALC
Hg*/Na	144	29.28	2.897	15	14.7
Hg*/K	132	36.31	3.574	21	21.4
Hg*/Rb	118	50.14	2.827	24	23.6

Since the rainbow is not observed it would be unfair to use the areas shown in table [6-12] to characterise the potential. It would be equally unfair to use the area bounded by $\chi = -\chi$ arb, $\chi = 0$ and the deflection function where χ arb is an arbitrary angle, since the asymptotic behaviour of the deflection function is by no means secure, as mentioned previously, and therefore the areas of the deflection function between $\chi=24^{\circ}$ and $\chi = 40^{\circ}$ have been chosen to compare all three potentials and between $\chi=24^{\circ}$ and $\chi = 70^{\circ}$ in the cases of Hg*/Na and Hg*/K. The results are displayed in table [6-13].

Table 6-13

Areas calculated within certain angular ranges

SYSTEM	ANGULAR RANGE	k ($\AA^{-1}$)	Area (arbitrary units)
Hg*/Na	24° - 40°	29.28	.7330
Hg*/K	24° - 40°	36.31	.9285
Hg*/Rb	24° - 40°	50.14	1.092
Hg*/Na	24° - 70°	29.28	1.955
Hg*/K	24° - 70°	36.31	2.443

Since the area bounded by the deflection function is equivalent to a phase shift it is possible to reduce the above areas by using $A^* = \frac{A}{k\sigma}$.

The results for the reduced areas are shown in table [6-14].

Table 6-14

The reduced areas for the Hg*/alkali systems

SYSTEM	ANGULAR RANGE	k ($\AA^{-1}$)	σ ($\AA$)	A	A*
Hg*/Na	24° - 40°	29.28	4.40	.7330	.00566
Hg*/K	24° - 40°	36.31	4.55	.9285	.00558
Hg*/Rb	24° - 40°	50.14	4.65	1.092	.00470
Hg*/Na	24° - 70°	29.28	4.40	1.955	.01520
Hg*/K	24° - 70°	36.31	4.55	2.443	.01492

It would appear from these results that the Hg*/Na and the Hg*/K deflection functions are consistent with the theory of corresponding states although the Hg*/Rb does not seem to fit into the general scheme of things. I am confident that the results for Hg*/Rb should fit into this general scheme and therefore I should be wary of any potential calculated using this deflection function until further tests have been carried out on the fitting procedure since as stated previously the rubidium is the least well resolved of the data.

Although there is a wide variation in the possible fits which can be made I am confident that the range of the potential is reasonably well defined although the shape may be incorrect. A semi empirical rule can be used to determine the equilibirium

separation [BER 1967];

$$r_m = r_1 + r_2 + 3.8 \text{ A.U.}$$

where r_m is the equilibrium separation and r_1 and r_2 are the orbital radii of the two atoms involved. This rule appears to give results within a deviation of ± 1 A.U. (according to Boyle [BOY 1971]). Using the orbital radius of the mercury atom calculated by Darwall [DAR 1972] and the radii for Na, K and Rb calculated by Waber and Cramer [WAB 1965], this rule has been applied in all cases. The results are displayed in table [6-15].

Table 6-15

Comparison of the observed and empirical values of r_m

SYSTEM	r_m (experiment) Å	r_m (calc) Å
Hg*/Na	4.83	5.24
Hg*/K	5.05	5.59
Hg*/Rb	5.20	5.71

It would appear that the calculated values of r_m are consistent with the measurements. The potentials [Figs 6-18, 6-19, 6-20] have been used in a monoenergy forward calculation and the scattering patterns obtained. The experimental and calculated centre of mass differential cross sections are displayed in figures [6-27, 6-28 and 6-29]. Considering the large number of extrema involved the systems show good agreement between the experimental and calculated positions of the maxima and minima. Therefore, it would appear that the assumption of a single effective potential is correct.

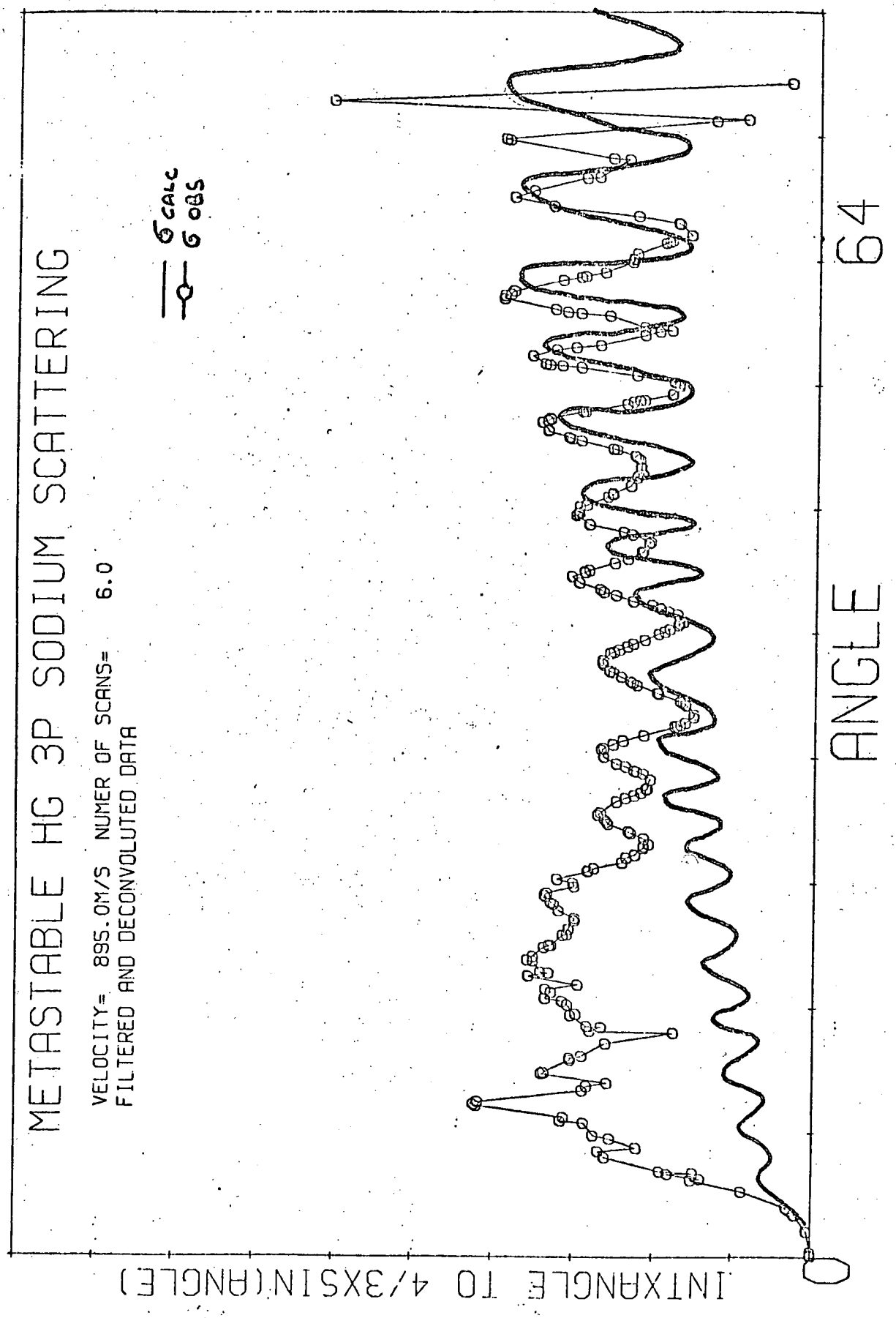

Comparison of observed and calculated differential cross sections. The calculated values have been produced by a forward calculation using the potential calculated from the fitting procedure.

Hg*/Na

Figure 6-27

Figure 6-28

Comparison of observed and calculated differential cross sections. The calculated values have been produced by a forward calculation using the potential calculated from the fitting procedure.

Hg*/K

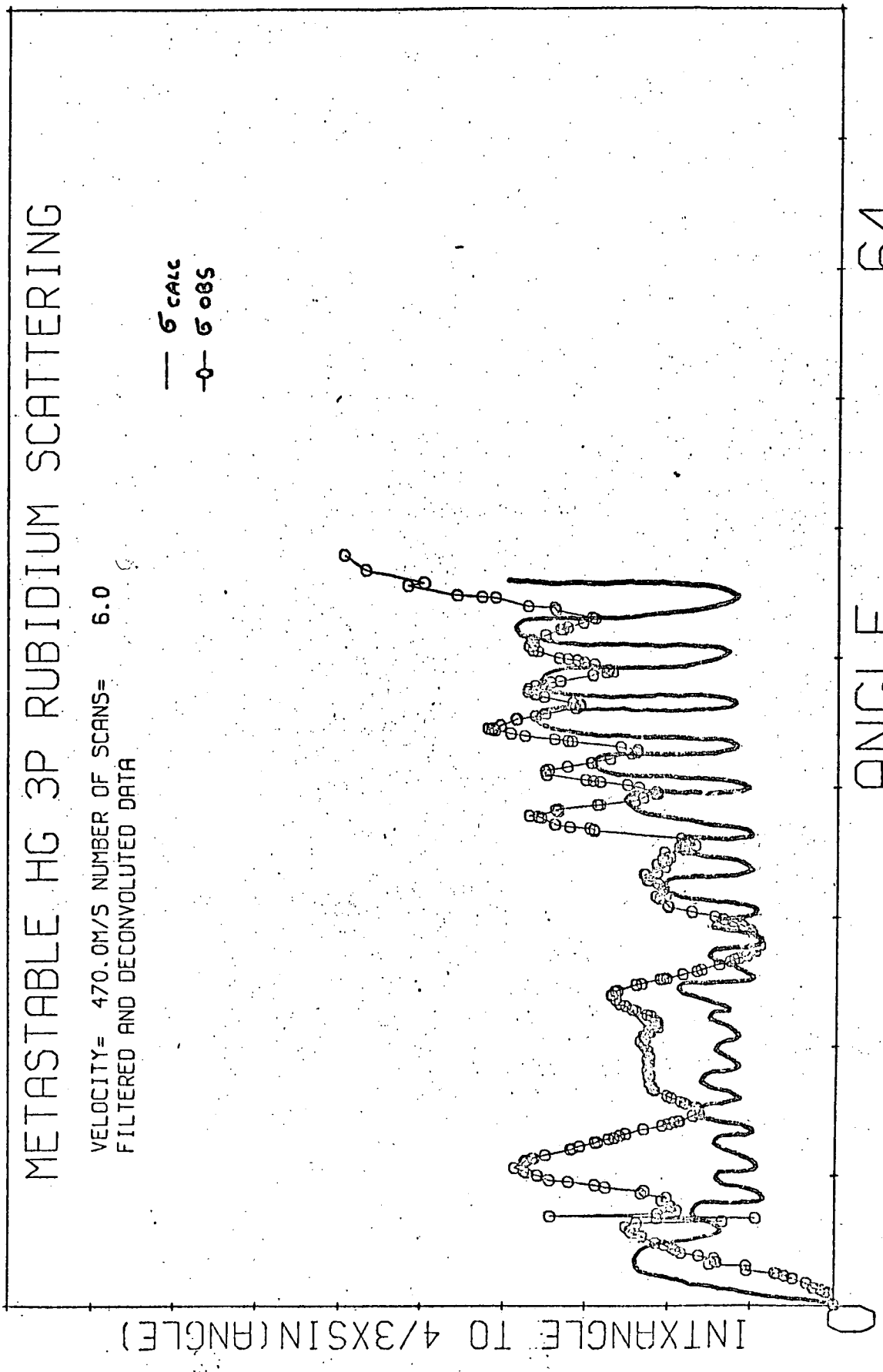

Comparison of observed and calculated differential cross sections. The calculated values have been produced by a forward calculation using the potential calculated from the fitting procedure

Hg*/Rb

Figure 6-29

Chapter 7

Discussion and Conclusions

7 Discussion and Conclusions

Discussion

In the discussion of potentials calculated from scattering patterns it is normal to plot the potentials in reduced units for comparison. This has been done for the experiments reported here, bearing in mind the inadequacies of the fitting procedure which result in a potential which may not be unique. The potentials for all three alkali mercury systems in reduced units are plotted [Fig 7-1]. Table [7-1] contains the corresponding size parameters of the potential: the well depth Σ and the equilibrium distance Rm.

Table 7-1

Size parameters for the Hg*/alkali potentials

SYSTEM	Rm(Å)	Σ (10^{-14} ergs)
Hg*/Na	4.83	23.06
Hg*/K	5.05	22.73
Hg*/Rb	5.20	22.03

The reduced potentials for Hg*/Na and Hg*/K are in very good agreement but there are slight discrepancies in the case of Hg*/Rb. (A similar situation was found in the case of the deflection function and the explanation is the same: the potential appears to encompass a smaller area and this is consistent with the deflection function arguments). The equilibrium distance Rm increases with increasing atom size as expected, whereas the potential well depths decrease

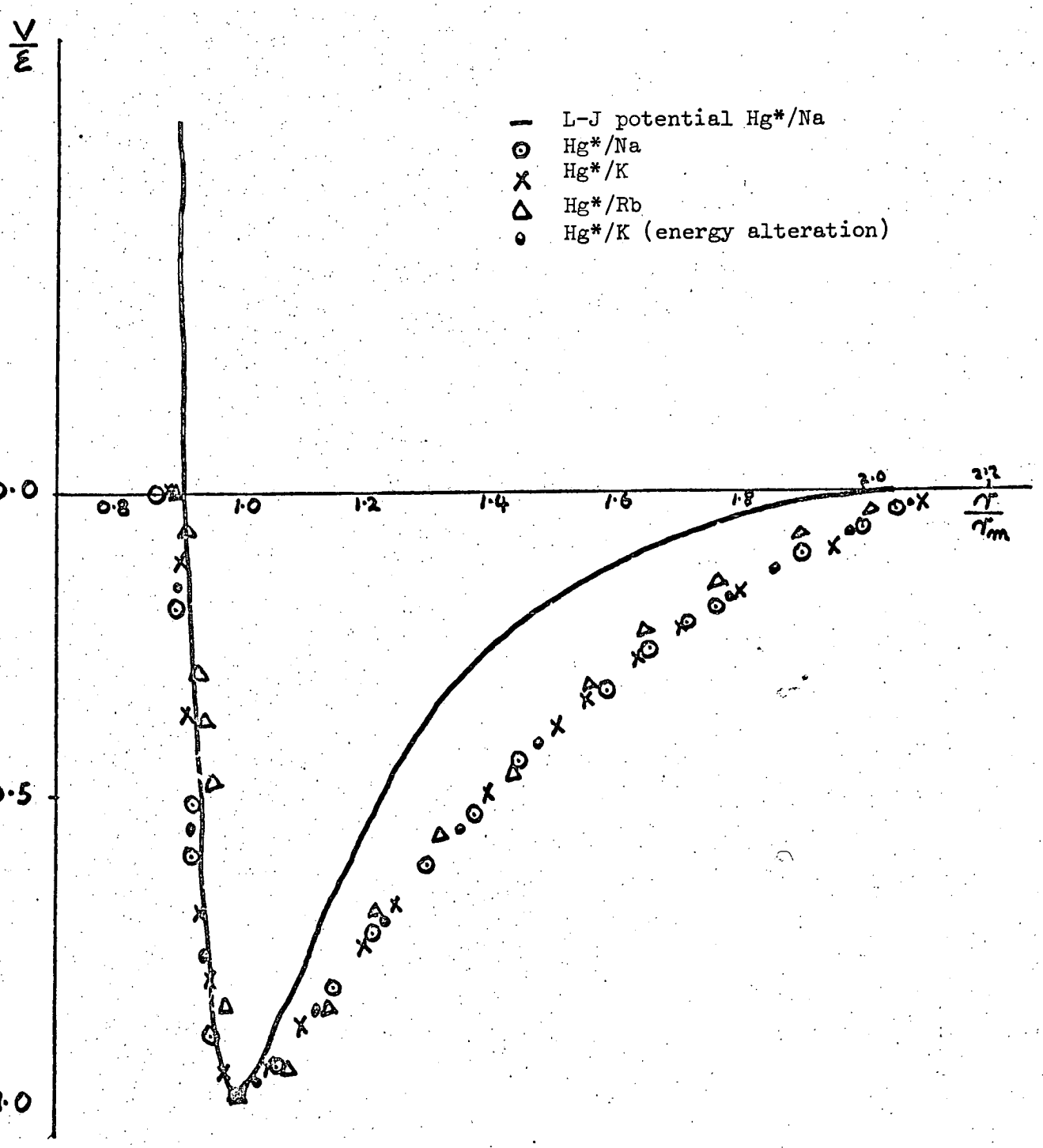

The reduced potentials from the scattering data

Figure 7-1

slightly in contrast to the behaviour of the alkali rare gas systems but in agreement with the results of Buck et al [BUC 1972] for the ground state mercury alkali systems. I should not, however, labour this point as, has been mentioned previously, the experimental results are not available in the rainbow region which defines the depth of the potential well.

It is also fashionable to compare calculated potentials with other parameterised forms of the potential (e.g. Lennard Jones 12:6 which was previously used a great deal in the characterisation of potentials). A reduced Lennard Jones potential, using the values of Σ and Rm from the Hg*/Na experiment, is also plotted in figure [7-1]. The potentials reported here are significantly different from the Lennard Jones potential especially in the attractive region, although this may be a result of the parameterised form used. It does appear, however, that the potentials are more attractive at intermediate ranges than would be expected from a pure $C_6 r^{-6}$ behaviour.

Given the parameterised deflection function used, nothing has yet been stated about the accuracy of the potentials calculated by this method. Unfortunately, this is difficult to do since the experiments have only been performed at one energy. However, an attempt has been made to determine the effect of an energy change by varying the most probable velocity of the potassium beam which is used in the fitting procedure and the Firsov inversion (i.e. the positions of the maxima and minima to be fitted are unchanged but the relative energy of the interaction is altered). The reduced potential determined for an increase in relative energy of

30% (in the case of Hg*/K) is also plotted in figure [7-1] and the potential obtained fits very well into the general scheme. The value of Rm was found to be 5.08Å which compares favourably with the value 5.05Å obtained using the correct most probable velocity for the potassium while the well depth increased as expected from 22.73×10^{-14} to 27.7×10^{-14} ergs. This suggests once again that the range of the potential is accurate whereas the well depth is less well determined because the rainbow was not observed.

The above rather crude analysis brings to light an important point which has hitherto been neglected and this is that the analysis has been carried out for the case in which both beams are monoenergetic whilst the experiments were performed using non velocity selected beams with their inherent velocity distributions. It might be expected that the Maxwellian distribution especially in the cross beam would result in a smearing affect so that interference structure would not be resolved. Forward calculations have been performed for a range of cross beam velocities (30% change on either side) and it was found that although the positions of the rainbow and the first two supernumeraries were shifted, the second supernumerary by $< 1^{\circ}$, the other supernumerary bows remained unaltered in the centre of mass cross sections. This confirms the statement of Buck [BUC 1971 (a)] that these extrema positions are almost independent of various angular and energy averaging processes in the primary and secondary beams. Having checked the centre of mass cross sections for this smearing effect it is also useful to ensure that "smearing" in the laboratory cross section does not occur as a result of these averaging processes. This has been

verified by finding the scattering angle Θ corresponding to a centre of mass angle χ for a range of cross beam velocities. The results for Hg*/Na are shown in table [7-2] and the situations for Hg*/K and Hg*/Rb are displayed pictorially in figures [7-2] and [7-3] respectively.

Table 7-2

The change in laboratory scattering angle Θ, for a given χ, with changing velocity

SYSTEM	Main Beam Velocity	Cross Beam Velocity	χ	Θ
Hg*/Na	2.475×10^4 cm s^{-1}	8.677×10^4 cm s^{-1}	35°	6.00°
Hg*/Na	2.475×10^4 cm s^{-1}	1.147×10^5 cm s^{-1}	35°	6.53°
Hg*/Na	2.475×10^4 cm s^{-1}	7.573×10^4 cm s^{-1}	35°	5.54°

The results suggest that, for the angular range studied, the smearing effect is such that structure with a period > 1° in the laboratory will be resolved.

So far the results have been analysed in terms of a single potential despite the fact that five "molecular states" (Chapter 4) evolve from the atomic pair Hg ($^3P_2$) + M ($^2S_{\frac{1}{2}}$). It, therefore, appears that these 5mj states are similar for the energy which has been probed. This scheme of a single effective potential has not so far, accounted for one feature of the scattering pattern and that is the size of the cross section at small angles. This "hump" is most pronounced in the case of Hg*/Na [Fig 7-4] although it is also an observable feature in the other systems. The scattering

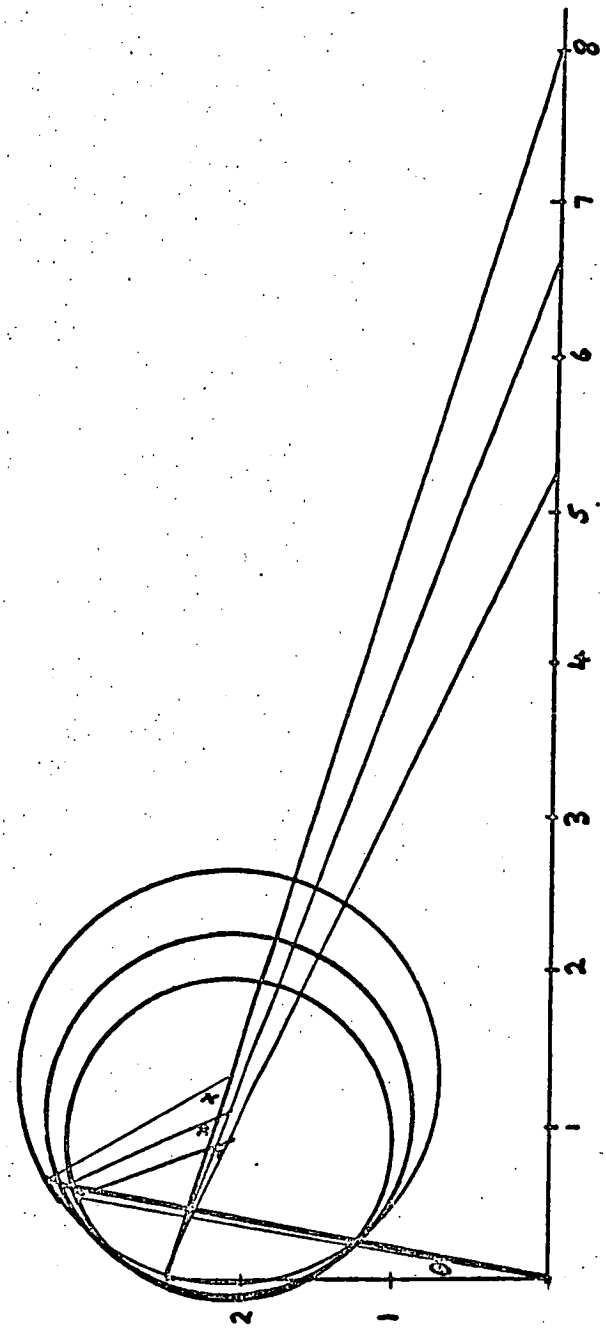

Newton diagram for Hg*/K showing the effect of the velocity spread in the cross beam on the laboratory scattering angle.

Figure 7-2

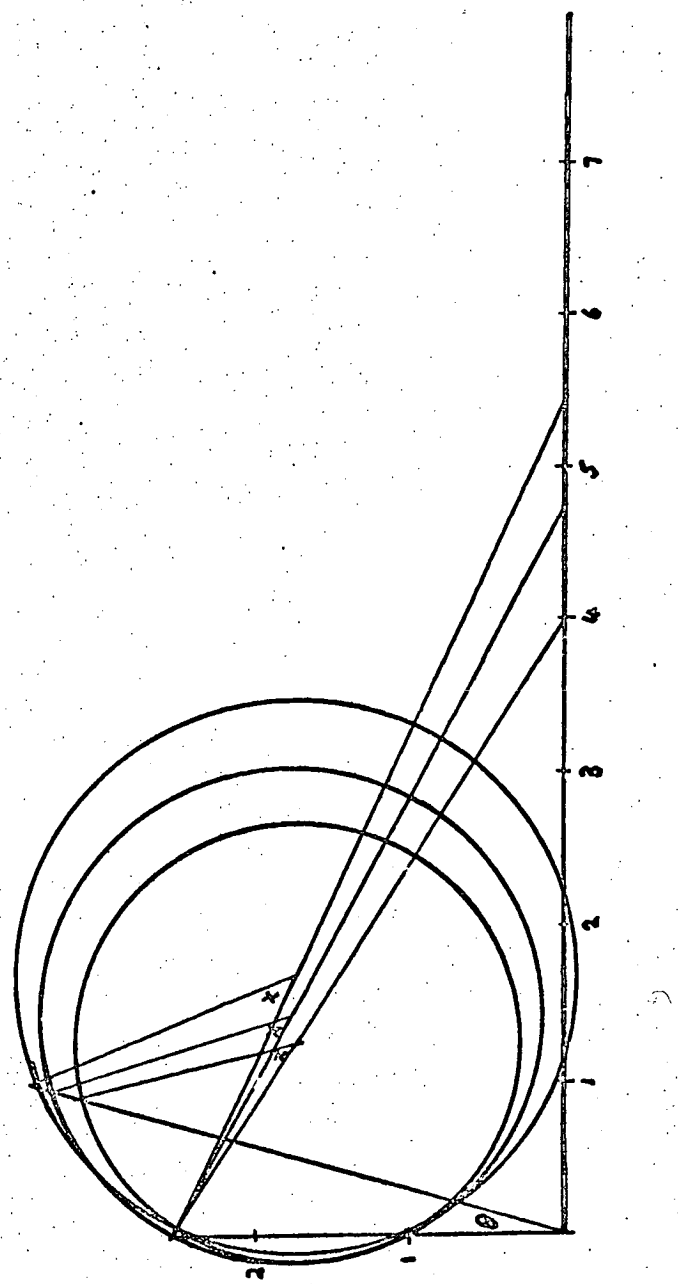

Newton diagram for Hg*/Rb showing the effect of velocity spread in the cross beam on the laboratory scattering angle.

Figure 7-3

pattern obtained by a monoenergy forward calculation is also shown in figure [7-4] and the discrepancy at narrow angles is quite pronounced. Neglecting for the moment the interference structure, the envelope of the scattering pattern can be given by the classical expression:

$$\sigma(\chi) = \sum_i \frac{bi}{\sin\chi \left|\frac{d\chi}{dbi}\right|} \qquad 7\text{-}1$$

The experimentally observed increase of intensity at narrow angles might be obtained if the derivative $\frac{d\chi}{db}$ was smaller at these angles and larger for wide angles. An exaggerated sketch of the requirements is shown in figure [7-5].

Considering the case of sodium, one possible reason for this increase in intensity at narrow angles is a much larger value of C_6 than the value calculated by Darwall of 590×10^{-60} ergs cm^6. Another alternative is that the asymptotic approach to zero has a power dependence of $C_2 < 6$ for the situation $V=-C_1 r^{-C_2}$ but this is physically unrealistic. A third possibility is that the value of C_6 is approximately correct but the deviation from $V=-C_6 r^{-6}$ is considerable as the internuclear separation decreases (The form of the potential is also found to deviate from $V=-C_6 r^{-6} - C_8 r^{-8}$ and the best fits were obtained with a value of $C_2 \sim 9.5$). A fourth alternative in the single potential argument is that the derivative of the inner branch of the deflection function is small but this again would be a physically unrealistic situation. The final possibility in terms of a single potential and deflection function is that the increased intensity at narrow angles is due to scattering

Figure 7-4

Comparison of forward calculation of the cross section and the experimentally observed cross section. The amplitude discrepancy at narrow angles is pronounced.

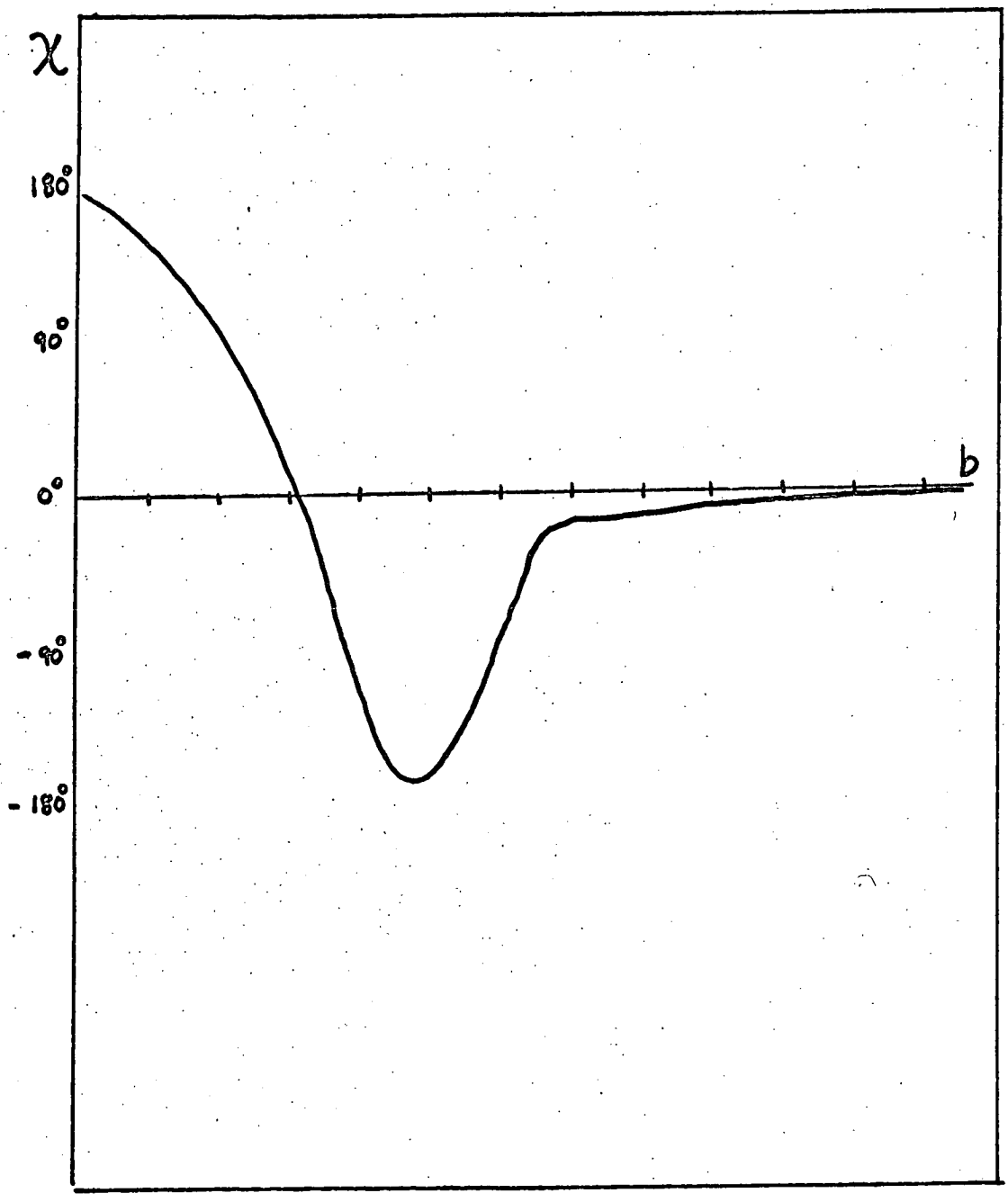

Deflection function which would produce greater intensity at narrow angles.

Figure 7-5

at angles >2π with a rainbow at 2π+χ where $\chi < 20^{\circ}$. However, this would greatly complicate the scattering pattern since it would increase the number of possible interferences. It is also unlikely that the amplitude of such a contribution would be large since the region of stationary phase would be small. Therefore the possibility which seems most reasonable is that the increased intensity at narrow angles is due to the shape of the outer branch of the deflection function. By calculating the mean relative cross section at all angles it should be possible to fit the cross section envelope using equation [7-1] in an extension of the multiparameter fit and therefore to determine the exact reason for this phenomenon. Also it should be possible to fit the amplitude variations in a final sophisticated version of the fitting routine. Unfortunately, I did not have a chance to do this but work is continuing in the laboratory in the hope of finding a more tightly constrained fit to the potential by using extrema positions, mean cross sections and amplitudes.

At the outset of this work it was thought that the Hg*/alkali interactions would be useful systems in which to investigate elastic scattering with concurrent inelastic processes by differential cross section measurements. Earlier in this thesis a brief review of inelastic processes was given and yet no inelastic scattering has yet been mentioned in these experiments. It may be that the inelastic scattering cross sections are so small as to be unobservable in comparison with the large elastic cross section but it is useful to consider whether the "hump" at narrow angles, or in this interpretation the decrease in intensity at wide angles, is due to

some form of quenching process. A crude calculation for the magnitude of the inelastic process was made using the procedure outlined by Greene et al [ROS 1966].

The probability that an inelastic collision occurs at the angle χ is given by

$$P(b) = \frac{\sigma\text{calc}\ (\chi(b)) - \sigma\text{obs}\ (\chi(b))}{\sigma\text{calc}\ (\chi(b))}$$

where σcalc is the calculated intensity at χ

σobs is the experimentally observed intensity at χ.

σcalc and σobs are normalised at $\chi = 20^{\circ}$. In terms of the inelastic probability function, P(b), the total inelastic cross section is given by:

$$\sigma = \pi \int_{o}^{bt} P(b)bdb$$

P(b) can be obtained from the shaded area in figure [7-6] and bt is the threshold (i.e. the largest value of b at which the inelastic process occurs). 24° is taken as the angle corresponding to onset of the effect of inelastic processes and this corresponds to an impact parameter of b = 10.2Å (from the experimentally obtained potentials), a rough calculation of P(b) gives an answer P(b) $\sim$ .2 and therefore the inelastic process has a magnitude of $\sim 60 Å^2$.

It is worthwhile considering the likely inelastic processes which might be occurring and their possible magnitudes. The various processes which can occur are:

a) intermultiplet transitions ΔJ which will be followed by quenching if the $^3P_1$ state is formed.

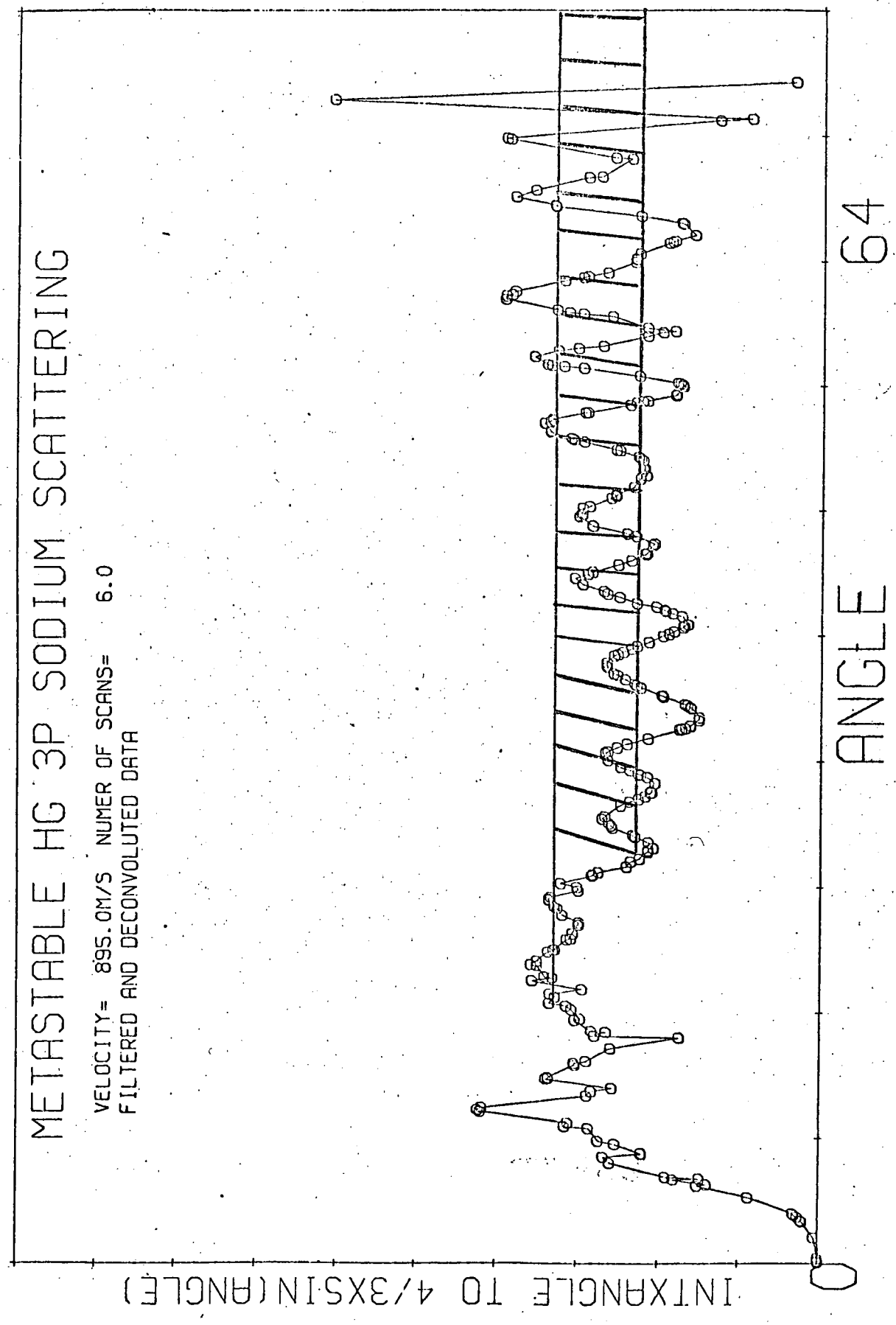

Shaded area denotes the proposed loss of intensity due to inelastic processes.

Figure 7-6

b) Δmj transitions within a given J state.

c) ionisation

d) transfer of electronic excitation to the alkali metal.

The relevant data for a consideration of such processes is given in table [7-3].

Table 7-3

ΔE(eV) for processes involving Hg* and alkali metals

Process	Na	K	Rb
Ionisation of M by $^3P_2$	-0.31	-1.11	-1.27
Excitation transfer to 1st excited state of M by $^3P_2$	-3.33	-3.82	-3.87
Ionisation of M by ^3P_o	+0.48	-0.32	-0.48
Excitation transfer to 1st excited state of M by $^3P_2$	-2.54	-3.03	-3.08

Process	Transition		
	$^3P_2 - {}^3P_1$	$^3P_2 - {}^3P_o$	$^3P_1 - {}^3P_o$
Intermultiplet transitions	-0.57	-0.79	-0.22

For the 6 $^3P_2$ state all channels (a → d) are open for the series Na → Rb though with fairly considerable exoergicities except for process b. For the 6 ^3P_o state and Na the ionisation channel is not open.

From the available experimental evidence for energy transfer processes (Chapter 2) it does appear that the processes with the largest cross section are those for which the internal energy change is smallest. It is possible that the Na atom may bring about a spin orbit relaxation of the Hg atom.

$$Hg\ (^3P_2) + Na\ (^1S_o) \rightarrow Hg\ (^3P_j) + Na\ (^1S_o)\quad j=0,1$$

but the changes in internal energy involved are ΔE_{21} = 0.57eV, ΔE_{2o} = 0.79eV and therefore the cross sections are likely to be small. (Cross sections for ΔE changes of this magnitude are typically $<.2\text{Å}^2$ [CZA 1973]). For Hg (^3P_o) colliding with Na (^1S_o) upward intermultiplet transitions are unlikely at normal temperatures since the energy involved is 0.22eV. The quenching of the ^3P_o state will result in the excitation of the 7S state of sodium [BLJ 1929] although once again the cross section is unlikely to be as large as 60Å^2 since the energy discrepancy is +.055eV and is therefore likely to be $\sim 5\ \text{Å}^2$ [CZA 1973]. It would be difficult to attempt, I think, to use any of the methods mentioned in chapter 2 for the treatment of energy transfer, since the amounts of energy to be transferred are large and a successful theory seems to have been developed only for small energy changes [NIK 1965].

Apart from the case ^3P_o + Na all other processes which quench the metastable to the ground state could result in Penning ionisation

of the alkalis. Typical Penning ionisation cross sections are $\sim 20\text{Å}^2 \rightarrow 30\text{Å}^2$ (e.g. [SCH 1970]) and the Penning ionisation of Na by $He(2^3S)$ has been found to be $\sim 15\text{Å}^2$ [HOT 1970] . It is unlikely that the cross section for Hg*/Na will be much larger than this. However, Martin [MAR 1972] has reported relative cross sections for associative and Penning ionisation so they are observable processes. It may be possible to do a calculation similar to that of Miller (Chapter 2) using the existing mercury wave functions and the calculated potentials to find an estimate for the cross section. If this cross section is found to be large it may be possible to look for the Na^+ ions although intensities will be very low since the Na^+ ions will be scattered over a very much larger solid angle than the Hg atoms. However, the possibility of detecting either the Na^+ ions or electrons by surrounding the scattering centre with some form of Faradaycage does exist so that a total cross section for the process may be easy to determine.

None of the above mentioned inelastic process seem to be able to account for the large inelastic cross section of 60Å^2 even if selective quenching of various mj states were an important process. Another possibility is the chance of selective quenching between the $^3P_2$ and ^3P_o states in the beam. The most likely inelastic process to differentiate significantly between the two states would be Penning ionisation which is an allowed process for $Hg(^3P_2)$ + Na but is unlikely for Hg (^3P_o) + Na at thermal energies. However, this increased intensity at narrow angles is present in the scattering patterns involving the other alkalis which seems to rule out this possibility.

It would, therefore, appear that the "hump" at narrow angles is a function of the "effective" potential and not a result of inelastic processes. A question then has to be asked about why one "effective" potential is seen when there are two different metastable states in the beam with, perhaps, similar lifetimes. Since the ^3P_o state population is only $^1/6$ of the total metastable beam, the states may be produced in their statistical ratio (Chapter 3), then the contribution to the total cross section from this state will be small. Also the ^3P_o state correlates with a deep "molecular" state corresponding to a $^2\Sigma$ state (Chapter 4); such a potential would probably correspond to orbiting for the energies used in these experiments and therefore the contribution to the cross section is likely to be small since $|\frac{d\chi}{db}|$ will be large for such a steep potential.

The picture of an "effective" potential originating from the five different mj states which have similar potentials has been produced and an explanation of this phenomenon requires an investigation of the dynamics of the collision.

The forces operating during a collision depend on whether mj in a space fixed system or in a rotating system is a good quantum number. Thus for collisions of large impact parameter the coupling of electronic motion to the interatomic motion is weak and the phase shifts depend only slightly on mj. That is, the adiabatic phase shifts (those calculated assuming mj a good quantum number) are scrambled. As the impact parameter decreases strong coupling ensues at first near the turning point. Finally, for collisions of small

impact parameter, mj in a rotating frame is a good quantum number and the phase shifts are well separated.

The impact parameter at which coupling becomes important is determined by the splitting of the adiabatic potentials. The dependence of the polarisability [DAR 1970] of the $^3P_2$ state on mj is less than 10% of the mean value and this presumably means a similarly small range of C_6 values. Taking the range of C_6 values to be given effectively by

$$\Delta C_6 = 4\Delta\varepsilon\sigma^6 \qquad 7\text{-}2$$

where $\Delta\varepsilon$ is the range of well depths one applies

$$b_c = \tfrac{3}{8}\left(\frac{\Delta C_6}{\hbar v}\right)^{1/5} \qquad 7\text{-}3$$

[FLU 1973(b)] to determine the critical impact parameter for coupling bc. In the first order computations (Chapter 4) relatively shallow wells ranging from 8×10^{-14} ergs to 13×10^{-14} ergs were found for the five mj states. (These well depths are all much less than the spin orbit splitting in mercury). Using the results of these potentials b_c is found to be $\sim 6\text{Å}$.

The following tentative picture is proposed. At small angles of scattering, the lack of coupling between the Hg* mj state and the passing atom results in a scrambling of the manifold of interatomic potentials to give one effective curve. As b decreases, coupling ensues but the potentials remain inherently similar and the interference structure from them coincides. The deflection functions associated with the various adiabatic potentials can not diverge appreciably until near the minimum where the resulting interference

structure from each state would be lost.

An effective potential has been calculated by taking an average of the five potentials evaluated in chapter 4 and the scattering pattern has been produced by a monoenergy forward calculation [Fig 7-7]. The similarities between this scattering pattern and the experimentally observed pattern [Fig 7-8] for Hg*/K are not striking although undulations cover the entire range. However, it should be remembered that these calculations were rather basic and had obvious limitations. L-S coupling was not included in the first order Hamiltonian and configuration interaction was ignored. Had these two considerations been included slightly deeper wells would have been produced, this in turn would have resulted in deeper deflection functions and the extrema in the calculated cross section would have been closer spaced. In short, the calculated cross section would have looked more like the experimentally observed cross section.

As mentioned in the introduction (Chapter 1) the collisions between ground state Hg atoms (^1S_o) and alkali metal atoms ($^2S_{\frac{1}{2}}$) have been studied in detail [BUC 1971(b), 1972] whereas only limited data on the corresponding interaction between alkali atoms and excited states of mercury is available [DAR 1972]. It is perhaps worthwhile effecting a comparison between the results of the work mentioned in the references above and the work performed here bearing in mind the limitations of each.

A comparison with the work of Buck has been a major feature of this discussion and the comments in the preceding chapter.

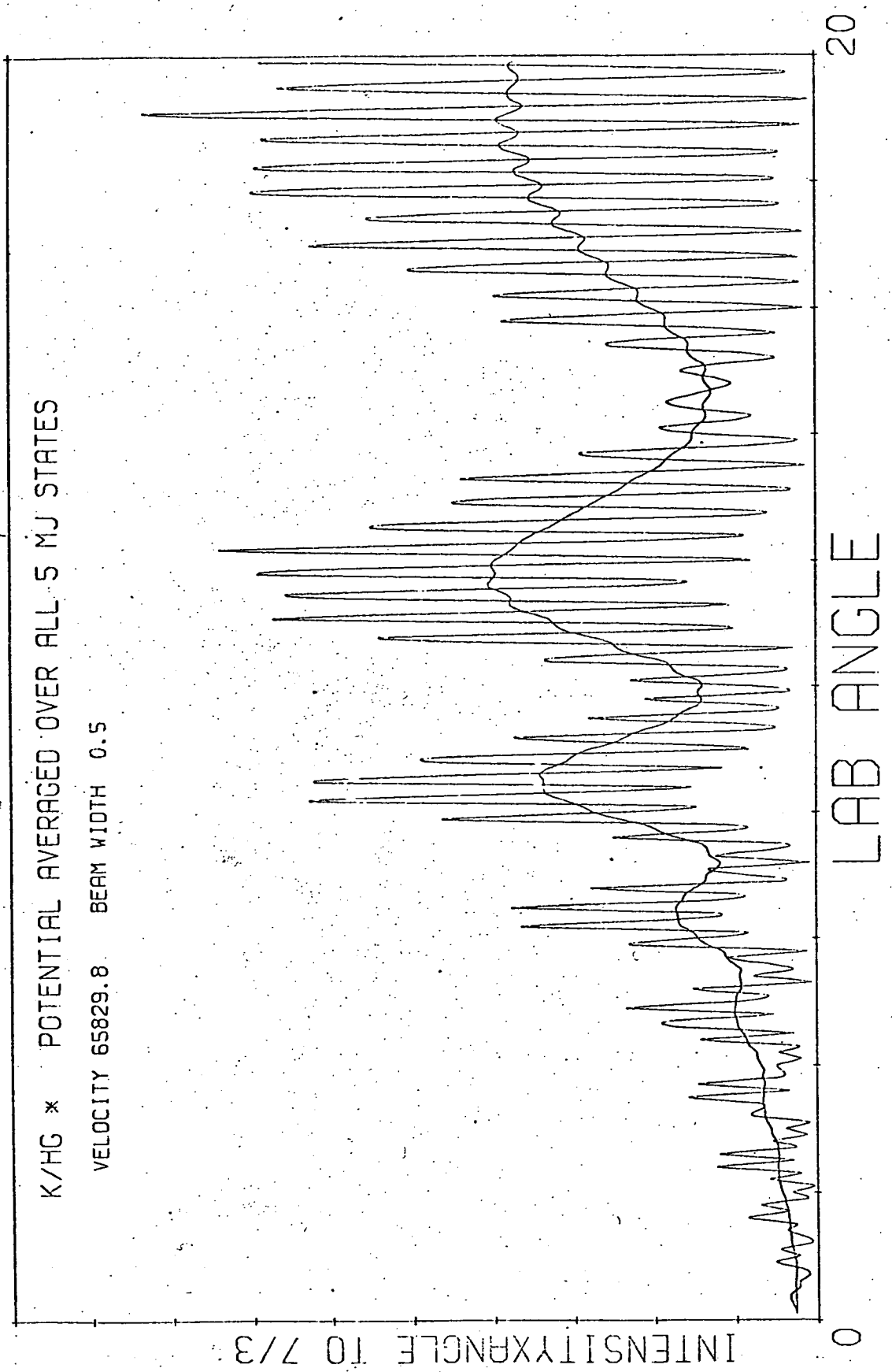

Laboratory differential cross section produced by a monoenergy forward calculation using an average potential. The average potential being calculated from the 5 potentials for Hg*/K produced in chapter 4 for the possible mJ states of the interaction.

Figure 7-7

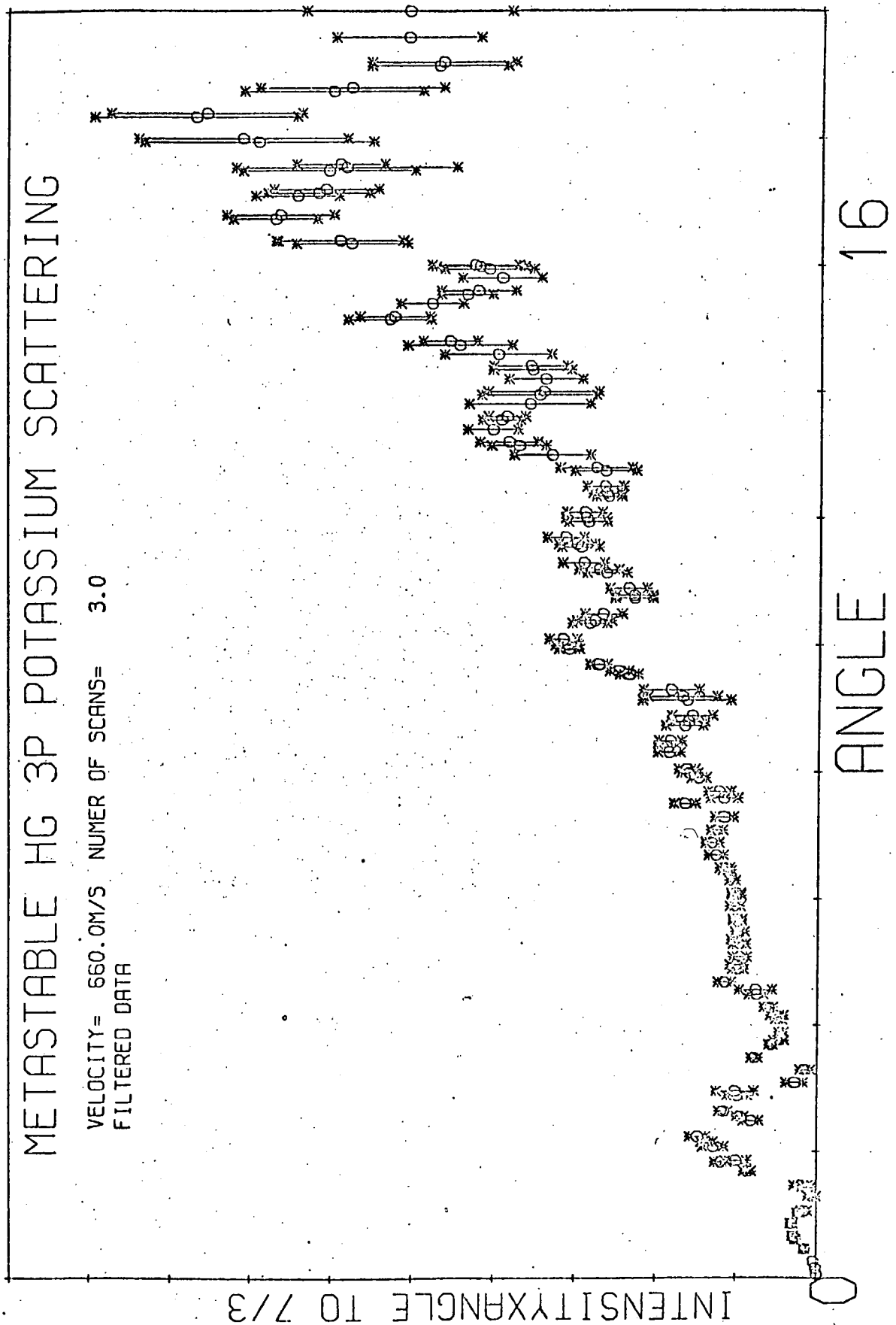

Observed laboratory differential cross section for Hg*/K.

Figure 7-8

Therefore, only the main points concerning the evaluated potentials will be re-echoed. It is useful to consider the potential parameters which are displayed in table [7-4] remembering that only one possible potential can operate in the ground state interaction whereas an effective potential is operating in the excited state counterpart.

Table 7-4

Comparison of Potential Parameters of the ground state and excited state mercury/alkali systems.

SYSTEM	Rm(Å)	ε (10^{-14}ergs)	Reference
Hg /Na	4.72	8.79	BUC 1971(b)
Hg*/Na	4.83	23.06	This work*
Hg /K	4.91	8.40	BUC 1972
Hg*/K	5.05	22.73	This work*

(*It should be noted that this may not be the final version of the potential parameters pending the results of the calculations in progress at Edinburgh on a more tightly constrained fit. However, it is not expected that the final version of the parameters will vary significantly from those calculated here although the potential shape may be found to be different). It can be noted from table [7-4] that the values of R_m are slightly greater for the excited systems. This is consistent with the fact that the metastable mercury atom will have a slightly larger orbital radius due to the promotion of a 6S electron to a 6p orbital. The much greater values of ε, the well depth, are more difficult to explain although

it may be, as mentioned in chapter 4, the result of some binding phenomenon due to the unpaired electrons.

The only previous excited mercury alkali work performed was carried out in this laboratory by Darwall [DAR 1972] using the same apparatus although modifications have been carried out to the turntable and the exciter since that time. Darwall investigated the Hg*/K interaction but unfortunately he only studied the angular range $0 \rightarrow 7^{\circ}$ in the laboratory and no centre of mass analysis of the results was performed. He did, however, observe periodic structure in this range and also the large intensity at narrow angles. His results were interpreted in terms of two effective potentials, one which produced a rainbow (the "hump") at 1.9° in the laboratory reference frame. This "rainbow" corresponded to 4 of the 5mj states while the other mj state was responsible for a "supernumerary" at 3.4° and a "rainbow" at 5.8°. Darwall also required that some inelastic process was occurring with a non negligible cross section to account for the fall off in intensity at angles beyond 3°. Had Darwall continued his investigations to wider angles he would undoubtedly have found that the oscillatory structure continued to these wider angles and that his results could then only have been attributable to a single effective potential. One interesting feature did arise from Darwall's investigations. He was puzzled that he saw this "structure" since he did not feel that the system was sufficiently good to resolve it. However, in his considerations of apparatus resolution he had assumed that the lifetime of the metastable was long compared to the flight time between the scattering centre and the detector and he came to the conclusion that his

assumption about the lifetime was wrong and decided that "a lifetime for the $^3P_2$ state of the order of 10^{-3}S correlates better with the data than a lifetime of 10^{-1}S". This anomaly has now been resolved and the lifetimes of the metastables have been found to be 1.3×10^{-3}S. (Chapter 3).

Conclusions

It has been found that the scattering patterns obtained for the Hg*/Na, Hg*/K and Hg*/Rb in which interference structure is resolved in all cases, suggest that the atoms interact by a single potential in the attractive region probed at these energies. This single "effective" potential arises because the potential energy curves for the 5 possible mj states are not significantly different and because the Hg*/alkali system corresponds to a weak coupling case especially for the lighter alkalis [FLU 1973(b)].

Using the positions of the extrema in the cross section, parameterised deflection functions have been produced using the method of Buck [BUC 1971(a)] and these deflection functions have been inverted to potentials by the Firsov technique. However, it has been found that potentials cannot be reliably determined using only the positions of the extrema. It appears that the positions of these oscillations define the magnitude of certain areas contained in the well of the $\chi(b)$ curve and that by altering the $\chi(b)$ curve, in a way that does not alter these areas, the main rainbow oscillations can be left unaltered. The reduced areas bounded by the deflection function curves show that the Hg*/Na and Hg*/K interactions agree with the theory of corresponding states but that the Hg*/Rb system does

not fit into this scheme of things. (Further investigations should be performed on Hg*/Rb and perhaps Hg*/Cs since I feel that they too should fit into this theory.)

Despite the fact that the positions of the oscillations do not themselves determine the potential absolutely it should be possible to produce a more realistic potential by utilising other information such as the mean relative value of the cross section and the relative amplitudes of the extrema together with their positions. Therefore, the potential parameters obtained in this work await final confirmation from a more sophisticated inversion procedure being developed in Edinburgh, although it should be stated that the potentials obtained here are more realistic than those which might be obtained from Lennard-Jones type potentials.

No attenuation of the interference structure is found and the observation of quantum structure sets an upper limit on the size of the quenching cross section since both branches of the deflection function must be present for this structure to be seen. Quenching is clearly not an important process for collisions with impact parameters greater than $\sigma = 4\text{Å}$ and the total quenching cross section can hardly exceed gas kinetic values. Selective quenching might be an important factor although it is difficult to see what the exact nature of such a process might be.

Considering the range and well depth, the single "effective" potentials found for the three systems are consistent with the ground state interactions. The scattering patterns are also in agreement with the limited data available from previous experiments on the same

system and there seems little doubt that this scattering pattern is produced by one "effective" potential.

Concluding Remarks

More data is needed on the Hg*/alkali systems for a complete unravelling of the physics and chemistry involved. It is extremely difficult to determine decisively the potential if differential cross sections are available at only one energy. A wide energy range could be made available by using a "seeded" beam or by producing "fast" mercury from an ion source and using charge exchange techniques before excitation. Unfortunately both of these methods would require considerable alterations to the present experimental set up.

Another useful alteration would be velocity selection of the alkali beam, however, this would considerably reduce the number of interactions at the scattering centre and the experiment would be difficult to perform especially at wide angles where the number of scattered particles would be small. It might be possible to increase the number of interactions by using, instead of the present main beam oven, a nozzle source which would also have the advantage that the collision energy would be increased and the rainbow for these interactions would move into the angular range of the experiments. However, such a nozzle source would probably require differential pumping and therefore considerable alterations.

Such a source is worth considering for future work, however, since a number of other experiments would then become available. With

increased intensity it should be possible to look at the scattering of specific mj states of the excited atom either by magnetic selection or by a coincidence counting technique in which excess excitation energy is used and the metastables produced by cascade from perhaps the 7^3S level in mercury. The light emitted at the exciter by cascade to a specific mj state would then be used to "gate" the detector in coincidence so that the scattering of specific states could be studied (Such a method would require very good counting statistics).

It does not seem worthwhile investigating the light emitted from the interaction region for Hg*/alkali systems since the cross sections would appear to be very small although an analysis of ions or electrons from the interaction region would be useful in determining the magnitudes of ionisation cross sections. These ions should be easily observable and such an investigation might only require some sort of Faraday cage round the interaction region. Information about the well depth of the potential can also be obtained directly from electron energy distributions.

All the above mentioned experiments would require significant alterations to the apparatus and at this time it might be better to concentrate on other target beams, e.g. CO, NO and N_2 where inelastic cross sections might be larger, which can be used in the present apparatus. Also it might be worthwhile repeating the Hg*/Rb system and perhaps doing the Hg*/Cs system to complete the picture for Hg*/alkali interactions.

Work must continue on the fitting procedure because it seems

such a waste that so much time is spent, in a molecular beam experiment, obtaining a potential only to find that the potential is not unique.

Appendices

APPENDIX I

Calculation of the deflected beam profile

In general, the measured intensity depends on the widths of the source, collimator and detector slits and on their relative position and is normally trapezoidal in shape [RAM 1956]. The procedures for calculating the deflected beam shape have been developed by Stern [STE 1927]. The calculation would be trivial if all the molecules were in the same molecular state and at the same velocity since to a first approximation the undeflected beam shape would merely be shifted by an amount equal to the magnetic deflection (equation 3-10). Complications arise, however, due to the smearing effects of the velocity distribution.

Let b be the position in the detection plane to which an atom goes in the absence of a field. Let x be the position to which an atom with the same displacement goes in the presence of a field. Then x-b is the magnetic deflection at the detector position. This situation can be represented schematically.

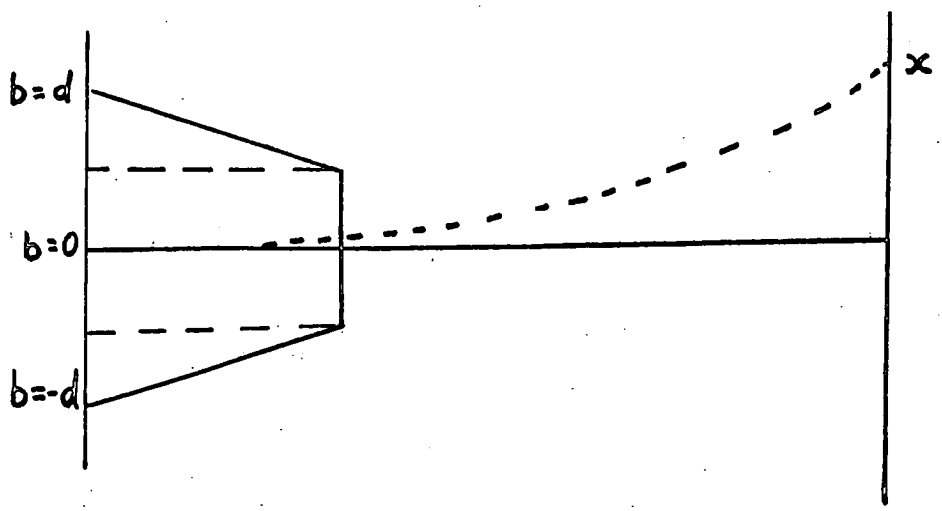

Since the deflection x is given by

$$x = \frac{A}{v^2} \qquad \text{[Equation 3-10]}$$

In the case of a Maxwell Boltzmann v^2 distribution

$$I(v)dv = Bv^2 \exp\left(-\frac{v^2}{\alpha^2}\right) dv$$

$$I(x)dx = \frac{A^{\frac{3}{2}} B}{2x^{\frac{5}{2}}} \exp\left(\frac{-A}{\alpha^2 x}\right) dx \qquad (1)$$

Equation 1 gives the deflected beam shape for molecules whose undeflected position in the detector plane is b = 0. For molecules with an arbitrary undeflected position b in the detector plane the expression becomes

$$I(x)dx = \frac{A^{\frac{3}{2}} B}{2(x-b)^{\frac{5}{2}}} \exp\left(\frac{-A}{\alpha^2(x-b)}\right) dx$$

To find the deflected beam intensity at a position x the contributions to the intensity from all elements of the undeflected beam shape must be added.

$$I(x) = N\int_{-d}^{+d} \frac{1}{(x-b)^{5/2}} \exp\left(\frac{-A}{\alpha^2(x-b)}\right) I_o(b)db \qquad (2)$$

where N = normalisation constant and $I_o(b)$ accounts for the undeflected beam shape.

When allowance is made for the lifetime τ in equation 2 the expression for I(x) becomes

$$I(x) = N\int_{-d}^{+d} \frac{I_o(b)}{(x-b)^{\frac{5}{2}}} \exp\left(\frac{-A}{\alpha^2(x-b)}\right) \exp\left(\frac{-d(x-b)^{\frac{1}{2}}}{\tau A^{\frac{1}{2}}}\right)db$$

A flowchart for the program to calculate the deflection pattern produced by passing a beam of atoms with a Maxwell Boltzmann v^2 distribution through a non homogeneous magnetic field is presented [Fig. A].

In the present experiment the main use of this program was to decide the slit dimensions necessary if only those atoms with zero effective moment are to be transmitted. The program was run for a variety of dimensions. The positions of the source, collimator, magnet and detector were fixed but the width of the source slit, the collimator slit and the lifetime were variable. The deflection patterns mapped onto a detector at the position of the magnet exit were then calculated. From these patterns the deflection x could be calculated for which the contribution to the total intensity from $m_J = \pm 2, \pm 1$ was zero. This value determined the size of the magnet exit aperture so that atoms with $m_J = \pm 2, \pm 1$ were discarded. Typical results are shown in Figures B and C.

The author would like to thank J.A. Robertson who was largely responsible for this program.

FIGURE A

Flowchart for the program to calculate the deflection pattern produced by passing a beam of atoms with a Maxwell Boltzmann v^2 distribution through a non-homogeneous magnetic field.

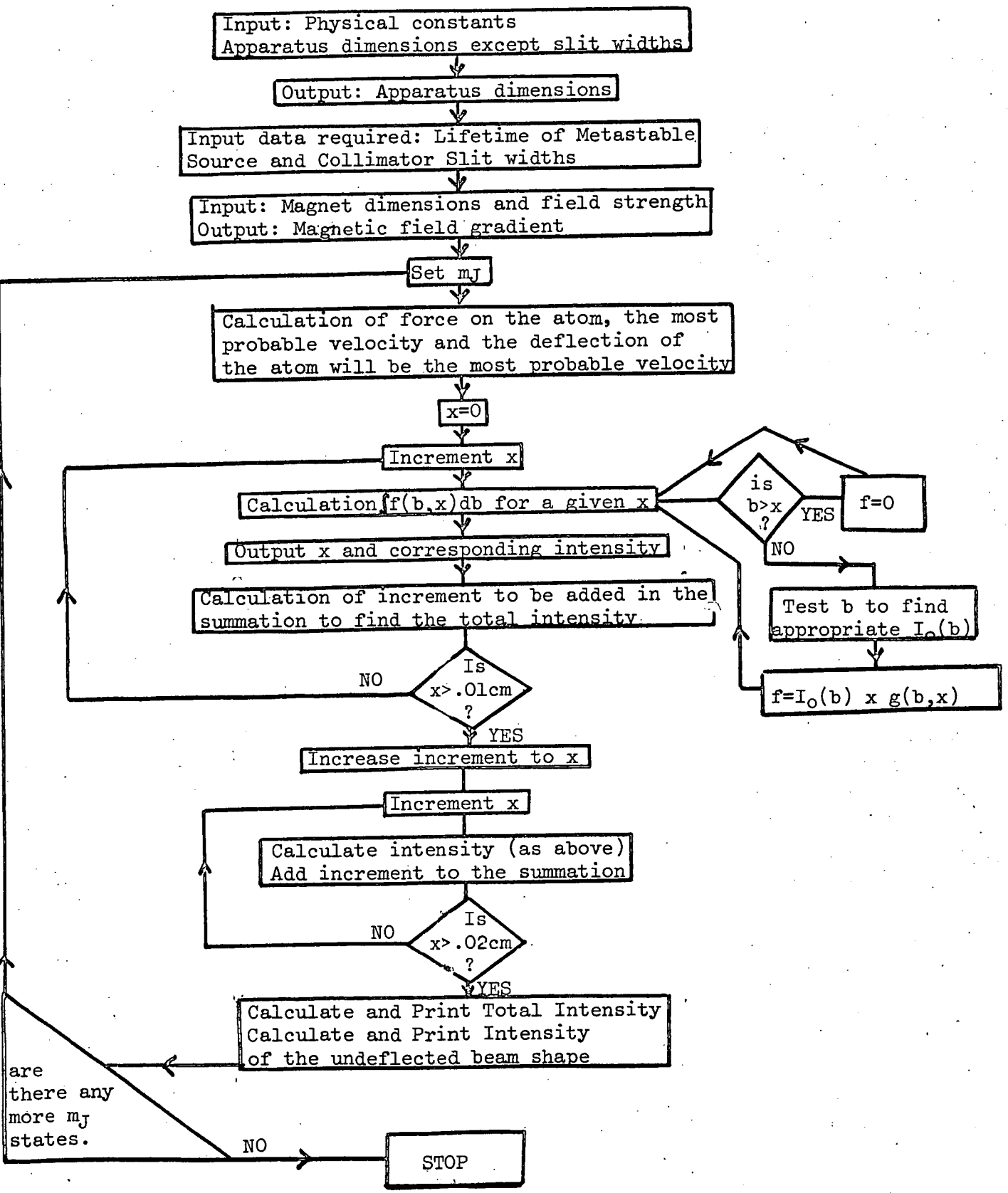

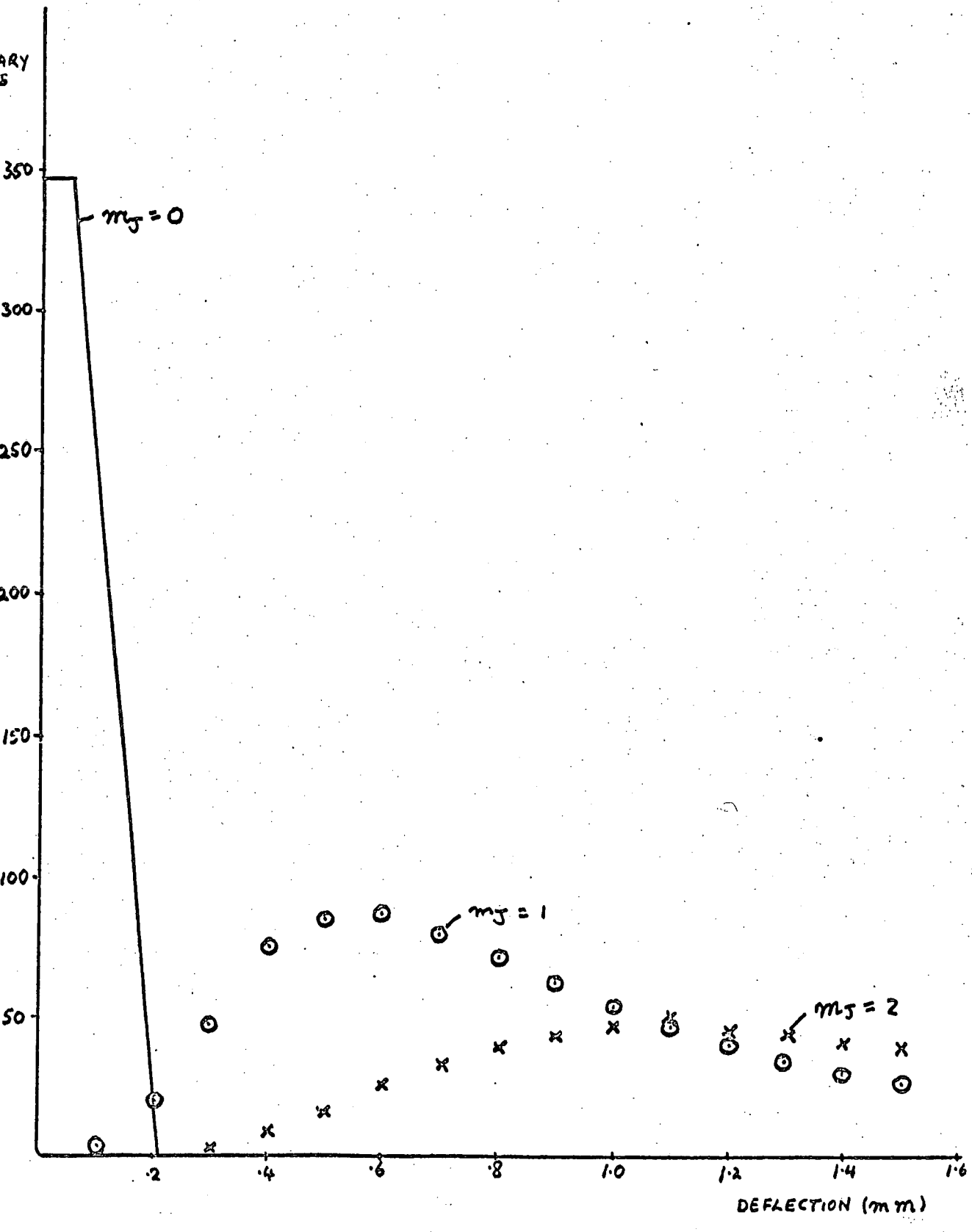

Computed deflections for the m_J = +2, +1 states of Hg* for a magnetic field of 7.5 KG and an entrance aperture of .01 cm mapped onto a detector .01 m from the magnet exit.

Figure B

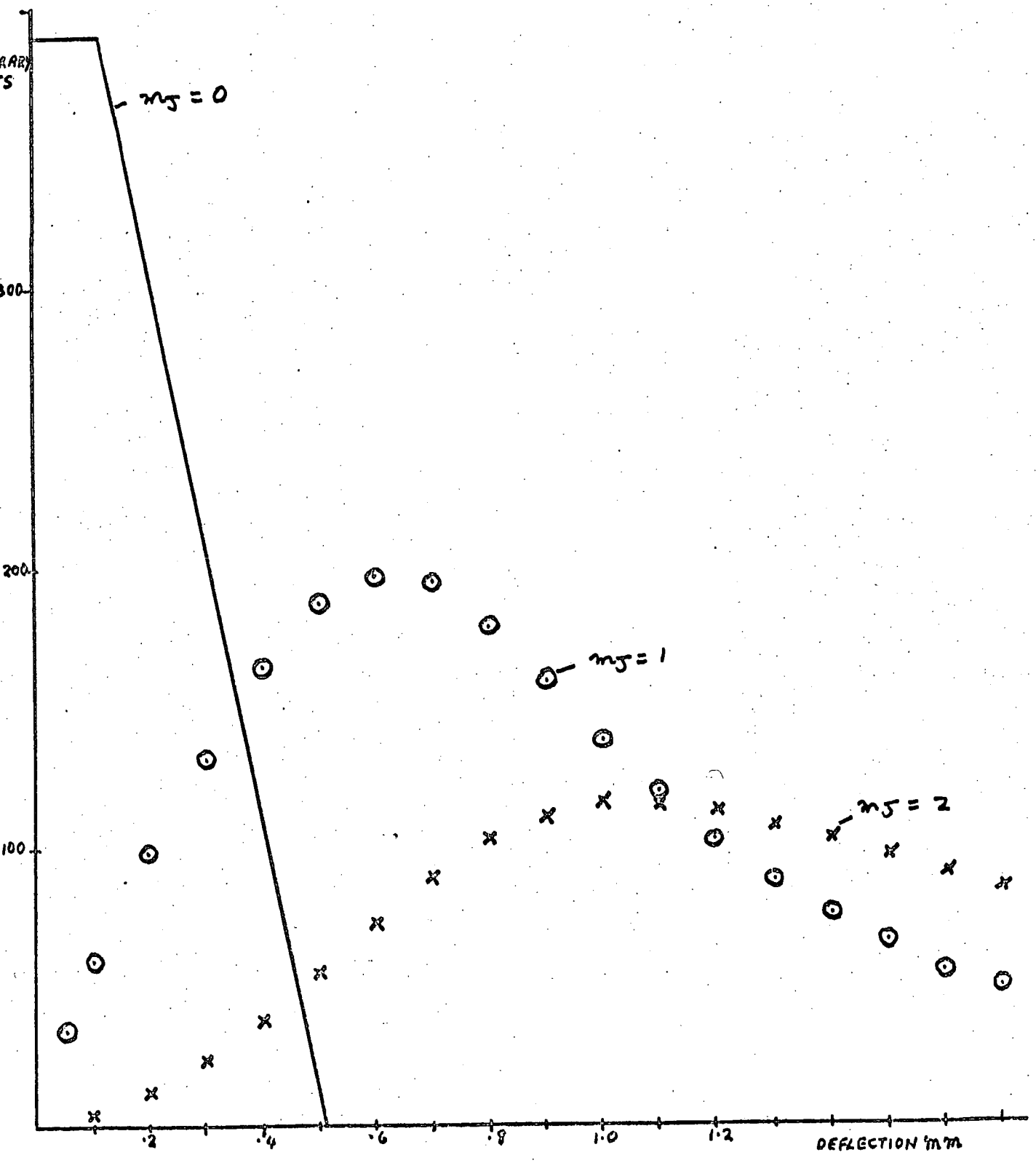

Computed deflection patterns for the m_J = +2,+1 states of Hg* for a magnetic field of 7.5 KG and an entrance aperture .025 cm mapped onto a detector .01 m from the magnet exit.

Figure C

APPENDIX II

Flow diagram for the evaluation of $\frac{1}{r_{12}}$ type integrals

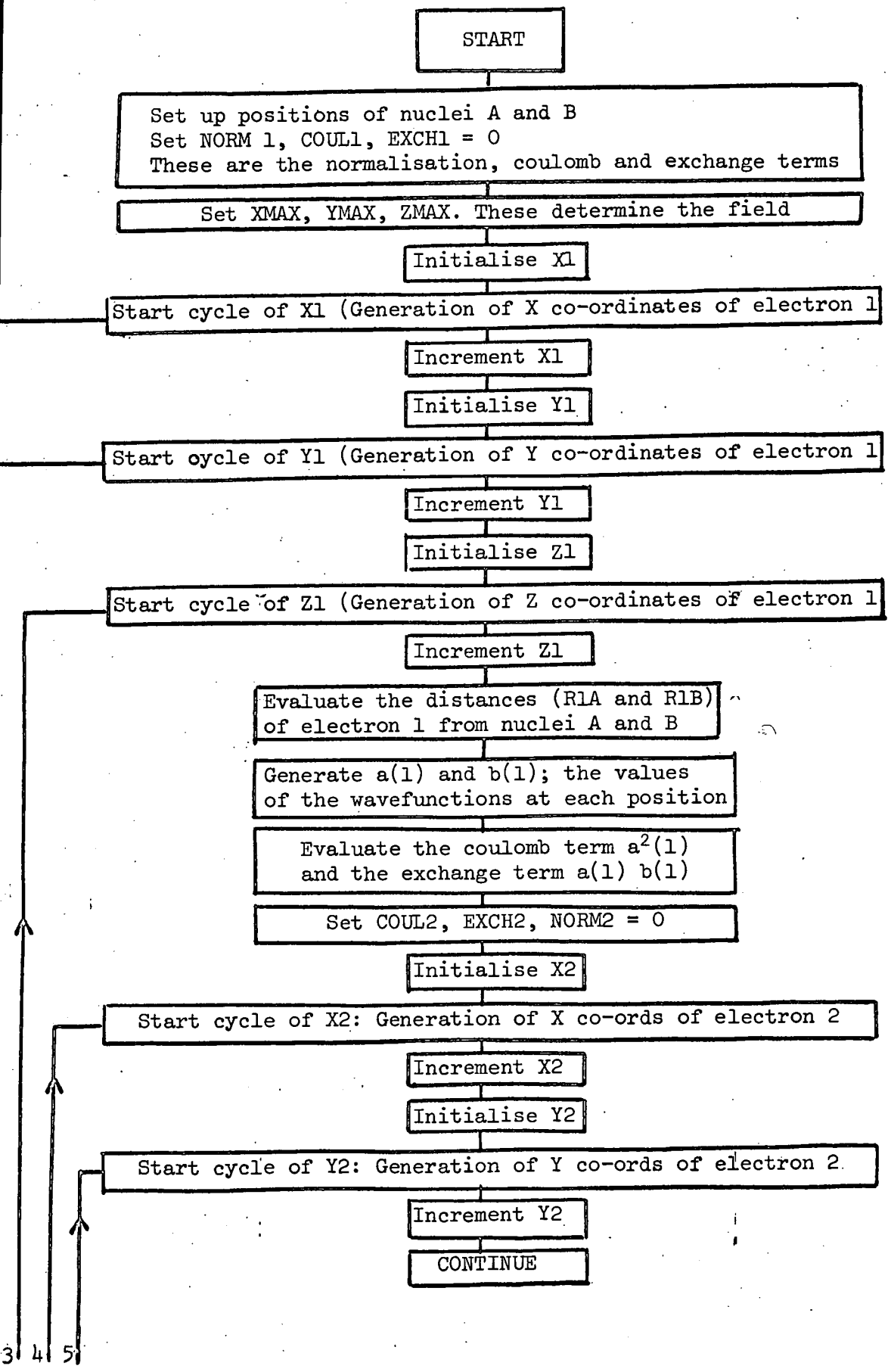

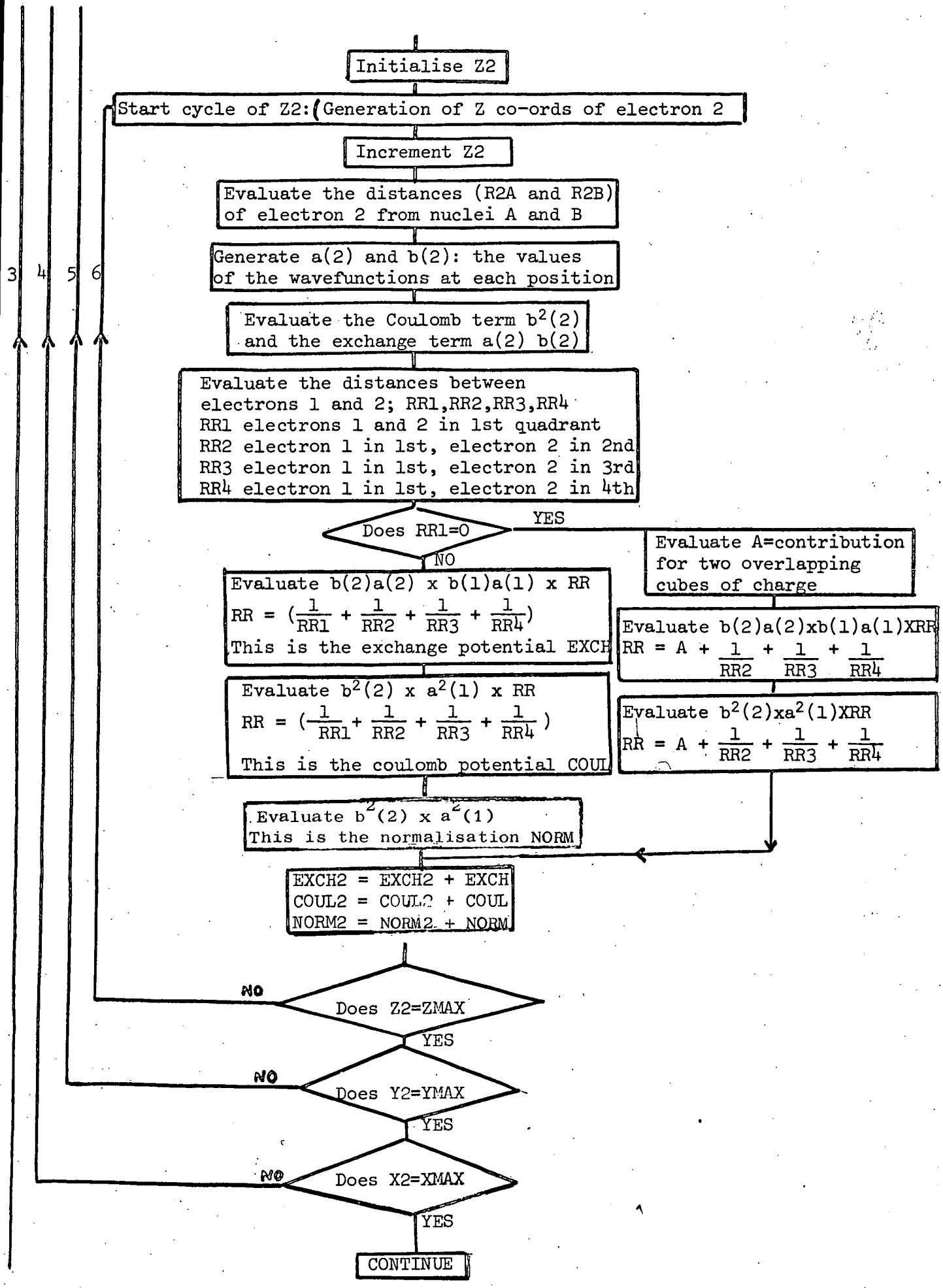
Initialise Z2
Start cycle of Z2: Generation of Z co-ords of electron 2
Increment Z2
Evaluate the distances (R2A and R2B) of electron 2 from nuclei A and B
Generate a(2) and b(2): the values of the wavefunctions at each position
Evaluate the Coulomb term b²(2) and the exchange term a(2) b(2)
Evaluate the distances between electrons 1 and 2; RR1,RR2,RR3,RR4
RR1 electrons 1 and 2 in 1st quadrant
RR2 electron 1 in 1st, electron 2 in 2nd
RR3 electron 1 in 1st, electron 2 in 3rd
RR4 electron 1 in 1st, electron 2 in 4th
Does RR1=0
YES
NO
Evaluate A=contribution for two overlapping cubes of charge
Evaluate b(2)a(2) x b(1)a(1) x RR
RR = (1/RR1 + 1/RR2 + 1/RR3 + 1/RR4)
This is the exchange potential EXCH
Evaluate b(2)a(2)xb(1)a(1)XRR
RR = A + 1/RR2 + 1/RR3 + 1/RR4
Evaluate b²(2) x a²(1) x RR
RR = (1/RR1 + 1/RR2 + 1/RR3 + 1/RR4)
This is the coulomb potential COUL
Evaluate b²(2)xa²(1)XRR
RR = A + 1/RR2 + 1/RR3 + 1/RR4
Evaluate b²(2) x a²(1)
This is the normalisation NORM
EXCH2 = EXCH2 + EXCH
COUL2 = COUL2 + COUL
NORM2 = NORM2 + NORM
Does Z2=ZMAX
NO
YES
Does Y2=YMAX
NO
YES
Does X2=XMAX
NO
YES
CONTINUE
3
4
5
6

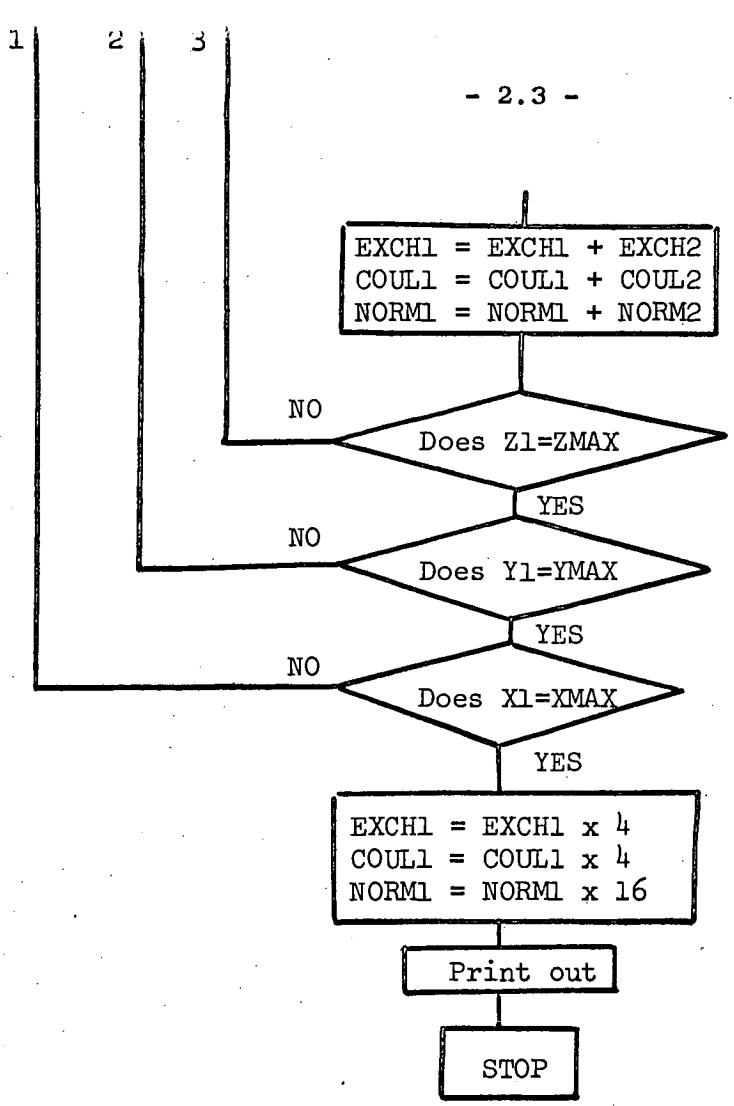
1
2
3
EXCH1 = EXCH1 + EXCH2
COUL1 = COUL1 + COUL2
NORM1 = NORM1 + NORM2
NO
Does Z1=ZMAX
YES
NO
Does Y1=YMAX
YES
NO
Does X1=XMAX
YES
EXCH1 = EXCH1 x 4
COUL1 = COUL1 x 4
NORM1 = NORM1 x 16
Print out
STOP

APPENDIX III

One of the molecular states arising from the collision $^3P_2 + {}^2S_{\frac{1}{2}}$ can be represented in the three electron approximation, by the Slater determinant.

$$\psi = \frac{1}{\sqrt{6}} \begin{vmatrix} 6S\alpha(1) & 6p_1\alpha(1) & K\alpha(1) \\ 6S\alpha(2) & 6p_1\alpha(2) & K\alpha(2) \\ 6S\alpha(3) & 6p_1\alpha(3) & K\alpha(3) \end{vmatrix}$$

This represents $^3P_{2,2} + {}^2S_{\frac{1}{2},\frac{1}{2}}$ and the final state which results has a value $m_J = \frac{5}{2}$.

For simplicity, the wavefunction may be represented as

$$Hg(1,2)K(3) - Hg(1,3)K(2) + Hg(2,3)K(1)$$

Let A = Hg(1,2)K(3)

B = Hg(1,3)K(2)

C = Hg(2,3)K(1).

As mentioned previously, an approximation to the Hamiltonian may be given by

$$\mu = -\tfrac{1}{2}\nabla_1^2 - \tfrac{1}{2}\nabla_2^2 - \tfrac{1}{2}\nabla_3^2 - VHg(1) - VHg(2) - VHg(3) - VK(1) - VK(2) - VK(3) + \frac{1}{r_{12}} + \frac{1}{r_{23}} + \frac{1}{r_{13}} + \frac{Z_A Z_B}{R}$$

On substitution of the wavefunction ψ and the Hamiltonian μ into the equation $E = \int \psi \mu \psi$

then $E = A\mu A + B\mu B + C\mu C - 2A\mu B - 2B\mu C + 2A\mu C$.

In evaluating E, it is useful to remember that

$$Hg(1,2)\left[-\tfrac{1}{2}\nabla_1^2 - \tfrac{1}{2}\nabla_2^2 - VHg(1) - VHg(2) + \frac{1}{r_{12}}\right] Hg(1,2) = E_{Hg}^*$$

and that $K(3)\left[-\tfrac{1}{2}\nabla_3^2 - VK(3)\right] = E_K$

Neglecting the fact that the overlap integral $\int 6p_1\alpha(1)K\alpha(1) = 0$

but remembering that $\int 6p_1\alpha(1)\ 6p_1\alpha(1) = 1$

$\int 6S\alpha(1)\ \ 6S\alpha(1) = 1$

$\int K\alpha(1)\ \ K\alpha(1) = 1$

the terms required in the evaluation of E are presented.

The symmetric terms which arise are as follows

$$\int K\alpha(2)\left[-VHg(2)\right] K\alpha(2)$$

$$\int 6S\alpha(1)\left[-VK(1)\right] 6S\alpha(1)$$

$$\int 6p\alpha(3)\left[-VK(3)\right] 6p\alpha(3)$$

$$\int 6S\alpha(1)\ K\alpha(2)\ \frac{1}{r_{12}}\ 6S\alpha(1)\ K\alpha(2)$$

$$\int 6p\alpha(1)\ K\alpha(2)\ \frac{1}{r_{12}}\ 6p\alpha(1)\ K\alpha(2)$$

$$+\ \frac{Z_A\ Z_B}{R}$$

The following non symmetric expressions are also required.

$$-\int 6S\alpha(1)\left[-\tfrac{1}{2}\nabla_1^2\right] 6S\alpha(1) \times \int 6p\alpha(2)\ K\alpha(2) \times \int 6p\alpha(3)\ K\alpha(3)$$

$$-\int 6S\alpha(1)\left[-VHg(1)\right] 6S\alpha(1) \times \int 6p\alpha(2)\ K\alpha(2) \times \int 6p\alpha(3)\ K\alpha(3)$$

$$-\int 6S\alpha(1)\left[-VK(1)\right] 6S\alpha(1) \times \int 6p\alpha(2)\ K\alpha(2) \times \int 6p\alpha(3)\ K\alpha(3)$$

$$-2\int 6p\alpha(2)\left[-\tfrac{1}{2}\nabla_2^2\right] K\alpha(2) \times \int 6p\alpha(3)\ K\alpha(3)$$

$$-2\int 6p\alpha(2)\left[-VHg(2)\right] K\alpha(2) \times \int K\alpha(3)\ 6p\alpha(3)$$

$$-2\int 6p\alpha(2)\left[-VK(2)\right] K\alpha(2) \times \int K\alpha(3)\ 6p\alpha(3)$$

$$-2\int 6S\alpha(1)\ K\alpha(3)\ \frac{1}{r_{13}}\ 6S\alpha(1)\ 6p\alpha(3) \times \int 6p\alpha(2)\ K\alpha(2)$$

$$-\int 6p\alpha(2)\ K\alpha(3)\ \frac{1}{r_{23}}\ 6p\alpha(3)\ K\alpha(2)$$

$$-\frac{Z_A Z_B}{R}\int 6p\alpha(2)\ K\alpha(2) \times \int 6p\alpha(3)\ K\alpha(3)$$

$$2\int 6S\alpha(1)\left[-\tfrac{1}{2}\nabla_1^2\right] 6p\alpha(1) \times \int 6S\alpha(3)\ K\alpha(3) \times \int 6p\alpha(2)\ K\alpha(2)$$

$$2\int 6S\alpha(1)\left[-VHg(1)\right] 6p\alpha(1) \times \int 6S\alpha(3)\ K\alpha(3) \times \int 6p\alpha(2)\ K\alpha(2)$$

$$2\int 6S\alpha(1)\ \left[-VK(1)\right]\ 6p\alpha(1)\ x\int 6S\alpha(3)\ K\alpha(3)\ x\int 6p\alpha(2)\ K\alpha(2)$$

$$2\int 6S\alpha(1)\ 6p\alpha(2)\ \frac{1}{r_{12}}\ 6p\alpha(1)\ K\alpha(2)\ \ x\int 6S\alpha(3)\ K\alpha(3)$$

$$2\int 6S\alpha(1)\ K\alpha(3)\ \frac{1}{r_{13}}\ 6S\alpha(3)\ 6p\alpha(1)\ x\int 6p\alpha(2)\ K\alpha(2)$$

$$-\int 6p\alpha(1)\ \left[-\tfrac{1}{2}\nabla_1^2\right]\ 6p\alpha(1)\ \ x\int 6S\alpha(2)\ K\alpha(2)\ \ x\int 6S\alpha(3)\ K\alpha(3)$$

$$-\int 6p\alpha(1)\ \left[-VHg(1)\right]6p\alpha(1)\ \ x\int 6S\alpha(2)\ K\alpha(2)\ \ x\int 6S\alpha(3)\ K\alpha(3)$$

$$-\int 6p\alpha(1)\ \left[-VK(1)\right]6p\alpha(1)\ \ x\int 6S\alpha(2)\ K\alpha(2)\ \ x\int 6S\alpha(3)\ K\alpha(3)$$

$$-2\int 6S\alpha(2)\ \left[-\tfrac{1}{2}\nabla_2^2\right]\ K\alpha(2)\ \ x\int 6S\alpha(3)\ K\alpha(3)$$

$$-2\int 6S\alpha(2)\ \left[-VHg(2)\right]K\alpha(2)\ \ x\int 6S\alpha(3)\ K\alpha(3)$$

$$-2\int 6S\alpha(2)\ \left[-VK(2)\right]K\alpha(2)\ \ x\int K\alpha(3)\ 6S\alpha(3)$$

$$-\int 6S\alpha(2)\ K\alpha(3)\ \frac{1}{r_{23}}\ 6S\alpha(3)\ K\alpha(2)$$

$$-2\int 6p\alpha(1)\ K\alpha(3)\ \frac{1}{r_{13}}\ 6p\alpha(1)\ 6S\alpha(3)\ x\int 6S\alpha(2)\ K\alpha(2)$$

$$-\frac{Z_A Z_B}{R}\ x\int 6S\alpha(1)\ K\alpha(1)\ \ x\int 6S\alpha(3)\ K\alpha(3)$$

The majority of the non symmetric terms listed above are small since they involve, in some cases, multiplication by two overlap integrals which, in the majority of cases at the internuclear separations considered in this calculation, are small. The terms involving the kinetic energy operator are evaluated by remembering that

$$\mu = -\tfrac{1}{2}\nabla_1^2 + V$$

$$\left[-\tfrac{1}{2}\nabla_1^2\right]\ \psi_i = \left[\mu - V\right]\ \psi_i$$

$$= \left[E_i - V\right]\ \psi_i$$

For the wavefunction considered the resulting state has a value $m_J = \frac{5}{2}$. However, if the potassium atom has β spin then the same terms can be used to compute a state with $m_J = \frac{3}{2}$, remembering the orthogonality relations.

A similar analysis is required for the other states involved in the interaction of metastable mercury and ground state potassium. The possible atomic states of mercury are given in expression [4-1]. When these expressions are combined with the potassium atom in the appropriate spin state they form the necessary wavefunctions for calculation of the "molecular" matrix elements.

e.g. The $^3P_{21}$ state of mercury can be written in the following form

$$^3P_{21} = C_1 \,|S\alpha(1)\; p_1\; \beta(1)| + C_1\,|S\beta(1)\; p_1\alpha(1)| + C_2|S\alpha(1)\; p_o\alpha(1)|$$

so that the resulting "molecular" wavefunction, in the case of $^3P_{2,1} + {}^2S_{\frac{1}{2},\frac{1}{2}}$, becomes

$$\psi = C_1\,|S\alpha(1)\; p_1\; \beta(1)K\alpha(1)| + C_1\,|S\beta(1)p_1\alpha(1)\; K\alpha(1)| + C_2|S\alpha(1)\; p_o\alpha(1)\; K\alpha(1)|$$

The atomic wave function for $^3P_{20}$ can be represented as

$$^3P_0 = C_3\,|S\beta(1)\; p_1\beta(1)| + C_4\,|S\alpha(1)\; p_{-1}\alpha(1)| + C_5\,|S\alpha(1)\; p_o\beta(1)| + C_5\,|S\beta(1)\; p_o\alpha(1)|$$

and so on. C_1, C_2, C_3, C_4 and C_5 are the Clebsch-Gordan coefficients.

The terms involved in computing these other states are similar to those presented above. Before any computing was performed the required integrals for each state were listed. The number of terms required varied due to spin orthogonality and the value of the overlap integral $\int 6p(1)\; K(1)$. (For the cases in which the wave functions are $6p_1$ and 6_{p-1} the overlap is zero). The algebra, which was tedious, has been rigorously checked.

It should be noted that, in the above description, spin orbit interaction has been omitted from the Hamiltonian. In general, the Hamiltonian can be considered as $\mu^o + \mu^1$ where μ^o is the Hamiltonian

without spin orbit interaction. The result for the spin orbit interaction energy of an electron in a central field with potential U(r) is

$$\mu^1 = \frac{1}{2m^2C^2} \left(\frac{1}{r} \frac{dU(r)}{dr}\right) L.S$$

where L is the orbital and S the spin angular momentum.

In this case it is possible to write

$$Hg(1,2) \left[\mu^1 + \mu^0\right] Hg(1,2) = E^{*}_{Hg_{12}}$$

however, exchange terms will arise in the "molecular" case and an estimate of the effect requires consideration. A full analysis of the central field problem is presented by Condon and Shortley [CON 1953] (p. 121) and it can be shown that the effect of exchange integrals of the form $\int 6S\alpha(1) \left[L.S\right] K\alpha(1)$ and $\int 6p\alpha(1) \left[L.S\right] K\alpha(1)$ will be small.

The molecular situation is not a central force situation but it is reasonable to assume that this effect will only be large for the electron near the nucleus and can therefore be looked upon as a central field problem. It seemed reasonable, therefore, to neglect this effect at the internuclear separations involved.

Spin orbit interaction is a large energy term in mercury and the absence of this term in exchange with potassium is perhaps one reason for its lack of binding in the "molecular" situation.

References

ALP 1949 D ALPERT, A O McCOUBREY, T HOLSEIN
Phys. Rev., 76, 1257, 1949.

BAL 1965 P BALTAYAN and J-C PEBAY PEYROULA
Comp. Rend., 260, 6569, 1965.

BAR 1966 P BARWIG, U BUCK, E HUNDHAUSEN, H PAULY
Z. Physik, 196, 343, 1966.

BAT 1962 Ed. D R BATES, "Atomic and Molecular Processes" Chapter 14, Academic Press, New York, 1962.

BAT 1965 Ed. D R BATES, I ESTERMANN
Vol 1, Adv. in Atomic and Molecular Physics, Academic Press, New York 1965.

BER 1967 R B BERNSTEIN, Adv. in Chemical Physics, Vol 12, p 389, Ed. J O Hirschfelder.

BER 1966 M V BERRY, Proc. Phys. Soc., 89. 479, 1966.

BEU 1929 H BEUTLER and B JOSEPHY
Z. Physik, 53, 747, 1929.

BIG 1967 M C BIGEON
Journ. de Phys., 28, 51, 1967.

BOR 1969 W L BORST
Phys. Rev., 181, 257, 1969.

BOR 1971 W L BORST and E C ZIPF
Phys. Rev., A3, 979, 1971.

BOY 1971 J F BOYLE, MOLECULAR PHYSICS, 22, 993, 1971.

BRO 1971 J C BROWNE, Adv. in Atomic and Molecular Physics, Vol 7, 47, 1971.

BUC 1952 R A BUCKINGHAM and A DALGARNO
Proc. Roy. Soc (London) A213, 506, 1952.

BUC 1968 U BUCK, and H PAULY
Z Physik, 208, 390, 1968.

BUC 1971a U BUCK, Journ. Chem. Phys., 54, 1923, 1971.

BUC 1971b U BUCK and H PAULY
Journ. Chem. Phys., 54, 1929, 1971.

BUC 1972 U BUCK, M KICK, H PAULY
Journ. Chem. Phys., 56, 3391, 1972.

BYK 1964 V K BYKHOVSKII, E E NIKITIN
Opt. Spectr. 16,, 111, 1964.

CAL 1965 J CALLAWAY and E BAUER
Phys. Rev., 140, A1072, 1965.

CAR 1922 G CARIO and J FRANCK
Z. Physik, 17, 202, 1923.

CER 1966 V CERMAK
Journ. Chem. Phys. 44, 3781, 1966.

CON 1935 E U CONDON, G H SHORTLEY
"Theory of Atomic Spectra", Cambridge University Press, 1935.

COU 1942 C A COULSON
Proc. Camb. Phil. Soc., 38, 210, 1942.

COW 1968 L T COWLEY, Ph.D Thesis, Edinburgh 1968.

CZA 1973 M CZAJKOWSKI, G SKARDIS, L KRAUSE
Can. J. Phys., 51, 334, 1973.

DAR 1970 E C D DARWALL, M A D FLUENDY, K P LAWLEY
Molecular Physics, 19, 673, 1970.

DAR 1971 E C D DARWALL, M A D FLUENDY, K P LAWLEY
Entropie, 42, 162, 1971.

DAR 1972 E C D DARWALL, Ph.D Thesis, Edinburgh 1972.

DEE 1971 J S DEECH, J PITRE, L KRAUSE
Can. J. Phys., 49, 1976, 1971.

DOE 1969 L J DOEMENY, F J VAN ITALLIE, R M MARTIN
Chem. Phys. Lett, 4, 302, 1969.

DUC 1971 B S DUCHART, Ph.D Thesis, Edinburgh 1971.

DUR 1968 R DUREN, G P RAABE, C h SCHLIER
Z. Physik, 214, 410, 1968.

FIR 1953 O B FIRSOV
Zh. eskp Fiz., 24, 279, 1953.

FIS 1967 E S FISHBURNE,
Journ. Chem. Phys., 47, 58, 1967.

FIT 1959 W L FITE, R T BRACKMANN, D G HUMMER, R F STEBBINGS
Phys. Rev. 116, 363, 1959.

FLU 1973a M A D FLUENDY, K P LAWLEY
"Chemical Applications of Molecular Beam Scattering"
Chapman Hall, London, 1973.

FLU 1973b M A D FLUENDY, I H KERR, K P LAWLEY
to be published.

FOR 1959 K W FORD, J A WHEELER
Ann. Phys., 7, 259, 1959.

FRE 1967 R S FREUND, W KLEMPERER
Journ. Chem. Phys., 47, 2897, 1967.

FUK 1926 M FUKUDA
Sci. Pap. Inst. Phys. Chem. Res., 4, 171, 1926.

GAR 1961 R GARRON, D TESTARD
Compt. Rend., 253, 1170, 1961.

GOL 1964 H GOLDSTEIN, "Classical Mechanics", Addison Wesley,
1964.

GRO 1968 J GROSSER, H HABERLAND
Phys. Lett, 27A, 634, 1968.

HAB 1973 H HABERLAND, C H CHEN, Y T LEE
Private Communication.

HEI 1927 W HEITLER, F LONDON
Z. Physik, 44, 455, 1927.

HER 1963 F HERMAN, S SKILLMAN
"Atomic Structure Calculations", Prentice Hall Inc. 1963.

HER 1966 Z HERMAN, V CERMAK
Coll. Czech. Chem. Comm., 31, 649, 1966.

HER 1968 J A HERCE, J R PENTON, R J CROSS, E E MUSCHLITZ
Journ. Chem. Phys., 49, 958, 1968.

HOR 1951 J A HORNBECK, J P MOLNAR
Phys. Rev., 84, 621, 1951.

HOR 1969 D S HORNE, Ph.D Thesis, Edinburgh 1969.

HOR 1971 H HORIGUCHI, S TSUCHIYA
Bull. Chem. Soc. Jap., 44, 1213, 1971.

HOS 1960 H U HOSTETTLER, R B BERNSTEIN
Phys. Rev. Lett, 5, 318, 1960.

HOT 1967 H HOTOP, A NIEHAUS
Journ. Chem. Phys., 47, 2506, 1967.

HOT 1968 H HOTOP, A NIEHAUS
Z. Physik, 215, 395, 1968.

HOT 1969a H HOTOP, A NIEHAUS
Z. Physik, 228, 68, 1969.

HOT 1969b H HOTOP, A NIEHAUS, A L SCHMELTEKOPF
Z. Physik, 229, 1, 1969.

HOT 1970 H HOTOP, A NIEHAUS
Z. Physik, 238, 452, 1970.

HUN 1964 E HUNDHAUSEN, H PAULY
Z. Naturfor., 19, 810, 1964.

HUN 1965 E HUNDHAUSEN, H PAULY
Z. Physik, 187, 305, 1965.

HUZ 1967 S HUZINAGA
Prog. Theor. Phys. Suppl., 40, 52, 1967.

JOH 1972 C E JOHNSON
Phys. Rev., A5, 1026, 1972.

KAL 1929 H KALLMAN, F LONDON
Z. Phys. Chem., 132, 207, 1929.

KAL 1973 A P KALININ, V B LEONAS
VIII ICPEAC, Belgrade, 1973.

KES 1950 K G KESSLER
Phys. Rev., 77, 559, 1950.

KIM 1960 G H KIMBELL, D J LEROY
Can. J. Chem., 38, 1714, 1960.

KIT 1956 C KITTEL
"Introduction to Solid State Physics", Wiley, New York, 1956.

KOD 1971 M KODAIRA, T WATANABE
Adv. Chem. Physics, XXI, p 167, 1971.

KOL 1969 H J KOLKER, H H MICHELS
J. Chem. Phys., 50, 1762, 1969.

KRA 1970 E K KRAULINYA, M L YANSON
Opt. Spect., 29, 239, 1970.

KRA 1972 H L KRAMER, J A HERCE, E E MUSCHLITZ
Journ. Chem. Phys., 56, 4166, 1972.

KRA 1973 H F KRAUSE, S DATZ, S G JOHNSON
Journ. Chem. Phys., 58, 367, 1973.

KRU 1937 A A KRUITHOFF, F M PENNING
Physica, 4, 430, 1937.

LAB 1972 Laboratory Manual, Edinburgh University Molecular Beams Group, 1972.

LEV 1969 R D LEVINE
"Quantum Mechanics of Molecular Rate Processes", Clarendon Press, Oxford.

LEV 1972 R D LEVINE, R B BERNSTEIN
Chem. Phys. Lett, 15, 1, 1972.

LIC 1957 W LICHTEN,
Journ. Chem. Phys., 26, 306, 1957.

LIC 1958 W LICHTEN,
Phys. Rev., 109, 1191, 1958.

LUO 1970 J R LUOMA,
Journ. Chem. Phys., 53, 129, 1970.

MAR 1972 R M MARTIN

Private Communication.

MAS 1971 H S W MASSEY, H B GILBODY, E H S BURHOP

"Electronic and Ionic Impact Phenomena III", Clarendon Press, 1971.

MAS 1967 M MATSUZAWA, H NAKAMURA

J. Phys. Soc. Jap., 22, 312, 1967.

MCA 1965 J E McALDUFF, D J LEROY

Can. J. Chem., 43, 2279, 1965.

MCC 1968 J C McCONNELL, B L MOISEIWITSCH

J. Phys., B, 1, 406, 1968.

MCL 1960 A D McLEAN, A WEISS, M YOSHIMINE

Rev. Mod. Phys., 32, 211, 1960.

MIL 1970a W H MILLER

Journ. Chem. Phys., 52, 3563, 1970.

MIL 1970b W H MILLER, H F SCHAEFER

Journ. Chem. Phys., 53, 1421, 1970.

MIL 1972 W H MILLER, C A SLOCOMB, H F SCHAEFER

Journ. Chem. Phys., 56, 1347, 1972.

MOR 1962a F A MORSE, R B BERNSTEIN

Journ. Chem. Phys., 37, 2019, 1962.

MOR 1962b F A MORSE, R B BERNSTEIN, H U HOSTETTLER

Journ. Chem. Phys., 36, 1947, 1962.

MOR 1963 J D MORRISON
Journ. Chem. Phys., 39, 200, 1963.

MOT 1965 N F MOTT, H S W MASSEY
"Theory of Atomic Collisions (3rd Edition)"
Oxford University Press, 1965.

MRO 1945 S MROZOWSKI
Phys. Rev., 67, 161, 1945.

MUS 1966 E E MUSCHLITZ
Advances in Chem. Phys., Vol 10, Editor J Ross,
Wiley, 1966.

NIK 1965 E E NIKITIN
Journ. Chem. Phys., 43, 744, 1965.

PAU 1935 L PAULING, E B WILSON
"Introduction of Quantum Mechanics", McGraw Hill,
New York, 1935.

PEN 1968 J R PENTON, E E MUSCHLITZ
Journ. Chem. Phys., 49, 5083, 1968.

PIT 1972 J PITRE, K HAMMOND, L KRAUSE
Phys. Rev. A6, 2101, 1972.

POL 1967 G KARL, P KRUUS, J C POLANYI, W M SMITH
Journ. Chem. Phys., 46, 244, 1967.

RAM 1956 N F RAMSEY
"Molecular Beams", Oxford University Press, 1956.

RAN 1960 B J RANSIL
Rev. Mod. Phys., 32, 245, 1960.

RAY 1927 LORD RAYLEIGH
Proc. Roy. Soc., (London) A117, 294, 1927.

ROS 1966 "Adv. in Chem. Phys. Vol 10", Editor J Ross, Wiley 1966.

ROT 1965 E W ROTHE, R H NEYBAYER, S M TRUJILLO
Journ. Chem. Phys., 42, 3310, 1965.

SCH 1970 A L SCHMELTEKOPF, F C FEHSENFELD
Journ. Chem. Phys., 53, 3173, 1970.

SLA 1951 J C SLATER
Phys. Rev., 81, 385, 1951.

SLA 1963 J C SLATER
"Quantum Theory of Molecules and Solids I", McGraw Hill, New York, 1963.

STE 1921 O STERN
Z. Physik, 7, 249, 1921.

TAN 1972 S Y TANG, A B MARCUS, E E MUSCHLITZ
Journal Chem. Phys., 56, 566, 1972.

THO 1961 W R THORSON
Journ. Chem. Phys., 34, 1744, 1961.

TIT 1965 K TITTEL
Z. Physik, 187, 421, 1965.

VAN 1971 R S VAN DYCK, C E JOHNSON, H A SHUGART
Phys., Rev. A4, 1327, 1971.

VAN 1972 F J VAN ITALLIE, L J DOEMENY, R M MARTIN
Journ. Chem. Phys., 56, 3689, 1972.

VAN 1972b R S VAN DYCK, C E JOHNSON, H A SHUGART
Phys. Rev. A5, 991, 1972.

VIK 1972 A C VIKIS, G TORRIE, D J LEROY
Can. J. Chem., 50, 176, 1972.

WAB 1965 J T WABER, D T CRAMER
J. Chem. Phys., 42, 4116, 1965.

WAT 1967 T WATANABE
Journ. Chem. Phys., 46, 3741, 1967.

WU 1962 T Y WU, T OHMURA
"Quantum Theory of Scattering", Prentice Hall Inc.
New York, 1962.